UNIVERSITÀ DEGLI STUDI DI NAPOLI
"FEDERICO II"

SCUOLA POLITECNICA E DELLE SCIENZE DI BASE
Department of Industrial Engineering

DOCTORAL THESIS IN INDUSTRIAL ENGINEERING

Preliminary Design of Hybrid-Electric Regional Aircraft with Reduced Environmental Impact

Supervisor:
Prof. Fabrizio Nicolosi

Coordinator:
Prof. Michele Grassi

Author:
Valerio Marciello
DR995127

March 2024

To my father Giovanni Battista,
to my beloved Maria Vittoria,
and to all who have illuminated
my path with their unceasing support.

Declaration of Authorship

I, Valerio Marciello, declare that this thesis, titled "Preliminary Design of Hybrid-Electric Regional Aircraft with Reduced Environmental Impact" is a product of my original research. I confirm that:

- The research and writing for this thesis were wholly or mainly conducted during my candidacy for a research degree at this University.
- In instances where any part of this thesis was previously submitted for a degree or any other qualification at this or any other institution, I have explicitly indicated so.
- Whenever I have consulted the published works of others, this was always clearly attributed.
- Any quotations from the works of others were properly cited, and except for these quotations, this thesis is entirely the result of my own efforts.
- I have acknowledged and cited all main sources of help.
- In cases where the thesis includes collaborative work, I have explicitly clarified the contributions made by others and those that are my own.

Date: 10^{th} March 2024

Sign: 

Abstract

Nowadays, the aviation industry faces unprecedented challenges in the context of environmental sustainability. Due to their smaller size and shorter route profiles, regional turboprop airplanes are identified as the ideal test bed for the integration of cutting-edge technologies. The integration of alternative propulsion systems, such as hybrid-electric architectures and alternative aviation fuels, is a necessary stride toward reducing regional aviation's environmental footprint, but their true potential can only be unlocked through a multidisciplinary approach. In light of the major impact of design choices on the technical, economic, and environmental performance of new aircraft, emphasis is placed on the role that the preliminary designer may have in influencing the industry's trajectory toward sustainability.

Literature on hybrid-electric regional aircraft highlights the sensitivity of the expected advantages to the assumed technological levels. This stresses the importance of a careful technology foresight, when the purpose is to provide a prospective analysis of the benefits expected in a specific time horizon. Furthermore, increasing sensitivity to the environmental problem imposes holistic considerations, which do not neglect life-cycle and cost considerations even in the preliminary design phases. The present thesis work, titled "Preliminary Design of Hybrid-Electric Regional Aircraft with Reduced Environmental Impact", aims to explore the challenges and opportunities that lie in integrating sustainability into the heart of aircraft design, posing the following research question:

How can preliminary aircraft designers support the transition to a future sustainable regional aviation, with a specific focus on hybrid-electric and hydrogen-based technologies, while including life-cycle considerations?

By addressing this multifaceted problem, the initial candidate's efforts have been focused on the development of a design framework for hybrid-electric aircraft in collaboration with the DAF research group of the University of Naples "Federico II". In this sense, active participation in several European research projects supported the candidate's research and the development of know-how on the topic. Thus, classic design methodologies have been adapted and generalized in order to manage innovative propulsion architectures as well as conventional aircraft. In particular, a general mathematical model is proposed, capable of describing a huge variety of propulsion systems involving alternative energy sources. The model is able to degenerate into specific architectures based on thermal engines, batteries, hydrogen fuel cell systems, or any combination of them. The model has been included in an in-house flexible design workflow that allows for an accurate, consistent, and complete design of new concepts. The workflow combines the generalized powertrain description with sophisticated methods for mass estimation, aero-propulsive interaction effects, and a design approach based on mission analysis.

An extensive study has been conducted to support the determination of a transition roadmap towards economically and environmentally sustainable regional aviation. Focusing on a 50-passenger regional platform, several future scenarios have been defined, representative of the most promising technologies available for three reference entry into service years. Starting from market-driven top-level requirements, a wide design exploration has been performed, using an accurate approach based on surrogate models and mission analysis. Detailed life cycle and cost analyses have been carried out for each scenario, highlighting that trade-offs emerge when considering innovative technologies. As an outcome of this activity, extensive and scalable life cycle inventory datasets have been generated and published in collaboration with expert partners, representing a first step toward the integration of sustainability considerations at the preliminary design level. Finally, the technical, economic, and environmental results of the study have been critically compared, electing the most promising scenarios. Sustainable aviation fuels and battery systems have been identified as valid transition technologies, while waiting for hydrogen-based propulsive systems to mature sufficiently. The conclusions have been summarized in a set of recommendations for aviation stakeholders and policymakers, seen as necessary steps toward the alignment with European environmental objectives.

Keywords: *aircraft design*; *sustainable aviation*; *hybrid-electric propulsion.*

Contents

List of Figures

List of Tables

List of Abbreviations

Abbreviation	Description
ACARE	Advisory Council for Aviation Research and Innovation in Europe
AEA	Association of European Airlines
AEO	All Engines Operating
Al	Aluminium
ATA	Air Transport Assosiation of America
ATAG	Air Transport Action Group
bat	Battery
BTF	Buy-To-Fly
CFD	Computational Fluid Dynamics
CG	Center of Gravity
CO_2	Carbon Dioxide
CORSIA	Carbon Offsetting and Reduction Scheme for International Aviation
CPI	Consumer Price Index
CSJU	Clean Sky Joint Undertaking
CS2	Clean Sky 2
DAF	Design of Aircraft and Flight technologies research group
DC	Direct Current
DEP	Distributed Electric Propulsion\Propellers
DOE	Design Of Experiments
DTU	Technical University of Denmark
EF	Environmental Footprint
EIS	Entry Into Service
ELICA	ELectric Innovative Commuter Aircraft
EM1	Primary Electric Machine
EM2	Secondary Electric Machine
E-ST	Electric Storage System
ETS	Emissions Trading Scheme
EU	European Union
FC	Fuel Cell
FEA	Finite Element Analysis
FL	Flight Level
FT	Fischer-Tropsch
GaN	Gallium-Nitride
GB1	Primary Gearbox
GENESIS	Gauging the ENvironmEntal Sustainability of electrIc aircraft Systems
GHG	Greenhouse Gas
GT	Gas Turbine
H_2, H2	Hydrogen
H_2O	Water
HC	Hydrocarbon
HEAD	Hybrid-Electric Aircraft Designer
HEFA	Hydro-Processed Esters and Fatty Acids
HHV	Higher Heating Value
HPC	High-Pressure Compressor
HPT	High-Pressure Turbine

Abbreviation	**Description**
IATA	International Air Transport Assosiation
ICAO	International Civil Aviation Organization
ICE	Internal Combustion Engine
IGBT	Insulated-Gate Bipolar Transistor
ISA	International Standard Atmosphere
LCA	Life Cycle Assessment
LCI	Life Cycle Inventory
LCIA	Life Cycle Impact Assessment
LHV	Lower Heating Value
$Li - Air$, $Li - O_2$	Lithium-Air
$Li - Ion$	Lithium-Ion
$Li - S$	Lithium-Sulfur
LMNO	Lithium-Manganese-Nickel Oxide
LPC	Low-Pressure Compressor
LPT	Low-Pressure Turbine
NMC	Nichel-Manganese-Cobalt
No.	Number
NO_x	Nitrogen Oxide
O_2	Oxygen
OEI	One Engine Inoperative
OPR	Overall Pressure Ratio
PAX	Passengers
P1	Primary Propeller
P2	Secondary Propeller
PEM(FC)	Proton Exchange Membrane (Fuel Cell)
pLCA	prospective Life Cycle Analysis
PMAD	Power Management And Distribution
PMSM	Permanent Magnet Synchronous Machine
PREE	Payload-Range Energy Efficiency
PT	Power Turbine
Q.ty	Quantity
RDTE	Research, Development, Test and Evaluation
Ref.	Reference
RPK	Revenue Passenger Kilometer
S1	Primary Shaft
S2	Secondary Shaft
SAF	Sustainable Aviation Fuel
SiC	Silicon-Carbide
SL	Sea Level
SO(FC)	Solid Oxide (Fuel Cell)
SO_2	Sulfur Oxide
SPK	Synthetic Paraffinic Kerosene
SSB	Solid-State Battery
TLAR	Top-Level Aircraft Requirement
TMS	Thermal Management System
TRL	Technology Readiness Level
UNINA	University of Naples “Federico II”
USD	United States Dollar
WP	Work Package

List of Symbols

Symbol	Units	Description
α	°, deg	Angle of attack
α_1	–	Subsystem's share fraction of a primary unit
a	–	Axial induction factor
a_t	–	Tangential induction factor
AC	mol H^+-eq.	Acidification
AR	–	Aspect ratio
β	°, deg	Sideslip angle
β_s	–	Slipstream correction factor
b	m	Span
BFL	m	Balanced field length
c	m	Local chord
C	$	Cost
C-Rate	1/h	Battery C-rate
CAPEX	$/flight	Capital expenditure
CAS	kts, km/h	Calibrated airspeed
Cd	–	2D drag coefficient
CD	–	3D drag coefficient
CD_0	–	3D parasite drag coefficient
Cf	–	Friction coefficient
Cl	–	2D lift coefficient
CL	–	3D lift coefficient
$C\mathcal{L}$	–	3D rolling moment coefficient
Cm	–	2D pitching moment coefficient
CM	–	3D pitching moment coefficient
$C\mathcal{N}$	–	3D yawing moment coefficient
CY	–	3D side force coefficient
δ	°, deg	Deflection angle of a control surface
Δ	–	Variation\Difference
DOC	$/flight	Direct operating cost
D_P	m	Propeller diameter
ε	–	Residual error
η	–	Efficiency
e	–	Oswald factor
E_Cell	Wh	Cell energy
E_bat	kWh	Battery energy
ECOTOX fresh	CTUe	Ecotoxicity (freshwater)
EI	kg/kg, g/kg	Emission Index
EUTRO fresh	kg P-eq.	Freshwater eutrophication
EUTRO marine	kg N-eq.	Marine eutrophication
EUTRO ter	mol N-eq.	Terrestrial eutrophication
φ	–	Shaft power ratio
ϕ	°, deg	Bank angle
Φ	–	Supplied power ratio
f	–	Frequency of occurrence
f_1	–	Fraction of residual primary units (subsystem)

Symbol	Units	Description
f_2	–	Fraction of residual secondary units (subsystem)
F	A s/mol	Faraday's constant
FF	kg/s	Fuel flow
g	m/s^2	Acceleration of gravity
GI	–	Gravimetric index
GWI	kg CO_2-eq.	Global warming potential
H	kW, hp	Heat
HTc	CTUh	Human toxicity (cancer)
HTnc	CTUh	Human toxicity (non-cancer)
i	°, deg	Angle of incidence
I	A	Current intensity
IOC	$/flight	Indirect operating cost
IR	kBq U235-eq.	Ionizing radiation
k	–	Constant\Correction factor
K	–	Matrix element
Λ	°, deg	Sweep angle
l	m	Longitudinal distance from wing's aerodynamic center
L	m	Length
LF	%	Load factor
LU	Point	Land use
m	kg	Mass
mm	g/mol	Molecular mass
M_∞	–	Flight Mach number
MAC	m	Mean aerodynamic chord
MLM	kg, tons	Maximum landing mass
MTOM	kg, tons	Maximum take-off mass
N	–	Number\Quantity
$\mathcal{N}$	N m, kN m	Yawing moment
n_1	–	Number of primary power units (subsystem)
N_1	–	Number of primary power units (system)
n_2	–	Number of secondary power units (subsystem)
OD	kg CFC-11-eq.	Ozone depletion
OPEX	$/flight	Operational expenditure
p	W, kW, hp	Power (subsystem)
P	W, kW, hp	Power
PM	Disease incidence	Particulate matter
POF	kg NMVOC-eq.	Photochemical ozone formation
Q	C	Charge
ρ_∞	kg/m^3	Air density
R	m	Radius
RE	MJ	Resource use (fossils)
Res	Ω	Ohmic resistance
RM	kg Sb-eq.	Resource use (minerals)
RPM	1/min	Revolutions per minute
RV	–	Residual value (fraction)
S	m^2, ft^2	Surface area
SE	Wh/kg, kWh/kg, MJ/kg	Specific energy

Symbol	Units	Description
SFC	kg/(kW h), lb/(hp h)	Specific fuel consumption
SOC	%	State of charge
SP	W/kg, kW/kg	Specific power
t	s	Time
T	N	Thrust
TAS	kts, km/h	True airspeed
TOC	$/flight	Total operating cost
TOFL	m	Take-off field length
$\overline{V}$	–	Volumetric ratio
V	V	Voltage
V_∞	m/s	Flight speed
V_0	V	Open-circuit voltage
V_{MC}	m/s	Minimum control speed
$V_{\text{Stall,1}}$	m/s	Stall speed at maximum take-off weight
W	N, lb	Weight
WU	m^3-world-eq.	Water use
x, X	m	X-coordinate \Distance along X-axis
X_{P}	m	Propeller disk's distance from leading edge
y, Y	m	Y-coordinate \Distance along Y-axis
z, Z	m	Z-coordinate \Distance along Z-axis

Subscript/Superscript	Description
$(\cdot)_a$	Aileron
$(\cdot)^{\text{Apex}}$	Surface's apex point
$(\cdot)_{\text{Av.}}$	Available
$(\cdot)_\beta$	Derivative with respect to the sideslip angle
$(\cdot)_{\text{c/2}}$	At half of the local chord
$(\cdot)_{\text{c/4}}$	At one-quarter of the local chord
$(\cdot)_{\delta_a}$	Derivative with respect to the aileron deflection angle
$(\cdot)_{\delta_r}$	Derivative with respect to the rudder deflection angle
$(\cdot)_{\text{e}}$	Electron
$(\cdot)_{\text{E}}$	Empty
$(\cdot)_{\text{E-ST}}$	Electric storage
$(\cdot)_{\text{E-ST1}}$	First-type electric storage
$(\cdot)_{\text{E-ST2}}$	Second-type electric storage
$(\cdot)_{\text{EE1}}$	Electricity from first-type electric storage
$(\cdot)_{\text{EE2}}$	Electricity from second-type electric storage
$(\cdot)_{\text{Element}}$	Generic (powerplant) component
$(\cdot)_{\text{EM1}}$	Primary electric machine
$(\cdot)_{\text{EM2}}$	Secondary electric machine
$(\cdot)_{\text{EM3}}$	Tertiary electric machine
$(\cdot)_{\text{Eng}}$	Related to the propulsive system
$(\cdot)_{\text{ETS}}$	Emissions Trading Scheme
$(\cdot)_{\text{f}}$	Fuselage
$(\cdot)_{\text{Failed}}$	Failed unit
$(\cdot)_{\text{FC}}$	Fuel cell
$(\cdot)_{\text{Flights, Year}}$	Flights per year
$(\cdot)_{\text{Fuel}}$	Fuel
$(\cdot)_{\text{Fuel, FC}}$	Fuel for fuel cells

Subscript/Superscript	Description
$(\cdot)_{\text{Fuel, GT1}}$	Fuel for first-type gas turbines
$(\cdot)_{\text{Fuel, GT2}}$	Fuel for second-type gas turbines
$(\cdot)_{\text{GB}}$	Gearbox
$(\cdot)_{\text{GB1}}$	Primary gearbox
$(\cdot)_{\text{GB2}}$	Secondary gearbox
$(\cdot)_{\text{GB3}}$	Tertiary gearbox
$(\cdot)_{\text{GT}}$	Gas turbine
$(\cdot)_{\text{GT1}}$	First-type gas turbine
$(\cdot)_{\text{GT2}}$	Second-type gas turbine
$(\cdot)_{\text{h}}$	Horizontal tail
$(\cdot)_{\text{H2}}$	Hydrogen
$(\cdot)_{\text{H2, Cell}}$	Hydrogen supplying one fuel cell
$(\cdot)_{\text{i}}$	Positional index
$(\cdot)_{\text{i}\neq\text{Failed}}$	Residual (not failed) unit
$(\cdot)_{\text{In, Element}}$	Input to a powertrain component
$(\cdot)_{\text{j}}$	Positional index
$(\cdot)_{\text{Max}}$	Maximum
$(\cdot)_{\text{ME}}$	Manufacturer empty
$(\cdot)_{\text{Min}}$	Minimum
$(\cdot)_{\text{Nec.}}$	Necessary
$(\cdot)_{\text{OE}}$	Operating empty
$(\cdot)_{\text{OFF, E-ST1}}$	Offtakes from first-type electric storages
$(\cdot)_{\text{OFF, E-ST2}}$	Offtakes from second-type electric storages
$(\cdot)_{\text{OFF, FC}}$	Offtakes from fuel cells
$(\cdot)_{\text{OFF, GT1}}$	Offtakes from first-type gas turbines
$(\cdot)_{\text{OFF, GT2}}$	Offtakes from second-type gas turbines
$(\cdot)_{\text{OFF, PMAD}}$	Offtakes from power management and distribution system
$(\cdot)_{\text{Out, Element}}$	Output from a powertrain component
$(\cdot)_{\text{P}}$	Total propulsive
$(\cdot)_{\text{P1}}$	Primary propulsive
$(\cdot)_{\text{P2}}$	Secondary propulsive
$(\cdot)_{\text{P3}}$	Tertiary propulsive
$(\cdot)_{\text{P,i}}$	Generic propeller
$(\cdot)_{\text{PMAD}}$	Power management and distribution system
$(\cdot)_{\text{Pollutant}}$	Pollutant species
$(\cdot)_{r}$	Rudder
$(\cdot)_{\text{S1}}$	Primary shaft
$(\cdot)_{\text{S2}}$	Secondary shaft
$(\cdot)_{\text{S3}}$	Tertiary shaft
$(\cdot)_{\text{S,i}}$	Generic shaft
$(\cdot)_{\text{Shaft, j}}$	Generic shaft
$(\cdot)_{\text{Shaft, Total}}$	Total shaft
$(\cdot)_{\text{Sound}}$	Sound
$(\cdot)_{\text{Source, i}}$	Generic energy source
$(\cdot)_{\text{Source, Total}}$	Total from energy sources
$(\cdot)_{\text{Supplied}}$	Total supplied
$(\cdot)_{\text{Tank, H2}}$	Hydrogen tank
$(\cdot)_{\text{v}}$	Vertical tail
$(\cdot)_{\text{w}}$	Wing

1 Introduction

Contents

1.1 Research Motivation

In an age where embracing sustainable innovation is imperative rather than optional, aviation stands on the cusp of a substantial paradigm shift. The aviation industry, historically lauded for its contributions to global connectivity and economic growth, now faces unprecedented challenges in the context of environmental sustainability. The escalating concerns regarding climate change, coupled with the increasing demand for air travel, necessitate a transformative approach in aircraft design and operation. The integration of hybrid-electric and hydrogen-based propulsion systems in regional aircraft design is a promising stride toward reducing aviation's environmental footprint. These cutting-edge technologies are pivotal in the quest for sustainable aviation, but their true potential can only be unlocked through comprehensive and holistic considerations. The scope of this transformation extends beyond mere technological advancements; it calls for a fundamental rethinking of the principles that govern the preliminary stages of aircraft design. Preliminary aircraft designers, who play a pivotal role in shaping the future of aviation, are uniquely positioned to influence the industry's trajectory toward sustainability. Their decisions in the design phase can significantly impact an aircraft's environmental footprint throughout its life cycle, from manufacturing to operation and eventual decommissioning. This expanded scope of considerations presents a unique set of challenges and opportunities for designers, urging them to innovate in ways that harmonize technological advancement with environmental stewardship.

This thesis aims to explore the multi-faceted challenges and opportunities that lie in integrating sustainability into the heart of aircraft design. By improving existing design methodologies and examining emerging technologies and trends, the study

seeks to understand the current landscape of regional aviation and its potential for sustainable evolution. Furthermore, it delves into the role of preliminary aircraft designers, investigating how their work can be aligned with the broader goals of environmental responsibility and sustainable development. In this sense, the need emerges for an integrated approach to aircraft design that prospectively considers the environmental and economic impacts at every stage of the aircraft's life. In light of these considerations, it is legitimate to ask:

How can preliminary aircraft designers support the transition to a future sustainable regional aviation, with a specific focus on hybrid-electric and hydrogen-based technologies, while including life-cycle considerations?

By addressing this multifaceted question, the thesis aspires to bridge the gap between innovative sustainable technologies and their practical application in aircraft design. It encompasses the study of advanced propulsion technologies and the environmental and economic implications of their adoption at the aircraft level. The research aims to offer insights into how preliminary aircraft design processes can be improved to harness the full potential of hybrid-electric and hydrogen-based technologies, thereby contributing to a sustainable future for regional aviation. Moreover, it seeks to provide a roadmap for preliminary aircraft designers, policymakers, and industry stakeholders, focusing on creating a sustainable future for regional aviation that aligns with global environmental ambitions. The research question will be particularized in the next section, where an overview of the international context will be offered. The state-of-the-art studies on hybrid-electric regional aircraft will be explored as well, appropriately locating the motivation of the present work. Finally, the document's structure will be introduced to the reader, illustrating the role of each chapter in addressing the purpose of this dissertation.

1.2 State of the Art

1.2.1 International Context

Over the last thirty years, environmental concerns have become the primary focus in numerous national and international discussions, prompting the need for urgent resolutions to mitigate the adverse effects of human activities on the natural world. The enhanced living standards achieved in Western nations since World War II, coupled with the economic surge of emerging countries like China, India, and Brazil, have significantly altered our ecosystem. Human activities have released substantial amounts of greenhouse gases (GHGs), notably carbon dioxide (CO_2), into the atmosphere, resulting in an average global temperature rise of 1.2 °C above pre-industrial levels. As illustrated in Fig. 1.1, this temperature increase is projected to reach 1.5 °C by 2034 if current trends continue. The Paris Agreement [1] set this value as the upper limit, as exceeding it could trigger more frequent and severe natural disasters, profoundly affecting our lives and habits.

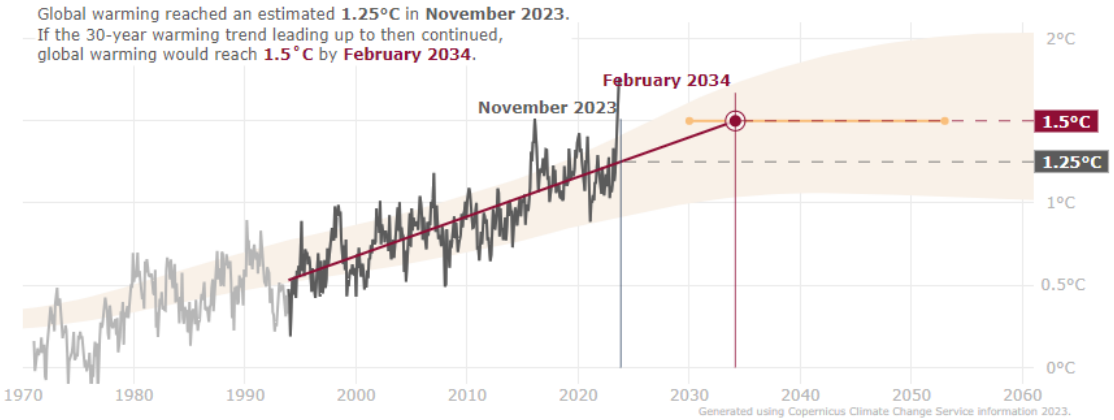

Figure 1.1: Future projections on global warming with respect to pre-industrial levels. The yellow area represents the uncertainty of the estimated 30-year average and of future climate projections. The orange line locates the 1.5 °C upper limit set out in the Paris agreement [1]. The plot has been obtained via the Global Temperature Trend Monitor by the Copernicus Climate Change Service [2].

The global civil aviation industry, like many other transportation sectors, is under increasing pressure to diminish its environmental footprint. Aviation is responsible for above 2% of annual global anthropogenic GHG emissions and about 12% of all transport emissions [3, 4]. Aircraft engines emit not just CO_2 but also a range of other gases and pollutants, including nitrogen oxides (NO_x), unburned hydrocarbons (HC), sulfur oxides (SO_x), water vapor (H_2O), and soot. These additional emissions exacerbate aviation's impact on global warming by contributing to the formation of contrail cirrus, ozone depletion, aerosol-radiation, and cloud interactions. Although the contribution of aviation to global GHG emissions may appear modest, the sector's rapid growth in recent decades makes it significant. As noted by Grewe et al. [5], there has been a consistent increase in both the total number of flights and passenger load factors. Before the COVID-19 pandemic, Airbus and Boeing forecasted average annual growths of 4.4% and 4.6% in revenue passenger kilometers (RPKs) for the coming decades, respectively [5]. Even considering the pandemic's impact, the aviation sector is expected to continue contributing significantly to global warming in the future [5], which underscores the importance of focusing on aviation to reduce its overall impact on climate change.

In a world where unsustainable production and consumption patterns increasingly harm human health, ecosystems, and natural resources, it is the responsibility of policymakers to guide aviation toward environmental sustainability. The aviation sector, in particular, is expected to contribute significantly to reducing transport emissions. This includes integrating market-based measures, operational improvements, and technological advancements. Committed to achieving climate neutrality by 2050, the European Union (EU) is currently implementing a variety of measures, including encouraging the development of sustainable aviation fuels (SAFs) and more efficient aircraft designs as well as revising the Emissions Trading System (ETS) [6, 7]. With a broader scope that covers multiple sectors and not just aviation, the EU's

ETS was launched in 2005 to combat climate change [7]. The system incentivizes companies to reduce their emissions and invest in cleaner technologies through the economic principle of supply and demand. A cap is set on the total amount of certain GHGs that can be emitted by installations covered by the system. Within this cap, companies receive or buy emission allowances, which they can trade with one another as needed. One allowance equals one ton of CO_2 or the equivalent amount of another GHG (CO_2-eq.). As the cap on emissions decreases over time, the overall emissions from sectors covered by the system are reduced. In 2016, with a major focus on the aviation sector, the International Civil Aviation Organization (ICAO) developed the CORSIA (Carbon Offsetting and Reduction Scheme for International Aviation) program to address GHG emissions produced by international aviation [8]. CORSIA runs on a voluntary basis from 2021 to 2026, becoming mandatory in 2027 for most countries. Its main objective is to stabilize CO_2 emissions at the 2020 level through the use of offsets and alternative energy sources. Airline operators that emit above a certain threshold of CO_2 must offset their emissions that exceed 2020 levels by purchasing carbon credits, which can arise from a variety of projects around the world for emissions reduction, such as renewable energy development or reforestation. This scheme is part of a broader ICAO effort to make aviation more sustainable, which also includes technological improvements, more efficient aviation fuels, and optimized flight routes to reduce fuel consumption and emissions.

The EU has soon accepted the commitment entrusted by ICAO. In this sense, the ICAO agenda for future sustainable aviation has been implemented in the EU by the Advisory Council for Aviation Research and Innovation in Europe (ACARE) [6]. In 2001, the ACARE outlined a 2020 vision for the European air transport system, setting ambitious environmental targets in its Strategic Research Agenda. These targets aimed for new aircraft designs to achieve a 50% reduction in CO_2 emissions, an 80% reduction in NO_x emissions, and a 50% decrease in perceived noise by 2020, relative to the top-performing aircraft models of 2000 [9]. In 2008, industry leaders convened at the Air Transport Action Group (ATAG)'s Aviation & Environment Summit, where they endorsed a strategic vision for the sustainable development of aviation by signing the Commitment to Action on Climate Change. The agenda included an average improvement in fuel efficiency of 1.5% per year from 2009 to 2020, a cap on net aviation CO_2 emissions from 2020, and a reduction in net CO_2 emissions of 50% by 2050 with respect to 2005 levels [10]. Also in 2008, the Clean Sky Joint Undertaking (CSJU), a collaboration between the European Commission and the European aerospace industry, launched the Clean Sky Program [11]. This initiative aimed to meet the ambitious goals set by ACARE in 2001, enhancing the competitiveness of the European aircraft industry globally. Following the success of its predecessor, the Clean Sky 2 (CS2) Programme was launched in 2014 [12] and will end in 2024, targeting a significant acceleration towards eco-friendlier aviation in the 2025-2035 timeframe. This has involved integrating, demonstrating, and validating new aircraft technologies to cut CO_2, NO_x, and noise emissions by 20 to 30% compared to 2014's state-of-the-art aircraft. These efforts aligned with ACARE's 2012 updated Strategic Research and Innovation Agenda, which set new and more

ambitious targets, including a reduction of CO_2 emissions by 75%, NO_x by 90%, and noise by 65% by 2050, relative to 2000 levels [13, 14]. Remarkably, funded projects under the CS2 program included the GENESIS [15], ELICA [16], IRON [17] projects, focused on quantifying the potential benefits brought by innovative technologies on small-medium range regional aircraft. In 2021, the CSJU evolved into the Clean Aviation Joint Undertaking. Building on the success of its predecessors, it will accelerate the achievement of carbon neutrality by 2050 by exploring cutting-edge technologies for regional and short-medium-range commercial aircraft. Founded on a consortium of 48 partners, the HERA project [18] fits into this context, exploiting distributed propulsion, batteries, and hydrogen-based systems to reduce regional and short-range air mobility emissions by 90%. The latest revision of the ACARE's agenda occurred in 2022, following the European Commission's introduction of the "Fit for 55" package targeting a 55% decrease in GHG emissions by 2030 [19, 20]. The vision underlying the current ACARE's agenda ("Fly the Green Deal") aligns with the Green Deal of the European Commission and extends beyond research to include new product development, energy, fuel, infrastructures, digitalization, and the implementation framework [6, 20]. In the context of regional aviation, the goals set by the ACARE agenda can be summarized in points as follows [6]:

- By 2030, net CO_2 emissions from all intra-EU flights and those departing the EU will be reduced by 55% compared to a 1990 baseline; moreover, non-CO_2 climate effects will be fully understood, managed, monitored, and reduction targets will be set in line with the latest scientific understanding and mitigation solutions.
- By 2035, new technologies, fuels, and operational procedures in service will result in a 30% reduction of non-CO_2 climate effects of all intra-EU flights and those departing the EU relative to a 1990 baseline.
- By 2050, net-zero CO_2 emissions will be achieved for all intra-EU flights and those departing the EU; moreover, new technologies and operational procedures in service will result in a 90% reduction in NO_x, non-volatile particulate matter, and warming contrail cirrus from all intra-EU flights and those departing the EU relative to the year 2000.

The aviation sector's efforts to pursue this sustainability roadmap include the development and adoption of new technologies, such as hybrid-electric architectures, and the use of alternative fuels, such as biofuels or hydrogen (H_2). It is also working to improve operational efficiency through advanced air traffic management and the design of more aerodynamic aircraft. The ultimate goal is to achieve a zero-impact aviation industry, in line with the global objectives of sustainability and reduction of climate change. The International Air Transport Association (IATA), in collaboration with the German Aerospace Center, proposed a technology roadmap for 2050, outlining potential technologies for achieving ACARE's goals [21]. These technologies were categorized based on their technology readiness level (TRL), with revolutionary designs like blended wing-body aircraft and hybrid-electric propulsion earmarked for the long-term (2035-2050), while more immediate advancements (2015-2035) focused on evolutionary airframe and engine technologies (Fig. 1.2). In

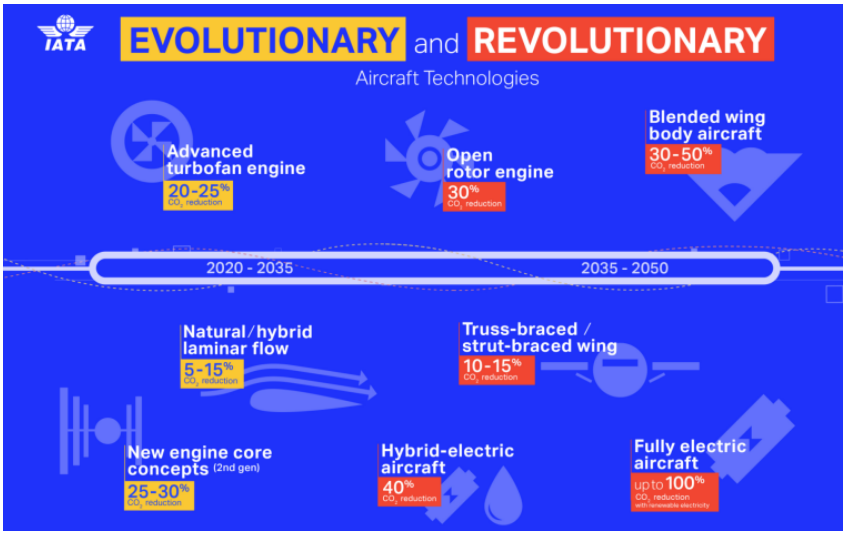

Figure 1.2: IATA infographic on evolutionary and revolutionary aircraft technologies [21].

2023, IATA further updated its environmental roadmap to align with the net-zero emissions target [22]. The new roadmap identifies a short-term solution in the use of 100% SAF blends, while waiting for batteries and hydrogen propulsion systems to mature and be tested with a view to long-term full-electric solutions.

The roadmap proposed by IATA identifies regional aircraft as the ideal testbed for new propulsion technologies [22]. Due to their smaller size and shorter route profiles, regional turboprop airplanes are ideally suited for integrating and evaluating cutting-edge technologies that might be too complex and risky for initial implementation in larger, long-haul aircraft [22, 23]. The introduction of hybrid-electric or hydrogen-based regional aircraft within the next decades will increase the experience connected to the integration of new technologies and new ground handling challenges, laying the foundation for the entry into service of larger aircraft. The development of these technologies in regional aircraft not only paves the way for scalability to larger fleets but also aligns with global decarbonization efforts. Despite contributing less than 10% to the aviation sector's overall emissions, regional aircraft exhibit the highest carbon intensity per RPK [24]. In 2019, CO_2 emissions per RPK from these smaller aircraft on short-haul flights were 80% higher compared to the average across all classes, including narrow and wide-body jets [24]. The growing regional market underscores the urgency of enhancing efficiency for this class. With over 34% world airports relying exclusively on regional turboprop aircraft, these aircraft are indispensable for connecting communities globally [23]. Beyond mere transport, regional aviation is pivotal for economic progress, facilitating the rapid establishment of tourism and business connections between smaller cities, thus integrating them into the global economy. In conclusion, the journey toward sustainable future aviation begins from the regional class, depending on the combined effort of policymakers, aviation stakeholders, and researchers in correctly selecting and implementing the most promising technologies.

1.2.2 Hybrid-Electric Aircraft Studies

First Steps Towards Hybrid-Electric Solution

The exploration of hybrid-electric technologies for regional aircraft has been a subject of intense study in recent years. These studies have focused on integrating electric propulsion systems with conventional aircraft engines, aiming to create a more efficient and environmentally friendly mode of air travel. The research especially focuses on understanding the basic feasibility and potential benefits of hybrid-electric systems, ranging from reduced carbon emissions to enabled possibilities for improving aircraft performance. Several projects and collaborations are emerging in this field, bringing together expertise from academia, industry, and regulatory bodies, which reflects the European and global desire to accelerate the decarbonization of the sector. The studies have differed significantly in both the adopted approaches and the results. A significant factor contributing to this divergence in conclusions is the variety of high-level assumptions and requirements that guide each project. More crucially, the outcomes are also heavily influenced by the assumptions about the future performance levels of the innovative technologies considered. Different hypotheses on battery energy density, electric motor efficiency, and other key technological parameters can dramatically alter the estimated advantages of hybrid-electric aircraft concepts.

A critical review of some of the most remarkable examples of hybrid-electric regional aircraft designs has been recently offered by Abu Salem et al. [25]. Among these, de Vries et al [26] present a detailed sizing methodology for the conceptual design of hybrid-electric aircraft, with a focus on a regional aircraft featuring leading-edge distributed propulsion. The study uses the top-level aircraft requirements (TLARs) of the ATR 72-600 regional aircraft as a benchmark, with a payload of 7 500 kg and a design range of about 825 nmi, and assumes a battery's specific energy of 500 Wh/kg. However, the numerical outcomes suggest limited promise for the hybrid solutions explored. Due to the long design range considered, the adoption of turbo-electric architecture leads to no significant fuel reduction; a serial architecture behaves even worse, with a 26.5% increase in maximum take-off mass (MTOM) and a 39.1% increase in fuel mass.

In the work of Voskuijl et al. [27], a hybrid-electric regional aircraft is designed based again on the ATR 72-600 and using a parallel propulsion system. The design maintains a constant power split between thermal engines and batteries throughout the flight, including diversion and loiter stages. However, this strategy results in carrying extra battery weight, impacting the aircraft's standard operations efficiency [25]. The study assumes a specific energy of 1 000 Wh/kg, leading to a 28% reduction in mission fuel mass and a 14% increase in MTOM. The work of Voskuijl et al. also includes a sensitivity analysis on the specific energy and supplied power ratio, underlying the predominant impact of these assumptions on the final results [27].

Similar considerations are made in the work of Antcliff et al. [28], where the ATR 42-500 is used as the reference baseline. The study examines different degrees of hybridization based on the electric motor's shaft power fraction. Interestingly, a

higher degree of hybridization increases the MTOM and the total energy required for the flight, but does not proportionally increase the mass of energy sources, due to enhanced efficiency associated with parallel hybrid-electric powertrain.

Finger et al. [29] compare different hybrid-electric powertrain architectures using current technology standards, specifically a battery specific energy of 200 Wh/kg. In this study a different approach is used, considering a fixed baseline conventional aircraft (similar again to the ATR72) with the original MTOM serving as an upper limit. Under these hypotheses, the full-electric architecture is deemed unfeasible for a design range of 270 nmi, while a parallel architecture is identified as the most promising solution with advantages up to -20% in fuel consumption [29].

Overall, the results of preliminary studies suggest that fuel burn reductions are quite limited for battery technology levels realistically achievable in the coming years. This has led to the need to explore even more disruptive solutions, targeting the complete decarbonization of aviation. A promising solution in this sense is represented by using hydrogen as an alternative fuel. In particular, when coupled with fuel cell (FC) systems, hydrogen would emit exclusively water vapor as a waste product. Palladino et al. [30] propose a study on an aircraft similar to the ATR 72, hybridized to combine thermal engines in parallel with FC systems based on liquid hydrogen. Once again, the MTOM of the conventional baseline is assumed as an upper threshold, thus limiting the obtainable degree of hybridization. The model used considers the additional mass penalties of tanks, FCs, and cooling systems. By also considering the effects of the production and distribution of hydrogen in the calculation of emissions, the best solution found by the study sees a reduction of 24% CO_2 and 40% in NO_x for a 200 nmi mission [30].

An alternative solution consists of the complete electrification of the aircraft based on batteries and hydrogen FC systems. In this sense, Eissele et al. [31] have demonstrated the feasibility of this concept for a 50-passenger regional aircraft assuming technological levels for an entry into service (EIS) year 2040, with even an estimated possibility of reducing direct operating costs (DOCs) compared to a conventional platform.

In summary, the major sensitivity of results with respect to technological levels highlights the need for robust technology assumptions, especially when the purpose is to try to anticipate the realistic benefits of innovative technologies in a specific time horizon. As discussed, the adoption of different approaches to design also influenced the diversity of conclusions of past studies, underlining the need for a refined and general design workflow.

Tools for Hybrid-Electric Aircraft Design

Aircraft design is an intricate and multifaceted process that requires a harmonious blend of engineering, creativity, and innovation. It encompasses a variety of factors, including aerodynamics, propulsion systems, structural integrity, safety measures, and environmental considerations, thereby mandating a comprehensive and holistic approach. The conceptual and preliminary design of a new aircraft has long been

guided by classical methodologies, refined over decades to optimize conventional aircraft [32–43]. These established techniques have successfully supported the evolution of aviation. As a matter of fact, proprietary or commercially available programs or design environments, such as FLOPS (FLight OPtimization System) [44], APP (Aircraft Performance Program) [45], and Piano [46], rely on these conventional approaches.

However, the advent of unconventional hybrid-electric aircraft is challenging such consolidated methods. Traditional design tools, while effective for conventional aircraft, struggle to encapsulate the complexities of hybrid-electric systems. These systems introduce new variables, such as alternative energy sources, electric propulsion integration, and energy management, which significantly alter the aircraft's performance characteristics. Therefore, design methodologies should be adapted to consider alternative and multiple energy sources, and to correctly account for new mass penalties that affect the feasibility and performance of the aircraft. Typically, the preliminary aircraft design for conventional aircraft configurations is based on evaluating the fuel necessary for the mission through the Breguet range equation, from which the MTOM of the aircraft is estimated with an iterative approach. One recent strategy has consisted of the attempt to generalize the range equation to the case of hybrid-electric aircraft [47, 48]. However, this approach is limited by the variety of hybrid-electric technologies and configurations that can be considered, leading to the need to customize a new equation for each variant. To add further complexity to the scenario, pioneering projects like NASA's X-57 have brought to light the significant benefits of aero-propulsive interactions offered by distributed electric propulsion (DEP) systems, particularly when used in synergy with electric or hybrid powertrains [49–52]. These considerations underscore the necessity for a rethinking of preliminary aircraft design approaches, to generalize the available methodologies and keep up with the rapid and necessary innovation of the aeronautical sector.

In recent years, significant advances have been made in this direction, largely in the context of academic and specialized research. Preliminary design tools have been developed, reflecting a concerted effort to adapt and extend traditional design principles to meet the specific challenges posed by hybrid-electric aviation. An example is represented by THEA-CODE, a MATLAB® tool for the conceptual design of hybrid-electric aircraft recently developed and presented by researchers from the University of Pisa [25, 53]. The tool, which is suitable even for unconventional configurations such as box-wing aircraft, generalizes conventional sizing methodologies, followed by a mission performance analysis. However, the tool does not include a model for distributed electric propulsion capable of capturing interactions between propellers and lifting surfaces [53]. Furthermore, the mathematical modeling of the powertrain seems to be limited to classic hybrid architectures based on thermal engines and batteries, such as serial and parallel schemes [53].

Elsewhere, efforts have been made to extend the functionality of already available tools to include hybrid-electric propulsion architectures. A first example is offered by MICADO (an acronym for Multidisciplinary Integrated Conceptual Aircraft

Design and Optimization environment), a software developed at the Institute of Aerospace Systems of RWTH Aachen University [54]. The software was originally tailored for conventional turboprop, turbojet, and turbofan systems, basing the design process on component sizing followed by a detailed mission analysis. Since 2016, the software has been extended to enable the design and evaluation of electric propulsion systems, including batteries and aero-propulsive effects. However, the model-based approach adopted appears to make it complex to generalize the software further to include multiple and diverse propulsion sources [54].

The commercial software PACELAB APD, developed by PACE Aerospace, fits similarly in this context [55], offering the possibility to simulate and analyze various design configurations accurately, and allowing engineers to explore a wide range of hybrid-electric propulsion systems. The software's robust modeling capabilities facilitate the integration of electric components within traditional aircraft systems, ensuring a comprehensive design process. However, its reliance on pre-existing data and models can restrict innovation in uncharted areas of hybrid-electric aircraft design. Additionally, the complexity and specialized nature of the software require significant training and expertise, potentially limiting its accessibility and not being practical for preliminary design applications.

Researchers at the University of Stuttgart [56, 57] recently tried to generalize SUAVE, an open-source tool for preliminary aircraft design that includes common handbook methods [58]. The tool, equipped with a solver for mission analysis, allows for an iterative design of the aircraft using detailed models of the powertrain components that characterize their efficiency during the mission [58]. In this way, the tool allows for increased levels of fidelity of the results, compared to more classic sizing approaches based on the Breguet range equation. Although SUAVE offers a flexible and modular definition of the propulsion architecture, the existence of potentially unlimited possible energy networks, once again, makes it challenging to integrate them into the design tool in a single and general form. For example, the characterization of hydrogen fuel cell systems as the primary energy source has yet to be addressed [56, 57].

In the vast landscape of possibilities that technological innovation offers, it is necessary to have a general but simple modeling of the propulsion system, capable of degenerating into a multitude of specific cases and allowing for wide preliminary investigations at the preliminary design level. Some important progress in this sense has been made by researchers from TU Delft [26, 27, 59, 60], who introduced a mathematical description of the hybrid-electric powerplant based on systems of linear algebraic equations. The proposed model describes a series/parallel partial hybrid architecture that can also degenerate into simpler configurations, such as conventional, all-electric, parallel, and serial [26]. However, their approach presents room for improvement, being still quite limited in the nature and number of energy sources (in particular, hydrogen-based propulsion systems are not contemplated), as well as coupled with simplistic methods for estimating aircraft masses.

In light of the previous considerations, the research question introduced in Section 1.1 leads to the need for a flexible and general design workflow, representing

a compromise between accuracy and ease of use, and which is well-suited to the variety of concepts at the frontier of innovation:

How can traditional preliminary design methodologies be generalized and adapted into a flexible, multidisciplinary workflow to address the diversity of hybrid-electric propulsion architectures in regional aircraft?

To reflect the needs of designers engaged in the search for innovative solutions, the following characteristics are desirable for a preliminary design tool:

- It should be *simple* to use, in view of the typical lack of information available to the aircraft designer in the preliminary stages of the aircraft design process. This is even more true when seeking innovative solutions, where there is also a scarcity of data coming from statistics.
- At the same time, it should be *accurate* enough not to risk focusing on the direct advantages of innovative technologies without grasping side effects at the aircraft level that could diminish or cancel the promised benefits. In this sense, an approach based on mission analysis is preferable to considerations based exclusively on the evaluation of point performance.
- It should be *quick*, in order to allow for extensive exploratory studies aimed at analyzing and optimizing a large number of possible solutions in a reasonable time.
- It should be based on *general* methodologies, valid for both conventional and alternative powertrain configurations. This is crucial for a correct assessment of the advantages and disadvantages associated with innovative technologies, providing intrinsically consistent results.
- It should be *flexible*, based on a modular framework that facilitates the adaptation and integration of various components and systems. This is fundamental in order to keep up with research, supporting a broad spectrum of hybrid-electric aircraft designs and, more generally, innovative solutions. In addition, to facilitate collaborative design, it is desirable that the tool structure is open enough to allow for the integration of external contributions (e.g., surrogate models).
- It should feature *comprehensive* simulation capabilities, reflecting the multidisciplinary nature of the problem. It needs simulation methodologies for accurate modeling of aerodynamic, propulsive, and inertial characteristics, including also possible interdependencies of one on the other (e.g., aero-propulsive effects). Moreover, it should incorporate the assessment of sustainability and economic metrics, which are essential for evaluating the long-term viability of the designed concepts.

In this context, the DAF research group of the University of Naples "Federico II" (UNINA) has contributed to this research need with the development of novel design workflows for hybrid-electric aircraft, which will be presented in Chapter 2. The presented methodologies further develop the approach originally proposed by de Vries et al. [26], combining it with more accurate and general methods for mass estimation and with an approach focused on mission and performance analysis.

Life-cycle considerations in preliminary design

The aviation industry's environmental footprint extends beyond its direct emissions during flight operations, encompassing various ancillary systems such

as airports, fuel production, and the broader aircraft life cycle, which includes production and end-of-life. Issues such as the use of scarce metals (e.g., cobalt or chromium) and the toxicity impacts of released chemicals also contribute to potential harm to human health, biodiversity, and resource depletion [61]. As the demand for air travel increases, there is a pressing need for a robust framework that not only measures these environmental challenges but also guides design solutions for environmentally sustainable growth in the air transport sector. In this sense, life cycle assessment (LCA) offers a comprehensive approach to evaluate the environmental and health impacts associated with all stages of a product or service's life, from material extraction to manufacturing, usage, and final disposal or recycling. This iterative, ISO-standardized [62, 63] process starts from the goal and scope definition, passes through the construction of a life cycle inventory (LCI) that describes the system, and culminates in a life cycle impact assessment (LCIA) and the interpretation of the results.

Several review studies have explored the aviation sector's environmental concerns and the effectiveness of LCA in addressing them [64–67]. However, these studies tend to have a narrow focus and carry important limitations in scoping the aviation sector, either providing a limited perspective or lacking a comprehensive impact assessment. Some research, such as the study of Calisir et al. [64], has delved into the life cycle impacts of aircraft and their components, focusing predominantly on carbon footprints and often overlooking other environmental impacts or alternative fuel and propulsion options. Other studies focused on the carbon footprint of traditional and non-traditional aviation fuels, but disregarding other environmental impacts, and overlooking some significant types of fuel and propulsion methods like liquid hydrogen and battery systems [65, 66]. Greer et al. examined sustainability metrics and methods applicable to airport operations, but neglected the potential impact of on-ground aircraft operations [67]. Sector-scale research studies, like the ones of Facanha et al. [68] and Chester et al. [69], compared different modes of transport quantifying and inventorying specific emissions, including GHGs, NO_x, SO_x, and particulate matter (PM), pinpointed as the main contributors to life-cycle impact. These studies, although restricting the analysis to only evaluating climate change impacts, provided a first perspective of the most influential contributors to total life cycle emissions, with direct emissions from fuel combustion being the main driver, followed by fuel production [68, 69]. Other studies using process-based approaches found that the contribution of aircraft manufacturing to the sector's GHG emissions was between 1% and 3% [70, 71].

Additional LCA studies have been performed at the level of the whole aircraft, or at the level of specific technologies and components. Some of them consist of cradle-to-grave LCA studies addressing a specific aircraft model or a specific fleet [72–76]. For instance, Lopes performed an environmental impact assessment of the Airbus A330-200 aircraft gathering the necessary data from aircraft flight manuals [74]. Johanning and Scholz addressed the entire life cycle of the A320-200, also introducing the effect of altitude-dependent emissions of NO_x and contrails generated by jet

engines during cruise [75, 76]. Other studies only focused on material extraction and production of parts possibly used for aircraft manufacturing [77–80].

Data accessibility poses a significant obstacle as well. In their comprehensive literature review, Keizer et al. scrutinized the data sources employed in aviation-related LCA studies, pointing out that 64% of researchers rely on literature data, and 47% utilize the Ecoinvent electronic database for their analyses [81]. In this sense, the active involvement of aerospace companies in enhancing the availability of data becomes crucial. While Airbus demonstrates a commitment to sustainability by annually publishing reports detailing the environmental impact of its operations [82], this level of transparency is not uniformly adopted across the major entities in the aerospace industry. The picture is further complicated when emerging technologies are considered, requiring the inclusion of a prospective dimension in life-cycle considerations. In this sense, Rupcic et al. offer a comprehensive review of existing LCA studies on potential alternative propulsion systems for aviation [61]. The scope of the review ranges from studies that analyze the environmental impacts of different batteries and drop-in fuels to preliminary studies that compare their potential impacts at the system level. The authors conclude that prospective life cycle analysis (pLCA) studies are needed to reliably assess the environmental impacts of future hybrid-electric regional aircraft, integrating technology foresight for the innovative technologies and their projected energy densities to match aircraft's TLARs. In this sense, the role of the preliminary designer becomes fundamental again. The designer has the responsibility of predicting the potential advantages that enabling technologies offer, as well as their effects at the aircraft design level. The identification of the best technologies cannot be based exclusively on the impact at the aircraft level, regardless of life-cycle considerations. Rather, a holistic evaluation becomes necessary that covers the full spectrum of potential environmental impacts associated with innovative aircraft solutions.

Although some first steps for the integration of LCA considerations at the design level have already been taken by Johanning et al. [83, 84], further efforts are needed to cover the wide spectrum of aircraft classes and technologies employed. For instance, the simplified LCA-AD tool proposed by Johanning [84] starts from a fixed LCI database tailored for aircraft similar to the Airbus narrowbody and widebody families. The method was taken up by Kossarev et al. [85] for a comparative analysis of different solutions with an EIS 2040 based on alternative fuels (kerosene, biofuel, and hydrogen) to evaluate their life-cycle impacts and operative costs. However, once again, the scope of the analysis was on larger airplanes rather than on regional turboprop aircraft, on which this dissertation intends to focus. To the author's knowledge, no equally detailed studies are available in the literature in relation to small or medium-sized regional turboprop aircraft. Therefore, the need emerges for the integration of pLCA considerations at the early stages of the design of a new regional aircraft, which can guide involved stakeholders in the decision-making process. In Chapter 4 of this dissertation, an extensive preliminary design study will be proposed, which seeks to contribute to this research need. The study has been carried out in collaboration with numerous experts in the emerging and most

promising aviation technologies, allowing technology foresight to be combined with aircraft-level considerations. Several future scenarios will be presented, using a 50-passenger regional aircraft as a reference platform. In light of all the previous considerations, the study will address the following more specific research questions:

How can integrating life-cycle and cost considerations into the preliminary design of a 50-passenger regional aircraft, with either conventional or hybrid-electric architecture, assess the real impacts of the most promising technologies over time? How can this study inform the development of an environmental database and provide actionable recommendations for technology selection to policymakers, aviation stakeholders, and aircraft designers?

1.3 Thesis Objective and Outline

The present thesis aims to respond to the research needs that emerged above from the analysis of the state of the art. At the same time, it will retrace the candidate's research path, including his international collaborations and training experiences. The rest of the document is structured into three chapters, organized as follows:

- **Chapter 2** will introduce the hybrid-electric aircraft design framework developed in collaboration with the research fellows from UNINA's DAF research group. The chapter addresses the need for research into tools, in the hands of the preliminary designer, that allow to capture the benefits and drawbacks of innovative technologies in a holistic and multidisciplinary vision, generalizing and integrating classic literature methods with innovative approaches. Along the lines of the mathematical modeling of a hybrid-electric powertrain originally proposed by de Vries et al. [26], a generalization is proposed, capable of describing a much larger number of propulsion architectures with the same approach. Further details regarding the model will also be found in the Appendix A and Appendix B. The sizing workflow, originally developed by Orefice [86], is presented briefly as it is functional for the discussion of the following chapter. The candidate's contributions will be duly highlighted. Particular emphasis will be dedicated to the workflow assembled by the candidate, which is based on mission and performance analysis and allows for greater time efficiency, flexibility, and accuracy of the design process. Finally, the development and testing of a workflow for estimating DOCs will be discussed.
- **Chapter 3** will explore the outcomes resulting from the candidate's participation in the CS2 research project ELICA [16]. Lasting 3 years, the project engaged the candidate for the first part of his career as a doctoral student, allowing him to gain experience in the context of collaborations with international industrial partners, and participation in workshops and conferences for the dissemination of the results. The presented application is on the design of a commuter class aircraft with 19 passengers, which aims for near-zero emissions with EIS in 2035. Several assessment loops were necessary to converge on a final output, and these will be briefly reviewed. Despite the confidential nature of many of the project's findings, the chapter is nevertheless functional to illustrate the lessons learned from the ELICA experience, which contributed to correcting the author's approach to research. In particular,

the difficulties and inefficiencies encountered justify the choice to make changes to the design workflow compared to what was proposed by Orefice, including a greater focus on mission analysis, and the generalization of the powertrain model to include hydrogen FCs.

- **Chapter 4** will describe in detail an original study conducted to support the determination of a transition roadmap towards economically and environmentally sustainable regional aviation. The case study will involve a regional platform with 50 passengers, and a large number of scenarios will be defined, representative of the most promising technologies available. With reference to three different future time horizons, several aircraft concepts will be selected, preliminarily designed, and critically analyzed. As arising from the literature, the assessment of the benefits of emerging technologies for aviation strictly depends on their TRL and on the hypotheses made about their performance levels in terms of efficiency and mass. For this reason, the study aims to base aircraft design on technological trends and estimates promoted by industry experts, both from industry and academia. Participation in the GENESIS project was functional in this sense, allowing for a careful and conservative definition of the most probable scenarios for near and remote time horizons. In this way, the study aims to provide a reliable indication of possible future scenarios. The workflow described in Chapter 2 and the previously gained experiences of Chapter 3 will both be instrumental to the design activity. The latter will involve the exploration of thousands of combinations of design parameters, aimed at minimizing fuel consumption. The constraints for the design will consist of a set of TLARs appropriately chosen on the basis of market considerations. The overview will be completed by an evaluation of the operating costs of the aircraft, which will allow for taking a look at the economic competitiveness of the most environmentally sustainable concepts. A detailed LCA for each scenario will mitigate the expected benefits of the technologies considered, highlighting that environmental trade-offs emerge when considering different impact categories. As will be discussed, the work has also enabled the development of a LCI database in collaboration with industrial partners and experts. The database, instrumental for the LCA performed, is scalable, publicly available, and is believed to represent a first step towards the integration of LCA considerations at the preliminary design level. The technical, economic, and environmental results of the study will be critically compared, electing the most promising scenarios and proposing a transition roadmap towards sustainable regional aviation. A set of recommendations for aviation stakeholders and policy makers will be proposed as well, reflecting the main conclusions of the study and the author's vision.

The structure of each chapter will be outlined in more detail in its introductory section. Furthermore, at the conclusion of each chapter's first section, tables will delineate the author's original contributions alongside a compilation of his scientific publications pertinent to the chapter's content. Finally, after Chapter 4, the overall conclusions of the thesis work will be summarized, together with prospects for future developments.

2

Hybrid-Electric Aircraft Designer

Contents

2.1 Introduction

The preliminary design phase of aircraft, specifically for hybrid-electric powertrain architectures, is of paramount importance to evaluate the expected advantages or disadvantages of innovative technologies. This chapter delves into an innovative preliminary aircraft design framework developed by the DAF research group from the University of Naples, able to incorporate cutting-edge technologies in the design of regional aircraft. The framework integrates a collection of libraries, methods, and workflows, which fall under the unique name *HEAD*, an acronym for *Hybrid-Electric Aircraft Designer*. The tool was originally conceived by Dr. Francesco Orefice, and its detailed description and validation of the methods is the subject of his

doctoral thesis [86]. However, this chapter aims to offer an overview of the design methodologies and workflows composing HEAD, in light of the author's contributions to its development and ongoing improvements. In the literature, the interested reader will find more insights into the tool as well as various applications relating to commuter, regional, or general aviation aircraft [86–97]. In the Introduction chapter, the research question was detailed in the need for methodologies for preliminary design that generalize the classic design chains for conventional aircraft:

How can traditional preliminary design methodologies be generalized and adapted into a flexible, multidisciplinary workflow to address the diversity of hybrid-electric propulsion architectures in regional aircraft?

This chapter will try to respond to this need, underlining the significance of HEAD in terms of its ability to streamline the design process, enhance predictive accuracy, and offer flexibility across various hybrid-electric configurations. The proposed tool addresses a more integrated and holistic approach to the preliminary design phase, enabling designers to efficiently evaluate and optimize various aspects of hybrid-electric aircraft, such as energy management, propulsion system configuration, and overall aircraft performance. All methods and workflows illustrated in this chapter will be instrumental for the studies conducted in Chapters 3 and 4 of this dissertation.

Implemented mainly in MATLAB® language and following an object-oriented paradigm, HEAD collects traditional and innovative methods for estimating the geometric, aerodynamic, inertial, and propulsive characteristics of the aircraft, generalized to the case of hybrid-electric architectures. The routines for calculating aircraft properties are implemented in the form of utility functions, called by different modules within the tool to compose several design and analysis workflows. As conceived by Orefice, HEAD is composed of three main toolboxes, or modules, which retrace three fundamental steps of conceptual design [86]:

- The *pre-design module*, devoted to the definition of a baseline reference aircraft, initializes the conceptual design process. The module is based on purely statistical considerations, applying semi-empirical correlations between top-level requirements and geometrical parameters.
- The *sizing module*, useful for carrying out the preliminary sizing activity, generalizes classical design approaches to hybrid-electric architectures. Compliance with requirements and aviation regulatory constraints is verified, basing the identification of the wing loading and the necessary power to be installed on assigned point performance requirements.
- The *analysis module*, devoted to the accurate evaluation of aircraft performance and mission analysis. The module is designed to verify the compliance of the sized aircraft with its design mission, as well as its performance in off-design conditions. A simulated approach is used, where the characteristics of the aircraft (including propulsion) are evaluated at regular time intervals, allowing for reliable estimates of energy consumption and emissions.

In the following sections, the tool's core functionalities and their potential impact on the future of aircraft design will be examined. Section 2.2 will cover aircraft modeling, with particular attention to the development of a general mathematical model for the hybrid-electric powertrain for which the author was responsible. Details about the estimation of aerodynamic and inertial characteristics will be given, particularly emphasizing the differences from traditional conventional design chains.

Section 2.3 will present the HEAD preliminary sizing workflow, originally developed by Orefice, which generalizes the traditional sizing methods available in the literature. The workflow encompasses the pre-design and sizing modules, allowing for the design of a conventional or hybrid-electric aircraft starting from an assigned set of TLARs and designer's preferences.

The mission and performance analysis usually follows the sizing phase, aiming to verify the performance on a reference mission and for a more accurate evaluation of power and energy demands. However, the difference in accuracy between the methods used in the sizing process and those underlying the analysis module can likely lead to discrepancies in the results. The mission analysis may reveal the need to adjust the outputs from the sizing module in light of requirements that have not been well verified, or even to repeat the entire sizing process with more conservative assumptions. Sometimes, the impossibility of replicating the accuracy of the mission analysis at the sizing level translates into the need for multiple, non-automatic iterative loops, which can be time-consuming and undermine the effectiveness and flexibility of the design tool. In light of this issue, an alternative design workflow was assembled by the author of this dissertation, in collaboration with his research fellows from the DAF research group. The new workflow, presented and validated in Section 2.4, aims for greater levels of automation of the design process. In particular, the design workflow is based on the accurate analysis of the reference mission and flight performance, ensuring consistent and accurate results in reasonable calculation times. In particular, it gives the possibility of integrating surrogate models and efficiency maps to be interrogated at each time step of the mission, which allows for a practical integration of higher fidelity models provided in the context of collaborations with academic and industrial research partners. The time-stepped simulation of the design mission also allows for greater consistency of the results with the set of requirements imposed by the designer, as well as a more precise estimate of energy consumption and emissions.

Finally, in Section 2.5, the module for estimating the DOCs of an aircraft with any hybrid-electric architecture, developed under the responsibility of the candidate, will be presented in more detail.

Author's Contributions

The author was involved in the development and refinement of the tools proposed in this chapter. The conceptualization and early development of HEAD were carried out by Dr. Francesco Orefice, being the subject of his doctoral thesis. Dr. Orefice's focus was on the development of a design chain based on a generalization of the classic sizing methodologies, integrating the possible presence of batteries and distributed propulsion systems.

Author's Contributions (Cont.)

At the beginning of his experience as a doctoral candidate, the author was paired with Dr. Orefice to be informed of the tool and trained in its use. However, the author also actively contributed to the development of vital parts of the software. As will be discussed in Section 2.2.1, the author was responsible for generalizing the tool to more complex propulsion architectures involving hydrogen fuel cell systems. The generalization also involved the estimation of the masses, as specified in Section 2.2.2. The author has constantly been maintaining the software, helping to increase computational efficiency, and improving its structure to increase the flexibility of use. This culminated in the creation of an alternative workflow, described in Section 2.4, which features a greater accuracy provided by the mission analysis while recalling the already existing libraries for the geometric, aerodynamic, inertial and propulsive characterization of the aircraft. The author was helped by his fellow researchers, Dr. Mario Di Stasio and Dr. Manuela Ruocco, in the creation and verification of the workflow. Last but not least, the author led the development of the cost estimation module which will be presented in Section 2.5, being supported by Dr. Vincenzo Cusati (UNINA\Smartup) in acquiring the theoretical background, in the conceptualization, and in the validation phase.

Related Publications

One journal publication covers some of the methodologies discussed in this chapter:

> [93] **Valerio Marciello**, Francesco Orefice, Fabrizio Nicolosi, Danilo Ciliberti, and Pierluigi Della Vecchia. *Design of Hybrid-Electric Aircraft with Fault-Tolerance Considerations.* Chinese Journal of Aeronautics, 36(2):160–178, 2023. The article presents a model developed by the author for simulating the effect of failures for hybrid-electric architecture with DEP. The model, suitable for preliminary design, was tested on a hybrid-electric commuter aircraft designed in the context of the CS2 ELICA project. The main content of this publication is reported in Appendix B. The article also contains the verification of the sizing module of Section 2.3.

One additional work has been produced, submitted to a high-rank journal, and is currently undergoing the review process:

> [97] **Valerio Marciello**, Vincenzo Cusati, Fabrizio Nicolosi, Karen Saavedra-Rubio, Eleonore Pierrat, Nils Thonemann, and Alexis Laurent. *Evaluating the Economic Landscape of Hybrid-Electric Regional Aircraft: A Cost Analysis Across Three Time Horizons.* Submitted to Energy Conversion and Management *(under review)*. The work presents the workflow for the cost analysis of hybrid-electric aircraft discussed in Section 2.5, with an application on several future regional aircraft concepts.

Last but not least, the author participated in the following international conference (the speaker's name is underlined):

> [92] Francesco Orefice, **Valerio Marciello**, Vincenzo Cusati, and Fabrizio Nicolosi. *Powertrain Model Improvement for Hybrid-Electric Regional Aircraft.* In AIAA Scitech 2022 Forum, San Diego, California, 2022. The work proposes a refinement of the hybrid-electric powertrain equations originally proposed by TU Delft [26, 27, 59, 60]. The authors investigated the physical feasibility of each operating mode and provided an algorithm for mode selection. More details will be given in Section 2.2.1. Conceptualized together with Dr. Francesco Orefice, the author of this dissertation was responsible for the investigation and for drafting the paper. The application, concerning a hybrid-electric regional concept, consists of the mission analysis of the aircraft, also simulating the battery discharge profile as described in Section 2.2.1.

2.2 Design Methodologies

2.2.1 Powerplant Model

Propulsive Architecture Scheme

When modeling hybrid-electric or full-electric aircraft, the first and most profound difference in describing the aircraft model is represented by the propulsion system. The classical design chains often lack adaptability to innovative powertrain architectures since semi-empirical methods cannot be applied in the case of electric propulsion systems. In general, the propulsion system of innovative configurations is complicated by new elements, including a variety of multiple alternative energy sources (e.g., thermal engines, FC systems, electric storages) and multiple propulsive lines, including primary propellers and DEP. Due to the increased number of design degrees of freedom, new design variables and approaches are necessary to simulate the actual operative condition of each powertrain component during flight. Designers are motivated to explore various propulsive configurations and optimize parameters before delving into subsystems' detailed analysis and design [98–102]. Thus, it becomes important to describe complex systems in the most simple way, to adapt to the needs of preliminary design without giving up the variety of possible solutions. While some studies simplify powertrain assumptions [103, 104], others propose generalized sizing methods for electric aircraft but often omit multiple propulsive lines and related aero-propulsive interactions [99, 105, 106].

Considering the extensive range of enabling technologies available that the designer might wish to explore, the need emerges for more general approaches for modeling hybrid-electric powertrains at preliminary design stages. A robust and adaptable modeling approach is essential to navigate the variety and complexities of these technologies effectively. Research initiatives by the Delft University of Technology have made progress in this direction [26, 27, 59, 60]. In order to provide a wider choice of propulsion architectures, they introduced a system of linear algebraic equations referred to as *powertrain equations*. The equations, in addition to depending on the efficiencies of the individual components, also depend on well-defined hybridization parameters that reflect the desired usage strategy of multiple sources and propulsion lines. The form of the equations is consequent to the chosen propulsion architecture model, which de Vries et al. generically defined as a series/parallel partial hybrid[1], with conventional internal combustion engines (ICEs), battery, and two propulsion lines [26]. The model is also capable of degenerating

[1]According to the nomenclature proposed in Ref. [107], *series/parallel partial hybrid* systems represent the most general example of a hybrid architecture, with some propellers driven directly by a gas turbine, and other propellers driven exclusively by electric motors powered by batteries or turbine-driven generators. A *turbo-electric* architecture consists of combustion engines that provide propulsive power with all (*full turbo-electric*) or some (*partial turbo-electric*) of the engine power output converted to electricity. In a *parallel* hybrid-electric system, a battery-powered motor and a turbine engine are both mounted on the same propeller shaft. In a *serial* hybrid-electric system, only the electric motors are mechanically connected to the propellers, while the gas turbine drives an electrical generator that produces power to drive the motors and/or charge batteries.

into simpler configurations, such as conventional, all-electric, turbo-electric, parallel, and serial [26]. Finally, their model manages different possible operations (or *operating modes*) of versatile components, such as electric machines that can work both as a motor and a generator, as well as batteries that are rechargeable in flight. Although the model of de Vries et al. offers a good level of generality, it is limited in the nature and number of energy sources. In an uncertain landscape, where the combustion of hydrogen or its use in open electrochemical systems (i.e., FCs) seems to represent a promising response to the complete decarbonization of aviation, it becomes necessary also to consider these alternative energy sources. At the same time, it is important to formulate a single, more general definition of the powertrain model for preliminary design applications compared to the current state of the art. Only in this way can it be possible for the designer to explore very different concepts, using a unique design workflow and ensuring consistency. A further limitation of de Vries's approach is that the choice of the operating mode is arbitrary, without taking into account the possible physical impossibility of the associated energy flows. To fill this gap, this dissertation proposes a generalized approach to describe complex systems at early design stages, which consistently controls the physicality of the operating mode and provides for its automatic adaptation. The proposed model is represented in Fig. 2.1.

In Fig. 2.1, five propulsion sources appear: two gas turbine engines (possibly representing thermal engines based on the combustion of different fuels, e.g., kerosene and hydrogen), a hydrogen-based FC system, and up to two different types of electric storage systems. The elements that appear in Fig. 2.1 actually represent groups of homologous and identical elements, allocated differently on board the aircraft. The secondary propeller group, for example, can represent a multitude of electric propellers distributed on the wing; multiple thermal engines or battery packs of the same type may be present as well. A total of three propulsion lines (or propeller groups) is included in the model, giving the analyst maximum flexibility in down-selecting the architecture. Primary and tertiary electric machines constitute the connecting elements between the propulsion lines, allowing for energy exchanges. Overall, the diagram represents a generalization of the powerplant architecture of a turboprop aircraft. However, as a future development, the scheme could also be adapted to the case of turbofan aircraft, e.g., properly characterizing the propeller elements to model the fans. Although complex and general, the model preserves the simplicity of the approach of de Vries et al. [26, 59] continuing to rely on linear systems of algebraic powertrain equations. The input and output powers of each element of the powerplant represent the unknowns of the problem, provided that at least one power (e.g., the total required propulsive power) is known. The system matrix is obtained by combining relations based on the energy conservation principle, represented by Eq. (2.1).

$$\sum P_{\text{Out, Element}} = \sum P_{\text{In, Element}} \cdot \eta_{\text{Element}} \tag{2.1}$$

In Eq. (2.1), $P_{\text{Out, Element}}$ is the power flowing outward from the generic element, $P_{\text{In, Element}}$ is the input power to the element, and η_{Element} represents the element's

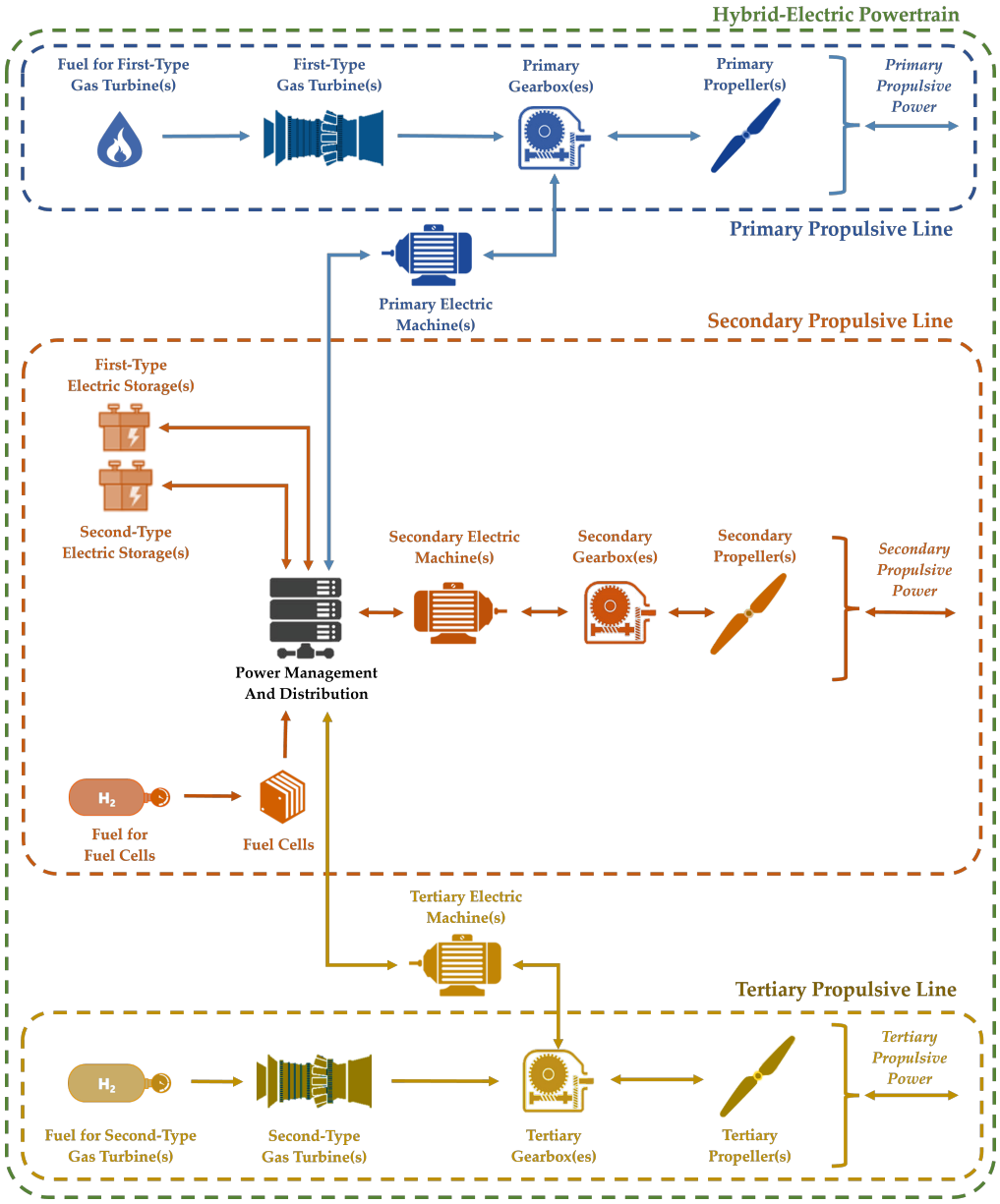

Figure 2.1: The most general propulsive architecture model implemented, featuring up to five energy sources, supplying power to up to three propeller lines.

efficiency. In addition to the energy conservation equations, some additional equations are required in order to specify the degrees of hybridization. Equation (2.2) defines the *supplied power ratio* Φ_i, representing the ratio between the i_{th} energy source and the total supplied power. Equation (2.3) defines the *shaft power ratio* φ_j, which represents the ratio between the power delivered to the shafts of the j_{th} propulsive line and the total shaft power.

$$\Phi_i = \frac{P_{\text{Source, i}}}{P_{\text{Source, Total}}} \tag{2.2}$$

$$\varphi_{\mathrm{j}} = \frac{P_{\mathrm{Shaft,\ j}}}{P_{\mathrm{Shaft,\ Total}}} \tag{2.3}$$

The sum of the supplied power ratios relating to the five sources must equal 1, as does the sum of the shaft power ratios. This implies the existence of up to 4+2 independent equations that specify the degree of hybridization. Combined with the equations representing the unknown powers exchanged by the components, they would lead to the definition of a system of more than 20 algebraic equations. Furthermore, the system is not uniquely determined unless the operating mode of the components with versatile behavior is specified, which could reverse the roles of $P_{\mathrm{In,\ Element}}$ and $P_{\mathrm{Out,\ Element}}$ in Eq. (2.1) for the corresponding element. The following can be considered as versatile elements:

- Electric machine groups, being able to work as motors or generators.
- Electric storage systems, being able to supply energy or recharge.
- Propeller groups, being able to produce thrust or harvest energy from the external flow.

In total, in Fig. 2.1, eight versatile elements with dual behavior can be distinguished, leading to $2^8 = 256$ possible combinations, or *operating modes* of the powertrain. Each operating mode will correspond to a slightly different system of equations, always given by the combination of Eqs. (2.1)– (2.3) but adapted to the specific behaviors of the components. Therefore, the operating mode becomes an additional parameter to be chosen by the designer. However, some of these operating modes are inherently unfeasible. For example, it is impossible for primary electric machines to work as motors (i.e., providing mechanical power to the primary line) while the primary propellers are in harvest mode because, in such circumstance, there would be no output gate for the primary gearbox. By excluding the intrinsically unfeasible modes, the number of combinations is reduced from 256 to 68. Moreover, the number of truly feasible combinations could be further reduced in specific circumstances, e.g., in the absence of some of the components of Fig. 2.1, or for certain combinations of efficiencies values. If, in formulating the powertrain equations, it is postulated that all the powers involved are defined as positive, it could happen that the solution presents at least one negative power value in any of the power nodes. This would be an indication of a non-physicality of the solution and, in turn, non-feasibility of the mode. Given the complexity of the architecture and the high number and diversity of power nodes, it could easily happen that the occurrence of similar circumstances escapes the eye of the designer, more focused on a few parameters of interest (e.g., consumption or total propulsive power). This leads to the risk of making mistakes and overestimating the potential benefits of an assigned architecture unless active control of the physicality of the operating mode is envisaged [92].

For the sake of brevity, further details on the mathematical model underlying the scheme of Fig. 2.1 will be relegated to the Appendix A. The discussion will continue below only in relation to two specific applications, which contemplate a reduced number of propulsion sources and propeller lines. Indeed, although it has been argued that the implementation of a robust and general model is important in order not to limit the validity of the method to any combination of enabling technologies,

it is unlikely that systems based on so many different energy sources and propellers will ever fly. In fact, a combination of complexity (e.g., implementation and control), reliability concerns, and cost and weight penalties would likely nullify the anticipated advantages. Rather, Fig. 2.2 and Fig. 2.3 are degenerations of Fig. 2.1 in the case of two-source hybrid-electric configurations. In particular, Fig. 2.2 refers to a hybrid-electric architecture based on one type of thermal engine and one battery group. Figure 2.3 represents instead the scheme for an all-electric configuration based on batteries and hydrogen FCs. The two derived architectures will also be taken into

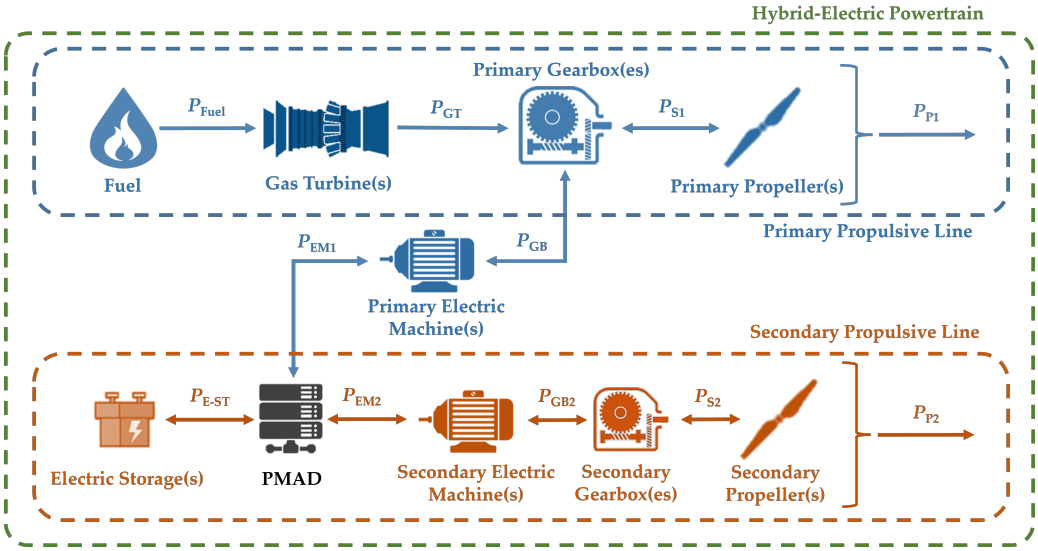

Figure 2.2: A general propulsive architecture model, featuring fuel-based thermal engines, electric storage system, and up to two propulsive lines.

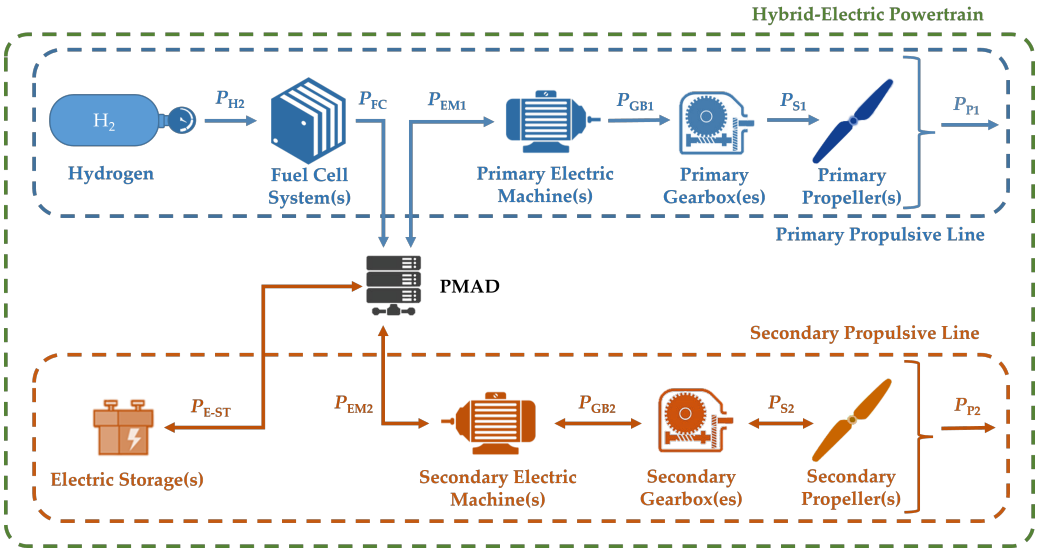

Figure 2.3: A general propulsive architecture model, featuring hydrogen-based fuel cell systems, electric storage system, and up to two propulsive lines.

consideration for the applications presented in Chapters 3 and 4. The nomenclature in Figs. 2.2–2.3 has been slightly adapted to facilitate the following discussion. As in the general case, in Fig. 2.2, the gas turbine (GT) converts the chemical energy of the fuel into mechanical power, which is transferred to the shaft (S1) and finally to the propeller (P1) after passing through a reduction gearbox (GB1). The latter also acts as a junction node with a primary electric machine (EM1) which exchanges electrical power with a battery (E-ST) and a line of secondary electric machines (EM2), which in turn move secondary (distributed) propellers (P2), provided or not the presence of reduction gearboxes (GB2). Acting as a hub for electrical power is a Power Management and Distribution (PMAD) system, associated with cables and control electronics. In the case of Fig. 2.3, the major difference lies in the presence of a FC system powered by H_2, which converts the chemical energy of hydrogen into electrical energy, which is eventually distributed on the two propulsion lines together with the additional power supplied by the battery.

For the architecture of Fig. 2.2, supplied and shaft power ratios are unique values and are redefined as in Eqs. (2.4)–(2.5)

$$\Phi = \frac{P_{\text{E-ST}}}{P_{\text{Fuel}} + P_{\text{E-ST}}} \tag{2.4}$$

$$\varphi = \frac{P_{\text{S2}}}{P_{\text{S1}} + P_{\text{S2}}} \tag{2.5}$$

In Eq. (2.5), P_{S2} is the secondary shaft (S2) power. In the case of Fig. 2.3, the supplied power ratio is defined by Eq. (2.6).

$$\Phi = \frac{P_{\text{E-ST}}}{P_{\text{H2}} + P_{\text{E-ST}}} \tag{2.6}$$

The possible operating modes for the two architectures are listed in Tabs. 2.1 and 2.2.

Table 2.1: Possible operating conditions of the propulsive scheme depicted in Fig. 2.2, defined based on the versatile behavior of the primary and secondary propellers, e-storage devices, and primary electric machines.

Mode	P1	P2	E-ST	EM1
1	Thrust	Thrust	Discharge	Generator
2	Thrust	Thrust	Charge	Generator
3	Thrust	Harvest	Charge	Generator
4	Thrust	Thrust	Discharge	Motor
5	Thrust	Harvest	Discharge	Motor
6	Thrust	Harvest	Charge	Motor
7	Harvest	Thrust	Discharge	Generator
8	Harvest	Thrust	Charge	Generator
9	Harvest	Harvest	Charge	Generator

Table 2.2: Possible operating conditions of the propulsive scheme depicted in Fig. 2.3, defined based on the versatile behavior of the primary and secondary propulsors, and e-storage devices.

Mode	P1	P2	E-ST
1	Thrust	Thrust	Discharge
2	Thrust	Thrust	Charge
3	Thrust	Harvest	Discharge
4	Thrust	Harvest	Charge
5	Harvest	Thrust	Discharge
6	Harvest	Thrust	Charge
7	Harvest	Harvest	Charge

The number of operating modes could be further reduced if the architecture degenerates further or if the versatility of some elements is prevented. The system of powertrain equations for modes 1 and 4 of the architecture in Fig. 2.2 is given below in Eqs. (2.7) and Eqs. (2.8), respectively. In the proposed form, P_{GT} constitutes the known power value. However, the equations can easily be inverted to be expressed as a function of a known total propulsive power (P_{P}) or any other node power.

$$\begin{bmatrix} -\eta_{\mathrm{GT}} & 0 & 0 & 0 & 0 & 0 & 0 & 0 & 0 & 0 \\ 0 & 1 & 1 & 0 & 0 & 0 & 0 & 0 & 0 & 0 \\ 0 & 0 & -\eta_{\mathrm{P1}} & 0 & 0 & 0 & 0 & 1 & 0 & 0 \\ 0 & -\eta_{\mathrm{EM1}} & 0 & 1 & 0 & 0 & 0 & 0 & 0 & 0 \\ 0 & 0 & 0 & -\eta_{\mathrm{PMAD}} & -\eta_{\mathrm{PMAD}} & 1 & 0 & 0 & 0 & 0 \\ 0 & 0 & 0 & 0 & 0 & -\eta_{\mathrm{EM2}}\eta_{\mathrm{GB2}} & 1 & 0 & 0 & 0 \\ 0 & 0 & 0 & 0 & 0 & 0 & -\eta_{\mathrm{P2}} & 0 & 1 & 0 \\ \Phi & 0 & 0 & 0 & (\Phi-1) & 0 & 0 & 0 & 0 & 0 \\ 0 & 0 & \varphi & 0 & 0 & 0 & (\varphi-1) & 0 & 0 & 0 \\ 0 & 0 & 0 & 0 & 0 & 0 & 0 & 1 & 1 & -1 \end{bmatrix} \begin{bmatrix} P_{\mathrm{Fuel}} \\ P_{\mathrm{GB1}} \\ P_{\mathrm{S1}} \\ P_{\mathrm{EM1}} \\ P_{\mathrm{E\text{-}ST}} \\ P_{\mathrm{EM2}} \\ P_{\mathrm{S2}} \\ P_{\mathrm{P1}} \\ P_{\mathrm{P2}} \\ P_{\mathrm{P}} \end{bmatrix} = \begin{bmatrix} -P_{\mathrm{GT}} \\ \eta_{\mathrm{GB1}}P_{\mathrm{GT}} \\ 0 \\ 0 \\ 0 \\ 0 \\ 0 \\ 0 \\ 0 \\ 0 \end{bmatrix} \tag{2.7}$$

$$\begin{bmatrix} -\eta_{\mathrm{GT}} & 0 & 0 & 0 & 0 & 0 & 0 & 0 & 0 & 0 \\ 0 & -\eta_{\mathrm{GB1}} & 1 & 0 & 0 & 0 & 0 & 0 & 0 & 0 \\ 0 & 0 & -\eta_{\mathrm{P1}} & 0 & 0 & 0 & 0 & 1 & 0 & 0 \\ 0 & 1 & 0 & -\eta_{\mathrm{EM1}} & 0 & 0 & 0 & 0 & 0 & 0 \\ 0 & 0 & 0 & 1 & -\eta_{\mathrm{PMAD}} & 1 & 0 & 0 & 0 & 0 \\ 0 & 0 & 0 & 0 & 0 & -\eta_{\mathrm{EM2}}\eta_{\mathrm{GB2}} & 1 & 0 & 0 & 0 \\ 0 & 0 & 0 & 0 & 0 & 0 & -\eta_{\mathrm{P2}} & 0 & 1 & 0 \\ \Phi & 0 & 0 & 0 & (\Phi-1) & 0 & 0 & 0 & 0 & 0 \\ 0 & 0 & \varphi & 0 & 0 & 0 & (\varphi-1) & 0 & 0 & 0 \\ 0 & 0 & 0 & 0 & 0 & 0 & 0 & 1 & 1 & -1 \end{bmatrix} \begin{bmatrix} P_{\mathrm{Fuel}} \\ P_{\mathrm{GB1}} \\ P_{\mathrm{S1}} \\ P_{\mathrm{EM1}} \\ P_{\mathrm{E\text{-}ST}} \\ P_{\mathrm{EM2}} \\ P_{\mathrm{S2}} \\ P_{\mathrm{P1}} \\ P_{\mathrm{P2}} \\ P_{\mathrm{P}} \end{bmatrix} = \begin{bmatrix} -P_{\mathrm{GT}} \\ \eta_{\mathrm{GB1}}P_{\mathrm{GT}} \\ 0 \\ 0 \\ 0 \\ 0 \\ 0 \\ 0 \\ 0 \\ 0 \end{bmatrix} \tag{2.8}$$

Equations (2.9) instead represent the powertrain equations for mode 1 of the all-electric architecture visualized in Fig. 2.3.

$$\begin{bmatrix} \eta_{\mathrm{FC}} & 0 & 0 & 0 & 0 & 0 & 0 & 0 & 0 & 0 \\ 0 & -\eta_{\mathrm{GB1}} & 1 & 0 & 0 & 0 & 0 & 0 & 0 & 0 \\ 0 & 0 & -\eta_{\mathrm{P1}} & 0 & 0 & 0 & 0 & 1 & 0 & 0 \\ 0 & 1 & 0 & -\eta_{\mathrm{EM1}} & 0 & 0 & 0 & 0 & 0 & 0 \\ 0 & 0 & 0 & 1 & -\eta_{\mathrm{PMAD}} & 1 & 0 & 0 & 0 & 0 \\ 0 & 0 & 0 & 0 & 0 & -\eta_{\mathrm{EM2}}\eta_{\mathrm{GB2}} & 1 & 0 & 0 & 0 \\ 0 & 0 & 0 & 0 & 0 & 0 & -\eta_{\mathrm{P2}} & 0 & 1 & 0 \\ \Phi & 0 & 0 & 0 & (\Phi-1) & 0 & 0 & 0 & 0 & 0 \\ 0 & 0 & \varphi & 0 & 0 & 0 & (\varphi-1) & 0 & 0 & 0 \\ 0 & 0 & 0 & 0 & 0 & 0 & 0 & 1 & 1 & -1 \end{bmatrix} \begin{bmatrix} P_{\mathrm{H2}} \\ P_{\mathrm{GB1}} \\ P_{\mathrm{S1}} \\ P_{\mathrm{EM1}} \\ P_{\mathrm{E\text{-}ST}} \\ P_{\mathrm{EM2}} \\ P_{\mathrm{S2}} \\ P_{\mathrm{P1}} \\ P_{\mathrm{P2}} \\ P_{\mathrm{P}} \end{bmatrix} = \begin{bmatrix} P_{\mathrm{FC}} \\ 0 \\ 0 \\ 0 \\ \eta_{\mathrm{PMAD}}P_{\mathrm{FC}} \\ 0 \\ 0 \\ 0 \\ 0 \\ 0 \end{bmatrix} \tag{2.9}$$

To keep the diagrams in Figs. 2.1–2.2 simple, the presence of inverters coupled to electric machines and converters for batteries and FCs has been omitted. However, their presence can be taken into account by including a penalty in the efficiencies of the associated elements in Eqs. (2.7)–(2.9).

As anticipated, even the apparently legitimate choice of one of the listed modes could lead to unfeasible solutions. Figure 2.4 shows a parametric analysis of the powertrain equations' solutions as the shaft power ratio and operating mode vary. The purpose of Fig. 2.4 is to point out that, for certain combinations of operating mode, hybridization, and efficiencies, certain powers may exhibit a negative sign as a symptom of the non-feasibility of the mode. In general, this happens when the required shaft power distribution is incompatible with the assigned powers of the individual sources, which flow following directions constrained by the chosen operating mode. In Ref. [92], the author of this dissertation offers an even more detailed analysis of the phenomenon, interpreting each possible mathematical result from a physical point of view. Also in Ref. [92] the interested reader can find explicit mathematical expressions of the asymptotes visible in Fig. 2.4, which can support consistency checks and preventively guide the choice of the operating mode. However, providing further details here would go beyond the scope of the discussion. In fact, in the implementation of the final powertrain model, the search for mathematical expressions that identified zeros and asymptotes of the powertrain equations was avoided, due to the enormous difficulty of obtaining exact solutions in the more general case of Fig. 2.1. A simpler, easier-to-replicate approach has been adopted, where the designer's choice of operating mode only serves as an initial guess. The power vector resulting from the powertrain equations is checked, and if at least one negative value exists, an automatic switch to another operating mode is performed. In this sense, the designer is free to set up the order of destination modes as preferred. It is possible that several consecutive changes will be necessary before arriving at a consistent solution. In the present context, the preferred destination mode is chosen trying to minimize differences from the original mode in terms of component behaviors. A change in the behavior of electric machines is prioritized, followed by battery and propeller behaviours. Mode 4 of Table 2.1, for example, mirrors mode 1 and vice versa. Modes 5 and 7 are complementary as well, as it also emerges from the trends in Fig. 2.4. In this way it is guaranteed that a valid solution is provided in any case, avoiding meaningless final results.

The powertrain mathematical model described in this paragraph is believed to provide important added value compared to the state of the art. The remarkable generality and replicability of the model, combined with its simplicity (only linear algebraic equations are used), make it suitable for conceptual and preliminary aircraft design applications and allow for the description of any propulsion architecture the analyst can think of. The model is also easy to generalize further, to include even more systems and degrees of freedom. As a final note, it is worth noting that the powertrain equations are linear only to the extent that the component efficiencies of the system matrix are constant numbers. In the case of nonlinear dependencies, the powertrain equations need to be solved iteratively until the powers converge.

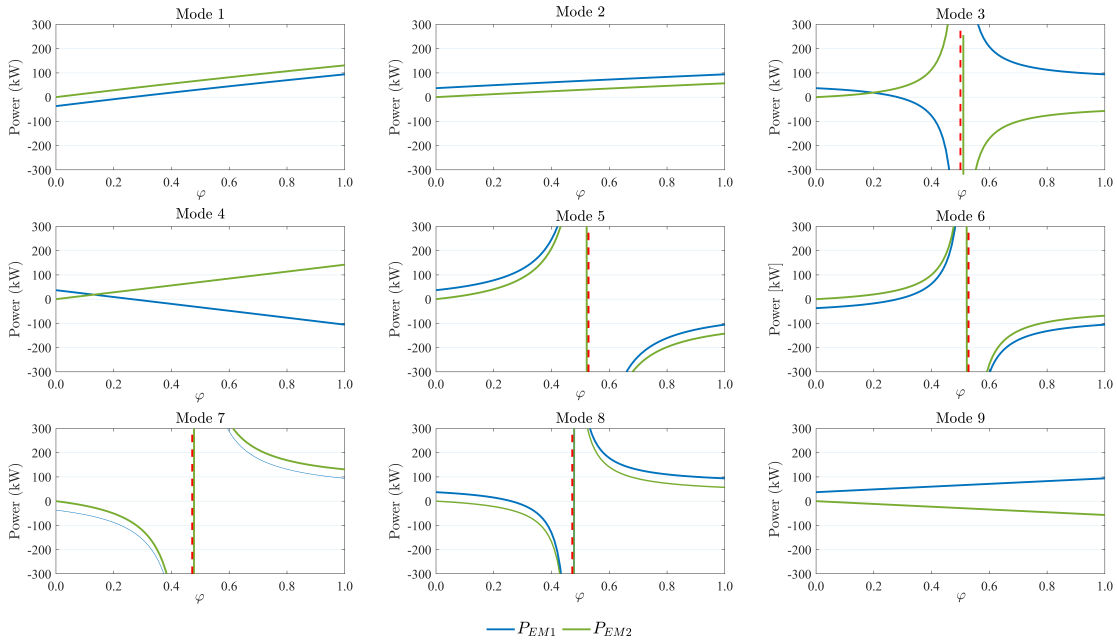

Figure 2.4: Powers of electric machines calculated solving powertrain equations for all different operating modes and shaft power ratios, at constant efficiencies and supplied power ratio ($P_{\mathrm{GT}} = 100$ kW, $\Phi = 0.10$, $\eta_{\mathrm{GT}} = 0.30$, $\eta_{\mathrm{EM1}} = \eta_{\mathrm{EM2}} = 0.95$, $\eta_{\mathrm{GB1}} = 0.99$, $\eta_{\mathrm{GB2}} = 1.00$, $\eta_{\mathrm{P1}} = \eta_{\mathrm{P2}} = 0.70$, $\eta_{\mathrm{PMAD}} = 1.00$). The reference powertrain architecture is the one described in Fig. 2.2. Negative values correspond to unfeasibility domains for the corresponding mode (adapted from Ref. [92]).

In the next subsection, the estimation of the efficiencies of the individual elements of the hybrid-electric powertrain will be explored in more detail, preparatory to the construction of the system of equations discussed so far.

Gas Turbines

When modeling the behavior of an ICE, the performance of the entire engine as a whole is typically considered without the necessity to make distinctions between its parts. However, as seen in the previous paragraph, in the case of hybrid-electric configurations, it may be convenient to separate the behavior of the gas turbine, gearbox, and propeller, which are seen as independent power nodes. Therefore, the need arises to separately characterize the efficiencies of the individual propulsion components:

- The **thermal efficiency**, associated with the gas turbine, representing its ability to extract energy from the fuel and convert it into mechanical power.
- The **mechanical efficiency**, associated with the gearbox, representing the mechanical losses in transferring the mechanical power to the shaft.
- The **propulsive efficiency**, representing the fraction of the net mechanical power that the propeller is able to convert into propulsive power.

The gas turbine (thermal) efficiency, η_{GT}, can also be expressed equivalently in terms of specific fuel consumption (SFC), i.e., the mass of fuel consumed per unit power and time, as in Eq. (2.10).

$$\eta_{\mathrm{GT}} = \frac{1}{SFC\ SE_{\mathrm{Fuel}}} \tag{2.10}$$

In Eq. (2.10), SFC is expressed in kg/(kW h), and SE_{Fuel} is the specific energy of the fuel (e.g., about 12.0 kWh/kg for kerosene). In the first instance and for preliminary sizing purposes, a constant SFC value can be attributed to the engine for a specified range of operating conditions or flight phases. Once the necessary power of the thermal engine is known, the fuel flow in kg/s can be estimated by Eq. (2.11).

$$FF_{\mathrm{GT}} = \frac{P_{\mathrm{GT}}}{3\,600\ SE_{\mathrm{Fuel}}\ \eta_{\mathrm{GT}}} \tag{2.11}$$

Finally, once the fuel consumed in the unit of time is known, it is also possible to estimate the emissions of pollutant species per unit of time, provided that their associated emission index (EI) is known. A general definition of EIs is given in Eq. (2.12), where m_{Fuel} is the consumed fuel mass, and $m_{\mathrm{Pollutant}}$ is the emitted mass of the pollutant species associated with $EI_{\mathrm{Pollutant}}$.

$$EI_{\mathrm{Pollutant}} = \frac{m_{\mathrm{Pollutant}}}{m_{\mathrm{Fuel}}} \tag{2.12}$$

In general, thermal engine performance varies as a function of operating conditions. In addition to the pilot's degree of freedom represented by the throttle setting, which scales the mechanical power delivered by the engine, there are typically also effects related to the flight Mach number, altitude, and deviation from the International Standard Atmosphere (ISA) model's temperature [33, 108–110]. Since atmospheric conditions can vary significantly even within the same flight phase or condition analyzed (e.g., during the climb up to cruise altitude), the assumption that the SFC remains constant may sometimes not reflect a realistic engine behavior. In parallel, the maximum power output could be limited by the increase in altitude. To take these effects into account, a convenient approach is to use rubberized *engine decks*, i.e., dimensionless performance maps of thermal engines. Engine decks may provide power and SFC (or, in turn, fuel flow) as settings and operating conditions vary. Moreover, multiple settings can be defined, characterizing different operating conditions (e.g., take-off, flight idle, ground idle, max continuous, climb, and cruise). In addition, the engine deck can also contain information on the EIs of the main pollutant species, which can alternatively be estimated using semi-empirical approaches [111]. Under the convenient hypothesis that the characteristics of a given type of engine do not vary excessively as the rated power varies, engine decks are a valid tool for preliminary design as they can be dynamically rescaled during the powertrain sizing phase. During a simulation-based mission analysis, engine decks allow for estimating the SFC at each time step, overall increasing the accuracy of the simulation. The knowledge of the atmospheric conditions and the

throttle setting is, in fact, sufficient to query the engine deck and estimate its output performance. In particular, the throttle could be fixed (as it happens in the case of take-off simulation where maximum throttle is assumed, or in descent for which a flight idle setting can be defined), or calculated through the powertrain equations on an iterative basis as a function of the propulsive power necessary for the flight (as happens for example in cruise). In the latter case, the value of the power (and the throttle) is also limited by the hybridization ratio chosen. In this way, for each time step, a new efficiency (and power) value is calculated, and the powertrain equations can be solved again by propagating the increased accuracy to the other powertrain components. In addition, limitations on the fraction of rated power that can be actually delivered also provide direct feedback useful to resize the engine in the event that the power is insufficient to meet the assigned requirements. In the case that the specified consumption is associated with the overall efficiency of the gas turbine plus gearbox, the model in Fig. 2.2 can still be adopted by pretending η_{GB1} to be unitary and including both thermal and mechanical efficiencies into η_{GT}. HEAD provides several rubberized engine decks, which are representative of different engine types, but the use of custom decks different from the default ones is allowed, as long as they comply with the required format [86]. An example of an engine deck is visually offered in Fig. 2.5, which refers to a PW127-like engine in take-off conditions. In practice, the engine deck can be provided as an external database (in .xls format) and interpolated as needed. This approach, used for the study conducted in Chapter 3, is useful in contexts that see close cooperation between the aircraft designer and an engine expert, the latter providing information to properly characterize the engine deck. An alternative approach, which is recently emerging

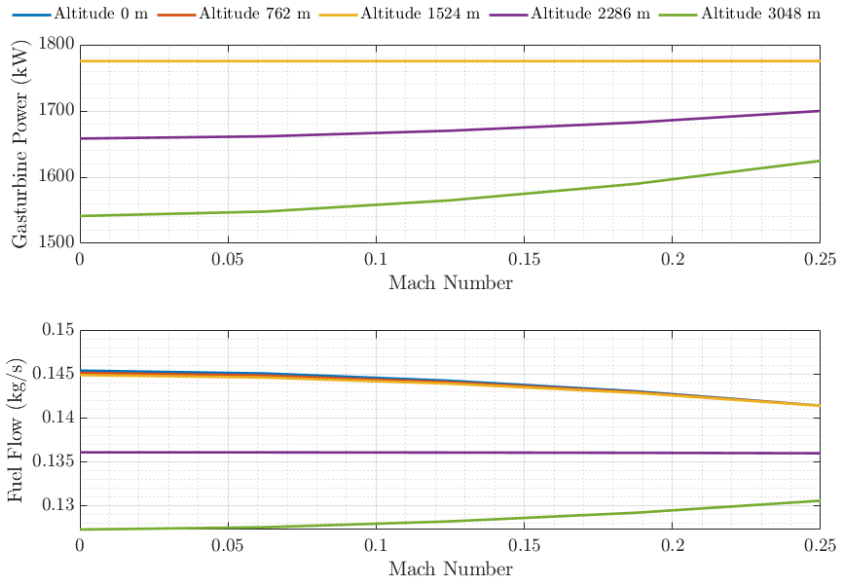

Figure 2.5: An example of an engine deck model for a PW127-like engine from the HEAD library [86, 112, 113]. Power and fuel flow are visualized as a function of altitude and Mach number. The figure refers to the take-off rating, at maximum throttle and in ISA conditions.

in the literature and which will be adopted for the application in Chapter 4, is to estimate the engine deck in advance by means of surrogate models [109]. In both cases, the use of engine decks allows for increasing the level of integration of the engine design process into the design workflow of the entire aircraft, reducing the number of iterations needed with the engine manufacturer.

Propellers

Accurately estimating the efficiency of a propeller involves considering various factors such as its design, the aerodynamic properties of the blades, and operating conditions like air density and aircraft speed. Advanced computational methods and empirical data would be necessary to model and predict propeller performance. However, simpler approaches are required for preliminary design applications, where a detailed characterization of the propeller may not be available. HEAD gives the possibility to estimate the propeller efficiency based on its characteristic curves [86], as classically done in the literature [33, 40]. These curves represent the propeller's performance under various operating conditions and are typically expressed in terms of adimensional thrust and power coefficients against the blade advance ratio [33, 40]. Assuming that, in light of its non-dimensionality, the characteristic curves can scale with the rated power, and the propeller efficiency can thus be characterized for different flight regimes, as already seen for the gas turbine. However, a simpler approach is mentioned below, which has also been used in the present context for the application of Chapter 4. The adopted method is based on the Rankine-Froude *momentum theory*, also known as the *actuator disk theory* [40]. Developed in the late 19^{th} century, it provides a theoretical framework for understanding how propellers generate thrust. The theory is suitable for preliminary calculations during the early design phase, but since it does not consider the design of individual propeller blades, then the momentum theory is inadequate if the propeller design is of interest [40, 114]. The momentum theory models the propeller as an actuator disk that imparts a velocity increase to the airflow, thereby creating thrust. By considering the energy and momentum changes in the flow through the propeller disk, the momentum theory helps in estimating propeller efficiency and performance, although the results are generally optimistic. According to the theory, the propeller's axial induction factor $a_{\text{P,i}}$ can be estimated as a function of the produced thrust T, the propeller's diameter $D_{\text{P,i}}$, the air density ρ_∞, and the relative speed V_∞, as expressed by Eq. (2.13) [40].

$$a_{\text{P,i}} = \frac{1}{2}\left[-1 + \sqrt{1 + 8\,\frac{T_{\text{P,i}}}{\rho_\infty\ \pi\ {D_{\text{P,i}}}^2\ {V_\infty}^2}}\ \right] \tag{2.13}$$

The axial factor represents the fraction between the propeller-induced velocity and the asymptotic speed. The effective propulsive power $P_{\text{P,i}}$ is always given by the product of the thrust and the flight speed, as in Eq. (2.14).

$$P_{\text{P,i}} = T_{\text{P,i}} \cdot V_\infty \tag{2.14}$$

However, the shaft power required must take into account the energy lost to accelerate the flow downstream of the propeller, and can be estimated by multiplying the thrust by the total velocity including induction. The ratio between propulsive power and shaft power provides the propeller efficiency, which can be formulated by Eq. (2.15).

$$\eta_{\mathrm{P,i}} = 0.85 \, \frac{1}{1 + a_{\mathrm{P,i}}} \tag{2.15}$$

As anticipated, the momentum theory overestimates the efficiency as it does not take into account effects such as the presence of the hub (which reduces the disk area), reduction of lift distribution near the tip and hub, and so on [40]. For this reason, a correction factor of 0.85 has been considered in Eq. (2.15) following Gudmundsson's suggestion [40]. The above efficiency estimating relationship does not depend on the number of revolutions per minute (RPM). However, a rough estimate of RPM can be useful for surrogate models for estimating the mass or efficiency of other components (namely gearboxes and electric machines). As the tips of the propeller blades approach sonic speeds, they can cause a significant increase in drag, noise, and potential structural damage due to shock waves. In this sense, the RPM can be estimated starting from the flight speed and the diameter of the propeller, constraining the Mach number to the blade tips to never exceed a limit value to avoid compressibility effects. If a margin of 10% is assumed with respect to the sonic condition, the RPMs can be estimated as in Eq. (2.16), where M_∞ is the Mach number and V_{Sound} is the sound speed.

$$RPM_{\mathrm{P,i}} = \frac{V_{\mathrm{Sound}} \, \sqrt{0.90^2 - {M_\infty}^2}}{D_{\mathrm{P,i}} \, \pi/60} \tag{2.16}$$

As a final note, the propulsive power at the static point is equal to zero according to the definition given in Eq. (2.14). In case it is necessary to estimate the static thrust without having the characteristic curves of the propeller available, the momentum theory also provides an estimating relationship, reported here in Eq. (2.17) [40].

$$T_{\mathrm{P,i,\ Static}} = \sqrt[3]{\frac{1}{2} \, \rho_\infty \, {D_{\mathrm{P,i}}}^2 \, {P_{\mathrm{S,i}}}^2} \tag{2.17}$$

All relationships seen in this paragraph can be used to characterize the propellers of all the propulsion lines that appear in Figs. 2.1–2.3.

Electric Storages

Batteries are key components in the decarbonization of the transport sector. In the present context, batteries play a pivotal role, supporting the power requirements of hybrid-electric aircraft and partially replacing carbon-based fuels in the process of direct decarbonization of flight. Hybrid and electric aircraft require high-voltage batteries composed of multiple cells arranged in series and parallel configurations.

A *cell* is the basic unit of an electric storage device. Multiple cells form modules, which are eventually assembled into battery *packs* [115]. The discharging features of all types of battery cells may be characterized as a function of the discharge current, I_{Cell} [115, 116]. In fact, the electric power delivered by a cell can be calculated by using the relationship in Eq. (2.18), simply representing the product between the voltage V_{Cell} and the current intensity.

$$P_{\text{Cell}} = V_{\text{Cell}} \cdot I_{\text{Cell}} \tag{2.18}$$

The discharge current is often expressed in terms of *C-Rate*, which normalizes it against the total cell capacity. By definition, a C-Rate of 1 means that the assigned discharge current will discharge the entire cell in 1 hour [116]. Higher C-Rates indicate faster charging or discharging capabilities. Still, they also require careful management to avoid reducing the battery's lifespan or causing safety issues due to overheating or overstraining the battery's components. In this sense, the current output from any battery cell may be limited by a maximum C-Rate value depending on battery type and chemistry [116]. It is also useful to express the instantaneous capacity as a percentage of maximum capacity, defined as the State Of Charge (SOC) of the cell. The usable energy supplied by the cell, E_{Cell}, is calculated as in Eq. (2.19) where Q_{Cell} represents the battery charge in Coulombs [116].

$$E_{\text{Cell}} = \int_{Q_{\text{Cell}}(SOC=SOC_{\text{Min}})}^{Q_{\text{Cell}}(SOC=SOC_{\text{Max}})} V_{\text{Cell}} \, dQ_{\text{Cell}} \tag{2.19}$$

Solving the integral of Eq. (2.19) between SOC = 0% and SOC = 100% gives the total energy that can be stored in the battery. The minimum SOC can be lower limited by the imposition of a cut-off voltage [116], affecting the maximum value of consumable energy according to the previous equation. Indeed, the expression of the output voltage produced by the cell can be approximated as the linear model in Eq. (2.20), where Res_{Cell} represents an equivalent Ohmic resistance, $V_{0,\text{Cell}}$ is called the open-circuit voltage, and V_{SOC} is the derivative of the voltage with respect to the SOC [116, 117].

$$V_{\text{Cell}} = V_{0,\text{Cell}} - Res_{\text{Cell}} \, I_{\text{Cell}} - V_{\text{SOC}} \, SOC \tag{2.20}$$

An example is provided by the characteristic curves in Fig. 2.6. The parameters of Eq. (2.20) could be obtained by regression starting from assigned characteristic curves or directly assigned by the battery manufacturer [118].

If the bus voltage is already known based on architectural considerations [119, 120], it is possible to size the battery by arranging a number of cells in series whose total voltage (calculated as the sum of the individual cell voltages) reaches the nominal requirement. Multiple modules obtained in this way can then be arranged in parallel to form a battery pack that meets the overall power and energy requirements [115]. However, in case of high power demands, the coupling of converters may also be useful to avoid excessive increases in current intensity and, thus, power losses. In this sense, the battery voltage is an integer multiple of the

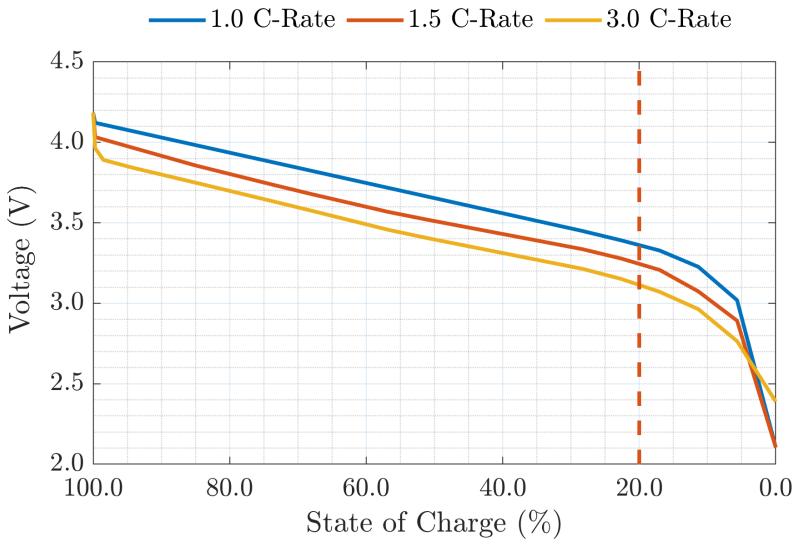

Figure 2.6: An example of cell discharging curves for a Samsung 18650-30Q lithium-ion battery (adapted from Ref. [118]). In the figure, a minimum SOC of 20% is suggested by the dashed red line.

single-cell voltage, assuming that the cells discharge uniformly during operation. As also emerges from Fig. 2.6, the cell (and battery) supplied voltage is usually an inverse function of the current intensity, and the cause lies in the losses due to the internal resistance of the battery. By modeling these losses exclusively as Ohmic, the battery efficiency can be estimated by Eq. (2.21).

$$\eta_{\text{E-ST}} = \frac{V_{\text{Cell}}}{V_{\text{Cell}} + Res_{\text{Cell}}\ I_{\text{Cell}}} \tag{2.21}$$

Combining Eq. (2.18), Eq. (2.20) and Eq. (2.21), if the battery power demand is known for an assigned operational flight, it is possible to deduce the minimum C-Rate required, therefore the associated voltage and efficiency. Consequently, the maximum power that can be delivered by the cell is the result of the maximum allowable C-Rate. Reaching the minimum SOC before the end of the mission can lead to the need for a resizing of the battery, based on the energy criterion rather than on the power demand.

The model described in this paragraph allows for a simulation of battery discharge based on an electrical model of battery systems. In Ref. [92] the author presents an application for a hybrid-electric regional aircraft, reporting the estimated discharge history of the battery. The model, although simple, is considered already quite elaborate for conceptual design purposes, especially for the very early stages of the design process. A substantially less elaborate approach consists of considering a constant efficiency value for the battery, relative to an intermediate value of discharge current and SOC. Typically, and as it can be noted from Fig. 2.6, the voltage losses due to increases in the C-Rate are in the order of 5–10%. Therefore,

battery efficiencies are generally very high, above 90%, and assuming a conservative reference value is a valid approach for preliminary applications. At the same time, as will be seen in Subsection 2.2.2, the battery energy and maximum power can be evaluated directly starting from the mass, through figures of merit such as the battery specific energy, rather than passing through the knowledge of the number of cells and their charge capability. Instead, the use of battery characteristic curves is useful in case of collaborations with industries or battery experts to increase the level of integration in the aircraft design flow, in a similar way to what has already been said regarding thermal engines.

Fuel Cells

Incorporating FCs into aircraft design chains represents a significant advancement in aviation technology, offering a more sustainable and efficient alternative to traditional propulsion systems. Fuel cells are electrochemical systems capable of converting the chemical potential of a fuel (e.g., hydrogen) into electricity. When hydrogen is used and made to react with external air, water vapor is the only waste product to be theoretically emitted [121, 122]. Regardless of the type of FC, it consists of three components [121–125]:

- The *anode*, the electrode at which the oxidation reaction occurs;
- The *cathode*, the electrode at which the reduction reaction occurs;
- The *electrolyte*, a substance that dissolves into ions, allowing for the passage of electric current.

In some FC types such as Proton Exchange Membrane Fuel Cells (PEMs or PEMFCs), a catalyst at the anode initiates oxidation reactions, generating ions and electrons. These ions traverse through the electrolyte to the cathode, while electrons create direct current (DC) electricity as they travel through an external circuit. At the cathode, another catalyst facilitates a reaction between ions, electrons, and oxygen, resulting in water formation. In the case of other FC technologies like Solid Oxide Fuel Cells (SOFCs), the electrochemical reaction occurs in a slightly different manner, involving oxygen ions moving through a ceramic electrolyte to the anode, where they react with hydrogen to form water and release electrons. In any case, the overall electrochemical reaction at the basis of hydrogen-based FCs' operating mechanism is well represented by Eq. (2.22) [121, 122].

$$2H_2 + O_2 \rightarrow 2H_2O \tag{2.22}$$

As demonstrated in the literature, the efficiency of the FC is directly related to the produced voltage [121, 122, 125]. In fact, in the first place, the FC efficiency is the ratio between the useful electrical power produced and the power associated to the energy extractable from the redox reaction. The latter is related to the flow of moles of hydrogen (in mol/s) multiplied by the hydrogen's specific energy (SE_{H2}). As shown by Eq. (2.23), the hydrogen moles can be rewritten in terms of the electric current intensity produced, I_{Cell}, through the Faraday constant

($F = 96\,485.33$ A s/mol), the number of electrons involved in the reaction ($N_e = 2$) and the molecular mass of hydrogen ($mm_{H2} = 2.016$ g/mol) [121, 122].

$$P_{\text{H2, Cell}} = \frac{I_{\text{Cell}} \cdot SE_{\text{H2}} \cdot mm_{\text{H2}}}{N_e \cdot F} \tag{2.23}$$

In Eq. (2.23), SE_{H2} is the reference specific energy of the hydrogen and is usually equal to the Lower Heating Value (LHV) of 120 MJ/kg or 33.33 kWh/kg. Sometimes, when the produced water leaves the stack in vapor form (i.e., in the case of high-temperature FCs), the Higher Heating Value (HHV) equal to 142 MJ/kg or 39.44 kWh/kg can be used instead [121, 122]. The electric power provided by the FC is defined by Eq. (2.24) as the product of voltage and electric current.

$$P_{\text{Cell}} = V_{\text{Cell}} \cdot I_{\text{Cell}} \tag{2.24}$$

Due to the high power demand in aviation applications, multiple FCs are packed in series forming what is called *stack*, and multiple stacks are eventually packed in parallel to provide the necessary power [126]. Combining Eq. (2.23) and Eq. (2.24) the efficiency as the ratio between the two powers can be obtained, and it is reported in Eq. (2.25).

$$\eta_{\text{FC}} = \frac{V_{\text{Cell}} \cdot N_e \cdot F}{SE_{\text{H2}} \cdot mm_{\text{H2}}} = \frac{V_{\text{Cell}}}{V_{\text{Ref.}}} \tag{2.25}$$

In the equation, the efficiency of the single cell has been confused with that of the entire FC system, under the assumption that the cells work in parallel (i.e., the stack voltage is the sum of the cell voltages) and that the losses due to other components (e.g., air compressor) are negligible. The constant parameters that appear in Eq. (2.23) have been recombined into the single constant $V_{\text{Ref.}}$. The latter is equal to 1.252 V if the LHV has been chosen as the reference value, otherwise 1.484 V if the HHV has been chosen [122]. However, note that the choice of the reference value does not affect the calculation of hydrogen consumption. The hydrogen fuel flow, given by Eq. (2.26) is, in fact, connected to the energy extracted from the fuel divided by the specific energy, thus eliminating the dependence on the chosen reference heating value.

$$FF_{\text{FC}} = \frac{I_{\text{Cell}} \cdot mm_{\text{H2}}}{N_e \cdot F} \cdot N_{\text{Cell}} \cdot \frac{1}{\eta_{\text{Utilization}}} \tag{2.26}$$

In Eq. (2.26), N_{Cell} is the total number of cells composing the FC system, estimable as the ratio of the system's power demand and the power supplied by the single cell. Hydrogen consumption, however, can be penalized with a further utilization factor, representing the fraction of hydrogen extracted from the tank that the FC is capable of reacting. Typical values range between 0.70–0.90 [127, 128], but in this context they only influence the fuel consumption without affecting the power or emissions of the system. The amount of hydrogen reacted is associated with a mass of water produced linked to the stoichiometric ratios of the redox reaction. For

every molecule of hydrogen and oxygen atom, one molecule of water is produced. It follows that the EI of water, given by the ratio between the mass of emitted water vapor (mm_{H_2O} = 18.015 g/mol) and the mass of reacting hydrogen, is a constant value equal to 8.936 kg/kg.

In Eq. (2.25), the explicit dependence on the current intensity disappears, with the efficiency depending only on the voltage supplied divided by a constant. However, the output voltage may still depend on the value of the current intensity (and power) produced by the cell. This dependency is visible in Fig. 2.7, representing the characteristic curve of a real FC in terms of input current intensity and voltage response. When a similar model is available, the designer can query it to get the voltage associated with a given value of current intensity, the latter directly related to the power demand. From the voltage, the efficiency can be estimated as well by means of Eq. (2.25). In practice, powertrain equations (e.g., Eqs. (2.9)) can be solved initially for a first-guess value of efficiency. Therefore, the efficiency can be recalculated as explained above, and the powertrain equations can be solved in a new iteration step. As for other powertrain components, HEAD also offers the opportunity to model FC efficiency as a constant. However, as the efficiency can vary significantly with power demand, the characteristic curve approach is preferable when viable.

As a final consideration, it is possible to correct the estimate of efficiency and output power by including further penalties related to the presence of other components such as the centrifugal air compressor, typically associated with FC stacks to provide the necessary oxygen from the external air [122]. This is useful to capture the effects on the system performance of the high altitude conditions characterizing the flight, as the behavior of the compressor depends on the air characteristics. In this sense, the method described by Larminie and Dicks is also

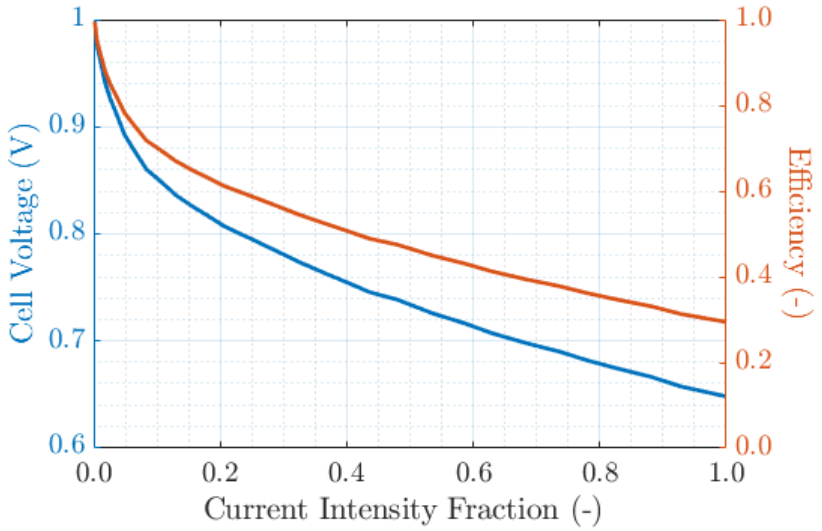

Figure 2.7: An example of fuel cell polarization curve for a Sinavy PEMFC (module FCM 34). Adapted from Ref. [129].

implemented in HEAD to describe the efficiency of a centrifugal compressor [122]. The required air flow rate for the reaction can be estimated from the stoichiometric ratios in the redox reaction. Therefore, the airflow can be used to estimate the flow conditions at the compressor inlet, assuming that isoentropic transformations occur in the air intake. Finally, through an efficiency map characterizing the compressor, it is possible to trace the efficiency of the compressor and the power loss associated with its use. In Ref. [130] the author proposes an application using a FC model coupled with a rubberized centrifugal compressor [122, 131, 132]. However, the inclusion of the compressor and the consequent variations in efficiency with operating conditions represents a second-order effect [130], overall negligible in the preliminary phase of the design. In Chapter 4, the proposed application will be based on already known efficiency functions provided by experts, which made it possible to calibrate the result of Eq. (2.25) without passing through the introduction of a compressor model.

Gearboxes, Electric Drives and Power Electronics

As for the powertrain components previously discussed, HEAD offers flexibility to integrate models as needed, for the characterization of secondary components such as gearboxes, electric machines, and power electronics [86]. Such an approach is effective in catching the aircraft-level effects of realistic models of industrial components. This flexibility will prove useful in applications involving cooperation with manufacturers or technology experts and will be exploited for the application in Chapter 3. As an alternative, it is possible to opt for methods adapted from the literature [133–135] or to assume constant values for the efficiencies, provided that the efficiency of the mentioned components is typically close to unity and generally undergoes negligible variations for a first approximation. This second approach is useful for preliminary applications, when detailed characterization of the components is still missing.

2.2.2 Mass Estimation

When dealing with hybrid-electric aircraft, one common mistake is to focus exclusively on the direct benefits of electrification in terms of fuel saving and emissions, without correctly evaluating the inertial penalties entailed by it. State-of-the-art batteries have a specific energy tens of times lower than the specific energy of fossil fuels. Hydrogen, although it has a specific energy up to three times higher than kerosene, needs to be stored in very heavy pressurized or cryogenic tanks. Overall, hybrid-electric systems include several elements preparatory to the generation, transmission, and conversion of electrical power, which affect the empty weight of the aircraft. Correctly characterizing the mass penalties due to hybridization is fundamental, as the consequent detriment of performance, the increase in necessary power, and the increase in energy demand for flight missions have the potential to reduce or compensate all the promised benefits. In this subsection, the aircraft mass estimation methods implemented in HEAD will be briefly discussed. Established

methods for mass estimation of the airframe and conventional systems are adopted from classical literature. They are complemented by methods for estimating the mass of typical components of hybrid-electric powerplants to obtain an estimate of the manufacturer empty mass (m_{ME}), and thus of the empty mass (m_{E}) also including the mass of furnishings $m_{\mathrm{Furnishing}}$ (see Eq. (2.27)).

$$m_{\mathrm{E}} = m_{\mathrm{Airframe}} + m_{\mathrm{Systems}} + m_{\mathrm{Powerplant}} + m_{\mathrm{Furnishing}} \tag{2.27}$$

Adding the mass of crew (m_{Crew}) and of the operating items (m_{Items}) to the empty mass leads to an estimation of the operating empty mass (m_{OE}), as in Eq. (2.28).

$$m_{\mathrm{OE}} = m_{\mathrm{E}} + m_{\mathrm{Crew}} + m_{\mathrm{Items}} \tag{2.28}$$

Finally, adding the mass of the payload (m_{Payload}) and fuel for the mission (kerosene or hydrogen), the aircraft's MTOM is obtained (Eq. (2.29)).

$$MTOM = m_{\mathrm{OE}} + m_{\mathrm{Payload}} + m_{\mathrm{Fuel}} \tag{2.29}$$

The weight estimation proposed in the literature for hybrid-electric aircraft is usually based on I-class methods, i.e., statistical approaches related to the category of interest, adapted to unconventional aircraft configurations. In this sense, de Vries et al. [26] have proposed a modification of classic methods for conventional aircraft [32, 34]. The I-class method proposed by Roskam et al. [34] based on weight fractions was adapted to the case of hybrid-electric aircraft [26]. However, the adapted method only allows for a preliminary estimate of the operating empty mass. For instance, the authors propose to evaluate the empty mass of an equivalent conventional aircraft, subtract the mass of the powertrain, and finally add the mass of the hybrid-electric powertrain including the innovative components [26]. In practice, at least II-class mass methods are necessary to characterize the mass breakdown at the system level properly. Methods proposed in classic literature are based on a preliminary knowledge of few geometric and propulsive characteristics but are tailored for conventional aircraft classes [32, 34, 36, 39, 40]. To be compliant with hybrid-electric architectures, existing II-class methods require the integration of new approaches to estimate the weight of the additional components of the propulsion system. In the present context, the main difference with classical methods deals with the evaluation of the propulsion system mass breakdown. A reference mass breakdown is visually represented by Fig. 2.8. In the following subsections, more details will be given about the several items that appear in Eqs. (2.27)–(2.29).

It is worth noting that estimating masses in a design workflow is a highly iterative process, suffering from the *snowball effect* resulting from any changes in geometry, power demand, or design conditions in general. In this sense, the mass estimation typically takes place multiple times within a single design cycle, being itself the primary reason for the highly iterative nature of preliminary design. Although some methods will be explicitly mentioned and presented in the next subsections, it is important to consider that the HEAD framework offers enough flexibility to easily enrich its library of methods by integrating new relationships for mass estimation. In

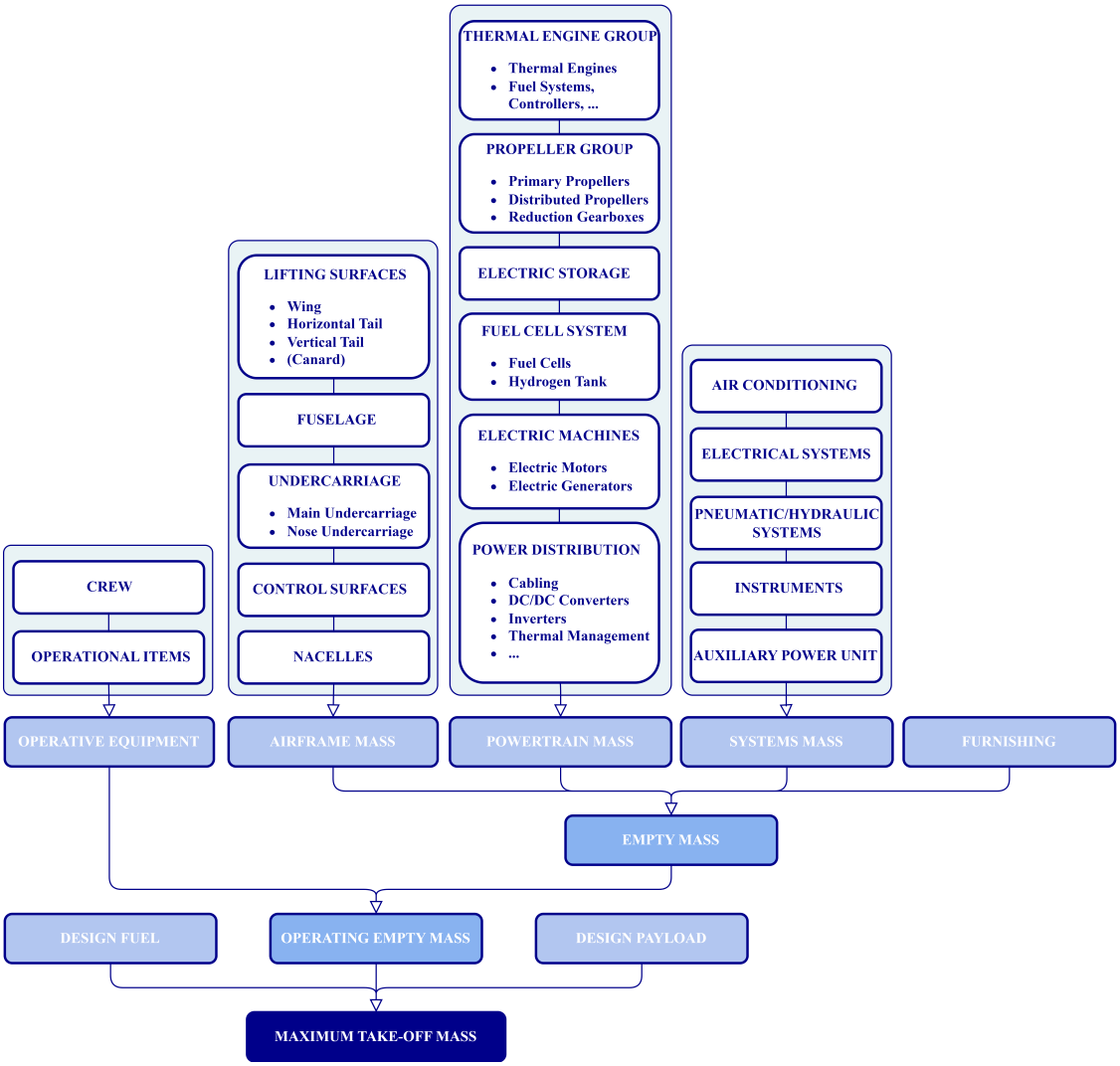

Figure 2.8: Components of the maximum take-off mass of an aircraft considered in the design tool.

the context of research projects involving collaboration with industrial and academic partners, this feature will prove useful in reducing the number of iterative steps and calibration processes that usually characterize collaborative design activities.

Airframe Mass

The mass of the airframe can be characterized as the sum of the contributions of the main structural components. This includes the mass of lifting surfaces, control surfaces, fuselage, and undercarriage. Also, primary and secondary nacelles have been included among the airframe components, leading to the general expression of Eq. (2.30)

$$m_{\text{Airframe}} = m_{\text{Lifting Surfaces}} + m_{\text{Undercarriage}} + m_{\text{Control Surfaces}} + m_{\text{Nacelles}} + m_{\text{Fuselage}} \tag{2.30}$$

The mass of the lifting surfaces can further be broken down into the masses of the wing and tailplanes. In this context, the classical Torenbeek's method is still considered useful for estimating the mass of these components [32]. Wing mass is primarily related to the geometry of the wing, including the wing area, the aspect ratio, the planform shape, and the distribution of chords and section thickness [32]. Moreover, the method allows for penalties in case there are spoilers, breaks, and nacelles installed on the wing [32]. Finally, the dependence on the MTOM supports the need for multiple iterations to estimate the mass of the aircraft [32]. The method is considered valid in light of the conventional nature of wings for regional aircraft, and has been adopted for the application in Chapter 3 lacking better alternatives. However, it is anticipated here that in Chapter 4 Torenbeek's method will be replaced by a novel method generated thanks to international collaborations in the context of the GENESIS project [15, 136, 137]. The method used in Chapter 4, calibrated for a 50-seat regional aircraft, will allow for better consideration of the impact of multiple nacelles distributed on the wing structure [136, 137]. As for the horizontal and vertical tailplanes, both will be treated by using Torenbeek's estimating relationship. Again, Torenbeek links mass to surface geometry and the aircraft category (e.g., *regional turboprop*) [32]. Masses of the main and nose undercarriage, control surfaces, and nacelles are estimated as well using Torenbeek's formulation [32].

Systems

For estimating conventional onboard systems, classic estimating relationships have been adopted as well. The contributions taken into account are summarized in Eq. (2.31).

$$\begin{aligned} m_{\text{Systems}} = m_{\text{Air Conditioning}} + m_{\text{Electrical}} + m_{\text{Pneumatic/Hydraulic}} \\ + m_{\text{Instruments}} + m_{\text{Auxiliary Power Units}} \end{aligned} \tag{2.31}$$

Primarily, Torenbeek statistically connects system masses to aircraft category, cabin volume, design payload and range, and manufacturer empty mass and take-off mass of the aircraft [32]. Only for the estimation of the air conditioning and anti-icing system, the method proposed by Nicolai et al. has been preferred, in light of its combined sensitivity to the dimensions of the fuselage and the number of occupants [36].

Furnishing, Crew, and Operating Items

According to Torenbeek's definition, $m_{\text{Furnishing}}$ includes contributions related to thermal and acoustic insulation, emergency equipment, seats, galleys, lighting, and water installation [32]. The formulation proposed by the same author in 2013 has been preferred for estimating the furnishing mass, seeing the dependence on the dimensions of the fuselage [39]. The mass of the crew is calculated by considering a mass of 95 kg (inclusive of baggage) for pilots and flight attendants [32, 138, 139]. The operational items, according to Torenbeek's formulation, are proportional to the number of passengers [32].

Payload and Fuel

While the payload is generally a top-level requirement and is assigned, the mass of assigned fuel (or fuels) can be estimated in different ways depending on the desired degree of approximation. Weight fraction method combined with the Breguet range equation is useful for a preliminary estimate [26, 32, 34]. After the sizing phase, if the time durations of each flight phase and the necessary powers are known, the necessary fuel can be obtained by combining the energy consumed with the fuel specific energy. According to the same criterion, in a simulation-based mission analysis, the fuel mass is calculated for each time step, querying efficiency maps and engine decks for a more accurate estimate. In the case of hybrid-electric architectures, fuel (or hydrogen) consumption must take into account the hybridization ratio used, as explained in Subsection 2.2.1. Finally, in the present context, a fuel reserve is typically considered sufficient to perform a diversion to an alternative airport, a loiter phase, and an additional % reserve in the tank.

Powertrain

The mass of the powertrain constitutes the main difference compared to the mass breakdown of conventional aircraft. In the context of the applications that will be presented later, the total powerplant mass is particularized as in Eq. (2.32).

$$\begin{aligned} m_{\text{Powertrain}} = m_{\text{Thermal Engines}} + m_{\text{Propellers}} + m_{\text{Electric Storage}} \\ + m_{\text{Fuel Cells}} + m_{\text{Electric Machines}} + m_{\text{Power Distribution}} \end{aligned} \tag{2.32}$$

In the absence of more elaborate models, a practical way of defining the mass of the generic powertrain component is through the specification of its specific power, i.e., the nominal power it is capable of generating or exchanging divided by its mass. Once the power is known, the mass of the generic component can therefore be estimated through Eq. (2.33), where SP_{Element} represents the specific power in kW/kg and P_{Element} is the nominal power in kW.

$$m_{\text{Element}} = \frac{P_{\text{Element}}}{SP_{\text{Element}}} \tag{2.33}$$

The reference power is chosen as the peak power required to satisfy the flight mission requirements and all the other constraints imposed as top-level requirements for the aircraft. In this sense, the resolution of the powertrain equations seen in Subsection 2.2.1 is useful for translating the propulsive power requirement (or at the level of any specific power node) into requirements for each other component. This approach can potentially be used for any component, including the FC system, electric motors and generators, and power electronics. The mass of converters and inverters can be estimated by considering the power of the component with which they are associated. As for the mass of the cables, it might be more convenient to consider a specific power per unit of length, as will be done for the applications presented below. In this case, the length of the cables can be estimated as a first

approximation by considering the distances of the wing-mounted electric machines from the locations of the electrical power supply devices.

In the case of FC systems, it may be convenient to isolate the mass of the tank, as it is a function of the mass of hydrogen to be stored. In this regard, the ratio between the mass of the stored hydrogen and the mass of the full tank is defined as *gravimetric efficiency*, or *gravimetric index* GI (Eq. (2.34)). Even considering a fixed GI value, the mass of the tank is strongly affected by variations in the mass of stored hydrogen, especially for pressurized tanks for which typical values are below 10% [122, 140]. When evaluating the mass of the tank, m_{H2} should also include reserves and unusable fuel.

$$GI_{\text{Tank, H2}} = \frac{m_{\text{H2}}}{m_{\text{H2}} + m_{\text{Tank, H2}}} \tag{2.34}$$

As for batteries, it should be noted that the power requirement is not always the most demanding since it can be used moderately for a long period of time, consuming all the energy without ever reaching peak power. This happens, for example, when the battery is mainly used in long cruise phases, where if the mission duration is fixed, the energy demand can easily become more limiting than the power requirement. In general, it is a good approach to evaluate, case by case, which is the most demanding one between the power and energy requirements. Thus, the estimate of the mass of the electric storage system is given by Eq. (2.35), where $SE_{\text{E-ST}}$ and $SP_{\text{E-ST}}$ are, respectively, the specific energy and the specific power at the system level.

$$m_{\text{Electric Storage}} = max\left(\frac{P_{\text{E-ST}}}{SP_{\text{E-ST}}}\ ,\ \frac{E_{\text{E-ST}}}{SE_{\text{E-ST}}}\right) \tag{2.35}$$

The total energy capacity, $E_{\text{E-ST}}$, is estimated on the basis of the assigned mission profile and may also account for a lower limitation on the SOC, as discussed in Subsection 2.2.1. Eq. (2.36) gives an approximate relationship that links the specific energy to the specific power, useful for determining the specific power starting from information on the maximum prescribed C-Rate. The formula is correct if the variations of the battery voltage with C-Rate and SOC are neglected, or if the definition of $SE_{\text{E-ST}}$ and $SP_{\text{E-ST}}$ is related to an operating condition where the voltage is equal to its integral average value.

$$SP_{\text{E-ST}} = C\text{-}Rate \cdot SE_{\text{E-ST}} \tag{2.36}$$

If the specific power of any component does not also take into account the thermal management system (TMS), the latter can be considered separately. In this case, the sizing power is equal to the produced heat H_{Element} to be dissipated, which can be calculated as the product between the power and the complement to the unity of the component's efficiency, according to Eq. (2.37)

$$H_{\text{Element}} = P_{\text{Element}}\ (1 - \eta_{\text{Element}}) \tag{2.37}$$

Regarding the conventional components, classical methods are adopted from the literature. Gudmundsson provides semi-empirical relations for estimating engine

dry mass as a function of rated power [40]. Alternatively, HEAD's library also integrates the surrogate model developed by Di Stasio et al. [109], better discussed in Chapter 4. The contribution of the fuel system and engine controls has been included using the relationships proposed by Raymer [141], while the mass of the engine starter is estimated with the approach of Nicolai et al. [36]. The latter has also been preferred to estimate the mass of the primary and secondary propellers [36]. Gearboxes are estimated using the correlation found by Hendricks et al. [142], which relates mass to exchanged torque. However, the relation is strictly valid for spur gearboxes and should not be used for planetary gearboxes unless there are no better alternatives. As already mentioned, the HEAD library also contains some surrogate methods derived from regressions on real data. In this sense, in Refs. [86, 91] the reader will find useful estimating relationships, the result of the close collaboration between the University of Naples and industrial partners in the context of the ELICA project [16]. The formulas are useful for estimating the mass of electric machines and gearboxes as the gear ratio and exchanged torque vary.

Balance

The balance module allows to calculate the aircraft's center of gravity (CG) position at different weight conditions (e.g., operating empty, maximum take-off), starting from an estimation of the CG position of each component, as well as the boarding diagram and the operative CG positions. Once again, semiempirical methods are useful for estimating the position of conventional components [32, 41]. However, in the case of the presence of innovative components such as batteries, FCs, and hydrogen tanks, the choice of position on board the aircraft is left free to the user, but could have a significant impact on the balance. Batteries or tanks located at the rear of the fuselage could lead to significant setbacks in the CG which would lead to stability problems in a classic tube-wing configuration. In design exploration applications such as the one presented in Chapter 4, a simplified approach is preferable as also anticipated in Section 2.4, in which it is assumed to always be able to balance the aircraft in light of the possibility of allocating the masses (e.g., batteries, FC systems) based on the designer's freedom of choice.

2.2.3 Aerodynamics Estimation

Aircraft aerodynamics play a crucial role in the design and performance of any aircraft. HEAD implements classic relationships from the literature for estimating the main aerodynamic characteristics of an aircraft, to which the individual airframe components wetted by the air contribute [36, 39, 41, 86, 143, 144]. These include lifting surfaces, nacelles, and landing gears, as well as penalties for interferences and corrections related to flight Reynolds number. In terms of lifting surfaces, the starting point is the definition of airfoils' characteristics. The analyst may choose to manually assign each aerodynamic parameter required to model the lift curve, or to select a generic NACA airfoil from a dedicated internal database, based on the data

reported in Ref. [143]. From the database, all necessary values to automatically produce the curves of lift, drag and pitching moment are collected. To estimate the friction drag of lifting surfaces, it is first necessary to evaluate the skin friction coefficient as a function of the Reynolds number, the latter including the effect of altitude and flight speed [41]. The assessment of the fuselage aerodynamics is done using the FusDes method developed by the DAF research group [144] which also provides an estimate of the moment coefficients. The lateral-directional aerodynamics are mainly characterized by using the approach of Perkins [145]. Drag produced by the nacelles is assumed to be lift-independent and accounts for both skin friction and form drag, according to the equations reported by Nicolai et al. [36]. The drag contributions of the individual components are combined into the aircraft parasitic drag coefficient, CD_0, by evaluating the wetted surfaces of each of them on a geometric basis, then rescaling the drag coefficients with respect to the wing surface [36, 41]. In parallel, the Obert method is used to estimate the Oswald factor e [42]. Additional wave drag contributions, although included in the HEAD workflow, will be reasonably neglected for regional aircraft applications. Thus, the parabolic polar model of Eq. (2.38) can be used to estimate the aircraft drag, providing good approximation in subsonic conditions.

$$CD = CD_0 + \frac{CL^2}{\pi\ AR\ e} \tag{2.38}$$

In Eq. (2.38), AR is the wing aspect ratio. The aerodynamic drag is obtained by multiplying the drag coefficient by the reference (wing) surface and the dynamic air pressure. In the evaluation of a specific flight condition, if the parabolic polar coefficients are known, it is possible to evaluate the force necessary to counteract the total drag. The maximum lifting capabilities of the surfaces, mainly estimated with Sforza's method [41], are expressed in terms of the maximum lift coefficient obtainable in clean and flapped conditions. Changes in the lift curve, pitching moment, and drag coefficient due to flap deflection are considered as explained by Torenbeek [32]. The aircraft can, in general, be trimmed, in the sense of being balanced with respect to the longitudinal moment about the CG. In the case of the CG being forward of the wing's aerodynamic center, a tail down force is required, so that also the wing is required to produce a lift greater than that necessary to balance the weight of the aircraft [41]. The resulting increase in drag relating to Eq. (2.38), known as trim drag, is considered as well in HEAD [34, 41, 86]. Moreover, a forward CG can increase the stability of the aircraft but may also require more lift at the same angle of attack, which could affect the maximum lift coefficient negatively. Additional checks ensure that the aircraft's maximum lift coefficient does not exceed the maximum that can be trimmed [86]. Finally, the lift coefficient is useful for determining the stall speed, which is especially important for evaluating ground performance. In HEAD, it is possible to calculate the characteristic aerodynamic coefficients in a specified number of flight conditions, which reflect the reference altitude and speed conditions that will characterize the operational mission. By reasonably assuming constant coefficients within the same flight phase, it is in this

way possible to apply the method for a limited number of aerodynamic conditions avoiding simulations of the aerodynamics at each time step.

However, if on the one hand conventional aerodynamics depend on factors that vary weakly during the mission, the argument is different for aero-propulsive effects. Seen as one of the main enabling technologies for regional air transport, the aero-propulsive effects generated by means of propellers distributed along the wing are calculated by HEAD as described in Ref. [86]. Placing secondary propellers spanwise and upstream of the wing can increase the dynamic pressure, enhancing the wing loading [50, 114, 146–148]. Given the innovative nature of DEP systems that will be included in the applications presented below, some insights into the method used to correct conventional aerodynamics to take into account aero-propulsive benefits are given herein. The approach, inherited from Patterson's work [50, 114, 146], has its theoretical foundations in the propeller momentum theory already mentioned in Subsection 2.2.1. DEP systems can be used to augment high-lift capabilities at low speed. If properly designed, high-lift propellers aim to improve the wing-blowing. To improve the axial velocity, and thus the high-lift capability, a near-uniform axial velocity must be produced aft of the propeller [149]. The aerodynamic interaction between the propeller slipstream and the lifting surface can be used to increase the lift coefficient and reduce the necessary wing surface in ground phases requiring high lifting capabilities. However, this effect has the drawback of increasing the drag coefficient as well. In this context, the effects of the lifting surface on the propeller efficiency due to the upwash are not considered. The interaction between the propeller slipstream and the lifting surface, on which the propulsion system is mounted, depends on the geometry of the two elements. This requires a dimensionless description of the geometry of the wing as well as the geometry of the distributed propulsive architecture since geometry is not fixed yet at this stage.

With reference to Fig. 2.9, it is assumed that the system is characterized by N_{P} propellers ($N_{\mathrm{P}}/2$ propellers per half-span) of diameter $D_{\mathrm{P,i}}$ and radius $R_{\mathrm{P,i}}$. The position and the distribution of the propulsion system and the propeller disks can be defined by specifying the fraction of the wingspan covered by the DEP and the gap between two consecutive propellers. In this sense, $D_{\mathrm{P,i}}$ can be determined by equally dividing the space available by N_{P}. In the applications that will be presented, this approach will be used, considering the entire portion of the wingspan that goes from the wing tip to the primary propeller or, in general, to the wing kink. In addition, $X_{\mathrm{P,i}}/c$ specifies the axial position of the propeller disk from the leading edge divided by the local chord. The actuator disk theory drives the estimation of the axial induction factor at the propeller disk as a function of the thrust and the diameter of the propeller, as already seen in Eq. (2.13). However, the axial induction influencing the aerodynamics coefficient should be evaluated at the aerodynamic center of the lifting surface. In this sense, the axial induction factor aft the propeller can be corrected by Eqs. (2.39)–(2.41), which first calculate the *contraction ratio* of the slipstream at 1/4 of the airfoil chord (Eq. (2.40)), then they use it to quantify the

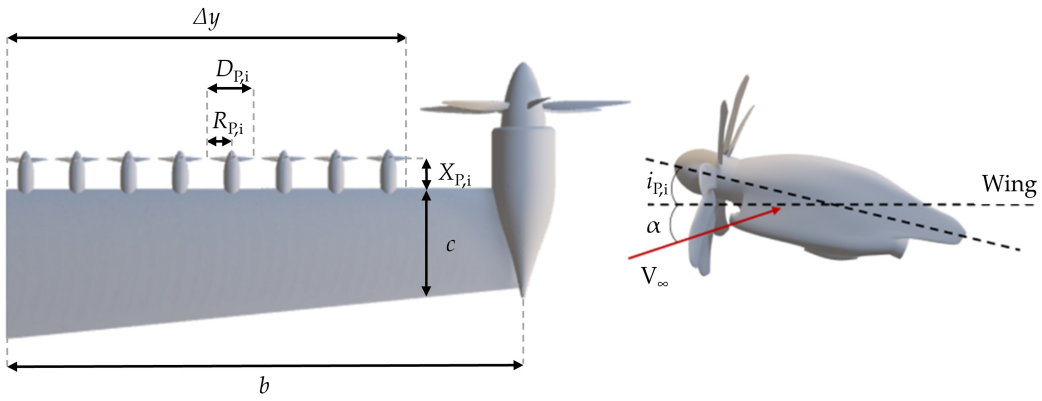

Figure 2.9: An example of a distributed electric propulsion system and its geometric description (adapted from Ref. [86]).

acceleration of the flow from the position of the propeller to the aerodynamic center of the surface, in terms of change in the axial flow at the new coordinate (Eq. (2.41)).

$$\frac{X_{c/4}}{R_{P,i}/c} = \frac{X_{P,i}/c + 1/4}{R_{P,i}/c} \tag{2.39}$$

$$\frac{R_{c/4}}{R_{P,i}} = \sqrt{\frac{1 + a_{P,i}}{1 + a_{P,i}\left(1 + X_{c/4}/\sqrt{{X_{c/4}}^2 + {R_{P,i}}^2}\right)}} \tag{2.40}$$

$$a_{c/4} = \frac{1 + a_{P,i}}{\left(R_{c/4}/R_{P,i}\right)^2} \tag{2.41}$$

The increase in induced speed translates not only into an increase in the total speed of the flow investing the airfoil but also into a reduction in the effective angle of attack [114]. In this sense, what contributes to the total lift is not only the increase in dynamic pressure but also a variation in circulation linked to the velocity component transverse to the flow, possibly caused by a non-zero angle of incidence of the propeller, $i_{P,i}$. From the Kutta-Žukovsky theorem, Eq. (2.42) gives the variation of the lift coefficient for the wing section.

$$\Delta Cl = 2\pi \sin\alpha \left[\left(1 - \frac{a_{c/4}\beta_s \sin i_{P,i}}{\sin\alpha}\right)\sqrt{1 + 2a_{c/4}\beta_s \cos\left(\alpha + i_{P,i}\right) + \left(a_{c/4}\beta_s\right)^2} - 1\right] \tag{2.42}$$

In Eq. (2.42), α is the aerodynamic angle of attack, and β_s is a correction factor accounting for the finiteness of the slipstream. The factor β_s takes on particular importance when $R_{c/4}$ is little compared to the local airfoil chord [114]. To estimate the value of this correction, HEAD adopts the surrogate model proposed by Patterson in Ref. [114] derived from computational fluid dynamics (CFD) analyses. As derived by de Vries et al. [26], once the increase in lift is known, it is also possible to estimate the increment in drag coefficient, composed of one component of induced drag and one linked to the skin friction coefficient C_f, as expressed by Eq. (2.43).

$$\Delta Cd \approx {a_{c/4}}^2 C_f + \frac{2\,CL\,\Delta Cl}{\pi\,AR\,e} \tag{2.43}$$

The first term represents the increase in friction drag on the wing surface due to increased dynamic pressure in the slipstream, while the second term depends on the three-dimensional lift coefficient CL of the lifting surface and represents the change in lift-induced drag due to the propeller-induced lift. As for the pitching moment coefficient, assuming that the aerodynamic center and the pressure center remain almost unchanged for subsonic flow, the change in pitching moment coefficient depends directly on the change in lift and can be estimated by Eq. (2.44) [51].

$$\Delta Cm_{\mathrm{c}/4} \approx \frac{\Delta Cl}{Cl} Cm_{\mathrm{c}/4} \tag{2.44}$$

As a final step, it is necessary to convert the two-dimensional coefficients into coefficients relating to the entire lifting surface. Strictly speaking, the evaluation of the three-dimensional coefficients should be obtained by integrating the lift and drag characteristics over a number of airfoil sections along the lifting surface. However, as suggested by Patterson, a simpler way to extend the method above to three dimensions consists of rescaling the two-dimensional result with respect to the fraction of the wing surface actually blown by the propellers [114]. As a first approximation, one could consider a rectangular wing planform or a mean reference chord [26]. This translates into multiplying the coefficients by the fraction $\Delta y/b$ of the wingspan b affected by the propellers, as in Eqs. (2.45)–(2.47) [26, 86].

$$\Delta CL = \Delta Cl \frac{\Delta y}{b} \tag{2.45}$$

$$\Delta CD = \Delta Cd \frac{\Delta y}{b} \tag{2.46}$$

$$\Delta CM_{\mathrm{c}/4} = \Delta Cm_{\mathrm{c}/4} \frac{\Delta y}{b} \tag{2.47}$$

As can be deduced from the presence of α in Eq. (2.42), the evaluation of the effective aerodynamic coefficients may require multiple iterations. In fact, if the lift coefficient needed by the aircraft in a given flight phase is known, an initial value of α can be estimated using Eq. (2.48), which relies on an approximation of the lift curve slope for finite wings [34].

$$\alpha \approx \frac{CL}{2\,\pi\,AR\,e} \left(2 + \sqrt{AR^2 \left(1 - {M_\infty}^2\right) \left(1 + \frac{\tan^2 \Lambda_{\mathrm{c}/2}}{1 - {M_\infty}^2}\right) + 4} \right) \tag{2.48}$$

In Eq. (2.48), M_∞ is the flight Mach number and $\Lambda_{\mathrm{c}/2}$ is the surface's sweep angle evaluated at half of the local chords. Therefore, the value found can be used to estimate ΔCL through Eqs. (2.42) and (2.45), from which a new estimate of the total CL of the lifting surface can be obtained. The process is repeated until convergence is achieved. In this way, the maximum lifting capabilities of the aircraft are also improved, although penalized by an increase in drag. The result is a reduction in stall speed and improved take-off and landing performance. This is in synergy with the application of electric propulsion because it combines the

practical distribution of thrust across multiple propellers with the possibility of balancing the mass penalty on ground performance entailed by electric systems. As said, the method implemented in HEAD benefits from the calibration carried out by Patterson; however, Orefice also offers in Ref. [86] additional sanity checks for regional aircraft applications, based on cross-validations with CFD results.

As a final note, HEAD is also capable of capturing the beneficial effect of a propeller tip installation on the drag coefficient. As a matter of fact, the wingtip vortex can be mitigated by installing a propeller at the wingtip. Similarly to what has been seen for the effect of distributed propulsion, the induced drag coefficient can be corrected by considering a reduction in the induced angle of attack, weighted by the portion of the wing surface actually blown by the tip propellers. This additional contribution was implemented and further verified by Orefice in Ref. [86]. Beyond the axial induction, the flow rotation due to the propeller slipstream can also have an effect on the components of the aerodynamic force produced by the local airfoil. Assuming a certain rotation direction of the propeller, the tangential induction is a measure of the ratio between the propeller's angular speed and the angular speed induced on the flow downstream of the propeller, and it can be used to estimate the vertical speed induced by the slipstream. The tangential induction due to the propeller can be computed through Eq. (2.49) [150]. As a consequence, the angle of attack induced by the propeller is approximated by Eq. (2.50) [86], and under the hypothesis of propeller rotating in the opposite direction with respect to the wing tip vortex (i.e., inner-up direction), this contribution mitigates the induced angle of attack and therefore the drag.

$$a_{\mathrm{t,P,i}} = \frac{1}{2} - \sqrt{\frac{1}{4} - \frac{{V_\infty}^2 \ (1 + a_{\mathrm{P,i}})\, a_{\mathrm{P,i}}}{\left(R_{\mathrm{P,i}} \ RPM_{\mathrm{P,i}} \ \frac{2\pi}{60}\right)^2}} \tag{2.49}$$

$$\alpha_{\mathrm{i,P}} \ \approx \ \frac{a_{\mathrm{t,P,i}} \ R_{\mathrm{P,i}} \ RPM_{\mathrm{P,i}} \ \frac{2\pi}{60}}{(1 + a_{\mathrm{P,i}}) \ V_\infty} \tag{2.50}$$

2.3 Point Performance

2.3.1 Sizing Approach

Aircraft sizing is a preliminary step in designing an aircraft, where its performance is estimated based on power and wing loading to meet assigned requirements and certification standards. In this sense, the classical approach described by Roskam is widely known and adopted [34]. Different relationships, representing performance requirements in different flight phases or certification constraints, are combined together and often represented as *constraint curves* in the form of a single *sizing plot*, where each point represents a combination of power-to-weight ratio and wing loading [34]. The constraints bound the area of the sizing plot compatible with all requirements, that is, the *design space*. Therefore, the choice of a *sizing*

point, combined with a preliminary estimate of the aircraft's mass, is sufficient to size the wing area and the necessary engine power. These parameters are the starting point for detailing the geometry of the entire aircraft, which can lead to more accurate estimates of inertial, aerodynamic, and propulsive characteristics and, ultimately, a new assessment of the aircraft's performance. Even in the case of unconventional aircraft, the constraint curves of the sizing plot are a function of aviation regulations [138, 139] as well as aircraft minimum performance requirements. In particular, Part 23, "Certification Specifications for Normal-Category Aeroplanes", is applied to "Aeroplanes with a passenger seating configuration of 19 or less and a maximum certified take-off mass of 8 618 kg (19 000 lb) or less" [138]. On the other hand, Part 25, "Certification Specifications for Large Aeroplanes", is applicable to turbine-powered large airplanes with any weight and size [139].

The introduction of hybrid-electric architectures requires some adaptations compared to the classic methodology. First, as pointed out by several authors [26, 60, 86, 151], since the sizing activity defines the boundaries of the design space, the introduction of the aero-propulsive effects can enlarge the design space leading to new design opportunities. Second, the sizing activity should be general and reproducible for any powerplant architecture, including conventional, full-electric, and hybrid-electric. Given the complex nature of the powertrain, it is important to express the power loading in terms of total propulsive power rather than installed source power, taking into account the different levels of hybridization adopted. HEAD implements a version of the classic constraint relationships that take into account aero-propulsive effects, adapting the original approach proposed by de Vries et al. [26, 86]. Semi-empirical constraints are adopted for take-off and landing phases, to link the requirements on take-off and landing distance to the propulsive power-to-weight ratio and the wing loading [32, 34]. Different from the classic literature, the lift coefficient is corrected to take into account the aero-propulsive benefits as described in Subsection 2.2.3. As already mentioned, the estimation of ΔCL requires an iterative approach, whose first attempt may consist of imposing the absence of aero-propulsive effects ($\Delta CL = 0$). The iterative process must be repeated for each point of the constraint curve in the sizing plot, i.e., for each value of the propulsive power. Combined with the propeller efficiency, the propulsive power leads to a thrust value according to statistical correlations [34]. The fraction of thrust relating to the DEP can be determined as a function of the shaft power ratio assigned by the designer for the phase. In the case of two propulsion lines, where the secondary line models the DEP, the thrust produced by DEP is given by Eq. (2.51).

$$T_{\mathrm{P2}} = \frac{T_{\mathrm{P1}} + T_{\mathrm{P2}}}{1 + \frac{\eta_{\mathrm{P1}}}{\eta_{\mathrm{P2}}} \left(\frac{\varphi}{1-\varphi} \right)} \tag{2.51}$$

The thrust produced by the single propeller can be also obtained by dividing T_{P2} by the number of distributed propellers N_{P}. The efficiencies η_{P1} and η_{P2} of the primary and secondary propellers respectively, can be assigned or calculated iteratively using

Eqs. (2.13) and (2.15). The resulting value of the axial induction factor is finally used to estimate the aero-propulsive effects, as explained in Subsection 2.2.3.

Similarly, the cruise constraint is modeled as in the classic literature as well [34]. The relationship between the wing loading and the propulsive power-to-weight ratio is based on the equilibrium along the vertical and longitudinal axes of the wind reference frame. In particular, the equilibrium along the vertical axis defines the relationship between the required lift coefficient and the assigned wing loading, while the equilibrium condition along the longitudinal axis relates the power-to-weight ratio to the drag coefficient. Although, in this case, the lift coefficient is dictated by the equilibrium condition, evaluating the aero-propulsive effects is still of interest for the calculation of the drag coefficient, influencing the necessary power-to-weight ratio. Finally, the power-to-weight ratio is rescaled by the aircraft mass fraction between cruise and take-off conditions, which can be assumed statistically [32, 34], in order to refer the constraint curve to the same reference condition in take-off. The same approach considered to evaluate cruise constraints can be adopted for the climb by also including a term referring to the required climb gradient into the equilibrium equations. Climb constraints are generally applied to flight phases immediately after the take-off phase or before the touchdown during the landing phase. Regulation constraints dealing with altitude, landing gear configuration, number of operative engines, climb gradient or rate of climb, and operating speed are specified in Refs. [138, 139]. More specifically, the normative references are §CS 23.65, §CS 23.67, §CS 23.77 for Part 23 [138], and §CS 25.111, §CS 25.119, §CS 25.121 for Part 25 [139]. Their implementation in the form of constraint curves, although it follows the procedure proposed in the classical literature [34], features a correction in the lift and drag coefficients (and, therefore, aerodynamic efficiency) to take into account the aero-propulsive effects [86–88]. The ceiling altitude in all engine operating (AEO) conditions preserves the classic definition. On the other hand, to preserve generality and simplicity at this stage, one engine inoperative (OEI) conditions can be considered by introducing a thrust loss factor, to be specified by the designer. The factor can be preliminarily assumed to be equal to 50% of the total thrust. However, in the case of DEP, this assumption may be too conservative, and a higher factor can be preferable (e.g., relating to the loss of only one propeller, parallel to the conventional case). In this regard, the reader will find in Appendix B details on a more refined model for the simulation of failure applied to aircraft with hybrid-electric architecture. Figure 2.10, adapted from Ref. [86], represents the entire sizing workflow based on the choice of the sizing point.

A set of TLARs, representing the set of product requirements or designer preferences, constitutes the real starting point for the design of a new aircraft. Based on TLARs, a statistical *pre-design* activity is carried out for initializing the aircraft geometry on a statistical basis and is accompanied by a preliminary (*I-class*) estimate of the aircraft masses. Statistics collected by the DAF group at the University of Naples are implemented based exclusively on conventional aircraft in light of the lack of data available for unconventional propulsion architectures. Despite this limitation, the pre-design only serves to initialize the sizing process,

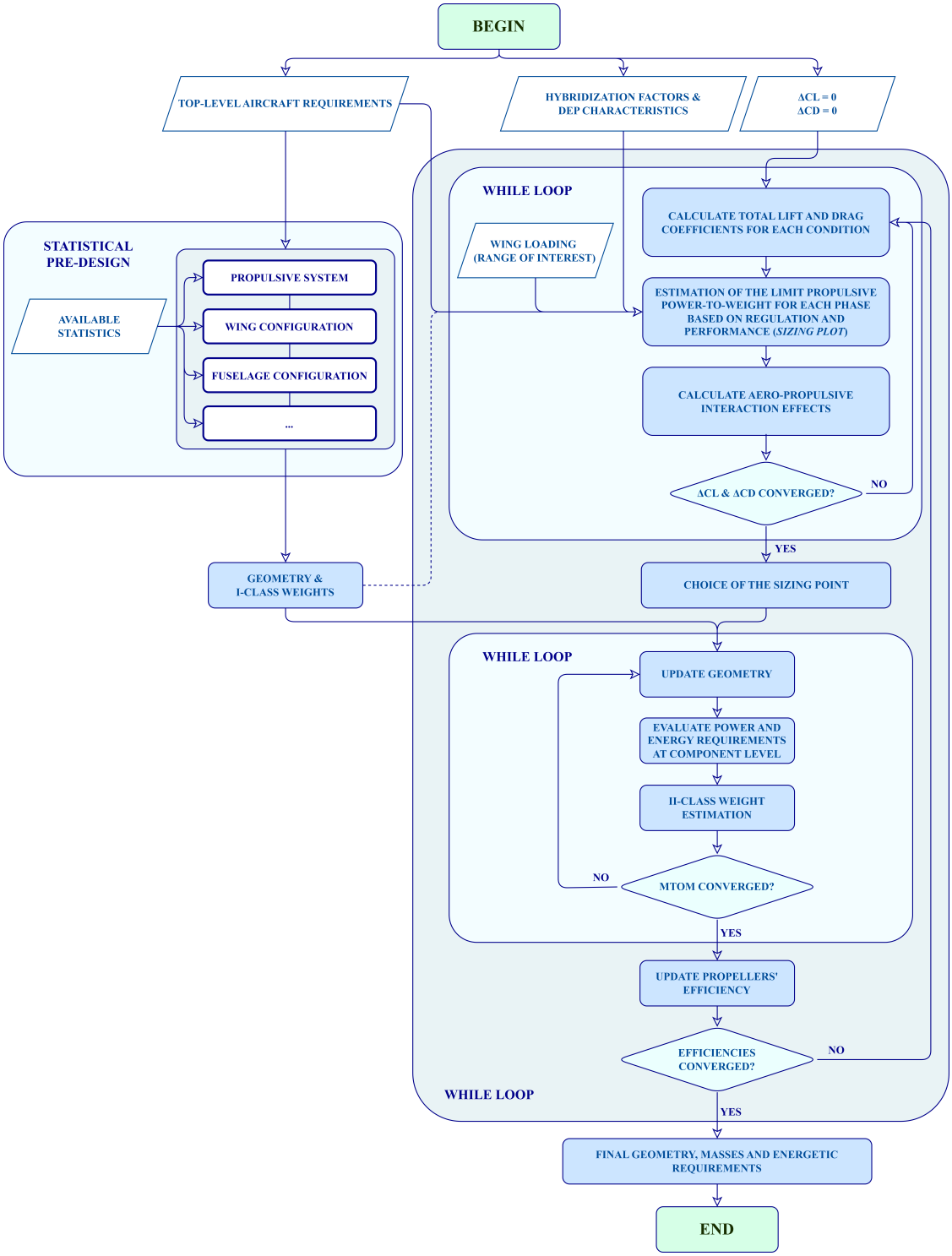

Figure 2.10: Conceptual design process based on point performance, as implemented in HEAD (adapted from Ref. [86]).

without affecting in a significant way the final result in light of the highly iterative nature of the sizing activity that will be discussed below. The designer is also asked to choose the propulsion architecture, specifying the number of propellers or

electric machines, the components' efficiency, and the hybridization ratios for the different flight phases. In the case of DEP, the percentage of wing area covered by distributed propellers is also considered as a design parameter. The sizing process begins with the construction of the sizing plot, i.e., the individual constraint curves discussed above in terms of wing loading and propulsive power-to-weight ratios. In the case of DEP, the aero-propulsive effects are initially neglected, to be then evaluated iteratively on the basis of the propulsive power values characterizing each curve. When the process ends due to the achievement of convergence, the designer can freely choose the sizing point, or automatically make the choice fall on the point of the available design space corresponding to the maximum wing loading and minimum weight-to-power ratio. Figure 2.11 shows an example of a sizing plot as produced by HEAD for a hybrid-electric regional turboprop aircraft with DEP. The figure also shows the advantage of the chosen hybrid-electric architecture compared to the conventional case. In the example shown, the hybrid-electric architecture is, in fact, able to significantly reduce the wing area (i.e., increase the wing loading), mainly thanks to the benefit of the DEP on take-off and landing performance.

Combined with the I-class estimation of the MTOM, the sizing point provides the values of the wing surface area and propulsive power. At this point, the geometry can be updated based on the new wing surface, according to different possible strategies. In this context, the update process is performed keeping some parameters constant, including the wing loading, the wing aspect ratio, the volumetric ratio of the tailplanes, the diameter of the primary propellers, the number of distributed propellers, and the fraction of wing span that they cover. The wing chords are updated to maintain the same aspect ratio and chord ratios assigned during initialization. The diameter of the secondary propellers is updated based on

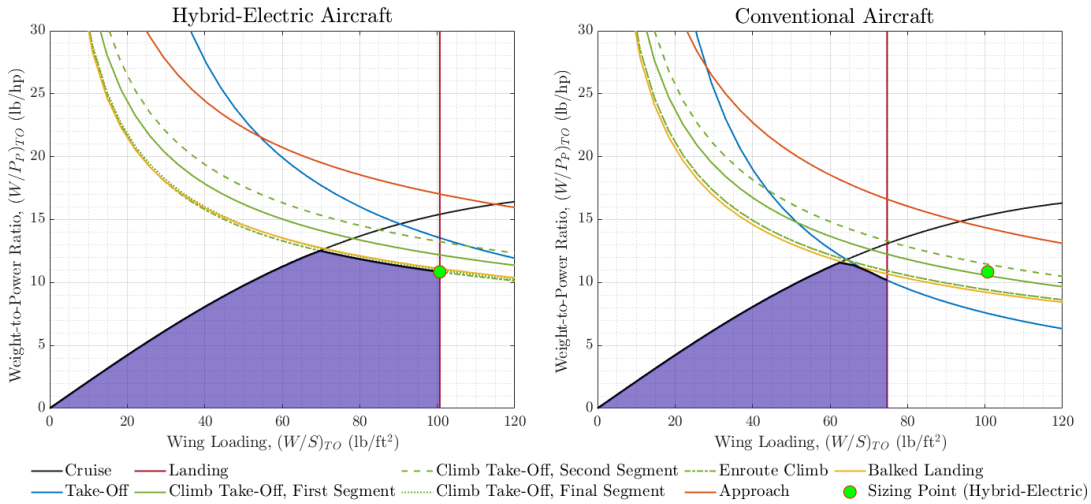

Figure 2.11: An example of a sizing plot produced by HEAD. The plot refers to a hybrid-electric turboprop aircraft featuring a series/parallel partial hybrid architecture with batteries and DEP. The figure also shows a comparison with conventional architecture, highlighting the benefits in terms of enlarged design space (colored purple).

the new wing span. The tail planes are resized as well, based on the new surface area that guarantees the same volumetric ratio. The geometry update is a necessary, but not sufficient, step to obtain a refined estimate of the aircraft's masses. In this sense, it is also necessary to evaluate the sizing powers of the individual powertrain components on the basis of the propulsive power requirement. The power-to-weight ratio that derives from the sizing point refers to the propulsive power requirement in the most demanding flight condition. Depending on the flight phase, different operating modes, hybridization factors, and efficiency characterize the powertrain and its components. Powertrain equations can be solved multiple times for each flight condition, starting from the selected value of (maximum) propulsive power. Hence, the highest values obtained for each element along the flight mission represent the sizing ones. Using the same approach, the powers associated with each energy source for each flight phase are also derived. Provided that TLARs also specify the duration of the individual flight phases or that the latter is deductible (e.g., by assigning cruise speed and range, it is possible to obtain the cruise time), energy consumptions can be estimated by simply multiplying powers and time durations. At this point, the mass breakdown of the aircraft can be estimated using more sophisticated (*II-class*) methods, discussed in Subsection 2.2.2. A new MTOM estimate is obtained, likely discordant from the I-class estimate resulting from the pre-design. For this reason, a new iterative loop is triggered, which updates the wing surface again based on the same wing loading derived from the sizing plot. The geometry and masses are refined again, and so on until convergence. Finally, the efficiency characteristics are updated again, with particular reference to the efficiencies of the propellers. In fact, when using certain models like the one represented by Eq. (2.15), the efficiency of the propellers may be linked to the diameter of the propellers and the thrust produced, both variables depending on the weight and the geometry of the aircraft. Since the propeller efficiency affects the aero-propulsive effects, the entire sizing process should be repeated in case of discrepancy with the initial estimate. Once convergence is achieved, the definition of the aircraft will finally be complete in terms of geometry, masses, and mission energy requirements. The resulting sized aircraft can be a useful starting point for the designer to make refinements to the geometry or installed powers, or for a subsequent more accurate evaluation of characteristics and performance. For instance, the mission analysis performed in the sizing phase in terms of energy and power requirement is very simplistic, as it only evaluates a point performance, without considering possible variations in efficiencies and operating conditions during the same phase. In this sense, a more accurate mission and performance analysis is often needed, and the HEAD module responsible for this will be discussed in Section 2.4. Before that, the next subsection proposes a verification of the results of the HEAD sizing module.

2.3.2 Validation

This subsection briefly presents a validation of HEAD's sizing workflow. In a context where there is a lack of information regarding flying hybrid-electric prototypes, the verification was based on a comparative analysis with similar methods in existing literature. The methodologies developed by FH Aachen and TU Delft have served this purpose [60]. Although the application of Chapter 4 will mainly be based on the alternative workflow presented in the next section, it recalls the same hybrid-electric aircraft model adopted in the sizing module and whose consistency is verified here. However, further validation of the alternative workflow will be proposed in the next section.

First, the reliability of the module in the case of conventional aircraft was demonstrated through a case study based on the DO-228NG [152], and the results are reported in Tab. 2.3. The similarity of the results regarding the conventional aircraft chosen as the baseline for the comparison was deemed satisfactory, always being under 5% error compared to expected values [60, 152], in some cases even providing better alignment than other methods.

For assessing the module's applicability to unconventional aircraft designs, analyses of both a parallel hybrid-electric and a full-electric concept were conducted. The figure of merit used as a reference for the comparison was the Payload-Range Energy Efficiency (PREE), defined as the product of payload and range divided by the energy required to complete the mission. The metric, originally chosen by the authors of Ref. [60], is emblematic in the context of hybrid-electric aircraft design, where the objective is to evaluate the influence of design parameters on fuel energy savings. All technological levels and assumptions have been considered the same as reported in Ref. [60]. Graphical comparisons in Fig. 2.12 reveal variations in PREE with changes in range and supplied power ratio, as also predicted by the other literature methods. The results of the comparison are also reported in Tab. 2.4, both in terms of PREE and MTOM. The differences are always less than 5% when compared with the TU Delft approach, and slightly higher when compared with the FH Aachen method. In any case, the differences are considered small and acceptable for design applications at the conceptual level, especially in light of the similarity of the trends shown in Fig. 2.12. Furthermore, HEAD's estimates appear to be more

Table 2.3: Validation of the sizing activity based on the comparison with methods proposed in Ref. [60], for the case of the DO-228NG [152] (adapted from Refs. [86, 93])

Parameter	Unit	DO-228NG	HEAD	FH Aachen	TU Delft
Wing Area	m^2	32.0	32.15 (+0.47%)	32.3 (+0.94%)	32.2 (+0.63%)
Wing Loading	N/m^2	1 962	1974 (+0.61%)	1 957 (-0.25%)	1 958 (-0.20%)
Power-to-Weight Ratio	W/N	18.44	18.61 (+0.92%)	18.65 (+1.14%)	18.63 (+1.03%)
Maximum Take-Off Mass	kg	6 400	6471 (+1.11%)	6 641 (+3.77%)	6 416 (+0.25%)
Operative Empty Mass	kg	3 900	3964 (+1.64%)	3 866 (-0.87%)	3 865 (-0.90%)
Fuel Mass	kg	540	547 (+1.30%)	615 (+13.89%)	591 (+9.44%)
Payload Mass	kg	1 960	1960 (+0.00%)	1 960 (+0.00%)	1 960 (+0.00%)
Engine Dry Mass	kg	349	350 (+0.29%)	356 (+2.01%)	354 (+1.43%)

Table 2.4: Change in PREE and MTOM for different supplied power ratios and ranges, as estimated by HEAD's sizing module, for a parallel hybrid-electric concept whose conventional baseline is the DO-228NG [152]. Results are compared with the sizing methods proposed in Ref. [60], using HEAD's predictions as the reference. Data related to the sweep on range is shown graphically in Fig. 2.12a, while the data related to the sweep on supplied power ratio is shown in Fig. 2.12b (adapted from Refs. [86, 93]).

Φ	Range	MTOM			PREE		
		HEAD	FH Aachen	TU Delft	HEAD	FH Aachen	TU Delft
Sweep on Range							
0.0	200 km	5 850 kg	-1.2 %	-0.6 %	0.60	+4.5 %	-1.3 %
0.0	300 km	6 069 kg	-1.3 %	-0.6 %	0.58	+3.4 %	-0.5 %
0.0	400 km	6 306 kg	-1.3 %	-0.6 %	0.56	+2.9 %	-0.4 %
0.0	500 km	6 561 kg	-1.3 %	-0.6 %	0.54	+2.4 %	-0.2 %
0.0	600 km	6 837 kg	-1.3 %	-0.6 %	0.52	+2.1 %	-0.4 %
0.0	700 km	7 137 kg	-1.3 %	-0.5 %	0.50	+1.8 %	-0.4 %
0.0	800 km	7 465 kg	-1.4 %	-0.5 %	0.48	+1.5 %	-0.6 %
0.0	900 km	7 823 kg	-1.4 %	-0.5 %	0.45	+3.3 %	+1.3 %
0.0	1 000 km	8 217 kg	-1.4 %	-0.5 %	0.43	+3.0 %	+0.9 %
0.1	200 km	5 917 kg	-1.1 %	-0.8 %	0.65	+2.9 %	+2.2 %
0.1	300 km	6 169 kg	-1.1 %	-0.8 %	0.62	+2.9 %	+2.3 %
0.1	400 km	6 446 kg	-1.1 %	-0.8 %	0.60	+1.7 %	+1.2 %
0.1	500 km	6 746 kg	-1.1 %	-0.7 %	0.57	+2.1 %	+1.8 %
0.1	600 km	7 077 kg	-1.2 %	-0.7 %	0.54	+2.8 %	+2.4 %
0.1	700 km	7 440 kg	-1.2 %	-0.7 %	0.52	+1.5 %	+1.2 %
0.1	800 km	7 837 kg	-1.1 %	-0.7 %	0.49	+2.2 %	+1.8 %
0.1	900 km	8 289 kg	-1.2 %	-0.7 %	0.47	+0.9 %	+0.6 %
0.1	1 000 km	8 813 kg	-1.5 %	-0.9 %	0.44	+1.6 %	+1.4 %
1.0	200 km	6 758 kg	-1.5 %	-0.4 %	2.41	+10.6 %	+2.1 %
1.0	300 km	7 468 kg	-1.6 %	-0.3 %	2.13	+9.3 %	+3.1 %
1.0	400 km	8 346 kg	-1.7 %	-0.2 %	1.88	+9.0 %	+3.8 %
1.0	500 km	9 456 kg	-1.8 %	-0.1 %	1.65	+8.6 %	+3.9 %
1.0	600 km	10 907 kg	-1.9 %	+0.0 %	1.42	+8.8 %	+4.4 %
1.0	700 km	12 885 kg	-2.1 %	+0.2 %	1.20	+8.6 %	+4.2 %
1.0	800 km	15 738 kg	-2.3 %	+0.4 %	0.98	+8.8 %	+4.1 %
1.0	900 km	20 215 kg	-2.7 %	+0.8 %	0.76	+9.3 %	+3.9 %
1.0	1 000 km	28 257 kg	-3.4 %	+1.5 %	0.54	+10.6 %	+3.9 %
Sweep on Supplied Power Ratio							
0.0	396 km	6 297 kg	-1.3 %	-0.6 %	2.41	+3.0 %	-0.2 %
0.1	396 km	6 434 kg	-1.1 %	-0.7 %	2.13	+1.8 %	+1.3 %
0.2	396 km	6 596 kg	-1.2 %	-0.7 %	1.88	+3.2 %	+2.7 %
0.3	396 km	6 767 kg	-1.3 %	-0.6 %	1.65	+2.6 %	+2.1 %
0.4	396 km	6 949 kg	-1.4 %	-0.5 %	1.42	+3.7 %	+3.0 %
0.5	396 km	7 143 kg	-1.4 %	-0.5 %	1.20	+4.0 %	+3.1 %
0.6	396 km	7 349 kg	-1.5 %	-0.4 %	0.98	+4.5 %	+3.3 %
0.7	396 km	7 568 kg	-1.5 %	-0.4 %	0.76	+5.3 %	+3.5 %
0.8	396 km	7 799 kg	-1.6 %	-0.3 %	0.54	+6.4 %	+3.8 %
0.9	396 km	8 043 kg	-1.6 %	-0.3 %	1.54	+7.6 %	+4.2 %
1.0	396 km	8 297 kg	-1.6 %	-0.3 %	2.54	+4.0 %	+4.0 %

conservative, leading to generally higher aircraft masses and, consequently, lower PREE compared with the other two approaches. This outcome is attributed to the application of II-class mass estimation methods in the module, which account for additional structural weight due to increased onboard battery mass. In general, when increasing the battery mass stored on board, the operative empty mass increases.

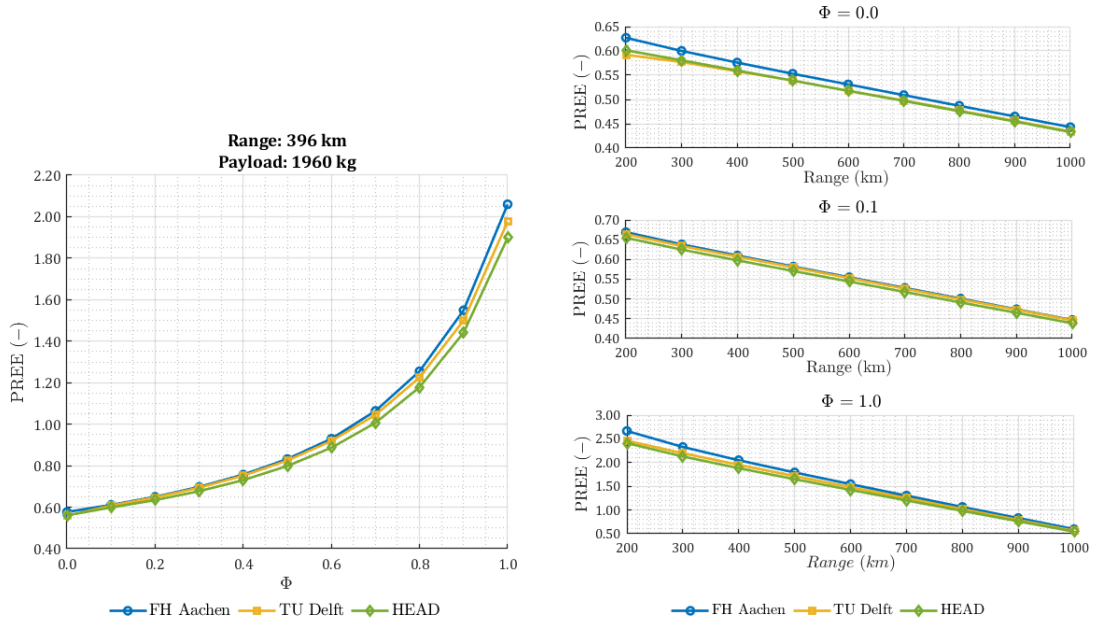

(a) Sweep on supplied power ratios **(b)** Sweep on ranges

Figure 2.12: Change in PREE for different supplied power ratios and ranges, as estimated by HEAD's sizing module, for a parallel hybrid-electric concept whose conventional baseline is the DO-228NG [152]. Results are compared with the sizing methods proposed in Ref. [60] (adapted from Refs. [86, 93]).

However, in the case of II-level methods, the masses of certain components, such as the undercarriage or wing, depend on the maximum zero-fuel mass of the aircraft, causing a more rapid (*snowball*) increase in the total weight of the aircraft [32]. This effect becomes more critical considering a higher range or a lower specific energy value for the battery. Being the operative empty weight higher, the same goes for the energy requirements for mission completion. In light of these considerations, the proposed cross-validation was deemed sufficient for the purposes of the analyses covered in the next chapters. In particular, the comparison made it possible to verify the correct implementation of the routines for estimating the inertial and propulsive characteristics of the aircraft, as well as for updating the geometries.

2.4 A Workflow Based on Mission Analysis

2.4.1 Mission Analysis and Performance

To perform a comprehensive simulation-based mission analysis, assessing the influence of hybrid-electric propulsion on various parameters throughout the aircraft's flight mission is crucial. Achieving a simulation-based analysis entails characterizing each step of the entire flight mission by considering its aerodynamic and propulsive characteristics. Consequently, aspects that define the aircraft's state at each step,

including Mach number, altitude, throttle setting, acceleration, rate of climb, etc., need to be determined to simulate the flight history accurately. The mission analysis of hybrid-electric aircraft also requires the definition of hybridization factors phase by phase. On the other hand, the approach proposed in this section relies on simplified hypotheses that make the mission analysis module suitable for the early stages of the aircraft design process. In particular, a major assumption consists of modeling the aircraft as a point mass, neglecting angular accelerations. Furthermore, time steps of approximately one minute are considered for most phases, since higher time resolution would increase the computational load without being necessary for preliminary design applications.

The following three phases of the algorithm are executed at each time step, with the order depending on the specific flight segment:

- The aerodynamic characteristics are computed from the flight conditions at the beginning of the flight segment.
- The power distribution across the propulsion system is determined based on the prescribed airspeed and altitude.
- The new flight conditions are determined by calculating both the effects of aerodynamic and propulsive forces.

In scenarios involving aero-propulsive interactions, the first two steps are chained in an iterative process [89]. Regardless of the flight phase, consumption and emissions are evaluated at each time step, through querying the engine deck and solving the powertrain equations. In fact, the power associated with each energy source also derives from the latter, which, when multiplied by the time duration, provides an estimate of the energy consumed. The decrease in the mass of the aircraft linked to fuel consumption is also taken into account for greater accuracy.

A detailed simulation of the *take-off* phase can be fundamental to evaluate some aircraft performance, such as balanced field length (BFL) and decision speed, or the necessary sizing power of some components of the propulsion system. To evaluate the take-off run, the approach proposed in Refs. [38, 43] is adopted in HEAD [38, 43, 86]. First, the phase is divided into time steps, characterizing the evolution of the speed, altitude, and thrust produced. Based on speed and altitude, the engine deck (see Section 2.2.1) is queried to estimate the thermal engine power at full throttle. Similarly, the efficiency maps of all powertrain components (where available) are interrogated, and the efficiency values feed the powertrain equations' system matrix. The resolution of the powertrain equations provides the total propulsive power based on the efficiency of each element at the time step considered. From propulsive power and airspeed, the total thrust can be determined. Then, the interactions between the propulsive slipstream and the lifting surfaces are considered to calculate the aerodynamic forces. During the ground roll, the total longitudinal force acting on the aircraft is given by thrust, aerodynamic drag, and friction. The effect of the aero-propulsive interactions on drag and lift is accounted for as well, directly affecting the acceleration and, thus, the time by which the lift-off speed is reached. The acceleration is calculated as well, depending on the aircraft mass. Finally, the equation that expresses the longitudinal equilibrium

of the body is integrated at the time step to eventually obtain an updated speed value. The ground phase ends when the lift-off speed is reached, here assumed as 1.10 times the stall speed. The latter is also affected by the use of DEP since an increment in the maximum lift coefficient implies a lower stall speed and, thus, lift-off speed. Continuing with a simplified approach, the second part of the take-off phase, represented by the airborne phase, is modeled as the portion of a pull-up maneuver performed at a constant speed, set at 1.15 times the stall speed. The latter is directly affected by aero-propulsive interactions between DEP and the main lifting surface. When simulating a failure during the take-off run, the procedure for measuring the BFL assumes that at each time step, the most critical failure for the propulsion system occurs. Starting from that moment, two different procedures can be adopted. On the one hand, the aircraft can continue the take-off phase with the residual propulsive power, requiring a longer run to reach the lift-off speed. On the other hand, the pilot can decide to abort, braking the aircraft within a certain distance. Both procedures are simulated to measure the BFL, that is the value where, at the occurrence of the failure, the distance to decelerate and stop is equal to the take-off distance. For the purposes of the analyses in Chapter 4, the reference failure will be represented by the loss of half of the primary propulsion system, in analogy with the case of a conventional twin-engine aircraft.

As for the simulation of the *climb* phase, HEAD subdivides the climb into two different segments. The adopted standard procedure considers a first segment of climb up to 1 000 ft performed at constant calibrated air speed (CAS). After an acceleration of 20 kts, thrust is cut back, and a second climb segment up to 3 000 ft is performed. Finally, after accelerating to the desired climb speed, one last segment is performed up to the cruise altitude [38]. The presence of acceleration phases and the use of take-off engine settings during the early steps of these procedures require a different approach in terms of supplied and shaft power ratios for the different climb phases. In fact, during the first climb steps, using the same value of shaft power ratio as in take-off would be beneficial in light of the limited flight speed and the high thermal power to be distributed. On the other hand, the use of shaft and supplied power ratios higher than zero in the following climb step have negligible or null benefits. The simulation of the climb phase occurs similarly to what has already been discussed for the take-off phase. At each time step, for the associated altitude, the climb setting of the engine deck is queried for the prescribed airspeed. Using the powertrain equations, the propulsive power is calculated, as well as the thrust and the aero-propulsive interactions. Finally, the rate of climb is calculated based on the excess of power available, and it is used to update the aircraft's altitude for the next time step.

The *cruise* phase is modeled considering constant, assigned values of the altitude and the flight Mach number. Also in this case, the propulsive characteristics are deducible from the assigned operating conditions, and moving from the associated value of thrust, the aero-propulsive effects on lift and drag can also be evaluated. However, different from the previous phases, the necessary throttle setting is determined by moving from the aerodynamic drag. In this sense, an iterative

process is necessary to correctly account for the variation in drag coefficient linked to the aero-propulsive effects.

The *descent* properly said ranges from cruise altitude up to 1 500 ft above airport altitude. The procedure for evaluating the propulsive and aerodynamic characteristics is similar to what has already been discussed for the climb phase, with the engine set to idle. Similar to the climb, an approach based on constant CAS is also applied to the simulation of the descent. A multi-stage descent procedure is applied as suggested by Filippone [38]. After decelerating to a descent speed, the first segment takes the aircraft down to 10 000 ft with a flight path constrained to an angle of $-3°$. Then, the aircraft is decelerated, and a new descent occurs to the target altitude of 1 500 ft [38]. The *approach* phase ranges from 1 500 ft above the ground to the reference obstacle height (50 ft). It is a complex phase managed by landing instruments that couples descent and deceleration while changing high-lift device settings [38]. In this context, each time step can be considered as a descent phase at constant CAS, following a rectilinear flight path constrained by a descent slope of $-3°$. The approach speed is set as a multiple of the landing stall speed (considering a factor of 1.3 for CS-23 [138] and 1.23 for CS-25 [139]), thus being affected by aero-propulsive effects.

The *landing* phase is the last step of the nominal flight mission. As for the take-off, it can be divided into an airborne phase and a ground phase, flown at a minimum power setting. The considerations dealing with the propulsion system and the aero-propulsive interactions made in the case of take-off also apply to landing. During the airborne phase, a descent is firstly carried out on a straight path, with constant flight angle and speed. Following, a flare segment joints the first part of the trajectory to the ground roll. The flare speed is set to an intermediate value between the approach speed and the touchdown speed [43, 138, 139]. After touchdown, the last segment is the ground run, which is governed by the same forces considered for the take-off run, with the only additional contribution to the force provided by brakes and any thrust reverser [38, 43, 86].

Last but not least, the taxi-in and taxi-out phases are approximately considered by HEAD in order to include an additional fuel reserve. By specifying the taxi time, fuel consumption can be estimated by querying the engine deck at the idle setting.

In case of air traffic congestion at the landing airport, or any critical or unexpected condition, the aircraft could be required to hold the flight path by the air traffic control. Therefore, to include energy reserves, additional phases may also be included in the mission profile, preceding the approach to landing. These include an *alternate* (or diversion cruise) to a different airport, which consists of an additional cruise phase at a constant altitude and Mach number. Also, a *loiter* (or *holding*) phase may be included, during which the aircraft is required to hold while waiting to land. In this context, both phases are managed as an additional cruise phase at constant altitude and Mach number. However, the loiter is characterized by a holding time rather than a range to travel. In these phases, the flight speed is usually reduced to increase efficiency and reduce energy consumption [38, 86]. In the case of hybrid-electric concepts, the use of electric energy during these

phases may not be recommendable, especially in the case of electric storage systems with low values of specific energy. In fact, the need to transport reserve energy could seriously penalize the mass and performance of the aircraft. Rather, for the applications that will be presented below, fuel consumption will always be preferred over secondary energy sources for the reserve phases.

2.4.2 Design Workflow

Typically, the sizing of an aircraft is conventionally conducted through a methodological approach [34], which, with some adjustments, can be applied to a hybrid-electric airplane, as outlined by Orefice et al. [86, 87] and seen in Section 2.3. However, employing such a method may result in significant disparities between the expected performance from the sizing phase and the outcomes derived from a detailed mission analysis, particularly considering the complexities introduced by hybrid-electric architectures. These disparities are influenced, for example, by assumptions of constant values for the efficiencies of various powerplant components. Conversely, simulating the entire mission and referencing lookup tables for the efficiencies of ICEs and other powertrain components can yield more accurate results and a more cohesive design approach. Hence, the need emerges for a new design workflow capable of precisely modeling and assessing the impact of hybridization ratios on performance and fuel consumption. The workflow, that is described in this subsection, will be adopted for the design explorations covered in Chapter 4. In that context, it will be helpful in accurately understanding the impacts of new technologies by modeling both their benefits and drawbacks through integrating several surrogate models and technology assumptions based on experts' judgment.

The exploration of hybrid-electric concepts introduces numerous novel design parameters, particularly when incorporating multiple unconventional power sources. For example, adopting DEP often implies opting for series/parallel partial hybrid architectures due to the necessity of managing two independent propulsion lines depending on the flight phase. From a designer's perspective, the value of the shaft power ratio at take-off holds significance as it not only dictates the extent of aero-propulsive effects but also influences the values of sizing power for the electrical components of the powertrain, such as electric motors and generators. Alongside managing two propulsive lines, designing any electric or hybrid-electric platform is complicated by the battery mass, along with all the associated mass penalties linked to hybridization. The greater the degree of hybridization (i.e., the supplied power ratio in individual flight phases), the higher the aircraft's mass. The optimal point, corresponding to maximum fuel reduction, relies on the battery use strategy during the flight mission. Utilizing batteries during longer phases directly reduces energy extracted from the thermal source. Simultaneously, employing electric power from the battery to assist primary power compensates for the aircraft's weight increase, preventing oversizing of thermal engines while maintaining the same performance. Given these initial considerations, determining the optimal set of hybridization parameters often requires a meticulous examination

of each combination's positive and negative impacts. Instead of selecting a fixed set of parameters, it is more advisable to fine-tune the hybridization strategy during parametric analyses to identify the most promising combinations between conventional and innovative propulsive solutions.

A systematic approach has been pursued to enhance result accuracy. The flowchart illustrated in Fig. 2.13 provides a simplified representation of the proposed design workflow, with a more detailed explanation available in Fig. 2.14. A flight simulation-based approach is implemented to comprehensively evaluate the effects of masses and efficiencies in all design phases. This includes integrating weight estimation models considering mass items typically excluded in the aircraft pre-design phase. The workflow follows an iterative process, estimating aircraft performance after determining geometric and aerodynamic characteristics in the preceding steps of the design loop. Initially, primary geometric characteristics are initialized based on a baseline aircraft, with key parameters like the size of lifting surfaces possibly varied. Concurrently, hybridization factors are chosen for each flight phase. The design mission, modeled according to specified requirements, undergoes simulation with minute-level time steps for most flight phases. Parameters such as take-off field length (TOFL) and service ceiling are also assessed. If installed powers prove inadequate for completing all mission phases or meeting one or more TLAR, adjustments are made accordingly. Similarly, powers are scaled down if they exceed requirements' demand. Component masses and aerodynamic characteristics, including aero-propulsive effects, are updated before starting a new mission simulation. In Fig. 2.14, the control variable for convergence is the

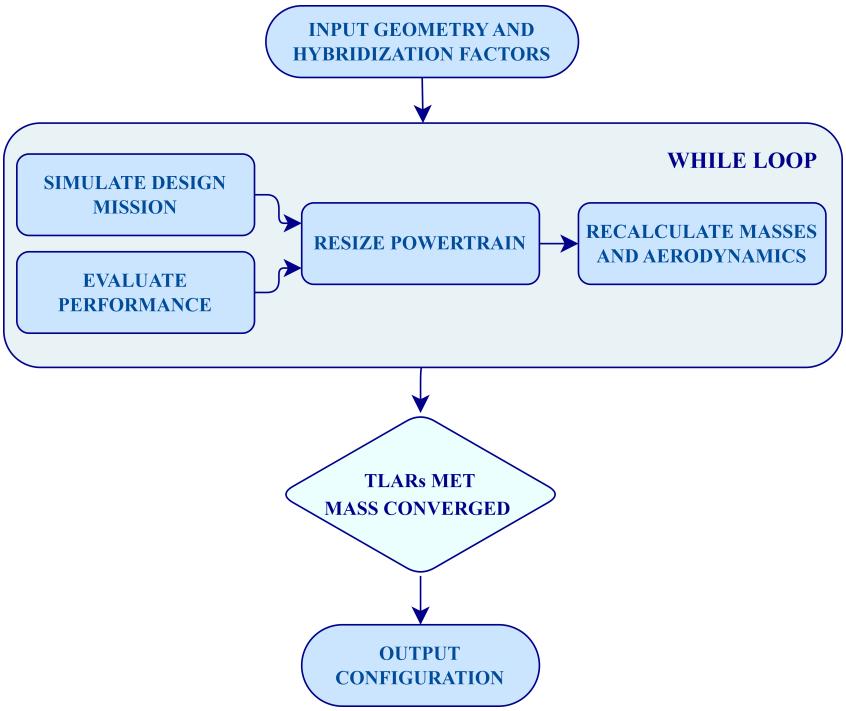

Figure 2.13: Simplified aircraft design workflow based on mission analysis (adapted from Ref. [153]).

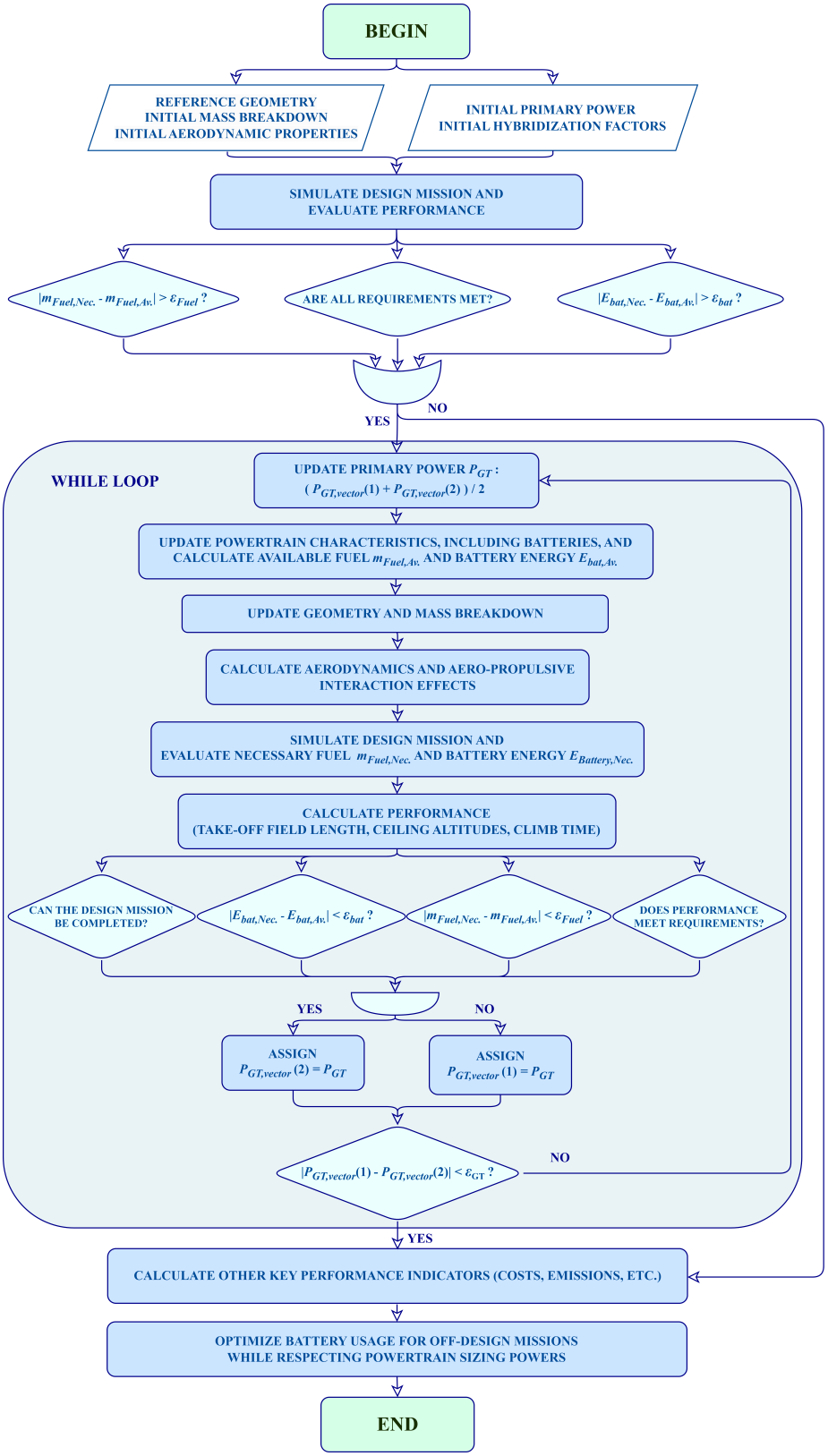

Figure 2.14: Detailed design workflow based on mission and flight performance analysis, suitable for hybrid-electric and conventional concepts (adapted from Ref. [153]).

power of the primary source (e.g., the thermal engine, or a FC system in case of hydrogen-based configurations) serving as the basis for updating sizing powers of other elements (e.g., electric machines, power electronics, energy storage systems).

The illustrated workflow can be used for investigating flight performance or designing a platform that fulfills a set of assigned mission and performance requirements. However, the starting point to initialize the process outlined in Fig. 2.14 is the definition of a particular powertrain architecture and specific geometric and hybridization parameters. These crucial parameters usually cannot be predetermined at the initial stages of the design process. Thus, design of experiments (DOE) studies may become necessary to identify the best combination of design parameters, aiming to minimize fuel consumption. DOE studies should also involve, in most cases, wing planform parameters to fulfill the entire set of requirements and design constraints, especially when faced with substantial increases in aircraft mass resulting from innovative propulsion technologies. To address this, a method has been developed and applied to systematically update both the wing and overall aircraft geometry when modifying the aforementioned wing geometry parameters. The original spanwise chord ratios are preserved when changes are made to the wing parameters in comparison to the baseline aircraft wing. First, the wing span is adjusted according to the updated area and aspect ratio. Consequently, the chords are extended or shortened in a manner consistent with the new wing surface and total span values. Finally, the horizontal and vertical tailplanes undergo resizing to ensure the volumetric ratios remain consistent with the original geometry of the baseline aircraft [32]. The horizontal tail volumetric ratio $\overline{V_h}$, defined as in Eq. (2.52), and the vertical tail volumetric ratio $\overline{V_v}$, defined as in Eq. (2.53), are kept constant as the wing area S_w varies.

$$\overline{V_h} = \frac{S_{\mathrm{h}} \cdot l_{\mathrm{h}}}{S_w \cdot MAC_{\mathrm{w}}} \tag{2.52}$$

$$\overline{V_v} = \frac{S_{\mathrm{v}} \cdot l_{\mathrm{v}}}{S_w \cdot b_w} \tag{2.53}$$

In the previous equations, MAC_{w} represents the mean aerodynamic chord of the wing, S_{h} and S_{v} are respectively the surface areas of horizontal and vertical tailplanes, l_{h} is the longitudinal distance between the aerodynamic centers of the wing and horizontal tail, and l_{v} is the longitudinal distance between the aerodynamic centers of the wing and vertical tail. For an assigned aspect ratio of the wing, a new value of the wing total span b_{w} is derived while preserving the plan form. After the wing geometry is updated, horizontal and vertical tails are modified accordingly, following the same approach adopted for the wing. In case updated planform areas lead to unfeasible geometries (i.e., vertical tail extending beyond the fuselage tail cone cap), l_{h} and l_{v} are also updated by adjusting the position of the tail. The update of the tail geometry is repeated until convergence is reached and the volumetric ratios match target baseline values. In case of innovative configurations such as involving hydrogen-based powerplants, it may be necessary to stretch the cylindrical portion of the fuselage to provide room for the installation of gaseous

or cryogenic hydrogen tanks, in addition to the controls of tail movables (i.e., elevator and rudder) and the auxiliary systems. In anticipation of this need, an algorithm for updating the fuselage geometry has also been implemented. When the fuselage is stretched, the longitudinal position of the wing in the body reference frame is automatically updated to keep the original relative position of the wing attachment, l_{w}, as in Eq. (2.54).

$$l_w = \frac{X_{\mathrm{w}}^{\mathrm{Apex}}}{L_{\mathrm{f}}} \tag{2.54}$$

In Eq. (2.54) $X_{\mathrm{w}}^{\mathrm{Apex}}$ is the absolute position of the wing apex in the body reference frame, and L_{f} is the length of the fuselage. When modifications to the fuselage length occur, tailplane characteristics are accordingly updated by keeping the same volumetric ratios as the baseline values.

Before using the workflow for the study of Chapter 4, its correct functioning has been verified based on an existing conventional aircraft, which will be covered in the next subsection.

2.4.3 Verification of the Workflow

For the purposes of verifying the mission analysis and performance model, the ATR 42-600 [154, 155] was selected as a case study. On the one hand, this choice is justified by the availability of data provided by the manufacturer which can provide a comparison [154, 155]. On the other hand, it is anticipated here that the application of Chapter 4 will consider the ATR 42-600 as a conventional reference baseline for the exploration of hybrid and electric solutions. In this sense, a verification of the analysis tool for the specific case of the ATR42 is particularly relevant, since the concepts explored later will rely on the correct modeling of the baseline. The ATR42 is a regional airplane designed and manufactured by ATR [154], a joint venture founded at the beginning of the 1980s by the French manufacturer Aerospatiale (now Airbus) and by the Italian Aeritalia (now Leonardo). The ATR42 was the first regional aircraft designed by this joint venture, shortly followed by the 72 variant, an updated version with a stretched fuselage allowing to carry on board a higher number of passengers [156, 157]. The ATR 42-600 is the latest version of the ATR42 model. It was presented in 2007 and, compared to the previous -500 version, it featured several improvements allowing to increase efficiency, reduce fuel use, and thus lowering operating costs and direct emissions. These improvements also came from adopting new engines: Pratt & Whitney PW127M engines replaced the 127E model as the standard engine option, granting improved take-off performance. In 2021, a further updated version of the PW127 engine for the ATR 42-600, called PW127XT-M, was presented by Pratt & Whitney, granting a 3% improvement in terms of fuel burnt [113]. The main characteristics of the airplane in terms of geometry, general layout, and powerplant are reported in Refs. [154, 158]. Here, Fig. 2.15 provides a visual representation of the aircraft, together with its digital reconstruction obtained in HEAD.

The 726 nmi mission given in Ref. [154], with 48 passengers at 95 kg each and including typical fuel reserves, was assumed as the design mission. In particular, a flat cruise at 24 000 ft was modelled at a target Mach number of 0.48, corresponding to 289 kts of true air speed (TAS) [154]. An alternate range of 100 nmi was assumed as reported in Ref. [154], with a target altitude of 10 000 ft. For the holding phase, 30 minutes at 1 500 ft were assumed, whereas, for the taxi phase, 20 minutes in total (i.e., including both taxi-out and taxi-in phases) were assumed, with the taxi-in phase corresponding to 34% of the total taxi phase, as suggested by statistics [159]. The workflow presented in this section was used for the analysis, implementing statistical relationships for the estimation of masses and aerodynamics, as well as for the prediction of performance, energy consumption, and emissions. The engine deck for the description of the thermal engine was selected from the HEAD library [86]. The precise calibration of the engine deck was the result of previous scientific collaborations between the DAF group and Leonardo [86]. It is anticipated here that the rubber engine model will be adopted in Chapter 4 as the basis for the definition of new engines with improved efficiency. Methods from the literature were used for the estimation of the EIs [111, 160]. Table 2.5 provides information about the main results and directly compares them with actual values reported in Refs. [154, 157].

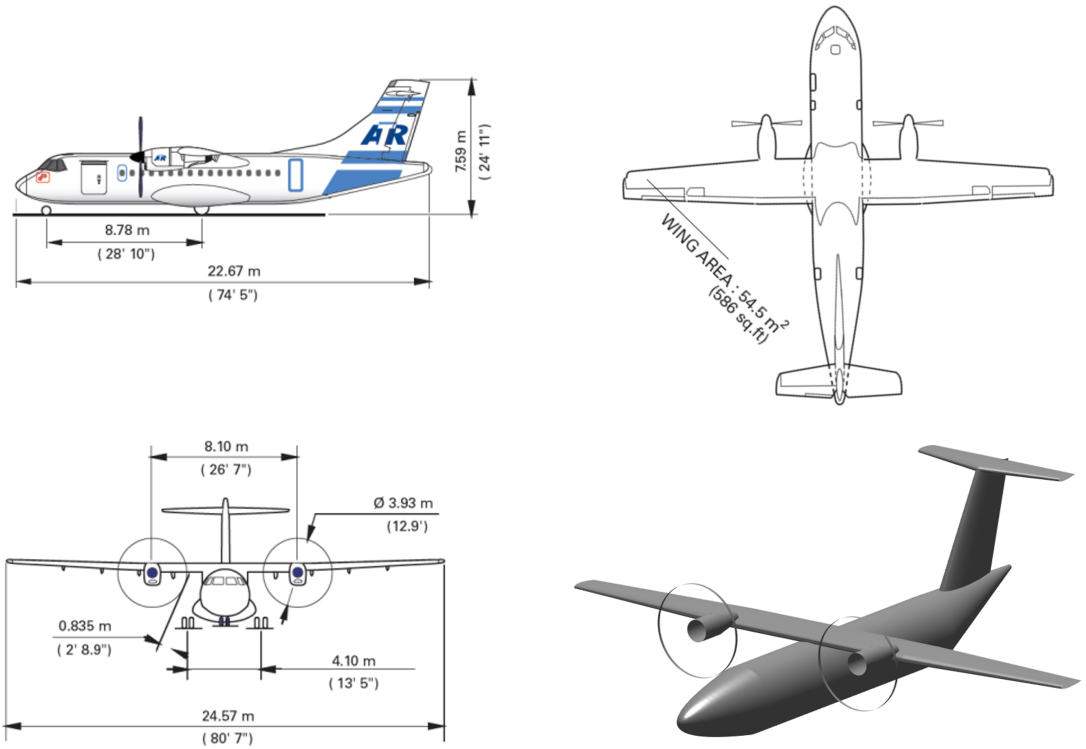

Figure 2.15: Three-view drawing of the ATR 42-600 (adapted from Ref. [158]) and 3D model of the digital counterpart as modeled in HEAD.

Table 2.5: Main performance indicators calculated for the ATR 42-600 modeled in HEAD, compared with expected data from Refs. [154, 157].

Parameter	Unit	Calculated	Expected	Deviation (%)
Maximum Take-Off Mass	kg	18 617	18 600	+0.09
Operating Empty Mass	kg	11 787	11 750	+0.31
Maximum Zero-Fuel Mass	kg	17 037	17 000	+0.22
Design Payload	kg	4 560	4 560	+0.00
Design Fuel Mass[1]	kg	2 270	–	–
Powerplant				
Number of Engines	–	2	2	–
Engine Rated Power	hp	2 381	2 400	-0.79
Performance				
Take-Off Field Length	m	1 096	1 107	-0.99
Landing Field Length	m	975	966	-0.93
Time to Climb (FL 170)	min	11.0	12.7	-13.39
Time to Climb (FL 240)	min	20.5	–	–
Service Ceiling (AEO)	ft	29 210	–	–
Service Ceiling (OEI)	ft	12 982	13 000	-0.14
Fuel Consumption (Cruise)	kg/h	618	620	-0.33
Mission Block[2] Distance	nmi	726	726	+0.00
Mission Block[2] Time	min	181	–	–
Mission Block[2] Fuel	kg	1 760	–	–

[1] Including reserves (climb to alternate, alternative cruise, descent from alternate, and holding).
[2] Including only nominal mission phases (i.e., taxi, take-off, climb, cruise, descent, and landing).

As seen from the table, the calculated values show good alignment with the expected values, with differences almost always below 1%. The operating empty mass calculated with HEAD differs from the actual one by less than 50 kg (0.3%). The difference between the two MTOM values is similarly low (0.1%), which means that the mission-required fuel is well estimated. The value of the maximum payload was imposed rather than estimated. As for the main performance indicators, HEAD provides results close to the values reported in Ref. [154] and Ref. [157]. The variations in terms of ground performance are negligible. On the other hand, a more significant discrepancy exists in terms of time to climb to flight level (FL) 170 (i.e., 17 000 ft), where a 13.4% deviation is registered. This difference could be associated with inaccuracies of the adopted engine model for the climb setting with respect to the real engine. However, it could also be due to discrepancies between the data: climb time reported in Ref. [157] could refer to different weight conditions of the airplane; moreover, intrinsic discrepancies exist between the aircraft data reported in Ref. [154] and Ref. [157], and the time to climb was taken from Ref. [157] which refers to a previous version of the ATR 42-600. In light of these considerations and of the fact that all other performance data were in line with the given ones, the deviation in the time to climb was not considered worrying for purposes of validation. Table 2.5 also compares the (average) cruise fuel consumption obtained from the mission simulation with respect to the value reported in Ref. [154], showing a quite negligible difference in this case too. More importantly, the power of the

combustion engine has been sized with less than 1% deviation compared to the rated power declared by the manufacturer. As seen, the workflow of Fig. 2.14 is based on sizing the power of the primary (thermal) engine, intended as the control variable, converging on the minimum power necessary to meet the minimum performance requirements. Therefore, since the expected performances were imposed as the minimum requirements, it is particularly significant for the purposes of workflow validation that the resulting power was aligned with the real one, and that, at the same time, all the controlled performances were matched accurately. As a final application, calculations were performed for several typical missions characterized by a shorter range. It is anticipated here that the results reported in Tab. 2.6 will provide additional reference values for comparison purposes in Chapter 4.

Table 2.6: ATR 42-600 fuel and emissions estimated by HEAD for three different mission ranges.

Parameter	Unit	200 nmi Mission	600 nmi Mission	726 nmi Mission
Block[1] Fuel	kg	610.7	1 481.5	1 760.1
Block[1] NO_x	kg	6.14	17.91	21.76
Block[1] CO	kg	4.77	5.54	5.78
Block[1] HC	kg	0.611	0.734	0.774
Block[1] CO_2	kg	1 923.2	4 665.1	5 542.6
Block[1] H_2O	kg	751.2	1 822.2	2 164.9
Block[1] SO_2	kg	0.51	1.244	1.478

[1] Including only nominal mission phases (i.e., taxi, take-off, climb, cruise, descent, and landing).

2.5 Cost Assessment

2.5.1 Cost Analysis Tool

In the literature, numerous classic methods for estimating operating costs have been documented [32, 34, 35, 37, 40, 141, 161–163]. These methods typically categorize various cost components based on their impact on the aircraft's operating costs. Certain elements, such as fuel expenses, maintenance costs, and depreciation, are directly affected by factors specific to the aircraft [35, 161–163]. These costs vary according to the performance and usage of the particular aircraft. Conversely, other cost items, including ticketing, sales, promotional activities, passenger services, and more, are not directly linked to the aircraft itself and remain independent of its unique characteristics. Thus, the operational component of an aircraft's total operating cost (TOC) can be dissected into two primary categories, as expressed mathematically in Eq. (2.55).

$$TOC = DOC + IOC \tag{2.55}$$

In Eq. (2.55), TOC encompasses all expenditures associated with operating the aircraft. DOC represents the direct operating cost, covering immediate expenses

directly tied to the aircraft's operation. Conversely, *IOC* stands for indirect operating cost, encapsulating costs indirectly related to the aircraft's operation. A thorough comprehension and effective management of these cost components are imperative for airline operations' financial success and sustainability. Adhering to the classical nomenclature introduced by Jenkinson [35], the DOC primarily includes costs associated with flight operations, such as fuel expenses, flight crew and cabin crew salaries, maintenance expenses, aircraft depreciation, loan interest, insurance premiums, navigation and landing fees, and carbon and noise taxes. These charges constitute essential components of airlines' overall operational expenses. In contrast, the IOC covers all remaining operating expenses not directly linked to the aircraft or its specific characteristics. This includes costs related to the depreciation of ground facilities and equipment, expenditures for sales and customer service activities, as well as administrative and overhead costs.

Operating costs play a pivotal role in the decision-making process for airlines and operators when selecting aircraft. As emphasized by Kundu [37], a commitment to cost-consciousness commences during the conceptual design phase. Initial cost evaluation becomes a crucial tool for choosing the most suitable design alternatives among various possibilities, including the aircraft's configuration and performance specifications, as these choices undeniably impact the overall project cost [35]. In summary, the absence of consolidated methods for estimating the costs of innovative aircraft poses a challenge in light of the significance of carefully evaluating economic feasibility to avoid misguided conclusions regarding achievable levels of environmental sustainability. In the following subsections, various methods will be outlined for estimating both DOC and IOC, applicable to conventional, hybrid, and electric aircraft. These methods, tailored for preliminary design applications, have been collected and adapted from existing literature to construct an original analysis workflow. The primary objective of this workflow is to enable the estimation of operating costs for a generic configuration in the early stages of the aircraft design process [34, 35, 41, 161, 162, 164]. Figure 2.16 provides a summary of the cost items considered in the analysis tool.

2.5.2 Indirect Operating Costs

Estimating IOC with accuracy can be challenging, given its close connection to how an airline opts to manage its operations. In contemporary approaches, IOC is frequently expressed as a percentage of the TOC. As a result, the IOC of an aircraft is influenced by a range of factors, encompassing fuel consumption, maintainability, reliability, noise emissions, and the overall time the aircraft remains in service. For the purposes of this study, the method proposed by Sforza [41] has been adopted, offering the advantage of correlating IOC with a limited set of overall mission and aircraft parameters. These parameters are typically available in the early stages of aircraft design and include the design mission range, the MTOM of the aircraft, and the number of passengers, while also accounting for the anticipated load factor (LF) of passengers.

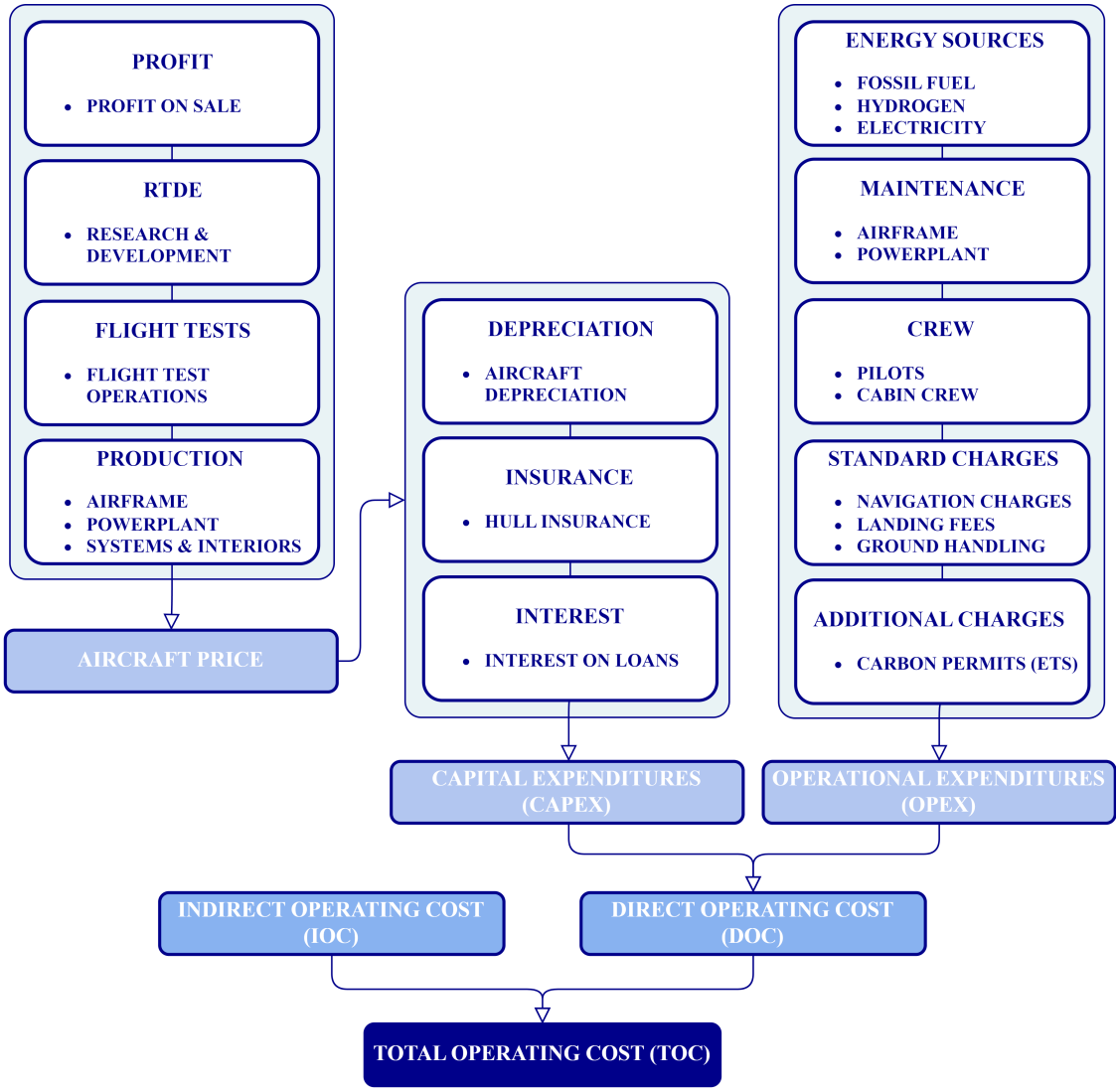

Figure 2.16: Components of the total operating cost of an aircraft considered in the analysis tool.

2.5.3 Direct Operating Costs

While DOC represents just one aspect of the economic viability of an airliner or private aircraft, it deserves considerable attention. This emphasis is justified by various factors that tie DOC directly to the technical and operational characteristics of the aircraft. Significantly, these factors fall within the direct control and influence of the design team [32]. Therefore, meticulous consideration and optimization of components related to DOC during the aircraft's design phase can significantly impact the overall economic feasibility of the aircraft. In this context, the DOC will be further dissected into two primary cost elements, specifically capital expenditures (CAPEX) and operational expenditures (OPEX), as illustrated in Eq. (2.56).

$$DOC = DOC_{\text{CAPEX}} + DOC_{\text{OPEX}} \tag{2.56}$$

While CAPEX is directly associated with aircraft ownership, OPEX is intimately tied to the operation of the aircraft throughout its operational lifespan. Equations (2.57) and (2.58) provide additional insights into the constituents of CAPEX and OPEX.

$$DOC_{\text{CAPEX}} = DOC_{\text{Depreciation}} + DOC_{\text{Insurance}} + DOC_{\text{Interest}} \tag{2.57}$$

$$DOC_{\text{OPEX}} = DOC_{\text{Energy}} + DOC_{\text{Crew}} + DOC_{\text{Maintenance}} + DOC_{\text{Charges}} \tag{2.58}$$

The subsequent subsections will delve deeper into the specific cost elements outlined in Eqs. (2.57)–(2.58).

2.5.4 Capital Expenditures

The process of determining the capital costs associated with acquiring a new aircraft is a complex undertaking, typically commencing with the assessment of the aircraft's market price. Various methods within aviation literature have been formulated for statistically estimating aircraft prices. One such method, outlined by Jenkinson et al. [35], adopts a straightforward approach by establishing a linear relationship between the market price of the aircraft and its operational empty mass. It is crucial to recognize that this relationship primarily aids in determining the market price of the aircraft but does not provide insights into the actual manufacturing costs. Jenkinson's method also correlates engine price with key engine parameters such as cruise thrust and SFC, primarily applicable to jet engines. This allows for a rough estimation of the airframe's cost by subtracting the engine price from the total aircraft cost. Sforza has developed an approach similar to Jenkinson's but incorporates more contemporary data, establishing a correlation between aircraft price and operational empty mass [41]. However, akin to Jenkinson's method, Sforza's approach concentrates on estimating costs at the aircraft level and does not offer specifics on isolated propulsion system costs. Acknowledging the necessity for approaches enabling the estimation of development and production costs of the airframe independently of the market value of the complete aircraft, alternative methods have been explored. An exemplary cost model is presented by Roskam [34], known for its versatility in estimating costs for both military and civil aircraft programs. Roskam's cost equations exhibit an exponential nature, with primary variables including the aircraft's mass, maximum speed, and production rates. Furthermore, Roskam provides relationships for estimating the costs of various engine types, encompassing turbofan, turboprop, and piston engines, along with a distinct estimate for propellers. For the current application, Roskam's method has been considered the most suitable choice for estimating the cost of the airframe and the conventional portion of the propulsion system. Roskam's definition of the aircraft price is summarized in Eq. (2.59).

$$Price_{\text{Aircraft}} = C_{\text{Production}} + C_{\text{Flight Tests}} + C_{\text{RDTE}} + Profit \tag{2.59}$$

In Eq. (2.59), $Price_{\text{Aircraft}}$ denotes the estimated market price of the aircraft. $C_{\text{Production}}$ represents the production cost, $C_{\text{Flight Tests}}$ encompasses the cost of flight

test operations, and C_{RDTE} covers research, development, test, and evaluation (RDTE) expenses. The program development cost is influenced by the complexity of the aircraft under analysis. The manufacturing company recovers this initial investment through the sale of a break-even production quantity of aircraft [34]. Equation (2.60) further breaks down the cost of aircraft production.

$$C_{\text{Production}} = C_{\text{Airframe}} + C_{\text{Powerplant}} + C_{\text{Systems}} + C_{\text{Interiors}} \tag{2.60}$$

Roskam's method provides a detailed process for estimating the various cost components mentioned in Eqs. (2.59)–(2.60), which, for brevity, are not explicitly outlined in this document [34]. The essential data required for estimating aircraft prices include manufacturing and engineering hourly labor rates, aircraft mass, maximum cruise speed, and a few other high-level descriptive parameters of the aircraft. Specifically, for powerplant cost estimation, Roskam offers empirical formulas primarily applicable to conventional (turboprop) engines and propellers. With a breakdown of powerplant costs for conventional components available, this approach can be easily extended to hybrid-electric architectures by summing the estimated cost of electric components. In this context, a generic approach based on unit pricing has been adopted. Unit prices could relate to unit power or unit capacity, depending on whether the component represents a power exchanger or a storage system. Therefore, the acquisition cost of a generic electric component is expressed by Eq. (2.61).

$$C_{\text{Electric Component}} = N_{\text{Components}} \cdot Price_{\text{Unit}} \cdot Size \tag{2.61}$$

In Eq. (2.61), $N_{\text{Components}}$ is the number of units of the same type, and the $Size$ parameter can be denoted in various measurement units, depending on the definition of the unit price $Price_{\text{Unit}}$ (e.g., USD/kW for power exchangers or USD/kWh for energy storage systems). This definition applies to various powertrain components, encompassing electric storage devices, power electronics, electric motors, electric generators, and FC systems.

Once the aircraft's price has been estimated, it becomes possible to calculate the CAPEX associated with each single flight, as expressed by Eq. (2.57). Depreciation accounts for the fact that the aircraft is gradually losing its initial value over time and can potentially be sold at any moment for its residual value. In Eq. (2.62), $Lifespan_{\text{Aircraft}}$ represents the anticipated lifespan of the aircraft in years, RV_{Aircraft} is the residual value of the aircraft at the end of its life (as a fraction of the initial price), and $N_{\text{Flights, Year}}$ indicates the number of flights per year.

$$DOC_{\text{Depreciation}} = \frac{Price_{\text{Aircraft}} \cdot (1 - RV_{\text{Aircraft}})}{Lifespan_{\text{Aircraft}} \cdot N_{\text{Flights, Year}}} \tag{2.62}$$

The insurance cost is computed as in Eq. (2.63), based on the total initial investment value and the annual insurance premium rate, $Premium_{\text{Annual}}$.

$$DOC_{\text{Insurance}} = \frac{Investment_{\text{Total}} \cdot Premium_{\text{Annual}}}{N_{\text{Flights, Year}}} \tag{2.63}$$

In Eq. (2.63), the total investment could represent the aircraft cost, inclusive of any spare parts. Finally, the interest cost pertains to the payments of fees accrued as interest on loans. This cost is determined as in Eq. (2.64), by applying an interest rate, $Rate_{\text{Interest}}$, to the total initial investment value, across a designated interest period expressed in years ($Period_{\text{Interest}}$).

$$DOC_{\text{Interest}} = \frac{Investment_{\text{Total}} \cdot Rate_{\text{Interest}} \cdot Period_{\text{Interest}}}{Lifespan_{\text{Aircraft}} \cdot N_{\text{Flights, Year}}} \tag{2.64}$$

2.5.5 Operational Expenditures

Energy sources

For a precise and accurate cost estimate, it is crucial to begin by obtaining information on the current prices of fuel and electricity. Typically, fuel prices are presented in dollars per gallon in the United States or Euros per liter in the EU, and this data needs to be sourced for the specific year for which the cost estimate is required. Fortunately, the IATA website serves as a reliable and up-to-date resource for such fuel price information [165]. However, the incorporation of alternative energy sources for propulsion necessitates a broader interpretation of this cost item, prompting the need for a more inclusive definition of *energy costs*. The cost of each energy source, whether conventional kerosene, SAF, H_2, or electricity, can be conveniently expressed in terms of cost per unit of available energy.

$$DOC_{\text{Energy}} = Price_{\text{Energy, Unit}} \cdot Requirement_{\text{Energy}} \tag{2.65}$$

For instance, in Eq. (2.65) $Price_{\text{Energy, Unit}}$ is expressed in USD/kWh assuming that the mission energy demand, $Requirement_{\text{Energy}}$, is given in kWh. In scenarios involving multiple energy sources employed to fulfill the same mission, as observed in hybrid-electric aircraft, the overall energy cost is derived from the summation of individual contributions associated with each source.

Crew Cost

The crew cost encompasses the salaries of both cockpit and cabin staff. As an initial approximation, the crew cost can be calculated by multiplying their salaries by the respective number of crew members.

$$DOC_{\text{Crew}} = \frac{Salary_{\text{Pilots}} \cdot N_{\text{Pilots}} + Salary_{\text{Attendants}} \cdot N_{\text{Attendants}}}{N_{\text{Flights, Year}}} \tag{2.66}$$

In Eq. (2.66), N_{Pilots} and $N_{\text{Attendants}}$ denote the numbers of pilots and flight attendants, respectively. However, it is important to note that the number of wages to be disbursed is not strictly equal to the number of staff members required on board for a flight. Under European regulations, the flight hours for each crew member cannot exceed 900 hours in the same calendar year [166]. This consideration can be factored into the crew cost calculation by adjusting the number of staff members based on the expected number of flight missions occurring every year.

Maintenance Cost

Prediction of maintenance costs presents challenges due to the lack of a standardized definition for items falling within this category. Estimating the overall costs involved has consistently proven to be a complex task, primarily due to the varied nature of maintenance tasks across different aircraft and the inherent variations in operational contexts. In practice, maintenance tasks are commonly categorized into airframe and engine components. A well-recognized approach is advanced by the Air Transport Association of America (ATA) [161]. This method adopts an integrated approach capable of estimating labor and materials for both (conventional) engines and airframe maintenance comprehensively. It encompasses costs associated with routine inspection, servicing, and overhaul activities related to airframes, engines, avionics, systems, and more. Due to its simplicity of implementation, the reduced number of required parameters, and especially the high level of standardization, the ATA method has been preferred for the present application. Interested readers can refer directly to the source for estimating relationships. Estimating the DOC for hybrid and electric architectures requires additional considerations to account for electric systems, including components such as batteries, FC systems, electric machines, and power electronics [164, 167, 168]. Zhang et al. modeled the acquisition and maintenance costs of electrical components as additive to the costs of conventional components, including battery replacement costs among maintenance expenses [167]. However, their study does not factor in any additional maintenance costs, such as those linked to electric machines and power electronics, nor does it address the influence of the reduced engine size due to hybridization on the maintenance cost of the combustion engine. Fioriti et al., following a task-based approach for estimating maintenance costs, concluded that the level of electrification can lead to significant reductions in the operational expenditures of regional transport aircraft [169]. In the case of hybrid-electric powerplants, the authors assumed a percentage reduction in maintenance costs compared to a similar conventional aircraft, rather than tying the estimate to the specific architecture. Other authors also roughly approximate the maintenance cost of hybrid-electric aircraft as a fraction of the maintenance cost of conventional aircraft [164, 170].

In the present context, the maintenance costs of the electrical components have been considered additive to the conventional cost items. Importantly, while ICEs often have lifespans equal to or longer than the aircraft they power, this is not the case for specific electrical components like batteries. In such cases, the cost of replacements is considered within maintenance expenses rather than as additional acquisition costs [167]. To summarize all these aspects, a general formulation for the estimation of the DOC per unit flight has been implemented, as shown in Eq. (2.67). In the equation, $N_{\text{Replacements}}$ represents the number of replacements expected during the service life of the aircraft and depends on the expected service life of the component itself. The cost of each replacement is modeled as the cost of acquiring a new unit, less any recovery obtainable from the residual value of the discarded component, $RV_{\text{Component}}$. Furthermore, additional base maintenance costs

can be taken into account by considering a maintenance labor rate, $LR_{\text{Maintenance}}$, the maintenance hours required, t_{Labor}, and the maintenance frequency, $f_{\text{Maintenance}}$, expressed as the reciprocal of the number of flights before the next check. The formula is valid for a generic hybrid-electric component of the propulsion system.

$$DOC_{\text{Maint,Component}} = \frac{N_{\text{Replacements}} \cdot Price_{\text{Component}} \cdot (1 - RV_{\text{Component}})}{Lifespan_{\text{Aircraft}} \cdot N_{\text{Flights, Year}}} + LR_{\text{Maintenance}} \cdot t_{\text{Labor}} \cdot f_{\text{Maintenance}} \tag{2.67}$$

Charges

In this context, the term *standard charges* encompasses navigation charges, landing fees, and ground handling charges. Navigation charges are prescribed by Eurocontrol and are determined as an increasing function of the MTOM and the distance flown [171]. However, the charged amount depends on factors such as the departure airport and the specific route, making it challenging to provide a general assessment in advance. Similarly, landing fees and ground handling charges vary across airports, with each levying fees differently. Generally, these charges are also dependent on the aircraft's mass and the number of passengers. To mitigate the dependence on specific airports, the Association of European Airlines (AEA)'s method for short-range aircraft has been adopted [162]. Similar considerations apply to taxation policies for both conventional and hybrid/electric aircraft, with individual European airports adopting charging systems that factor in polluting emissions. However, as of October 2022, only 43 out of 3 174 global airports listed in AirportCharges had implemented emissions-based charges [172]. Due to the uncertainty and airport-specific variations, it was chosen not to include this aspect in the analysis workflow to maintain generality. Instead, to account for potential incentives from authorities and airports in a preliminary manner, the alternative approach proposed by Scholtz et al. [164] has been incorporated. This model introduces a climate toll charging system based on the mitigation of standard air navigation charges, directly proportional to the aircraft's degree of hybridization [164]. Finally, additional charges consist of equivalent CO_2 emissions charges under the ETS [6, 7, 20]. In Eq. (2.68), $Price_{\text{Carbon, Unit}}$ represents the CO_2 allowance price, and $m_{\text{CO2, Flight}}$ denotes the mass of CO_2 emissions produced during each flight. The additional factor k_{ETS} considers the fraction of free-assigned emission certificates. As a preliminary approximation, a unit factor may be assumed for conventional aircraft, and a factor equal to zero in the case of exclusive use of alternative fuels (SAF or hydrogen), assuming free allowances will be allocated to promote sustainable fuels.

$$DOC_{\text{ETS}} = Price_{\text{Carbon, Unit}} \cdot m_{\text{CO2, Flight}} \cdot k_{\text{ETS}} \tag{2.68}$$

Inflation

When conducting economic assessments, analysts often rely on data and economic assumptions from diverse sources that pertain to different geographical contexts and reference years. Consequently, the presence of the *inflation* effect poses a substantial risk to the precision of economic calculations, introducing a dynamic element capable of distorting the actual value of monetary metrics over time if the economic assumptions do not uniformly refer to the same level of inflation. Hence, it is important to adjust all assumptions for inflation. An inflation correction factor is consistently applied to each collected value, expressing all costs in equivalent USD for the year 2020 (2020USD). The applied correction is outlined in Eq. (2.69).

$$C_{2020} = C_{\text{Reference Year}} \frac{CPI_{2020}}{CPI_{\text{Reference Year}}} \tag{2.69}$$

This same relationship is also utilized to correct the estimates generated by the adopted estimating relationships presented earlier in this section. For instance, methods for estimating aircraft price and standard charges pertain to the economic year 1989 [34, 162]. The ratio between the consumer price index (CPI) in 2020 and 1989 is 2.09, indicating that 1 USD in 1989 equals 2.09 USD in 2020 [173].

2.5.6 Tool Validation

To validate the cost tool, a case study involving the analysis of the ATR 42-500 has been selected. ATR provides the outcomes of an internal assessment of the DOC associated with this aircraft model for a 300 nmi mission [174]. To replicate the study, the same primary technical and economic assumptions presented by the source have been utilized, and are reported in Tab. 2.7 [174]. Additionally, no supplementary charges related to carbon permits have been taken into account. The cost analysis tool has been employed to estimate the costs of crew, maintenance, navigation charges, and landing fees, rather than assuming them as done in Ref. [174]. In both the ATR analysis and the present study, ground handling charges have been neglected.

Figure 2.17 illustrates the favorable correspondence between the computed cost and the expected result. The accuracy in CAPEX estimation can be attributed to a reasonable assessment of the aircraft's price. Specifically, the estimated aircraft price is 12.3 million USD. To gauge the accuracy of this result, it is noteworthy that the catalog price of the ATR 42-500 was 14.0 million USD in 2004, as reported by Jane's All World Aircraft 2007–2008 [175]. However, customary industry practices involve applying discounts to the catalog value. ATR, for instance, discloses a 10% discount on the catalog price [174]. Accounting for these factors, the value estimated by the cost tool is only 3.3% higher than the actual price. Furthermore, considering that the analysis tool appears to underestimate the program development cost, with an estimate of 24 million USD versus the 50 million USD reported by Jackson et al. [175], the 3.3% difference can be further reduced to 0.6% by calibrating the development cost estimate. Figure 2.18 provides a detailed comparison of

Table 2.7: Main economic assumptions for the cost tool validation. The case study is an aircraft similar to the ATR 42-500 [174].

Parameter	Value	Units
Depreciation	12 years with 20% residual value	–
Spares	10% aircraft price	–
Financing	85% of investment over 10 years	–
Insurance	1% of aircraft price per year	–
Fuel Price	2.06	USD/gal
Range	300	nmi
Block fuel (incl. taxi)	797.0	kg
Block time (incl. taxi)	1.28	h
Turnaround time	0.42	h
Annual utilization	1 800 flights per year	–

operating expenditures. The 4.0% discrepancy in crew cost can be attributed to the assumption of a different annual salary, which ATR does not explicitly report. The relatively small error (5.2%) on charges can be attributed to the statistical nature of the relationships employed by the cost tool. The same rationale applies to the errors in airframe and powerplant maintenance, which are 69.3% and 45.2%, respectively. Despite the high error in maintenance cost, this component constitutes only 18.7% of the total OPEX, resulting in an error of 10.6% on the OPEX and approximately 7.0% on the total cost. In conclusion, the predictions show satisfactory agreement with the reference data, which is particularly relevant given that the case study involves an aircraft in the same class as the application proposed in the subsequent chapter. This level of agreement is deemed sufficient for the purpose of comparative analysis. However, the statistical models for development cost, maintenance, and charges have been calibrated using corrective scale factors to eliminate the percentage errors associated with the case study.

2.6 Chapter Summary

This chapter has offered an extensive overview of the innovative preliminary aircraft design framework developed by the DAF research group at the University of Naples “Federico II”. The primary objective has been to comprehensively introduce new methodologies and workflows for the design and analysis of innovative regional aircraft, to which the candidate directly contributed. Particular emphasis has been given to their significance in addressing the challenges presented by hybrid-electric propulsion architectures in regional aircraft design.

Initially, the author has proposed a versatile and robust mathematical model capable of describing a wide array of propulsion systems incorporating alternative energy sources. This model demonstrates adaptability to various architectures based

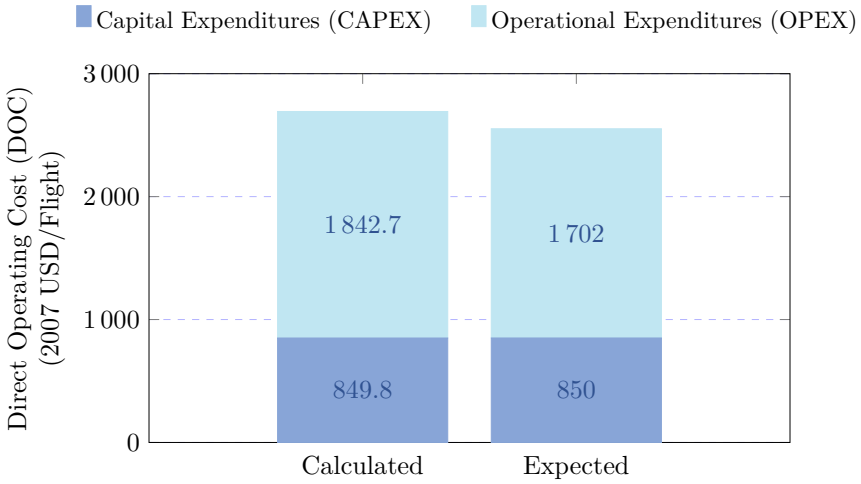

Figure 2.17: Comparison between calculated DOC and public data (adapted from Ref. [97]) The case study is an aircraft similar to the ATR 42-500 [174].

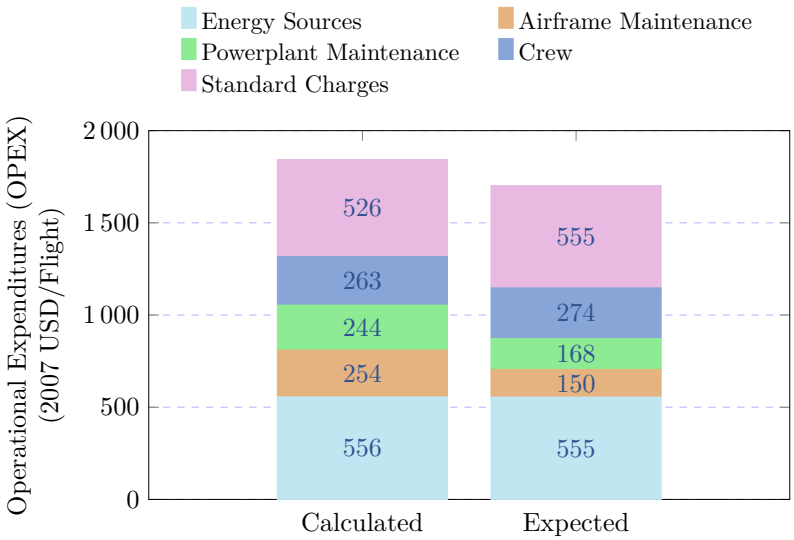

Figure 2.18: Comparison between calculated OPEX and public data (adapted from Ref. [97]). The case study is an aircraft similar to the ATR 42-500 [174].

on thermal engines, batteries, and hydrogen FC systems, while also encompassing DEP systems and the associated aero-propulsive effects. Its notable generality, coupled with the simplicity of the linear algebraic equations it employs, presents significant added value compared to state-of-the-art approaches, and addresses the diversity of potential innovative propulsion solutions for regional aircraft. Moreover, its flexibility allows for future generalization to include additional systems and degrees of freedom.

The integration of this model into a multidisciplinary design chain, combining the generalized powertrain description with mission analysis and II-class methods for mass estimation, enables a consistent and comprehensive conceptualization of new designs, enhancing accuracy compared to methods based on the evaluation of

point performance. Additionally, the development and validation of a module for estimating the DOCs of hybrid-electric aircraft represent a noteworthy enhancement to the functionality of the tool. This module, entirely developed by the author, offers crucial preliminary insights into the economic viability of hybrid-electric aircraft.

While limitations in publicly available data for flying electric prototypes hinder exhaustive verification of the tool, ongoing advancements in electric regional aviation research promise opportunities for further refinement and validation of these design methodologies.

The approaches and workflows discussed in this chapter will serve as foundational elements for the applications presented in the subsequent chapters. It is imperative to note that the maturation of these methodologies has resulted from a dynamic process intertwined with the execution of research activities involving the candidate. Notably, participation in the ELICA project played a pivotal role in refining the analysis workflow presented herein. The next chapter will delve deeper into this experience, providing additional insights into the motivations behind the selected methodological approach.

3

From Theory to Practice: The Experience of ELICA

Contents

3.1 The ELICA Project

Funded by the European Commission's CS2 program, the *ELICA* (*ELectric Innovative Commuter Aircraft*) project [16] answered to the thematic topic No. JTI-CS2-2018-CFP09-THT-03, "Conceptual Design of a 19-passenger Commuter Aircraft with near zero emissions". The project lasted 3 years, ending in October 2022, and involved the collaboration of industrial and academic partners under the coordination of Rolls-Royce Electrical Deutschland [176]. The activities were also monitored by an advisory board composed of Piaggio Aerospace [177]. The main focus was on the conceptual design of a 19-passenger commuter aircraft based on alternative propulsion concepts, targeting near-zero CO_2 emissions by 2035. The purpose was to demonstrate the potential advantage of the most promising disruptive technologies on this class of aircraft, particularly important for reducing the door-to-door time in Europe to less than four hours [13]. The project activities were organized into four different Work Packages (WPs):

- **WP2**, dealing with economic analysis for hybrid-electric commuter aircraft, supporting the definition of aircraft requirements and performance characteristics for the 19-passenger commuter aircraft.

- **WP3**, focused on the characterization of the hybrid-electric propulsion system, including architecture design, fault tolerance analysis, and modeling of electric components and thermal management concepts.
- **WP4**, dealing with the overall aircraft conceptual design and optimization, including increased fidelity analyses and life-cycle considerations.
- **WP5**, supporting the previous work packages with identification of enabling technologies, trade-off studies, and provision of technical recommendations for future aviation stakeholders.

Air s.Pace [178] was in charge of WP2, contributing to the definition of the aircraft requirements which will be presented in Section 3.2. UNINA's work was particularly concentrated in WP4 and WP5. Through preliminary analyses conducted with the tool described in Section 2.3, a preliminary assessment was carried out and will be briefly described in Section 3.3. Thanks to collaboration with industrial partners from Rolls-Royce [176] and Siemens Digital Industries Software [179], feedback on technology levels and surrogate models were integrated into the UNINA model, allowing for a better evaluation of the mission performance of the designed concepts. This evaluation led to the need for a new assessment covered in Section 3.4. Finally, during the last year of the project, new feedback on technological levels, as well as aerodynamic feedback supported by CFD analyses carried out by SmartUp Engineering s.r.l. [180], led to a final design loop and final considerations on the technical feasibility of the concepts, discussed in Section 3.5. The author invested effort and time in contributing to the success of the ELICA project. This chapter serves the function of showing a concise overview of the activities in which the author was involved, as well as their main outcomes. The focus will be mainly on UNINA's contributions to the project, on the general workflow, and on the difficulties encountered, which give room for improvement for future studies. The observations that will be presented in Section 3.6 constitute lessons learned, which the author drew from the ELICA experience and which contributed to improving his approach to research in the field of sustainable and innovative aircraft design. As a final note, despite the confidential nature of the project outcomes, the interested reader may refer to multiple works published in literature that directly fit into or were inspired by the project [88, 91, 93, 130, 149, 181–184].

Author's Contributions

The author of this dissertation was directly involved in the activities of WP4 and WP5 of the ELICA project. At the beginning of the project, coordinated by Mr. Qinyin Zhang (Rolls-Royce Electrical), Air s.Pace supplied a set of TLARs for the concept. Flanked by fellow researcher Dr. Francesco Orefice (UNINA), and under the coordination of Prof. Fabrizio Nicolosi (UNINA), during the first year of the project, the author provided support in the processing of the results for the preliminary assessment discussed in Section 3.3. During the second year, intensive data exchanges with the project partners were carried out, which required coordination between UNINA's group and the industrial partners of Rolls-Royce, represented by Mr. Zhang. In parallel, the author was responsible for the generalization of the design tool to manage systems based on fuel cells (already discussed in Chapter 2) in light of a sudden change of direction of the project towards full-electric solutions. During the second year, together with Dr. Francesco Orefice and Dr. Vincenzo Cusati (UNINA\SmartUp), the author participated in an intense analysis campaign aimed at integrating the surrogate models provided by the partners and producing a second-loop aircraft assessment. As will be explored in Section 3.4, the new design process used was time expensive and required dividing the workload equally among collaborators, in terms of combinations of design parameters to be analyzed. During the third year of the project, the results were transmitted to contracted collaborators for high-fidelity analyses. Dr. Cusati took care of CFD analyses on the hybrid-electric concept. Dr. Öngüt Emre (Siemens), Dr. Yves Lemmens (Siemens), and Dr. Vittorio Memmolo (UNINA) carried out a high-fidelity structural analysis to verify the structural mass of the wing with DEP. The author also interacted with Dr. Jonathan Menu (Siemens), who was responsible for a detailed fault-tolerance analysis to confirm an adequate level of safety for the selected propulsion architecture. Dr. Dominik Magner (Rolls-Royce Electrical) took care of the mass assessment of cooling systems, after interacting with the author for a correct communication of the design conditions. Approaching the end of the project, the partners' feedback was received and used for a reassessment of the configurations in charge of the author, which led to discrepancies compared to the previous assessment loop. Lacking time for a completely new design loop, new parametric investigations were conducted as part of WP5 to evaluate the impact of the degree of hybridization and uncertainty on the main technological assumptions. The author took care of this activity, discussed in Section 3.5, which led to the determination of final representative concepts for two different time horizons. The author was also responsible for the production of several technical reports of the results, their presentation to the project reviewers, and their public dissemination in international workshops and conferences.

Related Publications

The work conducted within the ELICA project has inspired the production of numerous scientific works. The following journal articles were published:

> [91] Francesco Orefice, **Valerio Marciello**, Qinyin Zhang, Guido Wortmann, Jonathan Menu, and Vincenzo Cusati. *Design of Hybrid-Electric Small Air Transports.* IOP Conference Series: Materials Science and Engineering, 1226:012075, 2022. The work proposes some estimating relationships obtained starting from the surrogate models provided by the ELICA project partners. The author of this dissertation contributed to the conceptualization and in writing and reviewing the paper.
>
> [93] **Valerio Marciello**, Francesco Orefice, Fabrizio Nicolosi, Danilo Ciliberti, and Pierluigi Della Vecchia. *Design of Hybrid-Electric Aircraft with Fault-Tolerance Considerations.* Chinese Journal of Aeronautics, 36(2):160–178, 2023. The article presents a model developed by the author for simulating the effect of failures in the presence of a hybrid-electric architecture with DEP. The model, suitable for preliminary design stages, was tested by the author on an intermediate version of the ELICA concept. The main content of this publication is also reported in Appendix B.

UNINA also participated in an intense dissemination activity of ELICA's outcomes at international conferences (for every item, the speaker's name is underlined):

> [130] Fabrizio Nicolosi, **Valerio Marciello**, and Francesco Orefice. *Conceptual Design of a Hydrogen-Propelled Aircraft with Distributed Electric Propulsion.* In AIAA Aviation Forum 2022, Chicago, Illinois, 2022. The work presents a comparative analysis of different full-electric commuter aircraft based on fuel cells, varying the number of DEP propellers. The author of this dissertation performed the analyses and led the drafting of the manuscript.
>
> [184] Fabrizio Nicolosi, **Valerio Marciello**, Vincenzo Cusati, and Francesco Orefice. *Technology Roadmap and Conceptual Design of Hybrid and Electric Configurations in the Commuter Class.* In 33rd Congress of the International Council of the Aeronautical Sciences (ICAS 2022), Stockholm, Sweden, 2022. The work, mainly written by the author, served to disseminate the partial assessments of the project's aircraft design activity, very close to those illustrated in Section 3.4.

Finally, the author gave additional presentations at the 12th EASN Conference and during a thematic workshop held in Naples, Italy in October 2022. The latter was organized by UNINA and SmartUp Engineering right after the end of the project. Both presentations served to disseminate the final outcomes at the international level, retracing the workflow of the entire project:

> [185] Qinyin Zhang, Fabrizio Nicolosi, **Valerio Marciello**, Vincenzo Cusati, Jonathan Menu, Emre Öngüt, and Maximilian Spangenberg. *Concept Designs of Hybrid-Electric Passenger Commuter Aircraft with Potential to Enable Zero-Emission Regional Air Transport.* In 12th EASN International Conference, Barcelona, Spain, 2022 *(presentation only).*
>
> [186] Qinyin Zhang, **Valerio Marciello**. *The ELICA Project.* In the Workshop on Commuter and Regional Hybrid-Electric Aircraft Design: Transition from Clean Sky 2 to Clean Aviation, Naples, Italy, 2022 *(presentation only).*

3.2 Requirements and Assumptions

To initialize the project's activities, Air s.Pace [178] made an essential contribution to defining the TLARs for the ELICA project. This was done by performing a detailed technical benchmark with relevant 19-seater commuter aircraft [181]. A *benchmark* is an effort to provide insights into the performance of a product or service from different suppliers or different sources. The dimensions measured can vary vastly from hard technical facts to subjective opinions on design and features. In this context, where no support was available from the aircraft manufacturer, this activity relied on publicly available information and internal knowledge about the principles of operation of the product. For the purposes of ELICA, nine 19-seater FAR-23/CS-23 airplanes were considered: Let L 410 NG, DHC-6 Twin Otter, Fairchild Metroliner, Beechcraft 1900D, Embraer EMB-110P2, BAe Jetstream 32, DO-228NG, Antonov AN-28, Harbin Y-12. Different figures of merit were compared in order to identify the performance parameters potentially most significant for the commercial success of the product, quantified in terms of number of sales. The parameters considered concerned size, installed power, mass and consumption, as well as take-off, cruise, and climb performance. The results of this comparison were also coupled with an economic feasibility study [181, 182]. According to the goals of Flightpath 2050, formulated by the European Commission, "90% of travelers within Europe are able to complete their journey, door-to-door within 4 hours" [13]. In this sense, regional air mobility has the potential to increase its commercial success in the coming decades, in light of the dense network of minor airfields covering Europe and the US. Their potential is further supported by potential cost savings due to a hybrid design, with Scotland and Norway that are heavily pushing electric aviation and can be considered as initial markets [187–189]. A preliminary set of TLARs was defined to support the economic feasibility of the final product. After being refined and shaped based on preliminary technical evaluations, the set of TLARs recommended for the ELICA project is the one reported in Tab. 3.1.

Table 3.1: Set of TLARs for the definition and design for the ELICA 19-seater commuter aircraft.

Description	**Value**	**Unit**	**Notes**
Design Range	500	nmi	
Typical Range	200	nmi	
Time to Climb (Design Mission)	< 6	min	At MTOM
Cruise Speed	375	km/h	FL 100
Maximum Field Length	$< 1\,000$	m	At SL, ISA and MTOM
Design Payload	1 797	kg	19 PAX – 93 kg per PAX
Alternate	100	nmi	FL 50
Holding	30.0	min	
MTOM	$< 8\,618$	kg	CS-23 Limitation [138]

3.3 Preliminary Sizing

3.3.1 Parametric Studies

While clear indications on technological levels were still lacking and the project was in a preliminary phase, UNINA carried out preliminary sensitivity analyses aimed at identifying a feasible preliminary configuration for a hybrid-electric commuter aircraft. The first application on a CS-23 aircraft aimed to study the combination of parameters that results in the highest fuel saving. After a review of the main enabling technologies available [149], the investigation was based on batteries and distributed propulsion, identified as the most promising technologies for an EIS year 2035. Fuel cells were initially excluded in light of their lower TRL. Furthermore, it is important to note that the workflow used for the preliminary analyses was the one discussed in Section 3.3 which, at the beginning of the project, did not contemplate in any case the possibility of including FCs in the propulsive architecture. The number of DEPs, the usage strategy for the flight mission, and different assumptions on the battery's specific energy were explored with the aim of maximizing the percentage of fuel saved compared to the conventional reference configuration. A specific power of 1 kW/kg was preliminarily assumed for the battery, and a specific power of 7.7 kW/kg was assumed for the electric machines. The analysis constraints were represented by the TLARs discussed in the previous section, with particular regard to the limitation on the MTOM, together with the purpose of minimizing fuel consumption. The propulsive architecture adopted for the application was the same as represented in Fig. 2.2. The different shaft power ratios considered phase by phase defined the DEP's usage, and the most promising strategy was identified in the use of distributed propulsion during take-off, landing, and climb. To make a fair comparison among three different specific energy values of the battery, the compared missions included only the block mission, without the loiter and alternate phases. Figure 3.1a explored different solutions evaluating the percentage of fuel saving for a 200 nmi mission, assuming 8 distributed propellers and with the battery supplying 10% of the total energy in all phases. However, by increasing the range, the hybridization of the platform may lead to higher fuel consumption with respect to the conventional baseline. Figure 3.1b shows the trend of MTOM penalties for a full-electric aircraft with respect to a conventional configuration as the range varies. These results highlight that, by increasing the battery specific energy, the maximum design range achievable with a CS-23 aircraft increases. From 100 nmi with 250 Wh/kg, the maximum design range reaches 300 nmi when the specific energy doubles. This limit is dictated by the 8 618 kg MTOM constraint, highlighted by the white dashed line in the figure.

Following, the effects of the number of propellers and the supplied power ratio on the fuel mass were investigated, considering a 500 Wh/kg battery. Distributed propulsion could mitigate, but not cancel, the impact of the mass increment related to batteries when exploiting aero-propulsive effects. Table 3.2 reports preliminary evaluations of the DEP effect on aerodynamic coefficients in typical take-off and

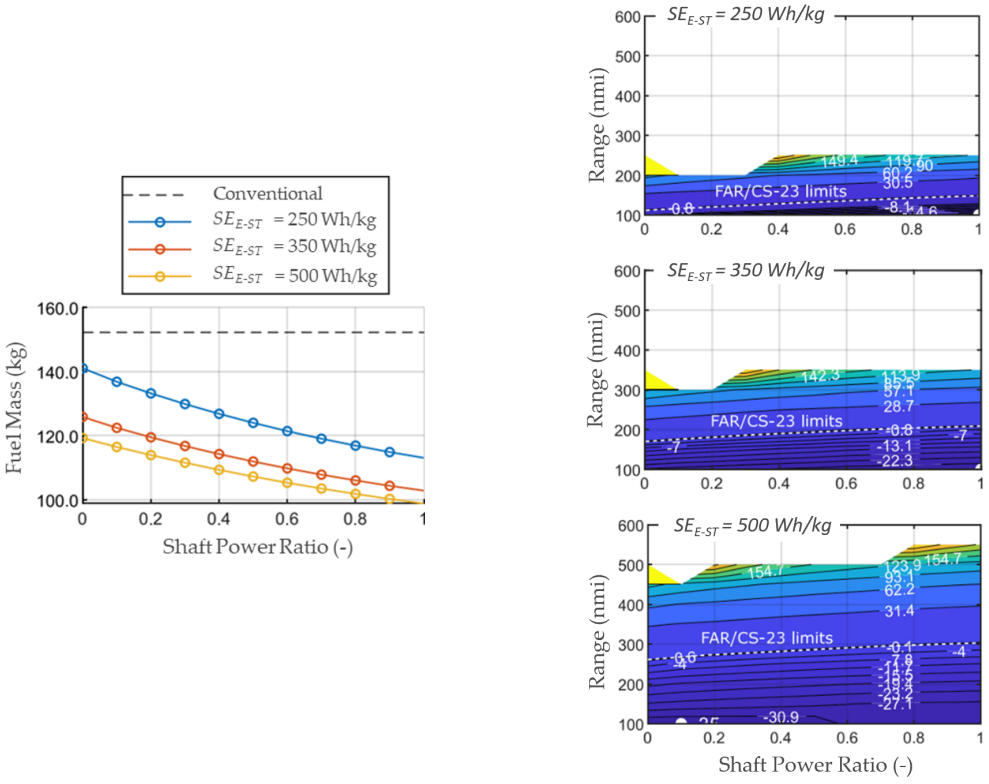

(a) Variations in fuel saving with shaft power ratio and battery's specific energy, for a 200 nmi mission and assuming $\Phi = 0.1$ in all phases.

(b) Variations in MTOM with range, shaft power ratio, and battery's specific energy for a full-electric commuter aircraft.

Figure 3.1: Preliminary parametric analyses on the ELICA hybrid-electric commuter aircraft, in terms of MTOM and fuel mass saving as the battery's specific energy and the DEP's utilization strategy change.

landing conditions. Figure 3.2a refers to a configuration with 8 distributed propellers, and Figure 3.2b refers to a configuration with 16 distributed propellers. The contour labels show the fuel mass saving with respect to the baseline aircraft with a conventional powerplant. The exploration revealed that DEP enables a fair fuel saving on turbo-electric aircraft with $\Phi = 0.0$ (i.e., featuring gas turbines whose output power is converted to electricity and eventually used to move DEP), especially on short ranges and for high shaft power ratios. The maximum fuel saving is about 15% for an 8 DEP wing and about 20% for a 16 DEP wing. The reason for this fuel saving is attributed to the higher wing loading values enabled by the use of DEP. The increase in the wing's lifting capability, due to the aero-propulsive effects, allows for the reduction of the wing area while guaranteeing the same ground performance. In turn, reducing the wetted area leads to a decrease in the aerodynamic drag generated throughout the mission and, thus, results in a decrease in the energy necessary for the mission.

Table 3.2: Preliminary estimation of the aerodynamic benefits of DEP for different numbers of distributed propellers.

Take-Off Condition (CL = 1.95)		
Number of DEPs	ΔCL	ΔCD
8	+0.75	+0.0779
12	+0.92	+0.0963
16	+1.03	+0.1073
20	+1.09	+0.1142
Landing Condition (CL = 2.20)		
Number of DEPs	ΔCL	ΔCD
8	+0.83	+0.0974
12	+1.03	+0.1205
16	+1.14	+0.1342
20	+1.21	+0.1429

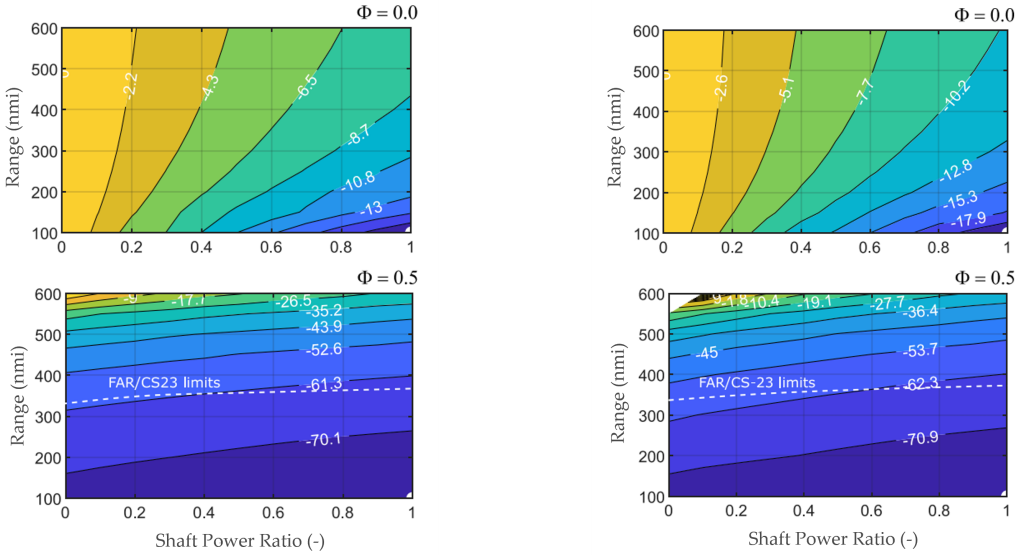

(a) 8 DEP. **(b)** 16 DEP.

Figure 3.2: Preliminary parametric analyses on the ELICA hybrid-electric commuter aircraft. Contour labels represent the % difference of fuel mass saving with respect to the conventional case. The assumed battery's specific energy is 500 Wh/kg.

When adding the contribution of batteries, the results also show that ranges longer than 375 nmi are not achievable within the CS-23 MTOM limit, already with $\Phi = 0.5$. With less optimistic assumptions about the battery technology level, this value would be further reduced. However, the effect of the number of distributed propellers becomes negligible for higher values of the supplied power ratio. As additional considerations, a higher number of electric drives and propellers would result in higher acquisition, installation, and maintenance costs. Moreover, the reduced propeller diameter would result in a troubling design to maintain high efficiency. Therefore, in light of the limited effect on fuel saving linked to

the increase in the number of DEPs, it was decided to select 8 propellers as a compromise between benefits and complexity, as also suggested by industrial designers in the advisory board.

Further preliminary considerations were made to pre-select the airframe architecture. A high-wing configuration was selected to favor clearance of the propeller blades from the ground, greater stability at high attitudes, and less risk of wake interference with the tailplane. Furthermore, a conventional tail configuration was preferred over a T-tail in light of its reduced structural weight. In this regard, the case of ELICA was not considered critical from the point of view of the controllability of the aircraft, thanks to the theoretical possibility of redistributing the thrust in case of failure, thus reducing the asymmetry (see also the case study in Appendix B).

3.3.2 First Assessment

The design and optimization activities of the project were characterized by an intensive exchange of data among partners, in particular with industrial partners in the ELICA consortium and the advisory board, in order to guide the analysis towards the most feasible configuration in terms of a realistic powertrain architecture, energy/power density assumptions, and so on. In this respect, a DEP configuration with 8 electric motors was frozen for several reasons related to maintenance and logistic costs, powertrain system complexity, and certification issues. To consolidate this choice, a further comparison between the DEP configuration and a hybrid configuration with just one electric propeller at the wing tip was also performed. A battery mass of 500 kg was considered leaving some margin compared to the certification limit on the MTOM. The comparison is summarized by Fig. 3.3, showing that a 20% reduction in the wing surface was attainable for the DEP configuration while continuing to meet the same TLARs. The main reason for the greater fuel saving is attributed to this, as the wing area is directly related to the aerodynamic drag generated throughout the mission.

Rolls-Royce's technical role was to provide technological guidance on the main technologies, as well as response surfaces for the accurate evaluation of the masses and efficiencies of powertrain components. In this regard, a new specific energy value for the battery was suggested by Rolls-Royce, equal to 270 Wh/kg, being close to the state of the art. Additionally, an engine deck was provided to describe the gas turbine. The sophistication of the models provided, as well as the need to accurately evaluate the energy savings associated with the mission, required a shift to an approach more based on mission analysis. As a matter of fact, a design approach based on preliminary sizing, such as the one described in Section 2.3, did not allow for an accurate evaluation of the flight performance and power and energy requirements necessary to meet the TLARs. Unfortunately, at that time, the analysis module was not yet included in an automatic workflow like the one described in Section 2.4. Therefore, the mission analysis had to take place downstream of the sizing phase, as was done for the preliminary assessment of the concepts in Fig. 3.3. The mission analysis often led to significant differences compared to the predictions

Technology Assumptions	
Battery's Specific Energy (Wh/kg)	270.0
Battery's Specific Power (kW/kg)	0.5

Option 1: 2 Primary Propellers + 8 DEPs

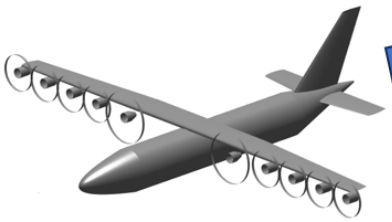

Geometry	
Wing Area (m^2)	33.94
Span (m)	22.58
Weights	
MTOM (kg)	8296.30
Battery (kg)	500.0
200 nmi Mission Block Fuel (kg)	158.8

Option 2: 2 Primary Propellers + 2 Tip-Mounted Secondary Propellers

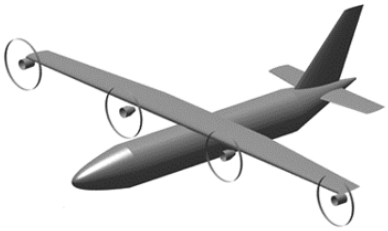

Geometry	
Wing Area (m^2)	42.43
Span (m)	22.58
Weights	
MTOM (kg)	8438.50
Battery (kg)	500.0
200 nmi Mission Block Fuel (kg)	175.25

Figure 3.3: Two different options for the hybrid-electric architecture of the ELICA concept. The use of DEP allows for a 20% reduction in the wing surface area which culminates in greater fuel saving.

made during the sizing phase. For example, it could provide feedback on a wing surface area that was too small, or on an installed power proving insufficient to meet a prescribed requirement. Similarly, the initially assigned amount of energy source (fuel or kerosene) could result in being insufficient to complete the mission. These shortcomings had to be corrected manually, relaunching the routines for estimating masses, aerodynamics, and performance. Multiple iterations were often necessary, requiring to manually repeat the verification of performance and the sizing update process. This activity required a long time (up to a day of work) for the assessment of a single aircraft, making it difficult to optimize the battery mass and its usage strategy in compliance with the certification limit and the other TLARs. Given the long calculation times required by the mission analysis module in its first version, the value of the battery mass was set at 500 kg, leaving a considerable margin compared to the certification limit on MTOM. The hybridization strategy, intended as a combination of shaft and supplied power ratio, was decided by trial and error to match the mission profile and discharge the battery up to 20% of the residual charge. Although rough, the preliminary assessment was useful in selecting the reference architecture for the subsequent refinement of the concept, discussed in the next section.

3.4 Second-Loop Assessment

This section briefly presents the results of ELICA's second-loop assessment, which served to provide the project's partners with a basis for conducting higher-fidelity analyses. The project timeline required freezing the configurations within the second year, limiting the time available for design refinement. These intermediate results have been partially disseminated in Ref. [184], and the main outcomes are reported in this section for discussion purposes.

During the second year of the project, further surrogate models were supplied by Rolls-Royce. These included models for gearboxes, electric machines, thermal engines, batteries, and power electronics. Each response surface, appropriately queried, could provide an estimate for the mass of the component as a function of independent variables such as the nominal power, the voltage, and the RPM number. These models were integrated into HEAD thanks to its flexible software structure, replacing the semi-empirical relationships used for the previous assessment. Efficiency maps were also provided for the components mentioned above, making an approach based on mission analysis even more appropriate. More details on the surrogate models are reported in Refs. [86, 91], which also propose semi-empirical relationships derived from the models themselves.

In parallel, the first annual review by the CSJU's Project Officer meant a substantial turning point in the project objectives. The preliminary estimate of the fuel consumed was still far from the near-zero emissions target. Thus, the demonstrated impossibility of creating entirely electric concepts without drastically reducing the range and commercial attractiveness of the aircraft (see Fig. 3.1 again) led to a change of direction towards a configuration based on hydrogen FCs. In light of the new needs, UNINA worked on the generalization of the powertrain model implemented in HEAD, already discussed in Section 2.2.1. Producing water vapor as the only waste product, a propulsion entirely based on electrical energy extracted from hydrogen promises a solution to the problem of decarbonization of this class of aircraft. However, hybrid-electric configuration based on thermal engines and batteries could still find a role as a necessary transition step starting from the conventional paradigm. In this sense, responding to the request of the Project Officer, a further time horizon with the reference year 2025 would have been considered to capture the possible evolution over time of the aircraft class under analysis. In this way, a transition roadmap towards clean aviation was configured, which passes through hybrid-electric concepts powered by both kerosene and batteries in 2025 and lands on a hydrogen-powered concept with EIS 2035. Figure 3.4 graphically summarizes the envisaged roadmap:

- **Short-term (EIS 2025)**: Serial/parallel partial hybrid aircraft powered with kerosene and lithium-ion ($Li-Ion$) batteries, featuring DEP.
- **Long-term (EIS 2035)**: All-electric aircraft powered with hydrogen PEM-FCs, featuring DEP.

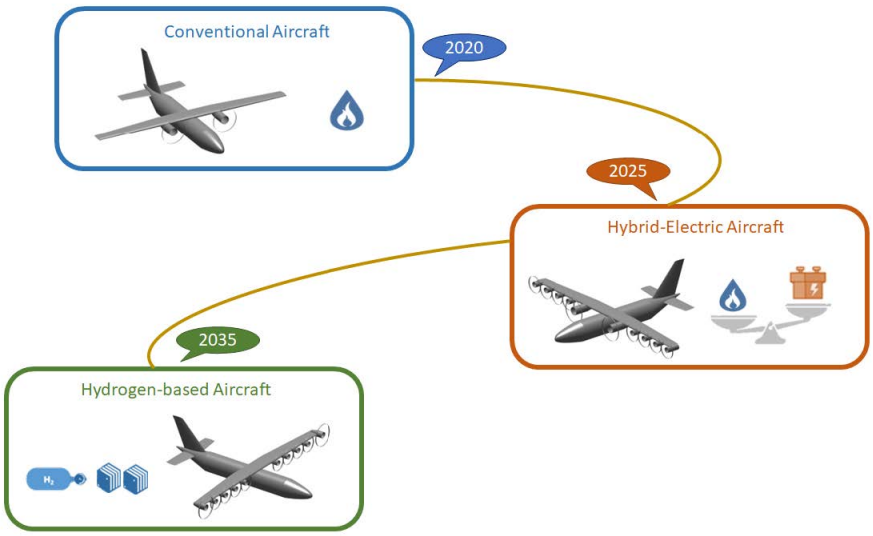

Figure 3.4: Roadmap towards greener commuter aircraft, according to the vision of the ELICA consortium.

As for the configuration with EIS 2025, the same hybrid-electric configuration with DEP as in Fig. 3.3 was adopted, using the secondary propellers in take-off, climb, and landing phases. During the cruise, all the power coming from the thermal engine and the battery is channeled to the primary propellers. In this sense, a series/parallel hybrid architecture (modeled as in Fig. 2.2) was selected in order to be able to split the power into two separated propulsive lines. The choice of the architecture was consolidated by a careful fault-tolerance analysis conducted by Siemens, which concluded that a dual architecture with two or four thermal engines is beneficial from a mass perspective while ensuring sufficient redundancy and controllability. Although analyzing the fault-tolerance of the aircraft was a task carried out by Siemens, the topic inspired the author to produce a work on the effects of failure in the case of DEP architecture. The interested reader will find more details in Ref. [93] and in Appendix B.

As for the EIS 2035 configuration, a partial turbo-electric architecture was selected. The choice criterion was based on the analogy with the short-term configuration, again including DEP and the same number of distributed propellers, placing the two larger propellers at the wing tips in order to mitigate the induced drag. Table 3.3 reports the main technology assumptions for battery and FCs for the two time horizons considered. The most promising estimates about today's specific power levels of a PEMFC are around 1.6 kW/kg, related to applications in the automotive sector [190]. Kadyk et al. estimate that this value could rise to 8 kW/kg in the future [191]. Considering that the specific power of the gas turbines is in the order of 4 kW/kg, it would be sufficient to reach at least this value at the system level in order to facilitate a complete replacement of conventional propulsion systems. Since 2035 is a relatively close target year, the less optimistic value of 2.5 kW/kg was assumed for the purposes of the ELICA project. The chosen value did not include

Table 3.3: Main technology assumptions for the design of the ELICA commuter aircraft, with respect to two different reference EIS years. All values are expressed at the system level.

Parameter	**Unit**	**Value**	
Configuration		**EIS 2025**	**EIS 2035**
Battery Specific Energy	Wh/kg	270.0	333.0
Battery Specific Power	W/kg	500.0	500.0
Fuel Cell Specific Power	W/kg	1 600.0	2 500.0

the weights of the thermal management system and the cryogenic hydrogen tank, the latter estimated separately following the approach proposed by Colozza [192]. However, the estimated GI, above 80%, was judged to be very optimistic compared to expectations, despite the future EIS [122, 140, 193]. The comparison between the specific power value of the FC system and the battery supported the exclusion of the latter from the long-term scenario, especially in light of the limited mass budget.

Table 3.4 reports the main geometry characteristics of the two concepts. The geometries were defined starting from a conventional aircraft serving as a reference baseline. The reference aircraft, having EIS year 2014, was suggested by the advisory board, and more details about its description are made available by the work of Romano et al. [194]. The geometric differences between the two ELICA configurations were limited, except for the distribution of the propellers and for a stretch of the fuselage necessary to accommodate the hydrogen tank in the rear part.

Table 3.5 reports details about the rated power of the main powertrain components of both configurations. These powers are the result of the assumptions about the hybridization ratios considered for the different flight phases. As for the short-term configuration, the shaft power ratio value was limited to 0.70 for the take-off and landing phase to avoid oversizing the secondary line that is not used during the cruise. The shaft power ratio in climb was assumed equal to 0.30. As for the supplied power ratio, it was manually calibrated in order to consume the expendable battery energy by the end of the design mission. This translated to a supplied power ratio of 0.07 in take-off and climb and 0.03 in cruise (raised to 0.09 for the shorter typical mission). As for the hydrogen-based configuration, the presence of a single energy source causes the definition of the supplied power ratio to lapse, while a shaft power ratio of 0.7 was assumed for all phases. For the evaluation of FC and battery efficiencies, the characteristic curves reported in Fig. 2.6 and Fig. 2.7 were adopted. The FC model was also equipped with an air compressor model, as discussed in Ref. [130], slightly reducing the overall efficiency.

Table 3.6 reports the mass characteristics of the two airplanes. For the short-term hybrid-electric solution, it was necessary to limit the battery mass to 700 kg due to the certification limit on MTOM. Although, in this way, a margin was recovered compared to the 500 kg of the preliminary assessment, this battery mass is still insufficient to allow for a significant reduction in fuel consumption and emissions. However, the advantage connected to hybridization goes beyond the

simple electric energy supply, since the use of the battery where peaks of power are required allows for limiting the size of the thermal engine. This not only has a direct advantage on the empty mass of the aircraft but also allows the gas turbine to be operated close to its nominal setting for almost the entire flight, avoiding drops in efficiency due to off-design conditions. In the case of the hydrogen-based configuration, a hydrogen utilization factor of 85% and a further 5% reserve were assumed for determining the total design amount of hydrogen.

The results of the mission analysis are reported in Tab. 3.7. The values refer to the block mission, i.e., the nominal mission excluding the alternate and loiter phases. As for the EIS 2025 configuration, the electrical energy consumed was around 80% of the total energy stored in the battery, equal to 189 kWh. However, a small difference exists between the two missions due to the aforementioned difficulty of manually iterating the analysis for different values of supplied power ratios. In order to judge the results in perspective, the reference aircraft discussed above was used as a comparison for the evaluation of fuel and energy savings. The intermediate results are reported in Tab. 3.8. Although promising, the estimated fuel savings for the hybrid-electric configuration, equal to -50% for the design mission and almost -60% for the typical, were only partially attributable to the limited mass of battery carried on board. From the engine deck provided by Rolls-Royce, a reference value can be extracted for the SFC in cruise equal to 0.40 lb/(hp h), i.e., approximately 35% less than the reference engine (the PTA6-52 [195]). Of the remaining percentage difference, part is attributed to the reduction in the wing surface enabled by DEP, to the higher aspect ratio, and, more in general, to slightly discordant aerodynamic and mission profile assumptions. Only between 10% and 15% was actually attributed to the direct reduction of fossil energy linked to the use of the battery, which confirms its limited usefulness in the presence of such a stringent limitation on MTOM. The block fuel saving of more than 80% reported for the EIS 2035 configuration is affected by the different chemistry of the fuel, and in particular by the different specific energy, which in hydrogen is almost three times higher than in kerosene. In this sense, the comparison between the energies associated with the fuels consumed is more significant. This saving, around 54% for the typical mission, highlights the high efficiency of the FCs compared to the conventional reference engine.

3.5 Final Loop

3.5.1 Parametric Analysis

During the last phase of the project, high-fidelity analyses were conducted by partners from Siemens and SmartUp Engineering. In particular, Siemens carried out Finite Element Analysis (FEA) on the wing structure in order to derive a more accurate estimate of the mass of the wing structure, based on an optimization of the structural parts given the aerodynamic loads and stress distribution [183]. Smartup conducted various analyses to support the aerodynamic and propulsive definitions

Table 3.4: Geometric parameters of the 19-passenger hybrid-electric concepts designed for the ELICA project (second-loop assessment).

Parameter	Unit	Value	
Configuration		**EIS 2025**	**EIS 2035**
Wing			
Surface Area	m^2	33.94	
Aspect Ratio	m	13.00	
Root Chord	m	1.85	
Taper Ratio	–	0.65	
Leading Edge Sweep	°	0.0	
Airfoil (Root/Kink)	–	NACA 23018	
Airfoil (Tip)	–	NACA 23015	
Horizontal Tail			
Surface Area	m^2	10.60	7.01
Aspect Ratio	m	4.60	
Root Chord	m	1.76	1.43
Taper Ratio	–	0.72	
Leading Edge Sweep	°	8.0	
Airfoil (Root/Tip)	–	NACA 0012	
Vertical Tail			
Surface Area	m^2	8.64	6.35
Aspect Ratio	m	1.63	
Root Chord	m	3.35	2.87
Taper Ratio	–	0.37	
Leading Edge Sweep	°	45.0	
Airfoil (Root/Tip)	–	NACA 0012	
Fuselage			
Length	m	16.25	18.00
Cross Section Diameter	m	2.15	
Propellers			
Number of Primary Propellers	–	2	
Primary Propeller Diameter	m	2.54	
Primary Propeller Y-Coordinate	m	2.88	10.50
Number of Secondary Propellers	–	8	
Secondary Propeller Diameter	m	1.79	
Secondary Propeller Y-Coordinates	m	$[5.06, 10.53]$	$[2.88, 8.31]$

Table 3.5: Rated power of main powertrain components for the ELICA hybrid/electric concepts designed (second-loop assessment).

	Short-Term (EIS 2025)		**Long-Term (EIS 2035)**	
Component	**Q.ty (–)**	**Rated Power (kW)**	**Q.ty (–)**	**Rated Power (kW)**
Thermal Engine	2	750.0 (×2)	–	–
Primary Electric Machine	2	500.0 (×2)	2	300.0 (×2)
Secondary Electric Machine	8	175.0 (×8)	8	150.0 (×8)
Fuel Cell System	–	–	2	750.0 (×2)
Battery	1	350.0 (×1)	–	–

Table 3.6: Mass breakdown of the 19-passenger hybrid-electric concepts designed for the ELICA project (second-loop assessment).

Parameter	**Unit**	**Value**	
Configuration		**EIS 2025**	**EIS 2035**
Airframe	kg	2 350.0	2 561.0
Powerplant	kg	2 550.0	2 218.0
Systems	kg	558.6	582.4
Furnishing	kg	418.7	418.7
Operating Equipment	kg	349.7	349.7
Operating Empty Mass	**kg**	**6 227.0**	**6 129.8**
Design Payload	kg	1 767.0	1 767.0
Design Kerosene	kg	615.0	0.0
Design H_2	kg	0.0	270.0
Maximum Take-Off Mass	**kg**	**8 609.0**	**8 166.8**

Table 3.7: Fuel and energy consumption of the 19-passenger hybrid/electric concepts designed for the ELICA project (second-loop assessment).

Parameter	**Unit**	**Value**	
Configuration		**EIS 2025**	**EIS 2035**
500 nmi Design Mission			
Block[1] Time	min	152.0	151.7
Block[1] Kerosene Consumed	kg	423.2	0.0
Block[1] H_2 Consumed	kg	0.0	162.5
Battery Energy Consumed	kWh	145.2	0.0
200 nmi Typical Mission			
Block[1] Time	min	63.0	62.7
Block[1] Kerosene Consumed	kg	158.3	0.0
Block[1] H_2 Consumed	kg	0.0	66.5
Battery Energy Consumed	kWh	159.0	0.0

[1] Excluding reserve mission phases.

Table 3.8: Block fuel and energy savings with respect to a reference conventional baseline with EIS 2014 (second-loop assessment).

	Today (Reference) (EIS 2014)	**Short-Term (EIS 2025)**	**Long-Term (EIS 2035)**
500 nmi Design Mission			
Block[1] Fuel (kg)	847.4	423.2 (-50.1 %)	162.5 (-80.8 %)
Block[1] Energy (kWh)	10 168.8	5 223.1 (-48.6 %)	5 318.7 (-47.7 %)
200 nmi Typical Mission			
Block[1] Fuel (kg)	390.3	158.3 (-59.4 %)	66.5 (-83.0 %)
Block[1] Energy (kWh)	4 683.6	2 058.6 (-56.0 %)	2 175.0 (-53.6 %)

[1] Excluding reserve mission phases.

of the concepts. In particular, propellers were designed in more detail, and their characteristic curves were provided to UNINA in order to replace the semi-empirical model used previously. Furthermore, CFD analyses were useful to re-evaluate the aerodynamics of the wing, with and without the aero-propulsive effects related to distributed propulsion. Feedback also came from the advisory board, which judged the aerodynamic drag to be optimistic and suggested its calibration with a view to a final reassessment. Given the limited duration of the project, the partners' analyses mainly focused on the EIS 2025 hybrid-electric concept, representing the original target of the project. However, the feedback allowed for a recalibration of the analysis tool, correcting the estimates of masses, efficiencies, and aerodynamic coefficients. From SmartUp's analyses, the lift coefficients, including aero-propulsive effects, turned out to be even higher than preliminary estimates by approximately 20%. Last but not least, Rolls-Royce provided an assessment of the mass of the thermal management systems for both concepts, which needed to be taken into account in the final assessment. In this sense, both air and liquid concepts were investigated for electric machines and battery systems, and innovative concepts were explored for FC systems [196]. Furthermore, in relation to the EIS 2035 configuration, it was deemed necessary to adopt more conservative assumptions about the specific power of FCs and about the GI of the hydrogen tank. The reasons listed above were judged more than sufficient to request a reassessment of both configurations. Unfortunately, under the new hypotheses, the concepts no longer matched the TLARs. In particular, the masses of both concepts proved to be higher than the certification limit imposed by the CS-23 certification basis. Since the latest feedback had arrived less than two months before the end of the project, it was impracticable to make radical changes to the configuration or start a new assessment loop. Nevertheless, the consortium agreed that a final assessment, although not supported by new high-fidelity analyses, could still be important in order to develop final recommendations as an output of the project. In this sense, based on the feedback received, UNINA conducted new parametric analyses. This time, different from the first loop discussed in Section 3.3, the study was based on accurate mission analysis rather than on the point performance of the aircraft.

The geometry was kept the same as in Tab. 3.4. As regards the hybrid-electric configuration with EIS 2025, the analysis was aimed at evaluating the effect of the battery mass and the technological level considered. Figure 3.5 shows the resulting trend. As already discussed, the analysis of each point was semi-automatic and required a fair amount of time and computation burden. As expected, the specific energy of the battery has a primary effect on the aircraft's weight and fuel consumption. More interestingly, as battery mass increases, the associated fuel reduction is progressively reduced, even to the point of providing the curve with a point of minimum. This result can be interpreted in light of the increased mass of the aircraft, which implies higher drag and total energy required for the mission. Where the specific energy of the battery is not high enough to justify the increase in mass of the aircraft, the necessary fuel does not decrease or even increase. Further justification is linked to the presence of the alternate and loiter

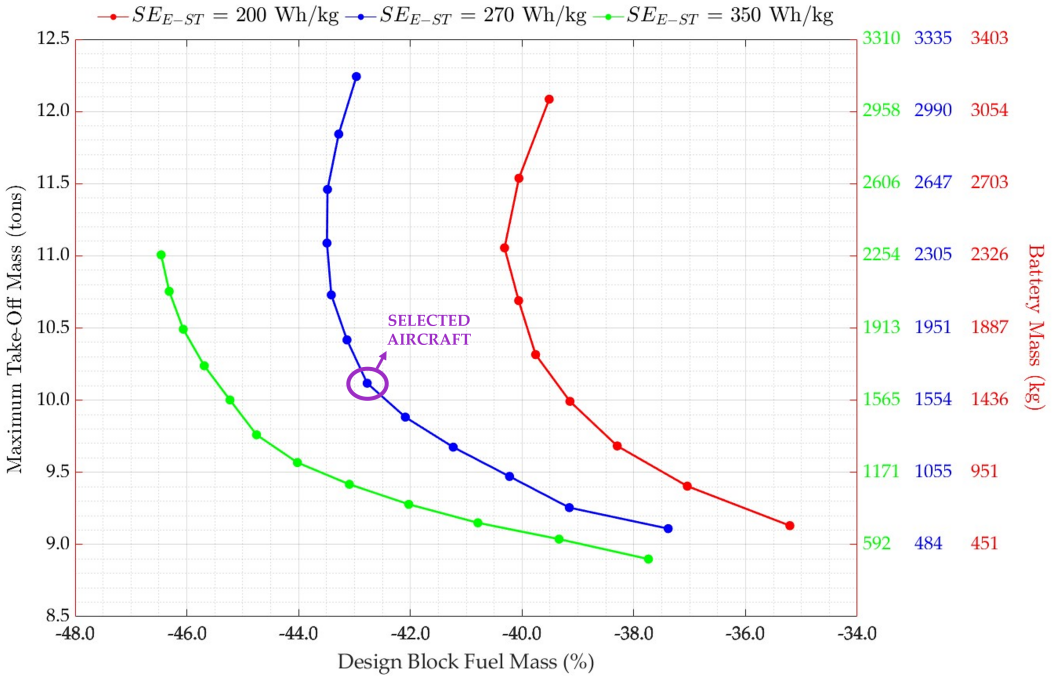

Figure 3.5: Effect of battery mass and specific energy on block fuel saving and maximum take-off mass.

phases, during which it was assumed to use exclusively the conventional propulsion line. In this sense, the reduction in the thermal engine's rated power due to the presence of a battery is possible as long as it cannot be further reduced due to the requirement imposed by the reserve phases. Therefore, further battery increases would increase the mass of the aircraft even more rapidly and have reduced effects on the total propulsive efficiency. Similar results and interpretations were found in the work of Eisenhut et al. [57]. To select a new reference design, the reference value for specific energy was confirmed as 270 Wh/kg. Since the certification limit could not be respected in any case, the new reference design point was chosen close to the identified minimum, on the knee of the curve.

As for the EIS 2035 case, a parametric analysis was performed to figure out the effects of different technological levels of PEMFC systems and cryogenic tanks. The results are visually represented by Fig. 3.6. For the ELICA final assessment, a more conservative specific power of the FCs (excluding the cooling) of 1.6 kW/kg was assumed. The mass of the cooling system was taken into account apart, based on the specific power indicated by Rolls-Royce at the end of the previous assessment loop. In this sense, the synergy with the GENESIS project consortium [15], in which UNINA was also involved, contributed to the recalibration of this assumption. Despite the more conservative assumption, the aircraft's MTOM still falls below the certification limit in the case of cryogenic tanks with adequately high gravimetric efficiency. On the contrary, pressurized tanks do not seem suitable for application on a commuter aircraft, in agreement with the results of other studies [193]. A

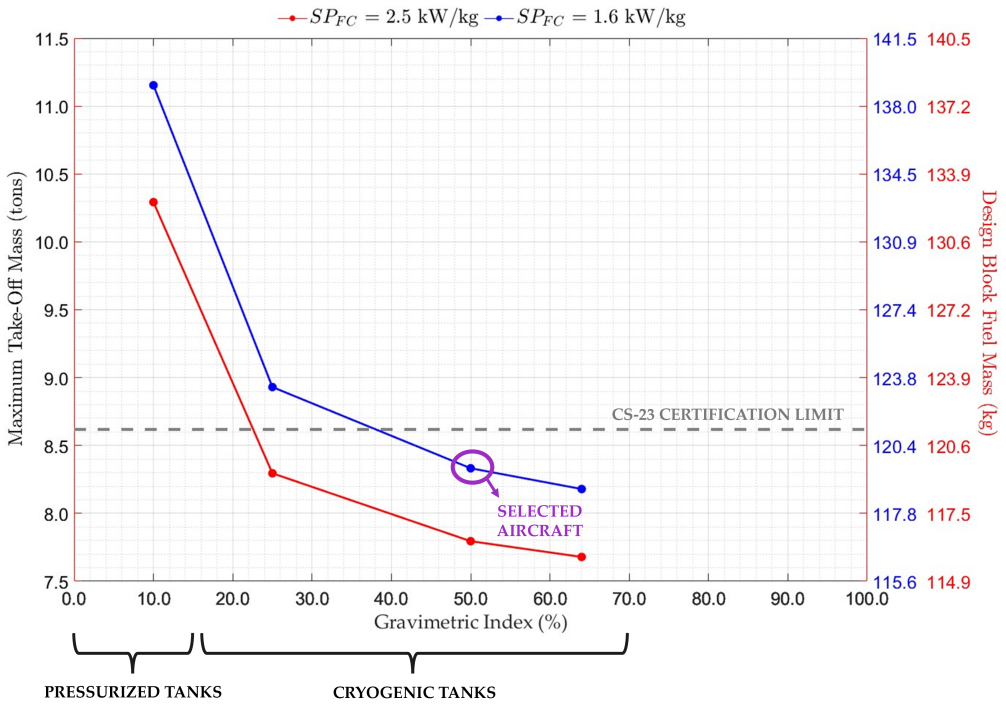

Figure 3.6: Effect of fuel cells' specific power and tank gravimetric index on block fuel (H_2) saving and maximum take-off mass.

new GI equal to 50% was assumed, more conservative than the one previously estimated. However, the figure shows that an efficiency close to 40% could still be compatible with the certification limit.

3.5.2 Final Results

The new mass breakdown of both configurations is reported in Tab. 3.9. This time a battery mass of 1 663.1 kg was considered for the EIS 2025 configuration, allowing for a greater benefit resulting directly from electrification. As anticipated, the solution is not compatible with a certification under the CS-23 regulation code. The mass assessment involved all the components of the powerplant, also including the cabling, whose length was evaluated by taking into account their distribution in detail (see Fig. 3.7). The voltage assumed for distribution is 850 V.

The hydrogen-based full-electric configuration was also refined by including the mass penalty due to the TMS, considering more conservative hypotheses for the mass of FC stacks and liquid hydrogen tanks. The specific power considered for the fuel cell system without cooling is 1.6 kW/kg, but the value dropped to about 1.13 kW/kg when considering the TMS mass.

Details about the cabin configuration and loading diagram are shown in Fig. 3.8 and Fig. 3.9. For the purposes of a more careful evaluation of the possible excursions of the CG, and for verification of the spaces available to house the innovative components, some hypotheses were made. As for the EIS 2025 configuration,

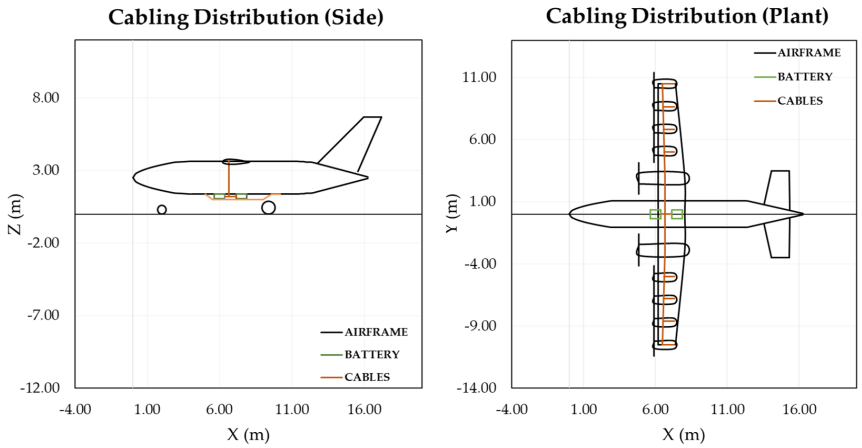

Figure 3.7: Battery and cabling arrangement for the ELICA concept with EIS year 2025. Battery packs are housed into a belly fairing under the fuselage (final assessment).

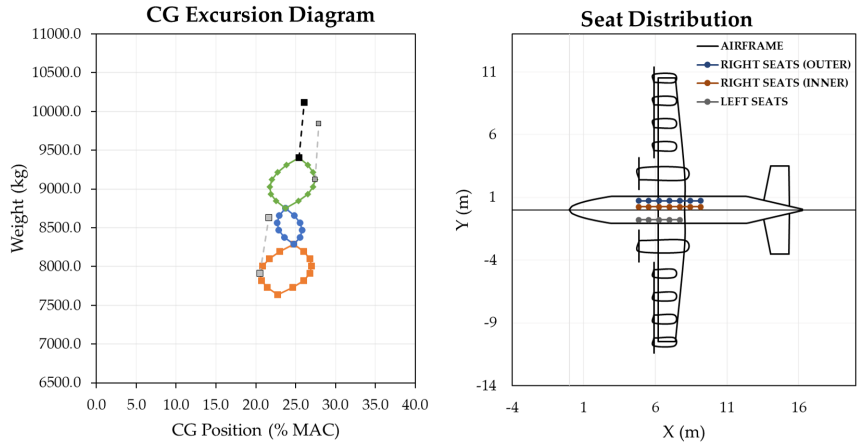

Figure 3.8: Distribution of seats and excursion of the center of gravity for the ELICA concept with EIS year 2025 (final assessment).

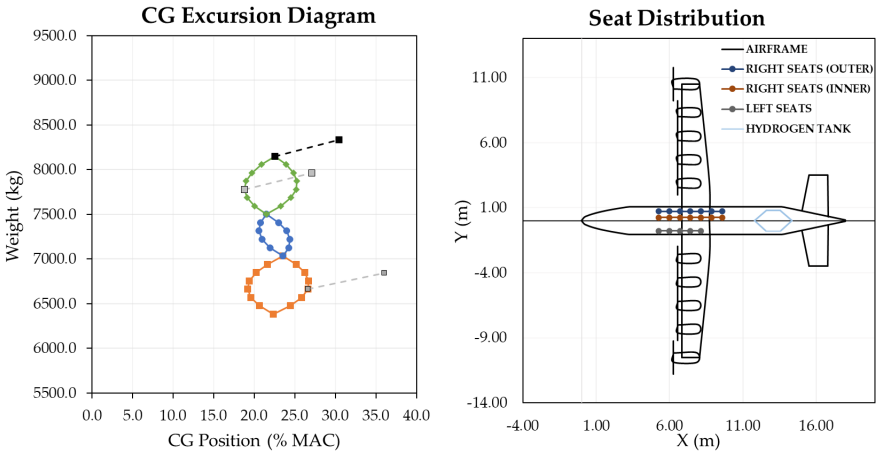

Figure 3.9: Distribution of seats and excursion of the center of gravity for the ELICA concept with EIS year 2035 (final assessment).

Table 3.9: Mass breakdown of the 19-passenger hybrid-electric concepts designed for the ELICA project (final assessment).

Parameter	**Unit**	**Value**	
Configuration		**EIS 2025**	**EIS 2035**
Airframe	kg	2 473.4	2 346.4
Powerplant	kg	3 780.4	2 649.7
(...of which battery)	*kg*	*1 663.1*	*0.0*
(...of which fuel cell plant)	*kg*	*0.0*	*1 464.7*
(...of which hydrogen tank)	*kg*	*0.0*	*182.2*
Systems	kg	609.0	593.5
Furnishing	kg	417.9	439.9
Operating Equipment	kg	353.7	353.7
Operating Empty Mass	**kg**	**7 634.4**	**6 383.2**
Design Payload	kg	1 767.0	1 767.0
Design Kerosene	kg	716.0	0.0
Design H_2	kg	0.0	182.2
Maximum Take-Off Mass	**kg**	**10 117.4**	**8 332.4**

Table 3.10: Rated power of main powertrain components for the ELICA hybrid/electric concepts designed (final assessment).

	Short-Term (EIS 2025)		**Long-Term (EIS 2035)**	
Component	**Q.ty (–)**	**Rated Power (kW)**	**Q.ty (–)**	**Rated Power (kW)**
Thermal Engine	2	750.0 (×2)	–	–
Primary Electric Machine	2	425.0 (×2)	2	250.0 (×2)
Secondary Electric Machine	8	200.0 (×8)	8	150.0 (×8)
Fuel Cell System	–	–	2	830.0 (×2)
Battery Packs	2	415.0 (×2)	–	–

the battery, divided into two packs with an estimated total volume of 0.75 m^3, was housed in a belly fairing under the fuselage (see Fig. 3.7 again). As a consequence, the excursion of the CG is contained between 20% and 26% of the mean aerodynamic chord, as visible in Fig. 3.8. A larger but still limited range was assessed for the EIS 2035 configuration (Fig. 3.9). The limited amount of hydrogen mass consumed during the mission, and the allocation of the FCs in the wing box in the absence of the kerosene tank, both contributed to the containment of the CG excursion, despite the presence of the hydrogen tank in the rear fuselage.

Table 3.10 reports the updated reference powers for the main powertrain components. Compared to the second-loop assessment, the installed powers are overall higher by virtue of the higher mass of the aircraft, except for small recovered margins on the primary electric machines. However, in the case of the EIS 2025 configuration, the increased availability of battery power made it possible to avoid oversizing the thermal engines. Table 3.11 reports the results of the mission analysis. While maintaining the same strategy as the second-loop assessment with regard to shaft power distribution, the supplied power ratio was recalibrated to guarantee

the consumption of 80% of the new value of available battery energy, equal to 449.0 kWh. For the EIS 2025 configuration, a supplied power ratio of 0.14 was used in take-off and climb and 0.054 in the design mission cruise (0.26 in the case of the typical mission). Figure 3.10 graphically reports the history of energy consumption during the design and typical mission phases.

For the final assessment, a preliminary noise analysis was performed as well. Noise estimation was based on the simulation of a certification (take-off) trajectory. Certification requirements for the 19-seat aircraft class are linked to the perceived noise at a point located at 2.5 km from brake release point [197]. The tool used

Table 3.11: Fuel and energy consumption of the 19-passenger hybrid/electric concepts designed for the ELICA project (final assessment).

Parameter	**Unit**	**Value**	
Configuration		**EIS 2025**	**EIS 2035**
500 nmi Design Mission			
Block[1] Time	min	159.1	151.1
Block[1] Kerosene Consumed	kg	488.1	0.0
Block[1] H_2 Consumed	kg	0.0	119.4
Battery Energy Consumed	kWh	359.4	0.0
200 nmi Typical Mission			
Block[1] Time	min	70.6	62.7
Block[1] Kerosene Consumed	kg	175.5	0.0
Block[1] H_2 Consumed	kg	0.0	50.4
Battery Energy Consumed	kWh	339.2	0.0

[1] Excluding reserve mission phases.

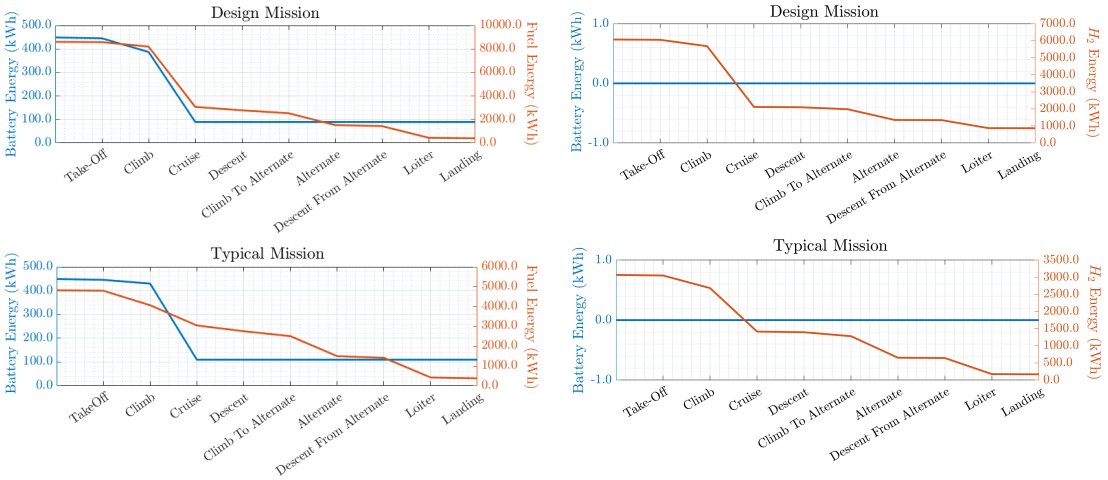

(a) EIS 2025 concept. **(b)** EIS 2035 concept.

Figure 3.10: Breakdown of the energy consumption of the ELICA concepts for both the 500 nmi design mission and the 200 nmi typical mission (final assessment).

for the analysis, named *ATTILA++*, is an application in C++ language capable of providing a preliminary evaluation of the noise footprint and reference noise values of the aircraft, in prescribed flight conditions. The development of ATTILA++ and its validation were the subject of the author's master's degree thesis [198]. The tool collects and adapts several semi-empirical methodologies, originally developed and published by ESDU [199]. In particular, ATTILA++ integrates semi-empirical methods for the prediction of airframe and engine noise, as well as propagation effects, including spreading, shielding, atmospheric absorption, and lateral attenuation [200–205]. For the purposes of ELICA, a powertrain noise map was generated using the methodologies illustrated in Refs. [204–206], constituting an input for the analysis tool. In particular, Refs. [204, 205] were used to estimate the noise coming from the conventional powertrain, while the work of Bruce et al. [206] provided information on the sound power level coming from the secondary components of the powertrain, including electric machines, gearboxes, and FC compressor. The resulting footprints are shown in Fig. 3.11, where the reduced acoustic footprint linked to an all-electric configuration emerges due to the absence of the thermal engine.

A final comparison with the reference aircraft is presented in Tab. 3.12. In addition to energy saving, the table provides some insights into the expected reduction in environmental impact for the two different concepts analyzed. In particular, the noise reduction was quantified in relation to the reduction of the noise footprint area for certain reference noise levels, following the procedure applied in Ref. [194] on the reference aircraft. Despite the increased mass of the aircraft, the expected reduction in CO_2 for the EIS 2025 configuration is promising, although far from the near-zero emissions target. It is important to note that the project initially included a life cycle assessment of the aircraft to take into consideration the effects of manufacturing, disposal, and production of energy sources on the real environmental impact of the aircraft. Nonetheless, the consortium soon realized that it was impossible to conduct such a study in the absence of a sufficient amount of industrial data and a systematic data collection and processing procedure. Furthermore, the environmental impact should be evaluated in a variety of different metrics, relating not only to global warming but also to resource depletion and direct damage to the territory and human health. Lacking the tools and resources to conduct a systematic study to meet the project's needs, the consortium agreed to limit the life-cycle considerations to a penalization of the CO_2 savings by considering the emissions due to energy source production. In this sense, the current European market mix was taken as a reference, and projections to the year 2025 were extracted from Ref. [207]. Furthermore, a reference value for the CO_2 emissions related to the production of 1 kg of kerosene, equal to 259 g, was assumed [75]. Under the hypothesis of green hydrogen, produced by electrolysis of water using renewable energy, the net emissions for the EIS 2035 remain confirmed at 100%.

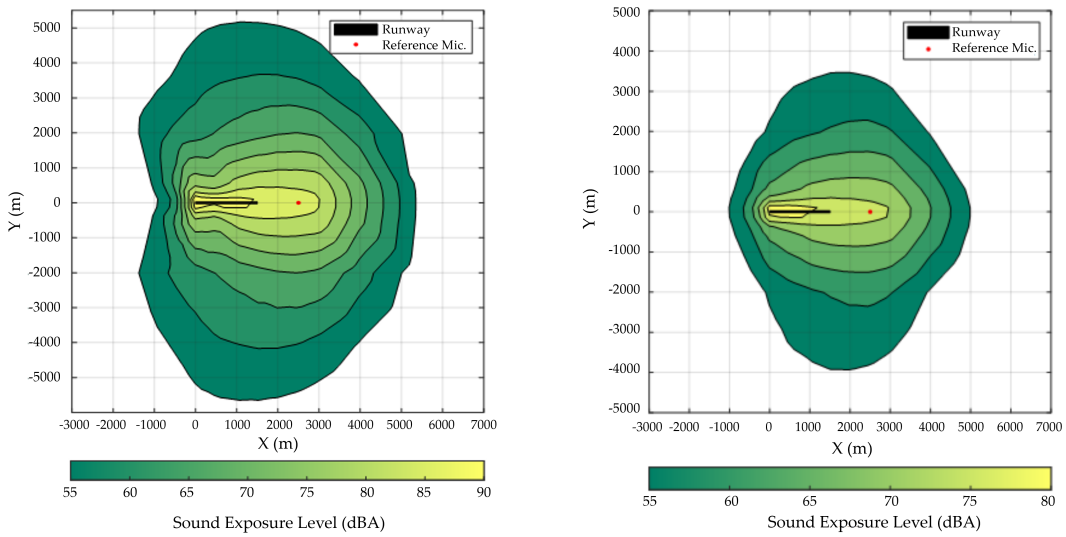

(a) EIS 2025 concept. **(b)** EIS 2035 concept.

Figure 3.11: Noise footprint of the ELICA concepts, represented in terms of sound exposure level (in dBA) at take-off (final assessment).

Table 3.12: Main environmental performance indicators compared to a reference conventional baseline with EIS 2014 [194] (final assessment).

	Reference (EIS 2014)	**Short-Term (EIS 2025)**	**Long-Term (EIS 2035)**
Noise			
Certification Noise Level (dBA)	81.1	78.3 (-3.5 %)	66.4 (-18.1 %)
Ref. Noise Footprint Area (m^2)	23.2	16.1 (-30.4 %)	7.2 (-69.0 %)
500 nmi Design Mission			
Block[1] Fuel (kg)	847.4	488.1 (-42.4 %)	119.4 (-85.9 %)
Block[1] Energy (kWh)	10 168.8	5 857.2 (-42.4 %)	3 981.0 (-60.9%)
Block[1] CO_2 Emissions[2] (kg)	2 899.0	1 732.7 (-40.2 %)	0.0 (-100.0 %)
200 nmi Typical Mission			
Block[1] Fuel (kg)	390.3	175.5 (-55.0 %)	50.4 (-87.0 %)
Block[1] Energy (kWh)	4 683.6	2 106.0 (-55.0 %)	1 678.2 (-64.2 %)
Block[1] CO_2 Emissions[2] (kg)	1 335.2	659.8 (-50.6 %)	0.0 (-100.0 %)

[1] Excluding reserve mission phases.
[2] Including emissions deriving from energy production.

3.6 Lessons Learned

In this chapter, the main activities of the ELICA project have been described, with particular reference to the outcomes of the preliminary design of two 19-seater hybrid-electric concepts. Project results suggest that electrification-induced mass penalties can lead to significant increases in aircraft mass even for limited levels of hybridization. In this sense, a hybrid-electric solution with batteries and thermal

engines could hardly be certifiable under CS-23. At the same time, electrification compatible with the certification basis could only be successful for very short flight missions, harming the economic competitiveness of the aircraft. In this sense, investing directly in hydrogen FCs could represent a more efficient solution for this class of aircraft, although various safety and certification challenges of the new systems would still need to be addressed. The results obtained in the project are not general, and a different outcome could be obtained under more optimistic assumptions on technological levels. In this sense, an albeit modest hybridization with batteries could still be effective, especially if combined with the exploitation of aero-propulsive interaction effects and with modern gas turbine engines with reduced SFC. In the vast landscape of enabling technologies for regional aviation, many of which are still in the development and certification phase, it is important to reliably predict the evolution of the TRL and performance indicators in future time horizons. In this sense, the consortium suffered from the lack of partners specialized in hydrogen propulsion systems. For the purposes of a complete exploration of the most promising scenarios, a diverse consortium is needed, capable of providing technological foresight as a basis for the assessment of impacts at the aircraft level. The advantages estimated for the ELICA concepts also lack a careful life cycle evaluation, which would nuance the estimated emissions reduction and could give rise to trade-offs between different impact categories. The experience highlighted the lack of environmental reports from aeronautical companies and the need for adequate public databases that support the impact of the industrial processes constituting the life cycle of the aircraft. Although predicting the life cycle impact of an aircraft would be essential to guide the designer's choices, such a multidisciplinary analysis requires vast resources and is not possible without the close collaboration of experts in the field. The study presented in the next chapter is founded on a collaboration motivated precisely by these considerations.

All in all, the activities conducted within the ELICA project have contributed to increasing the knowledge of the UNINA group on the research topic of hybridization of small transport aircraft. The project, which aimed to reach at least TRL 4 for the designed concepts, allowed for interaction with industrial partners, and to experience plausible technological levels for the main technologies considered. However, the need to carry out detailed analyses clashed with the need to select a single reference configuration, in a vast and complex landscape characterized by countless possible combinations of design choices. This, combined with the tight deadlines of the project and the shift in focus to hydrogen during execution, led to considerable difficulties in achieving a consistent final result compatible with the initial requirements.

From the aircraft designer's point of view, the greatest difficulty was represented by the absence of a quick and flexible design workflow, capable of integrating inputs from partners and allowing for extensive design explorations in a relatively short time. First, at the beginning of the project, the design workflow available to UNINA included a more rigid powertrain model, which exclusively contemplated architectures with thermal engines and batteries. The sudden need to consider hydrogen FC systems was the pretext for a generalization of the method, as already

discussed in Section 2.2.1 of the previous chapter. Similarly, the new software structure should have been flexible to the integration of mass estimation methods alternative to those presented in the literature. In the context of research projects like ELICA, the inclusion of surrogate models would have allowed for a reduction in discrepancies between expectations and results, thus reducing the number of necessary assessment loops with other partners. Furthermore, the need for accurate analysis of the mission through a simulated approach, including the query of efficiency maps, led to the development of an alternative design workflow focused on design mission analysis and performance evaluation. The workflow, already discussed in Section 2.4, was developed on the basis of the experience gained during ELICA, favoring optimization of calculation times and complete automation of aircraft sizing. The new workflow would have allowed for a complete and accurate design of a new aircraft, starting exclusively from a pre-sized reference aircraft and few more inputs about geometry and propulsion architecture. The time required for assessment for a single aircraft and for a single hybridization strategy (i.e., a combination of hybridization factors) would have been reduced from several hours to a few minutes, eliminating the need for manual designer intervention and reducing the risk of error. The parametric analyses discussed in Section 3.5.2 also suggested that there is a margin for the optimization of the hybridization level in terms of fuel consumed. Although the trends found are the result of a specific set of assumptions and TLARs and are not considered general, they allow deducing that possible trade-offs between the direct advantages of using electricity and the associated drawbacks (especially mass penalties) at the aircraft level should not be neglected. The need emerges to couple the analysis workflow with a DOE that contemplates an exhaustive number of combinations of geometric parameters, hybridization level and strategy, in order to identify the best compromise between aircraft mass and fuel saving. Unfortunately, the new workflow was not completed in time to be applied within ELICA. However, the refined approach was fundamental for the application presented in the next chapter, which benefited from all the lessons learned from the ELICA experience.

4

Technology Roadmap Towards Sustainable Regional Aviation

Contents

4.1 Introduction

4.1.1 A Path Towards Sustainable Aviation

The global civil aviation industry is under increasing pressure to diminish its environmental footprint. In response, the EU committed to attaining net carbon-neutral growth starting from 2020 [3, 6]. Besides climate change impacts, aviation also contributes to chemical pollution and resource depletion. A key strategy in this direction is to address the available propulsive technologies, which currently rely on petroleum-based fuels like kerosene. Transitioning to cleaner, alternative energy sources, as seen in the rise of electromobility in road transportation, is particularly viable for regional aircraft in the 50-seat class. These aircraft types are more adaptable to the potential constraints of new technologies compared to medium- or long-range aircraft. However, significant hurdles remain in achieving sustainable technology transition for these aircraft. In this sense, electric powertrain architectures are still in the early development stages, with no proven technology yet available for regional-class aircraft. Comprehensive studies exploring the technological capacity and potential for electric propulsion in the aeronautics sector are lacking. Future development of electric aircraft will require technology foresight studies and scenario analyses to foresee key technology requirements (like energy density), predict technological advancements, and design integrated aircraft systems, including implications for airframes and ground infrastructure. Furthermore, there is a notable absence of overarching studies that, in addition to focusing on conceptual design and preliminary assessments, allow for capturing life-cycle effects on the real benefits of promising technologies. Only by combining technical considerations, detailed environmental assessments, and considerations of economic feasibility will it be possible to provide reliable answers to the need for truly sustainable regional aviation. In Section 1, the above considerations were formalized in the following questions, which this chapter aims to address:

How can integrating life-cycle and cost considerations into the preliminary design of a 50-passenger regional aircraft, with either conventional or hybrid-electric architecture, assess the real impacts of the most promising technologies over time? How can this study inform the development of an environmental database and provide actionable recommendations for technology selection to policymakers, aviation stakeholders, and aircraft designers?

4.1.2 The GENESIS Project

In this context of uncertainty, it is also the responsibility of research to guide aviation towards environmental sustainability. Among all projects financed by the European Commission, the *GENESIS* project emerges for its specific objectives, which align with the search for truly sustainable solutions for future regional aviation. GENESIS (*Gauging the ENvironmEntal Sustainability of electrIc aircraft Systems*) [15] is a European, CS2-funded project (call H2020-CS2-CFP11-2020-01, project number 101007968) aiming at determining the environmental sustainability of hybrid-electric and all-electric aircraft platforms, by means of LCAs and propulsive technologies foresight. Lasted 30 months between 2021 and 2023, GENESIS ambitiously addressed the existing gaps, aiming to gauge the environmental sustainability of electric aircraft from a foresight perspective and provide a technology roadmap for a sustainable transition toward electric aircraft systems. The main focus of the project was on the identification of the most promising combinations of powertrain technologies for three different time horizons: *short term (2025–2035)*, *medium term (2035–2045)*, and *long term (2045–2050+)*. The reference platform for the aircraft design activities was a regional, 50-seat aircraft. The project comprised three technical WPs:

- **WP1**, dealing with aircraft design activities focused on the generation of hybrid-electric and all-electric aircraft concepts for the three time perspectives considered.
- **WP2**, focused on performing technology foresight analyses on conventional (gas turbines) and innovative (electric motors, batteries, FCs) powertrain elements for the three time horizons considered, supporting the aircraft design activities of WP1.
- **WP3**, developing LCIs for all the technologies and aircraft components, characterizing their production and end-of-life processes, to be used to perform prospective life cycle assessments for future configurations developed within WP1.

The application proposed in this chapter falls within the context of the activities conducted by the author as a participant in the GENESIS project. The collaboration with industrial partners, as well as the coordination role of the Technical University of Denmark (DTU) [208], allowed for obtaining valid results with a high level of detail and broad scope. In addition to being a good opportunity to put into practice the lessons learned from authors' past experiences and the already discussed improvements to the design workflow, participation in the project also proved synergistic in order to address the research question at the basis of the present dissertation.

4.1.3 Chapter Outline

The present chapter is structured as follows. Initially, Section 4.2 will illustrate the selection process of the TLARs for a 50-passenger regional aircraft. Starting from a technical benchmark based on the current market, a set of requirements will be derived to form the basis for subsequent design activities. Section 4.3 will digress on enabling technologies for future sustainable regional aviation. In particular, the most promising ones will be identified in relation to their level of maturity and expected technical characteristics, specifying how these hypotheses flowed into the aircraft design workflow. The subsequent sections, from 4.4 to 4.7, constitute the central part of the discussion. The identification of the most promising technologies available converges in the definition of scenarios representative of three future time horizons. The scenarios, presented in Sections 4.4 and 4.5, embody combinations of available innovative elements, so that an in-depth evaluation of their advantages and disadvantages can provide feedback on their potential impact on future regional aviation. In this sense, Section 4.4 also defines reference conventional aircraft for each time horizon, against which alternative solutions can be compared. The results will constitute a solid basis for the LCAs presented in Section 4.6, aimed at reducing the environmental benefits promised by mission analysis alone. This activity was possible thanks to the inclusion of this work within the GENESIS scope and started from data gathering and construction of models for aircraft concepts, in which the author of this dissertation had a role. In Section 4.7, the picture will be completed by a prospective cost analysis performed by the author, with the aim of providing future economic scenarios and evaluating the commercial feasibility of the proposed solutions. The technical, environmental, and economic results will finally be discussed in Section 4.8 where, for each time horizon, the solutions analyzed will be compared from a more multidisciplinary perspective. All considerations will flow into a proposed transition roadmap toward future aviation, which will be useful in trying to answer the research question underlying the present thesis. The roadmap will be accompanied by a set of recommendations for aviation stakeholders, seen as necessary steps to take to realize the author's vision and move towards a more sustainable regional aviation in the future.

Author's Contributions

The study that will be presented in this chapter was carried out in synergy with the objectives of the GENESIS project, coordinated by Dr. Alexis Laurent (DTU). In this sense, the author had a central role in the conceptualization and implementation of the aircraft design activities of WP1. Furthermore, the author was involved in WP2 activities, collaborating with industrial partners for the definition of technologies and their integration at the aircraft level. In WP3, the author contributed with an analysis of the direct operational costs of the scenarios considered, as well as the definition of a LCI database preparatory to the LCA. In summary, all the activities presented in this chapter involved the author of this dissertation to varying degrees. Moreover, the author was responsible for the production of several public technical reports [15], their presentation to the project reviewers, and their public dissemination at international conferences. First, the author participated in the definition of the TLARs discussed in Section 4.2.

Author's Contributions (Cont.)

This activity was mainly led by Dr. Manuela Ruocco (UNINA\SmartUp) and also received contributions from other fellow researchers from UNINA, including Dr. Francesco Orefice, Dr. Mario Di Stasio, and Prof. Fabrizio Nicolosi. Concomitantly, preliminary assessments of the aircraft's power and energy requirements were made by the author, providing a basis for discussion with WP2 partners specialized in innovative propulsive technologies. The author personally managed all interactions and data exchanges with partners, culminating in the identification of the most mature and suitable technologies for future regional aircraft and their expected performance levels. Particular credit is given to Mr. Markus Meindl and Mr. Christian Bentheimer (FAU Erlangen Nürnberg) for the foresight analyses relating to electric drives and power electronics; Mr. Bruno Lemoine and Prof. Priscilla Caliandro (Bern University of Applied Sciences) for their considerations on the potential of battery chemistries and SOFCs; Mr. Thomas Wannemaker and Dr. Nils Baumann (Proton Motor Fuel Cell GmbH) for the PEMFC systems; Dr. Benjamin Sala and Ms. Alexe Guiguemde (Mahytec) for the hydrogen storage systems. In parallel, within WP1, the author interacted with Dr. Zhijun Wang and Prof. Roeland De Breuker from TU Delft, providing indications useful for the development of a surrogate model for the structural mass estimation of a DEP wing. The output of these collaborations is reported in Section 4.3. The author coordinated the integration of surrogate models and technological assumptions within the design workflow described in Section 2.4, supported by Dr. Ruocco and Dr. Di Stasio. In this context, Di Stasio's method for modeling ICE characteristics was integrated as well. The author was responsible for the aircraft design activities that will be presented in Section 4.5. After setting up the workflow, he was supported by Dr. Ruocco and Dr. Di Stasio in the calculation execution and in postprocessing the results. A further but short interaction loop with the WP2 partners guaranteed coherence between the results of the aircraft design activity and the accurate definition of the individual powertrain components. In WP3, as discussed in Section 4.6, the author contributed to the preparation of a comprehensive LCI database, built starting from the previously designed scenarios. In particular, the author took care of the characterization of the aircraft's operational life and of aspects related to the airframe production. Dr. Di Stasio took care of the production and disposal of conventional powerplant components. The author was even more directly involved in WP3 activities during a three-month stay spent in person at DTU, in Copenhagen. During that period, which lasted from May to July 2023, he contributed with an economic impact assessment of future scenarios, discussed in Section 4.7. Cost assumptions related to innovative technologies were provided by the WP2 partners. Several researchers from DTU contributed to this work as well; in particular, Dr. Eleonore Pierrat collected projections about expected prices for energy sources, and Ms. Karen Saavedra-Rubio facilitated the management of input and output data. The LCA of Section 4.6 was formally performed by DTU researchers. Dr. Nils Thonemann coordinated the activity, supported in data curation by Ms. Saavedra-Rubio, Dr. Pierrat, Ms. Katarzyna Dudka, Ms. Julie Elleby, and Ms. Anna Lia Tromer Dragsdahl, under the coordination of Dr. Laurent. However, the research stay was also an opportunity to learn the rudiments of LCIA, so that the author could provide support and feedback to the analysis. In this sense, coordination was essential to align some operational assumptions underlying the LCA and the cost assessment. All results obtained, combined with observations by the expert partners on the pending technological challenges, were preparatory to the determination of the technological roadmap and a final set of recommendations, both required as a final output from WP1. The author was in charge of this final activity, and proposed the conclusions that will be presented in Section 4.8. However, the latter were shaped, refined, and discussed together with the partners from DTU and UNINA, taking advantage of the visit period in Copenhagen. The conclusions were finally shared by the entire consortium, reflecting GENESIS' vision for a future sustainable regional aviation.

Related Publications

The work presented in this chapter is linked to numerous scientific productions. In this regard, the following journal articles were published:

[94] **Valerio Marciello**, Mario Di Stasio, Manuela Ruocco, Vittorio Trifari, Fabrizio Nicolosi, Markus Meindl, Bruno Lemoine, and Priscilla Caliandro. *Design Exploration for Sustainable Regional Hybrid-Electric Aircraft: A Study Based on Technology Forecasts.* Aerospace, 10(2):165, 2023. The article focuses on the design exploration of sustainable regional concepts conducted for the purposes of this work and which will be recalled in Section 4.5. The author of this dissertation led the conceptualization of the work, the implementation of the design workflow (previously introduced in Section 2.4), the formal analysis, the discussion of the results, and the writing and revision of the manuscript. The presence of international co-authors is justified by their essential contribution to consolidating the technological assumptions at the basis of the design activities.

[209] Markus Meindl, Cor De Ruiter, **Valerio Marciello**, Mario Di Stasio, Florian Hilpert, Manuela Ruocco, Fabrizio Nicolosi, Nils Thonemann, Karen Saavedra-Rubio, Louis Locqueville, Alexis Laurent, and Martin März. *Decarbonised Future Regional Airport Infrastructure.* Aerospace, 10(3):283, 2023. The author of this dissertation contributed to the collection of data relating to the aircraft level, on the basis of which the first two authors evaluated potential solutions to adapt ground infrastructures and ground power supply to the new aviation paradigm.

[210] Nils Thonemann, Karen Saavedra-Rubio, Eleonore Pierrat, Katarzyna Dudka, Mathilde Bangoura, Nils Baumann, Christian Bentheimer, Priscilla Caliandro, Roeland De Breuker, Cor De Ruiter, Mario Di Stasio, Julie Elleby, Alexe Guiguemde, Bruno Lemoine, Martin Maerz, **Valerio Marciello**, Markus Meindl, Fabrizio Nicolosi, Manuela Ruocco, Benjamin Sala, Anna Lia Scharling Tromer Dragsdahl, Andrea Vezzini, Zhangqi Wang, Thomas Wannemacher, Julius Zettelmeier, and Alexis Laurent. *Prospective Life Cycle Inventory Datasets for Conventional and Hybrid-Electric Aircraft Technologies.* Journal of Cleaner Production, 434(3):140314, 2023. The work is the culmination of the intense collaboration between the partners of the GENESIS project, aimed at building a prospective LCI database for regional aircraft and for the technologies considered. The database, made publicly available [211], fills the lack in the literature of detailed aeronautical environmental datasets, particularly with respect to aircraft in the regional class. As will be clarified better in Section 4.6, the author contributed directly to the production of the database under the coordination of DTU.

In the context of the activities presented in this chapter, one additional work has been produced, submitted to a high-rank journal, currently undergoing the review process:

[97] **Valerio Marciello**, Vincenzo Cusati, Fabrizio Nicolosi, Karen Saavedra-Rubio, Eleonore Pierrat, Nils Thonemann, and Alexis Laurent. *Evaluating the Economic Landscape of Hybrid-Electric Regional Aircraft: A Cost Analysis Across Three Time Horizons.* Submitted to Energy Conversion and Management *(under review).* In this work, supported by Dr. Vincenzo Cusati in the development of the workflow for the cost analysis and by the other co-authors for the collection of economic assumptions, the author of this dissertation will propose an evaluation of the direct operating costs of future aircraft featuring innovative and sustainable propulsive technologies. The workflow has already been presented in this document in Section 2.5, while the results and their discussion will be the subject of Section 4.7.

Related Publications (Cont.)

In September 2022, the author also participated as a speaker at the 33rd ICAS Congress to disseminate the first results of the research activity (the speaker's name is underlined):

> [153] **Valerio Marciello**, Manuela Ruocco, Fabrizio Nicolosi, and Mario Di Stasio. *Market Analysis, TLARs Selection and Preliminary Design Investigations for a Regional Hybrid-Electric Aircraft.* In 33rd Congress of the International Council of the Aeronautical Sciences (ICAS 2022), Stockholm, Sweden, 2022. The work describes the determination of the TLARs starting from a technical benchmark study, as described later in Section 4.2. Essential contributions to the research work, market analysis, and determination of requirements were given by the co-authors.

The author contributed to additional presentations at the EASN Conference:

> [212] **Valerio Marciello**, Mario Di Stasio, Manuela Ruocco, and Fabrizio Nicolosi. *Design Exploration for Sustainable and Innovative Regional Aircraft.* In 12th EASN International Conference, Barcelona, Spain, 2022 *(presentation only).*
>
> [213] Fabrizio Nicolosi, **Valerio Marciello**, Mario Di Stasio, Manuela Ruocco. *Design of Sustainable and Innovative Regional Aircraft for Three Time Horizons.* In 13th EASN International Conference, Salerno, Italy, 2023 *(presentation only).*
>
> [214] **Valerio Marciello**, Vincenzo Cusati, Manuela Ruocco, Mario Di Stasio, Fabrizio Nicolosi. *Technology Roadmap for a Transition to Sustainable and Competitive Electric Aircraft Systems.* In 13th EASN International Conference, Salerno, Italy, 2023 *(presentation only).*

Finally, one additional paper has been submitted for presentation at the 2024 AIAA Aviation Forum:

> [215] Fabrizio Nicolosi, **Valerio Marciello**, Mario Di Stasio, Manuela Ruocco. *Technology Roadmap for a Transition to Sustainable and Competitive Electric Aircraft Systems.* To be presented at the AIAA Aviation Forum 2024, Las Vegas, Nevada, 2024 *(extended abstract submitted).* The work will disseminate the final results of the study covered in this chapter, with particular reference to the roadmap discussed in Section 4.8.

4.2 Definition of Requirements

4.2.1 Introduction

The design of new concepts integrating hybrid-electric architectures and highly efficient propulsion systems is a crucial aspect of future aviation. As the aviation industry evolves, the need for aircraft that not only meet technical benchmarks but also align with market demands becomes increasingly pronounced. A comprehensive understanding of the market landscape is imperative to anticipate and respond to emerging trends, regulatory shifts, and evolving consumer preferences.

As well known, conceptual design is an iterative process that aims to choose a single aircraft configuration in compliance with a set of well-defined boundary conditions. The latter are represented by aviation regulations and additional top-level constraints set by the designer. Therefore, the TLARs have a primary role in aircraft design activities, serving as the cornerstone upon which the aircraft design is

built, influencing performance parameters, operational capabilities, and eventually, economic viability. In this sense, choosing an adequate set of TLARs is essential to align the aircraft to be designed with market needs. As a matter of fact, the increase in operating costs associated with using alternative energy sources makes careful market analysis even more critical. Degradation of aircraft-level performance due to hybridization could drastically reduce the attractiveness of the final product. Therefore, ensuring minimum performance levels that match the end customer's needs is of the utmost importance. A different way of interpreting the set of TLARs is through the definition of a reference mission, which the appropriately designed aircraft must be able to complete. In this sense, the reference mission will be called the *design mission* in the remainder of the present dissertation. For this reason, the design mission must reflect the characteristics desired by the end customer. So its definition becomes the main objective of a market scenario analysis to make the final product economically attractive. Nonetheless, it is not necessarily said that the design mission corresponds to the *typical mission*, i.e., the mission that is best representative of the actual average use of the aircraft by the end operators.

This section will deal with the selection process of the TLARs for the 50-passenger regional aircraft that is the subject of this study. Subsection 4.2.2 will report observations on a technical benchmark of airplanes that are representative of the market segment of interest. Starting from the technical benchmark study results, a set of TLARs will be derived and fully reported in Subsection 4.2.3. The set of requirements will constitute the boundary conditions that will guide the design of the concepts in the following sections.

4.2.2 Technical Benchmark Study

To obtain a reliable forecast of future market scenarios and make the best design choices, it is indispensable to deeply search for data from the current air segment market and the whole international transport network, with particular attention to passenger demand.

In the present subsection, to define the aircraft TLARs, information was collected from regional aircraft with a seating capacity of up to 100 passengers operating predominantly on short-haul flights. The data were obtained from official sources, composed of type-certificate data sheets, airport planning manuals, and official statements by manufacturers [154–156, 216–230]. Table 4.1 reports the benchmark aircraft selected for this application. The benchmark included 3 jet aircraft and 5 turboprop-powered aircraft, closest to the case of interest, representing the 40-100 passenger class.

Once the benchmark was identified, the first and most important step was to define the parameters that are indicative of the product performance. The goal was to understand how the product works and how customer benefit is generated. The parameters considered for the present study are reported from Fig. 4.1 to Fig. 4.7. First of all, the maximum number of seats is compared to localize the 50-passenger target in the reference market (Fig. 4.1). Half of the aircraft considered have a

Table 4.1: Data collection of aircraft with up to 100 passengers representative of the regional class [154–156, 216–230] (adapted from Ref. [153]).

Aircraft	Manufacturer	EIS Year	Country	Max. Seats	Powertrain
ATR 42	ATR	1984	Italy–France	42–50	Turboprop
ATR 72	ATR	1989	Italy–France	66–78	Turboprop
CRJ 100	Bombardier Aerospace	1991	Canada	50	Jet
CRJ 700	Bombardier Aerospace	1997	Canada	66–78	Jet
Dash 8-Q300	Bombardier Aerospace	1989	Canada	45–56	Turboprop
Embraer E145	Embraer	1995	Brazil	49–55	Jet
Fokker 50	Fokker	1985	Netherlands	46–56	Turboprop
SAAB 2000	SAAB	1992	Sweden	50–58	Turboprop

nominal passenger number of around 50 passengers, as per the study under analysis. Among these, it is helpful to identify a main reference for the purposes of the design activities that will follow in the next sections. In fact, although this study aims to design new concepts, it is anticipated that a reference baseline will be very useful for initializing some design and architectural choices, as well as a term of comparison for the performance of the concepts designed. In particular, the ATR42 was chosen as the reference aircraft by virtue of its commercial success and the wide availability of public data [154–157, 174, 216, 231].

Figure 4.2 shows the distribution of the MTOMs of all airplanes in the benchmark. The highest value is related to the CRJ700, which, however, is a jet aircraft with significantly more seats than the aircraft under analysis. With the only exception of the CRJ700, the mass values are all below 24 tons. The ATR 42-600 has a certified MTOW of 18.6 tons for a nominal number of 50 passengers [155]. Considering that hybridization will lead to an increase in weight due to the mass of the electrical components, a threshold of 24 tons is a valuable reference for trying to contain the mass of the concepts to be designed, especially to reduce the acquisition and operating costs of the final products. However, this upper limit may not be sufficient for all-electric aircraft.

Following, the most interesting performance indicators are discussed. The design range gives the first relevant example. Figure 4.3 compares the ranges of all aircraft included in the benchmark. The effective range of an airplane is a function of the seating configuration and the number of passengers carried on board. However, the values shown in Fig. 4.3, referring to the maximum payload in sea level (SL) and ISA conditions, still constitute a first important indication for the selection of a reference design range. As a matter of fact, a wise choice of the design range is crucial as it

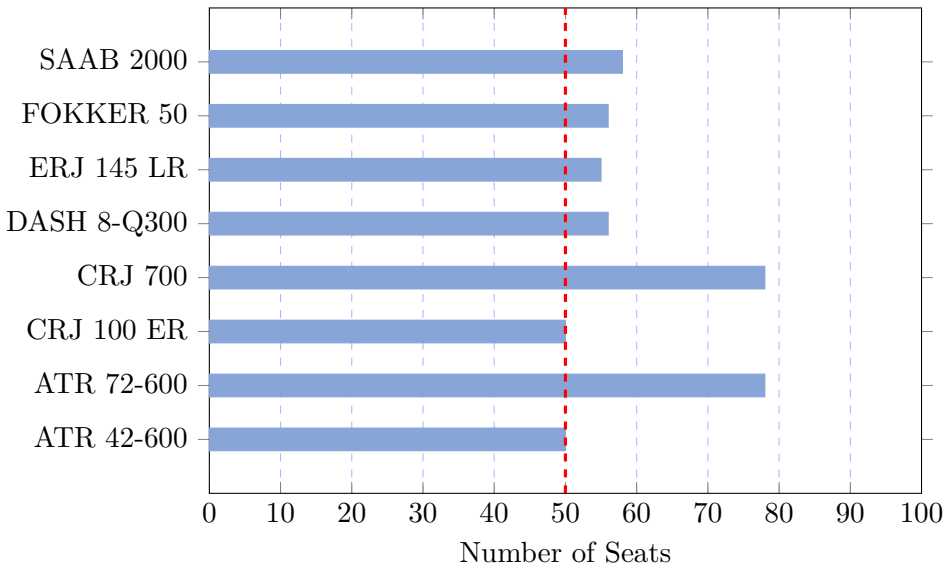

Figure 4.1: Comparison of data from the regional aircraft segment – Maximum number of seats. The red dashed line locates the aircraft of the present study [154–156, 216–230] (adapted from Ref. [153]).

influences which routes the aircraft will cover. Economic feasibility studies show that point-to-point connections not covered by narrowbody airplanes can be more profitable and a competitive niche for regional aircraft [232, 233]. In this sense, it is helpful to consider competitivity with other means of transportation. Compared to many regional transport systems, high-speed rail competes with air transportation in terms of time and distance factors. Airports are generally distant from city centers, while conventional and high-speed train stations are much closer. Conventional rail services are usually more competitive for short distances of less than 150 km (air transport is almost never flown over these distances) than high speed [233]. This is primarily attributed to the more frequent service schedules offered by conventional rail. High-speed rail typically operates within the main service window of 150 to 775 km, a range where it generally holds a time advantage over air transportation. However, for distances exceeding 800 km, air transportation usually becomes more advantageous. These aspects are visually summarized in Fig. 4.4, which compares door-to-door times between conventional, high-speed rail and air transport [233]. Considering a design range above 1 100 km (or about 600 nmi) would not only be in line with the average range of turboprop-powered aircraft in the benchmark but would also provide operational flexibility and a minimum margin with respect to the rail transport's competency area. These considerations led to a design mission of 600 nmi for the present application. However, it also emerges from Fig. 4.4 that, in case there were no high-speed rail services, air transportation would be more advantageous over distances of 370 km (200 nmi). This is especially true considering the extensive network of airports and regional airfields providing convenient access to various locations, especially in areas where larger airports may be less accessible.

This accessibility contributes to the expected growth in demand for regional

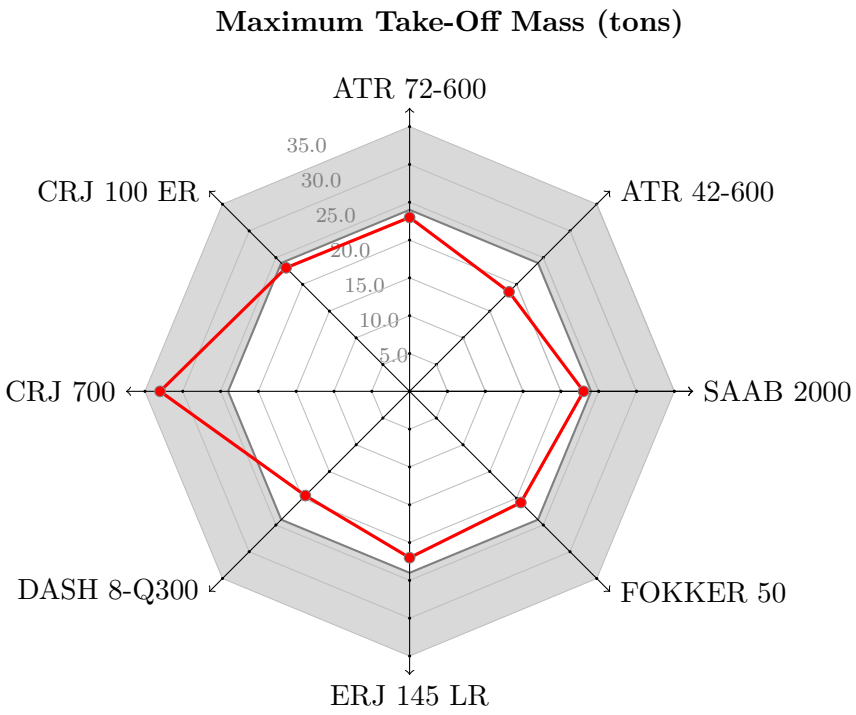

Figure 4.2: Comparison of data from the regional aircraft segment – Maximum take-off mass [154–156, 216–230].

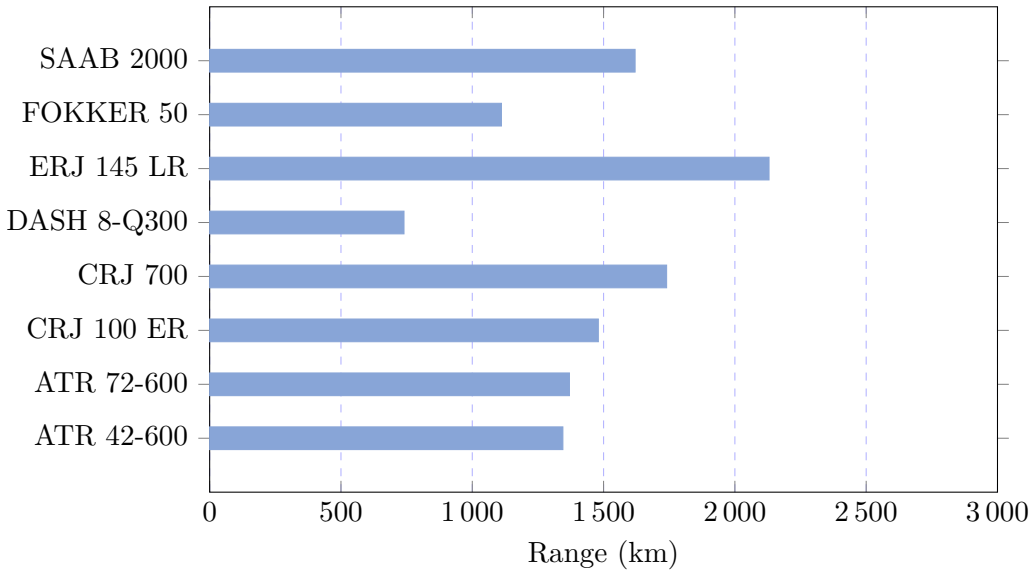

Figure 4.3: Comparison of data from the regional aircraft segment – Range at maximum payload (adapted from Ref. [153]).

flights using smaller aircraft [232]. In light of these considerations, a range of 200 nmi will be considered for the typical mission, assuming that the latter is better representative of the real operational use of the aircraft. The chosen value is also in line with the case of the reference aircraft since ATR indicates 200 nmi and 300 nmi as typical sectors for the operation of the ATR42 [174].

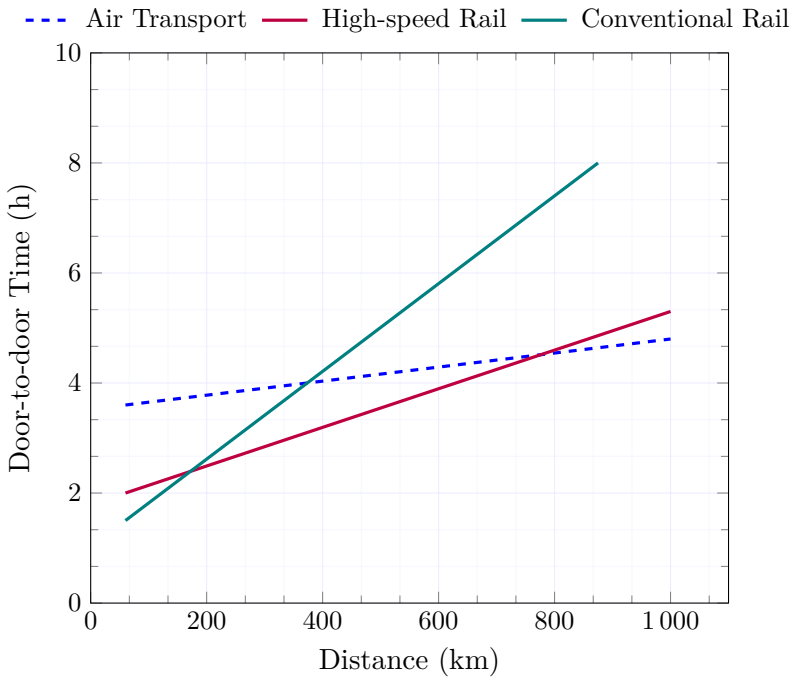

Figure 4.4: Break-even distance between conventional rail, high-speed rail, and air transport (adapted from Ref. [233]).

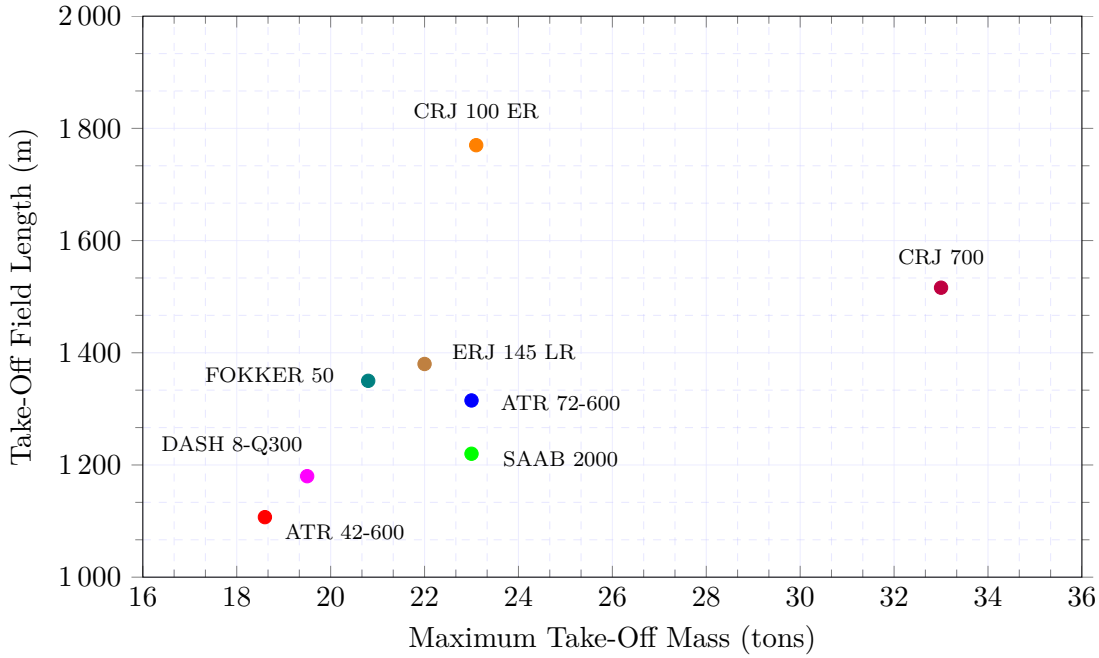

Figure 4.5: Comparison of data from the regional aircraft segment – Take-off field length [154–156, 216–230] (adapted from Ref. [153]).

Linked to the choice of reference ranges, a crucial aspect concerns the airports from which the aircraft will be operated. In this sense, a decisive factor is represented by the TOFL. Figure 4.5 reports the TOFL for all benchmark aircraft, showing

the correlation with the aircraft's weight. The average of the benchmark aircraft would suggest a take-off distance of 1 350 m. This value should be interpreted by considering that the take-off distance of regional airliners is often disregarded because the latter are usually operated from large airports with runways designed for bigger aircraft. However, this can no longer be true if the aim is to exploit as much as possible the vast global infrastructure network [232]. The shorter the required runway, the more airports can be part of the route network. Figure 4.6 show the frequency distribution of runway lengths for the major world airports [234]. As can be observed from the figure, a TOFL of 1 200 m would allow serving more than 90% of airports. This represents a rather ambitious target since the hybridization of the aircraft is expected to lead to a significant increase in MTOM. A too-low value of TOFL could lead to an increase in the required wing surface area, and in turn an increase in aerodynamic drag and energy demand for the mission. However, the presence of electric motors enables the use of DEP systems, and the exploitation of consequent propulsive benefits that can compensate for mass penalties without affecting the size of the lifting surfaces. In light of the possibility of providing DEP for hybrid-electric architectures and all the advantages it promises, a field length of 1 200 m was chosen to make the final product competitive in terms of maximum operational flexibility.

Finally, the cruise speed was also considered, since it affects the number of flights that can be carried out in a single day, and therefore the operating costs. It is evident from Fig. 4.7 that the average speed for jet aircraft is higher than for turboprop aircraft, the latter being of greater interest for the present application. Since cruise speed is an important parameter in determining the economic profitability of an aircraft, it is still vital to remain competitive in the market. For this reason, a cruise speed of about 545 km/h, close to the minimum in the benchmark, was assumed.

4.2.3 Selection of TLARs

The market considerations formulated so far helped identify the driving parameters that will be at the basis of further analyses. This preliminary phase led to the definition of a complete set of TLARs, here reported in Tab. 4.2. This set of parameters will serve as the boundary conditions for the design and optimization of aircraft. Two distinct missions were considered: a 600 nmi design mission, used to size the aircraft and assess its energy demand, and a 200 nmi off-design typical mission for evaluating typical fuel consumption and pollutant emissions. The cruise phase of both missions was assumed to occur at FL 200. The time to climb to cruise altitude should not exceed 13 minutes. This value was assumed starting from the climb rate of the ATR42, which can be deduced from ATR declarations to be around 1550 ft/min [174]. A 100 nmi alternate and a 30-minute holding were also considered after the cruise segment to account for reserves [154, 174]. Plus, an additional 5% contingency fuel was included. A taxi time of 20 minutes was assumed from the average of 90^{th}-percentile times observed at various airports [159]. Based on statistics, 66% of taxi time is associated with the taxi-out phase, while the

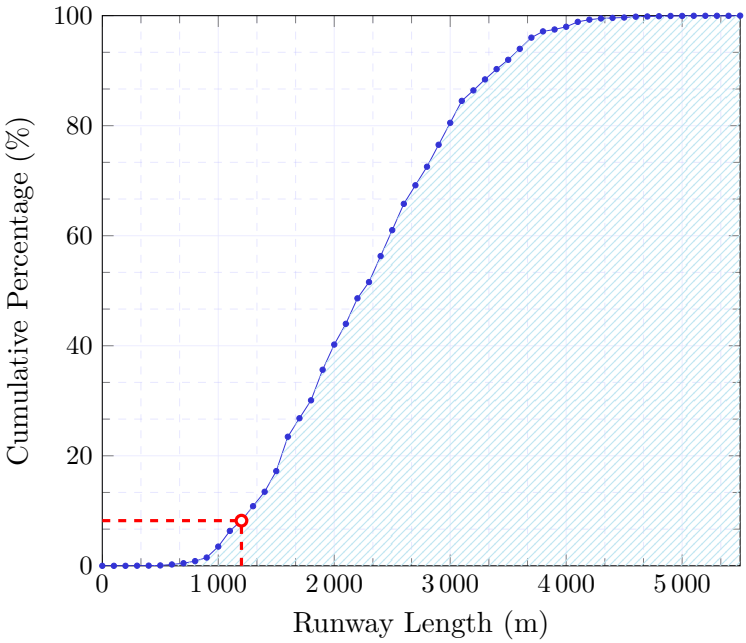

Figure 4.6: Frequency distribution of runway length for the major world airports (adapted from Refs. [153, 234]).

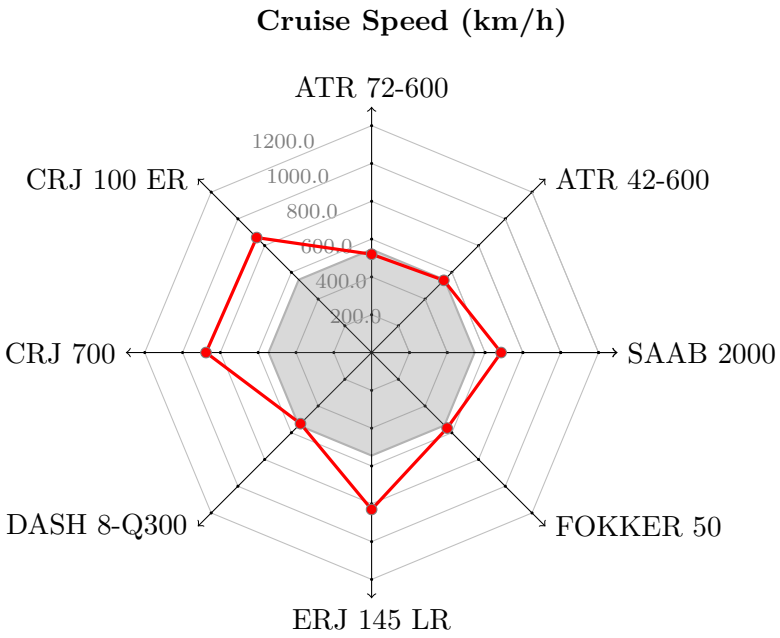

Figure 4.7: Comparison of data from the regional aircraft segment – Cruise speed [154–156, 216–230] (adapted from Ref. [153]).

remainder is associated with the taxi-in phase [159]. The resulting missions can be visualized in Fig. 4.8. The MTOM and the maximum landing mass (MLM) should be limited to guarantee the aircraft's operability from runways whose length is lower than 1 200 m at SL and in ISA conditions. The use of DEP is also prescribed for hybrid and electric concepts to support the achievement of this target. In addition,

Table 4.2: Complete set of TLARs for the definition and design of future aircraft concepts.

Description	Value	Unit	Notes
Design Range	600	nmi	
Typical Range	200	nmi	
Time to Climb (Design Mission)	13	min	At MTOM
Cruise Speed	295	KTAS	FL 200
Take-Off Field Length	$< 1\,200$	m	At SL, ISA and MTOM
Landing Field Length	$< 1\,200$	m	At SL, ISA and MLM
Design Payload	4 750	kg	50 PAX – 95 kg per PAX
Alternate	100	nmi	FL 100
Holding	30.0	min	
Taxi	20.0	min	34% taxi-in, 66% taxi-out
MTOM	< 24	tons	< 27 tons for hydrogen-based full-electric configurations.

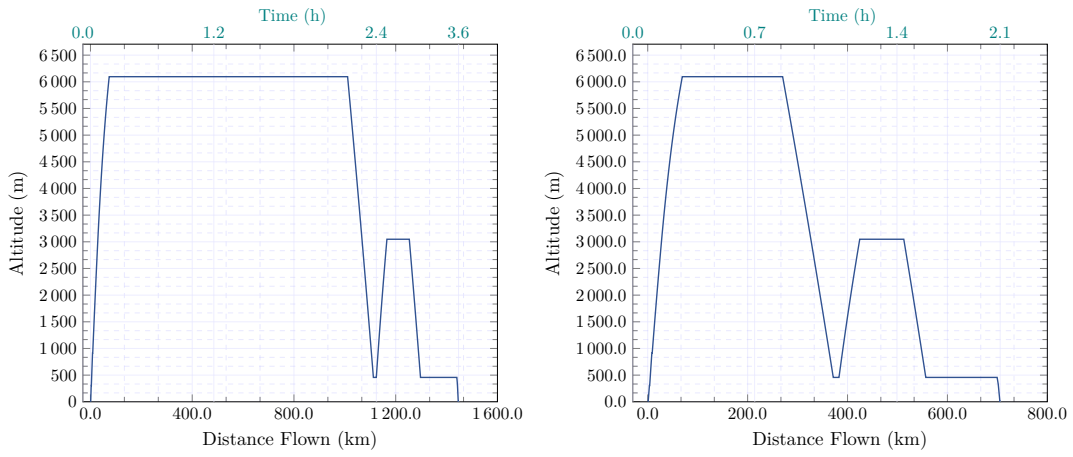

(a) **(b)**

Figure 4.8: Reference missions defined from the set of TLARs in Tab. 4.2. (**a**) 600 nmi design mission. (**b**) 200 nmi typical mission.

a limited weight correlates with lower maintenance, acquisition, and charge costs. For this reason, it is recommended that the MTOM does not exceed 24 tons for the hybrid-electric configurations that will be considered later in this study. However, this value may not be sufficient for a complete electrification of the concepts, due to the excessive weight penalties introduced by the energy storage systems and electric powertrain components. In light of this consideration, a higher mass limit, equal to 27 tons, will be considered for all-electric configurations based on batteries and hydrogen FCs. However, it is anticipated here that these mass limitations, rather than constituting a hard requirement or contributing to the definition of the design mission, will rather serve as an indication for the choice of the design point in the context of the design explorations that will be made in the following sections. Generally, the set of requirements derived in this section defines the design mission

profile, which is understood as the minimum requirements that all designed concepts must respect. As explained in this section, the requirements were built starting from market considerations, which should intrinsically guarantee good economic feasibility. Furthermore, the fact that all concepts will be designed based on the same constraints will make it easier to compare the different solutions in terms of technical performance, energy demand, costs, and environmental impact, which is one of the main objectives of this study. For these reasons, sensitivity studies aimed at further optimizing the set of TLARs go beyond the scope of this dissertation.

4.3 Technology Assumptions

4.3.1 Innovative Aviation Technologies

The dawn of sustainable aviation heralds a transformative era in the aerospace industry, marked by the advent and integration of novel enabling technologies. In reformulating the regional flight paradigm, a central role is assumed by advanced electric storage systems, electric motor drives, and hydrogen-based FC systems. In parallel, the increase in efficiency of structures and conventional thermal engines can also make a significant contribution to reducing the environmental impact of current aviation, especially if combined with the use of alternative fuels. The importance of reliable descriptions of the maturity levels of all these technologies cannot be overstated. Accurate performance assessments are essential for evaluating the potential benefits and feasibility of integrating these technologies at the aircraft level. They help in understanding the readiness of a technology for commercial use, its reliability, and its ability to meet the rigorous demands of aviation.

This section delves into the exploration of some of the most promising emerging technologies, selected for this study. In particular, Subsection 4.3.2 will discuss the thermal engine model adopted for the present study. Subsection 4.3.3 will deal with the most promising electric storage systems for aeronautical applications. Subsection 4.3.4 will focus on hydrogen FC systems capable of potentially reducing direct GHG emissions to zero. Subsection 4.3.5 and Subsection 4.3.6 will concern, respectively, electric motors and electric power distribution systems. In Subsection 4.3.7 the hypotheses made on the adoption of innovative materials for the wing structure will be presented. Finally, Subsection 4.3.8 will offer an overview of conventional and alternative aviation fuels. After a brief general introduction to each technology, a prospective assessment of their technical characteristics in terms of mass and efficiency will be provided. The data and models adopted for the present study were the result of the collaboration of UNINA with academic and industrial partners in the context of the GENESIS project [128, 235–241]. The evaluation of development trends and maturity levels presented here, based on expert assessments, will allow for the integration of reliable models within the aircraft design chain, and form the basis for the definition of representative scenarios for future regional aviation in the next section.

4.3.2 Internal Combustion Engines

Conventional turboprop engines represent a solid foundation in aviation, playing a significant role in powering commuter and regional aircraft especially thanks to their reliability and operating costs. Continuous advancements in design, technology, and performance have marked the evolution of conventional turboprop engines. Typically, a turboprop engine comprises three key components:

- A **gas turbine core**, that generates mechanical power, featuring one or more compressors, a combustion chamber, and one or more turbines.
- A **reduction gearbox**, that adjusts the engine's output shaft speed to the desired level.
- A **propeller**, that converts the engine's power into thrust, operating at a reduced rotational speed determined by the gearbox's gear ratio.

Decisions on the compressor group impact the overall pressure ratio (OPR), with choices for axial or radial compressors based on factors such as costs, size, weight, and target pressure ratio. The architecture of the turbine group involves considerations like the number of turbine stages, the cooling system, and the power transfer to the gearbox and propeller. A possible configuration involves integrating the gearbox on the same shaft as one of the compressors, while an alternative approach employs a separate Power Turbine (PT), leading to what is usually called a free-turbine turboprop engine.

In general, the process of developing a new turboprop engine is intricate and expensive, involving substantial investments in research, development, and the establishment of new production facilities. Consequently, aircraft manufacturers often opt to continue using older, proven reliable engines. A notable illustration is Pratt & Whitney Canada's PW100 family, a series of 1 300 to 3 700 kW turboprop engines [112, 242]. The PW100 engine's development started in the late 1970s, with its first production model operational in 1984 [243]. Since then, several engine variants were introduced, enhancing power-to-weight ratio and SFC. The latest advancement, the PW127XT, was introduced in 2021, designed to replace the PW127M variant on the ATR regional aircraft thanks to reduced maintenance costs and improved fuel efficiency [113, 154]. The PW127 models feature air-cooled High-Pressure Turbine (HPT) rotor blades, whereas the Low-Pressure Turbines (LPTs) do not require cooling [244]. A radial Low-Pressure Compressor (LPC), driven by a single-stage LPT, supercharges a radial High-Pressure Compressor (HPC) driven by a single-stage HPT. A third two-stage turbine, which is a PT, powers the propeller through a reduction gearbox [244, 245]. A drawing of the cross-section of this engine is reported in Fig. 4.9, highlighting all the significant components of the engine core. Since the ATR 42-600 aircraft was selected as the reference aircraft in Section 4.2.2, its PW127 engine was taken as the reference engine for subsequent considerations. The choice of the reference engine is also justified thanks to the availability of public data and models [109, 157, 244, 246].

In addition to the development complexities, the need for iterations in engine design within the broader aircraft design process poses another significant challenge

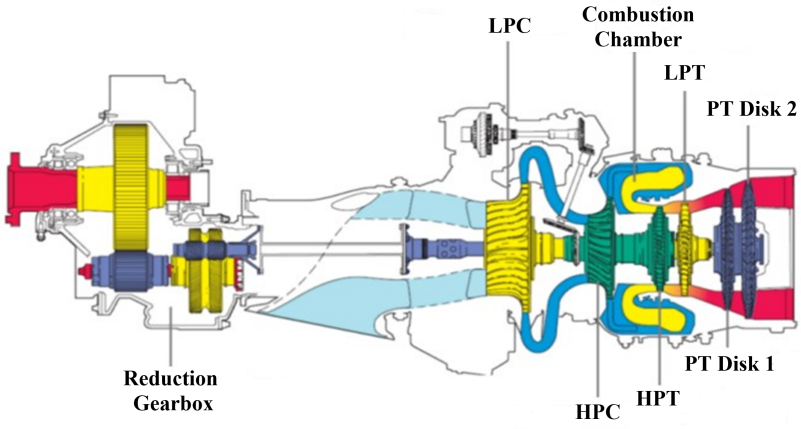

Figure 4.9: Pratt & Whitney PW127 engine configuration (elaborated from Ref. [245]).

to aerospace engineers and designers, affecting the entire program's efficiency, timeline, and cost-effectiveness. Mitigating these iteration challenges is crucial for streamlining the design workflow and ultimately producing aircraft with enhanced performance and functionality. In the context of the design of hybrid-electric configurations, where much of their advantage may depend on the optimization of the rating and operation of the combustion engine, reducing the separation of the two design processes has an even more critical role. According to Di Stasio, creating scalable performance models for aircraft engines is a practical approach to support the integration process within aircraft design workflows [109]. The importance of scalable models lies in their potential to reliably simulate and analyze the engine's behavior under different conditions, facilitating comprehensive assessments of the effects at the aircraft level by avoiding detailed engine design at each iteration. Aware of its advantages, for the purposes of this work, the design workflow model proposed by Di Stasio was adopted and integrated into the aircraft design chain [109]. The model was developed from simulations using GasTurb version 11 [109, 247]. GasTurb is a program capable of simulating the most common gas turbine configurations used for propulsion or power generation, allowing for the simulation of the gas turbine cycle in both design and off-design conditions [247]. Di Stasio implemented a set of engine design laws and automatic update strategies to reproduce a scalable engine model in GasTurb, starting from the characteristics of the PW127 engine. In particular, mathematical relationships were implemented to characterize the polytropic efficiencies of turbines and compressors, the burner efficiency, pressure ratios of low- and high-pressure impellers, pressure losses, and the relative amount of cooling air for the nozzle guide vane and rotor blades of the high-pressure turbine. Di Stasio's model directly links the aforementioned efficiencies with the EIS year of the engine, thanks to technological projections retrieved from the literature [248–250]. A parametric study was performed for future time horizons, involving thousands of design point cycle simulations to derive linear regression models for the time horizons of interest [109]. The surrogate models allow for

evaluation of the effect of required shaft power, burner exit temperature, OPR, and fuel LHV on key engine design and off-design performances, including SFC and NO_x emissions. The model is flexible enough to allow for in-loop optimizations of the burner exit temperature to minimize the SFC. This assumption was conveniently adopted for the purposes of this study. An estimate of the size and dry mass of the motor is also directly provided by the model, as a function of the entry mass flow rate and shaft power. The model, integrated within the aircraft design chain described in Section 2.4, allows for an automatic rescaling of a default engine performance deck (representative of the performance of the PW127 engine) starting from assigned values of EIS year, OPR, and shaft power demand, producing an engine deck useful for performance evaluation of the aircraft.

4.3.3 Electric Storage Systems

Batteries are widely considered to stay at the forefront of achieving complete decarbonization in regional aviation. The landscape of battery technologies is diverse, making it challenging to predict the most promising advancements over the next 30 years. However, a critical consideration for aviation is the specific energy of batteries, leading to the belief that lithium-based technologies are well-suited for this task. Lithium, as the third lightest element, is functional to achieve high gravimetric densities. Its low reduction potential also allows $Li-Ion$ batteries to attain the highest possible cell potential. Finally, a significant shortage of lithium is unlikely in the near future, even though there is expected to be a bottleneck in lithium production in the next decade [251]. According to the forecast technology roadmap envisaged by Batteries Europe [252], the current state of the art for mobility applications is represented by Generation 3 $Li-Ion$ batteries, but further improvements are deemed possible for this technology to enable higher energy and power density thanks to higher capacity and/or operating at higher voltage. Within the next decade, Generation 4 $Li-Ion$ batteries may achieve even better performance and safety, thanks to solid-state electrolytes, cathode materials, and anode materials enabling higher thermal and electrochemical stability [252]. Following, the introduction of advanced solid-state batteries (SSBs) and new conversion chemistries such as lithium-sulphur ($Li-S$), as well as the advent of lithium-air ($Li-O_2$ or $Li-Air$) batteries promise a further improvement in specific energy and performance of electric storage systems [252]. Figure 4.10, adapted from Park et al. [237], schematically shows the cell configuration for different chemistries. Based on the roadmap proposed by Batteries Europe, Lemoine et al. have proposed reference chemistries and performance indicators suitable for the regional aviation sector in the coming decades [237].

Generation 3 $Li-Ion$ batteries are currently being deployed in almost all electrified systems requiring high performance. However, $Li-Ion$ is a generic term that groups all batteries that use lithium as a charge carrier. Many different electrode materials can be used, drastically impacting performance [235, 252]. In light of this, advanced Generation 3 batteries were assumed for the short-term horizon by Lemoine

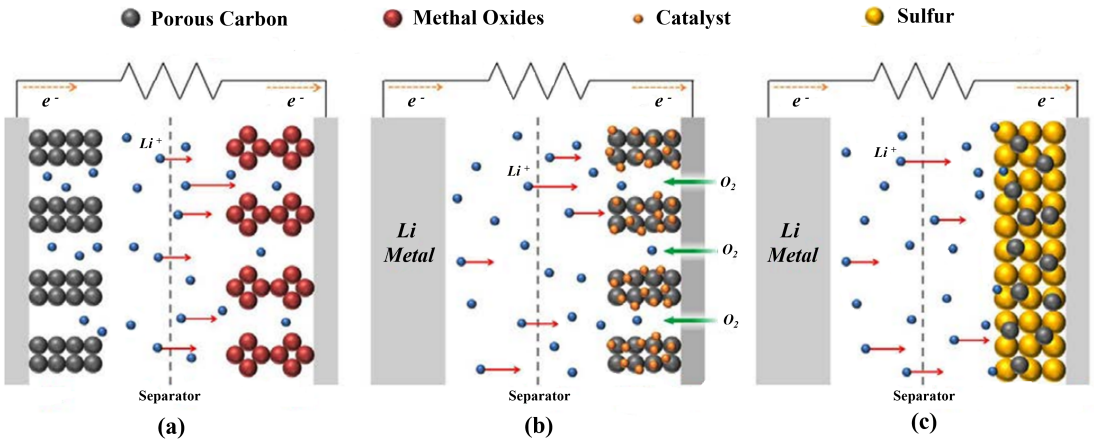

Figure 4.10: Schematic configurations of several lithium-based battery cells (adapted from Ref. [253]). **(a)** $Li - Ion$, **(b)** $Li - Air$, and **(c)** $Li - S$ batteries.

et al. and, in turn, for the purposes of the present study. Nichel-Manganese-Cobalt (NMC) oxides were assumed for the cathode, while the anode will be a graphite anode with a small percentage of silicon. In particular, NMC811/Silicon-Carbon chemistry was selected [235, 237]. The cathode is composed, by definition, of a lithium alloy of 80% Nickel, 10% Manganese, and 10% Cobalt. It is expected to have further improvements in structure and composition, which in turn will improve the cell's lifetime, safety, and performance of the cell [252].

In the medium term, Generation 4 batteries are expected to become available and widespread. SSBs and $Li - S$ batteries are both expected to challenge the current $Li - Ion$ market, but as of today, it is not expected that they phase out completely $Li - Ion$ [236, 252]. The working principle of SSBs is very similar compared to $Li - Ion$ batteries, differing mostly from containing a solid electrolyte. In this sense, the ongoing developments on cathode active materials from $Li - Ion$ batteries are expected to be completely transferrable to SSBs, and lithium-rich oxide cathodes should remain the mainstream solutions in the future. The high specific energy requirements coming from aviation aircraft could be fulfilled by cathode materials composed of lithium-manganese-nickel oxides or NMC. On the anode side, it is expected that the solid electrolyte allows for the implementation of lithium metal which would drastically improve the performance of SSBs over $Li - Ion$. In parallel, $Li - S$ batteries have recently received increased attention thanks to their extremely high theoretical energy density (up to 2 700 Wh/kg), which is 5 times higher than the theoretical limit of $Li - Ion$ batteries [254]. While this value is significantly lower practically, the technology has already demonstrated excellent performance in a technologically relevant cell format, featuring a specific energy close to 470 Wh/kg [255]. The promised performance of $Li - S$ batteries is extremely relevant to enable new applications such as aviation and large electric vehicles. In addition, sulfur is abundant, cost-effective, and environmentally friendly, which is very beneficial for reducing the environmental impact of the aircraft

industry [256]. However, challenges such as lifetime or power capabilities need to be overcome first [256]. The potential for cost reduction will also probably accelerate the commercialization and widespread of $Li-S$ batteries. Forecasts suggest that, with comparable performance, the cost of a $Li-S$ cell could become just half of a $Li-Ion$ cell [257].

In the long term, Generation 5, particularly non-aqueous $Li-Air$ chemistries, promise great potential for aircraft applications [252]. Their basic principle is that the lithium-based anode reacts with the oxygen-based cathode to produce lithium peroxide which releases electricity. During the charging process, the lithium peroxide is broken up into lithium and oxygen, which allows the cell to be re-used. $Li-Air$ cells would potentially show extremely high energy density. However, in practice, Girishkumar et al. predicted $Li-Air$ could only reach 1 700 Wh/kg due to the weight penalty of packaging and structural components [258, 259]. $Li-Air$ batteries still face many challenges such as low electrical efficiency, limited C-Rates, and low lifetime. Also, no practical applications of $Li-Air$ exist yet, even if $Li-Air$ batteries were already considered as a candidate to power the VoltAir aircraft planned and designed by EADS [260].

The review work by Lemoine et al. culminates in a prediction of the evolution of the technological readiness level for all battery technologies considered [237], which is visually reported in Fig. 4.11. The study also involved structural batteries as promising technologies for reducing aviation's environmental footprint. However, their current very low TRL suggests that their effective utilization as the main energy source for an aircraft may not be practical within the next 30 years, though they might find application in powering auxiliary systems. For this reason, they were not taken into consideration in this study. A parallel study conducted by the author of this dissertation in Refs. [95, 96] confirmed these expectations, showing that although structural batteries offer a way to reduce the mass penalties introduced by electrification, their specific energy is at least an order of magnitude smaller than necessary to achieve significant benefits for an aircraft application.

Considering intermediate years of EIS representative of the three time horizons analyzed in this study, i.e., 2030 (short term), 2040 (medium term), and 2050 (long term), and considering the forecasts in Fig. 4.11, reference technologies were selected for each horizon. For the short-term scenario, only $Li-Ion$ technology was considered as mature enough and widely available. For the medium term, both $Li-S$ and SSBs were considered. As a matter of fact, $Li-S$ batteries have a slightly better specific energy than SSBs. However, their ability to endure high C-Rates is limited. Consequently, the achievable power per unit of mass is significantly lower for $Li-S$ batteries when compared to SSBs. The battery technology selection is heavily influenced by whether the sizing criteria prioritize power or energy demand. Given these considerations, both battery models will be incorporated into the design workflow for medium-term analyses at the aircraft level, and the best choice will be made in accordance with the specific hybridization strategy under evaluation. Finally, with regard to the long term, $Li-O_2$ batteries are expected to be widely available by 2050. In addition, the same SSBs as in the medium term were also

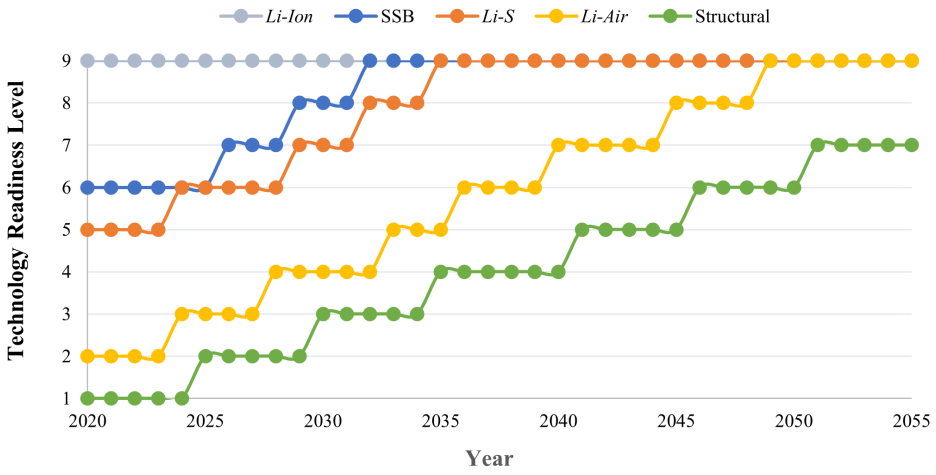

Figure 4.11: TRL forecasts for battery technologies (adapted from Ref. [237]).

considered for the long term as an alternative to $Li-Air$ batteries, in analogy with what has already been discussed for the medium-term horizon. For the purposes of this study, fundamental information for the sizing of the electric storage was also extrapolated from the work of Lemoine et al. and is provided in Tab. 4.3. The values of specific energy density reported in the table refer to the system level. To upscale from cell to pack performance, structural ratios were assumed by Lemoine et al. starting from current typical values and experts' evaluations [237]. The nominal specific power, also important in relation to the power requirement of the aircraft, can be estimated as the product of the specific energy and the nominal C-Rate.

Table 4.3: Gravimetric and volumetric characteristics of different types of batteries [94, 237], in different time horizons. Values are expressed at the system level.

		Short-Term (EIS 2030)	**Medium-Term (EIS 2040)**		**Long-Term (EIS 2050)**
Technology		$\boldsymbol{Li-Ion}$	$\boldsymbol{Li-S}$	**SSB**	$\boldsymbol{Li-O_2}$
Parameter	**Unit**	**Value**			
System Specific Energy	Wh/kg	280.0	675.0	585.0	945.0
Nominal C-Rate	1/h	2.0	1.5	4.0	2.0
System Energy Density	Wh/L	420.0	735.0	1 000.0	945.0

4.3.4 Fuel Cells and Hydrogen Storage Systems

In pursuing net-zero emissions in the aviation sector, a pivotal frontier emerges with exploring hydrogen FC systems for regional aircraft. Fuel cells can convert the chemical potential of hydrogen into electricity usable on board while emitting water vapor as the only waste product. At the state of the art, different technologies of

FCs are available. Nowadays, the most commonly used technology for aviation applications is low-temperature PEMFCs, typically fuelled with pure hydrogen and oxygen from ambient air at temperatures below 100 °C. A single cell consists of a so-called bipolar plate with an anode and a cathode side, gas diffusion layers, and a catalyst-coated membrane. Differently, SOFCs employ a non-porous solid ceramic electrolyte such as zirconium oxide stabilized with yttrium oxide and operate at high temperatures (600–1 000 °C). The oxygen air is fed to the cathode, and the electrolyte initiates the mobility of the ions. Water is formed through the chemical reaction occurring at the anode. Figure 4.12 schematically represents the difference between PEMFC and SOFC operation.

SOFCs have the potential to reach much higher electric efficiencies than PEMFCs, above 60% and very close to the theoretical thermodynamic efficiency. In addition, the high-temperature process in SOFCs could allow for direct internal reforming, although this further opportunity has not been explored in the present study. However, SOFCs have only recently started to be considered as a viable power source option for aircraft, and several technical challenges will need to be overcome before an application in an aeronautical context takes place. One of the main challenges with SOFC systems is high-temperature corrosion, which can be mitigated using an expensive protective layer of the current collector plates [261]. Additionally, the research dedicated to developing SOFCs will need to focus on increasing the power density of these systems to make them compatible with aeronautical requirements. In Refs. [128, 235, 236], Proton Motor Fuel Cell GmbH provides considerations on the state of maturation of FC systems, drawing on their experience of over 25 years in the production of emission-free hydrogen FCs [262]. The evolution of systems maturity, adapted to the time window considered in this study, is represented in Fig. 4.13.

Table 4.4 reports the assumptions on gravimetric and volumetric density values at the system (i.e., FC plant) level for two types of FCs, projected to the time horizons in which they were considered for this study. The very low specific power of current PEMFC systems has precluded their use in the short term. Figure 4.14

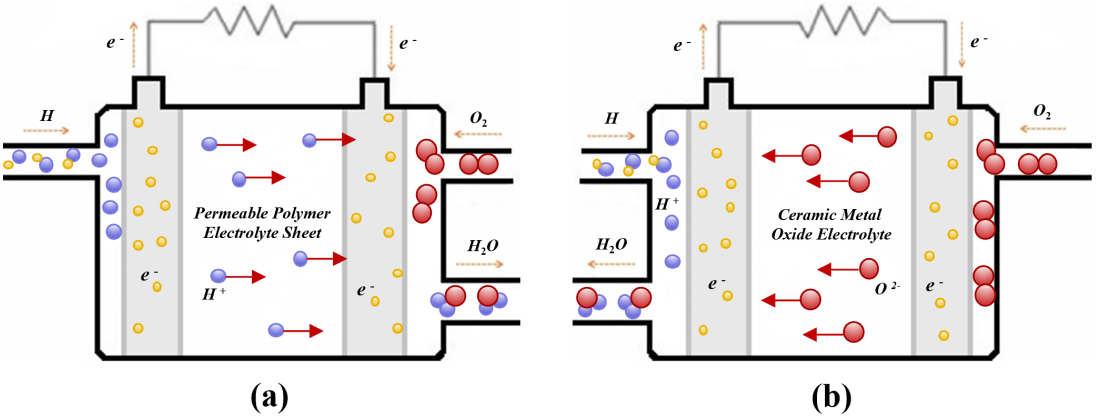

Figure 4.12: Schematic configurations of fuel cells (adapted from Ref. [263]). **(a)** PEMFCs. **(b)** SOFCs.

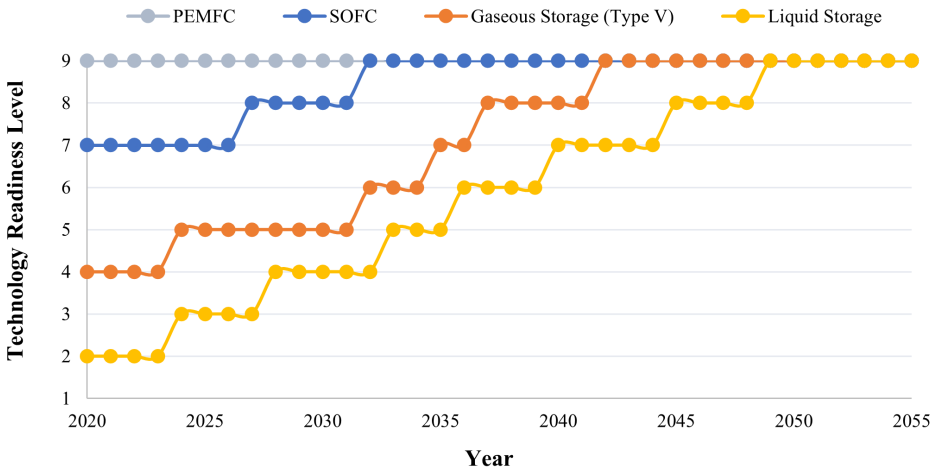

Figure 4.13: TRL forecasts for fuel cell and hydrogen storage technologies (adapted from Ref. [128]).

Table 4.4: Gravimetric and volumetric power density of fuel cell systems across different time horizons [94, 128, 264]. Values are expressed at the system (plant) level.

		Short-Term (EIS 2030)	**Medium-Term (EIS 2040)**	**Long-Term (EIS 2050)**	
Technology		**PEMFC**	**PEMFC**	**PEMFC**	**SOFC**
Parameter	**Unit**		**Value**		
Gravimetric Density	kW/kg	0.5	1.2	2.2	1.875
Volumetric Density	kW/L	0.3	0.8	1.5	1.5

shows the cell voltage and efficiencies of the systems as the nominal power fraction varies. Although PEMFCs are characterized by a lower electrical efficiency than SOFCs, the former feature higher power densities even in the long term. In light of this trade-off, added to the uncertainty about the level of maturity of SOFCs, it is worth considering both PEMFCs and SOFCs in the long term, especially since the market establishment of PEMFCs is such that their disappearance within the next 30 years is not realistic [128]. For both technologies, a fuel utilization of 85% will be used as a standard practice in modeling FCs [128].

The mass values reported in Tab. 4.4 do not include hydrogen tanks, for which separate considerations were made. Since the introduction of the first high-pressure hydrogen tanks in the late 19$^{\text{th}}$ century, the design of such tanks has undergone various technological advancements, continually enhancing their weight and volume efficiencies. The main challenge to using gaseous hydrogen in aircraft is the low gravimetric efficiency of the necessary pressurized tanks (around 6-7%) [140]. The first *gaseous tanks*, today known as Type I tanks, were composed entirely of metal, resulting in excessive weights [265]. The incorporation of continuous fibers first served as reinforcement for the cylindrical portion of the tank (Type II) and later

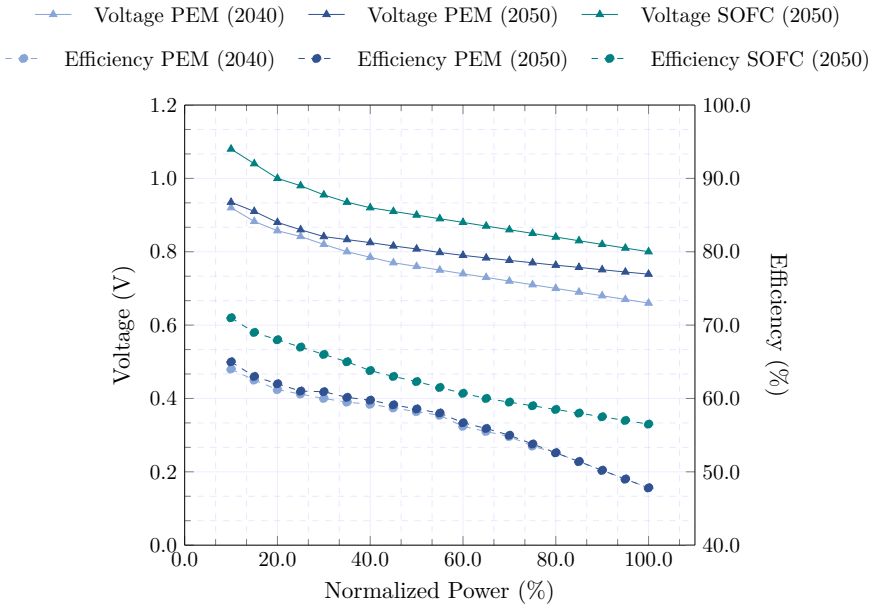

Figure 4.14: Anticipated cell voltage and system efficiency curves for future PEMFC and SOFC systems (adapted from Ref. [128]).

evolved into the sole pressure-bearing component, effectively reducing the tank's mass (Type III & IV) [265]. Specifically, Type III employs a single-part metallic liner with supporting functions, while Type IV utilizes a polymer liner tightly integrated with metallic bosses. These latter two technologies persist, coexisting due to trade-offs in terms of cost and operational conditions [265]. For instance, Type IV is particularly appealing for applications requiring hydrogen storage at high pressures, up to 700 bar, while keeping the mass low. The choice of high pressures is primarily convenient to increase the hydrogen density and, therefore, the volumetric efficiency of the tanks [128]. The next evolutionary step involves storing hydrogen directly in the pressure-bearing composite shell, eliminating the need for a liner altogether. This linerless tank technology is commonly referred to as Type V [265]. When considering a hydrogen mass to be stored of around 100 kg, Mahytec [266] estimated that the gravimetric efficiency of Type V tanks at 700 bar can reach up to 12.6 %, when considering a cylindrical shape, high-grade carbon fibers, vacuum-perlite insulation and a safety factor of 2.02 based on the current automotive standard [128]. Moreover, it is anticipated here that the tank sized in Ref. [128] has an external diameter of 1.0 m, making it possible to arrange up to 4 tanks in parallel in the aircraft's fuselage.

While gaseous tanks play on increasing the gas pressure to improve gravimetric and volumetric efficiencies of the tank, the same result can be achieved by decreasing the temperature of the hydrogen to increase its density. This is the main idea at the basis of *cryogenic tanks*. The technological challenges of liquid hydrogen are mostly temperature-related, due to significant changes in the mechanical properties of materials at cryogenic temperatures. In this sense, low-density aluminum alloys are the best candidates for this type of hydrogen storage in mobility applications.

Moreover, insulation concepts are crucial in minimizing heat transfer and preventing overpressure [128]. In the present context, a GI of 40 % was assumed for cryogenic tanks, considered as an achievable value for tanks operating at 20 K, cylindrical shape, vacuum-perlite insulation, and a boil-off rate of 5% after 6 hours, while keeping the output diameter below 1.0 m [128]. For both gaseous and cryogenic tanks, the longitudinal dimensions can be estimated starting from the hydrogen density and the stored mass, while keeping the same diameter.

Although cryogenic hydrogen tanks are already used in aerospace, one of the major disadvantages is the lack of knowledge about the fatigue behavior of these tanks in the long term [128]. In this sense, Fig. 4.13 also reports considerations on the current and future maturity level of gaseous Type V and cryogenic tanks. Pressurized tanks were favored for implementation in the medium term. In contrast, cryogenic tanks were considered for the long term as they are still in the early stage of development. As a final note, alternative hydrogen storage methods, such as solid storage based on hydrides, were excluded due to their low gravimetric and volumetric efficiencies which do not make them suitable for non-stationary applications [128]. The discussed assumptions on hydrogen storage systems are reported in Tab. 4.5.

Table 4.5: Gravimetric index of hydrogen storage systems across different time horizons [94, 128].

		Medium-Term (EIS 2040)	**Long-Term (EIS 2050)**
Technology		**Gaseous (Type V)**	**Cryogenic**
Parameter	**Unit**	**Value**	
Gravimetric Index	%	12.6	40.0

4.3.5 Electric Machines

Electric machines are the primary means of electric power transmission in hybrid-electric aircraft architectures. They drive the rotation of propulsion systems, namely the propellers, eventually generating the necessary thrust during all flight phases. In parallel, electric machines that can work as generators play a role in energy recovery during specific phases of flight. In the presence of distributed propulsion, generators also act as the fundamental connection elements between the propulsive lines. Very high efficiencies and specific powers generally characterize electric machines. However, it remains of considerable importance to accurately evaluate the impact of the most promising electric machine technologies on aircraft.

Meindl et al. [235, 236, 240] identified six main typologies of radial alternate current machines, which all have different characteristics, advantages, and disadvantages. These included switched reluctance machines, synchronous reluctance machines, separately excited synchronous machines, permanent magnet synchronous machines (PMSMs), slip ring induction machines, and squirrel cage induction machines. In

the case of synchronous machines, the rotor frequency is equal to the rotating frequency of the magnetic field in the stator. As for induction machines, the rotor frequency is higher (generator mode) or lower (motor mode) than the rotating frequency of the magnetic field in the stator. Müller et al. performed trade-off studies that compare the aforementioned types of electric machines in terms of several performance indicators, including efficiency, power density, maintenance demands, cost, and noise [267]. Their analysis, based on typical designs from each type of machine, concludes that PMSMs are overall the best performing although not the cheapest. Substituting rotor windings with permanent magnets leads to a reduction in the weight of the machine, resulting in better power density. However, for a hybrid or all-electric aircraft application, efficiency and power density are more important than cost, in light of their impact on the total weight and, in turn, on the energy demand. Considering the crucial role played by weight, the PMSM is deemed to be the most suitable option for electric drives in regional aircraft applications. In light of the same considerations, Meindl et al. focused on PMSM to define different regional aviation scenarios for future time horizons [240]. Different machine configurations were analyzed, with power requirements close to those of the present application, and imposing constraints on the size of the electric machine (the outer diameter was kept below 0.5 m for all designed configurations) [235, 236, 240]. Meindl et al. opted for a hairpin winding (rectangular winding) for short-term application to increase the power density. A Halbach magnet arrangement and directly cooled stator windings are proposed as optimization opportunities for future time horizon applications. In particular, the Halbach arrangement of permanent magnets utilizes a unique combination of radial and azimuthal magnet configurations, yielding a heightened magnetic field on one side of the arrangement and a near-zero cancellation of the field on the opposite side. This concentrated magnetic field reduces the rotor laminations' thickness without inducing magnetic saturation, consequently contributing to a smaller total mass of the machine [268, 269].

The work by Meindl et al. also contains a prediction of the technological readiness level for the aforementioned PMSMs technologies considered [240], reported here in Fig. 4.15. As can be noticed from the figure, the utilization of partially or fully superconducting externally-excited synchronous machines based on liquid hydrogen was also considered by Meindl et al. as a viable option for long-term applications [240]. Cryogenic temperatures of hydrogen have the potential to enable a superconducting state by producing zero-resistance conditions. However, when considering 2050 as the reference EIS year for the long-term horizon, superconducting machines are not expected to be mature enough for aeronautical applications. Therefore, they were conservatively excluded from the study covered by this dissertation. Table 4.6 provides an insight into the technology levels considered for three different time horizons. Electric machines installed on all long-term airplanes feature a specific power that is almost double that of the short-term. The efficiency of all the electric machines was reasonably assumed to be 95% for all machines operating at high rotational speeds [240].

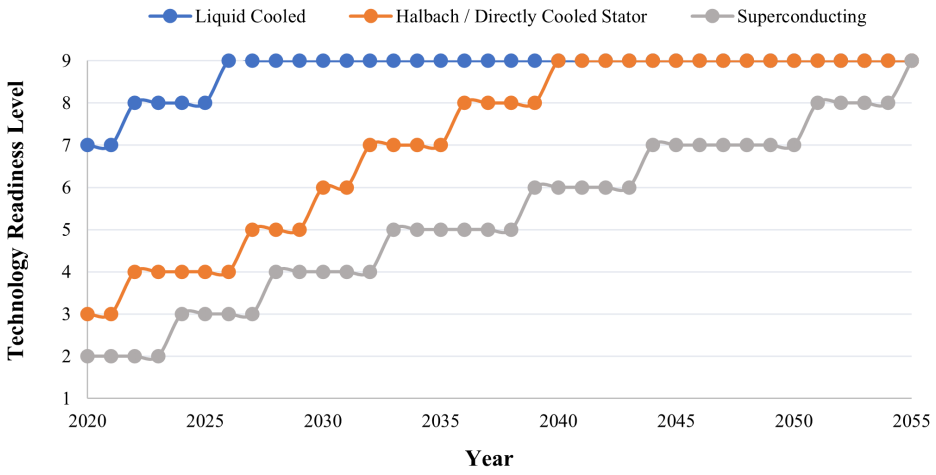

Figure 4.15: TRL forecasts for electric machine technologies (adapted from Refs. [94, 240]).

Table 4.6: Technology assumptions for electric machines [240].

		Short-Term (EIS 2030)	**Medium-Term (EIS 2040)**	**Long-Term (EIS 2050)**
Technology		Liquid Cooled PMSM with Hairpin Windings		Halbach Array PMSM with Direct Cooled Stator Windings
Parameter	**Unit**	**Value**		
Specific Power	kW/kg	5–6		9–11
Efficiency	%	95.0		95.0

4.3.6 Power Distribution and Power Electronics

Power distribution is becoming an increasingly important topic in the context of energy transition, in light of the very high power requirements coming from aviation. Selecting the appropriate DC bus voltage is preparatory for the choice and operation of power electronics, as it directly influences operational efficiency, current intensity, and system weight. If, on the one hand, the choice of high voltages leads to lower currents and lighter cables, on the other hand higher voltages lead to penalties in the efficiency of power electronics and unsolved safety concerns. For instance, high DC bus voltage increases the creepage and clearance distances [239], negatively affecting the physical size of the power electronics. In light of these considerations, 800 V was chosen as the reference voltage for future hybrid-electric aviation scenarios. The DC bus voltage of 800 V has been gaining much attention recently, becoming popular for the newest battery electric vehicle generation [120]. Accordingly, Meindl et al. conclude that 800 V is expected to represent the new standard for aviation, being an optimal compromise between operational efficiency, power density, and technological compatibility [239]. Following this assumption, a linear density of 1.455 kg/m was assumed based on state-of-the-art 800 V cabling systems [270, 271].

The total mass can be calculated by estimating the total length of the cables from the relative position of electric machines, FCs, and batteries on board.

Power electronics work as a link between the individual energy-producing and energy-consuming components, distributing energy on board. More specifically, DC/DC converters regulate and transform the electrical energy from batteries, FCs, and other sources, adjusting the voltage to the required level. Meanwhile, the motor inverters/controllers take center stage in translating electrical signals into mechanical motion, governing electric motors' speed, torque, and overall performance. Power electronic converters traditionally use silicon-based semiconductors like silicon insulated-gate bipolar transistors (IGBTs) for high voltage [239]. In the past decade, wide bandgap semiconductors, such as silicon-carbide (SiC) and gallium-nitride (GaN), have emerged. GaN is the newest class of market-available semiconductors with ongoing research, development work, and technical improvement. Although GaN electronics promise increased efficiency and reduced weight concerning current SiC technology, at the state of the art there is no GaN IGBT capable of operating at the chosen 800 V DC bus voltage. At the same time, some research work regarding SiC IGBTs is ongoing [272]. In light of these considerations, and based on experts' assumptions, Meindl et al. identify a technology roadmap for power semiconductor materials [239], here adapted and reported in Fig. 4.16. For the purposes of the present study, the use of GaN devices was limited to the long-term horizon only, while SiC converters were adopted for both the short and medium-term scenarios.

The specific power and efficiency values of converters and inverters are shown in Tab. 4.7. The reported values are extrapolated from the analytical estimates of Meindl et al., which consider similar power values and the same topology of the aircraft analyzed below [235, 236, 239]. An additional mass penalty connected to the TMS of power electronics was also considered. In this sense, a mass-to-power ratio of 2.0 kg/kW was considered for the short term, and 0.75 kg/kW was assumed for the medium term and long term [239, 271]. In this case, the sizing power is equal to the produced heat, which can be calculated as the product between the power and the complement to the unity of the efficiencies given in Tab. 4.7.

Table 4.7: Technology assumptions for power electronics across different time horizons [239].

	Short-Term (EIS 2030)	**Medium-Term (EIS 2040)**	**Long-Term (EIS 2050)**	
Component	**Silicon Carbide (SiC)**		**Gallium Nitride (GaN)**	
	Efficiency	**Power Density**	**Efficiency**	**Power Density**
Electric Machine Inverter	99.0%	63 kW/kg	99.0%	94.2 kW/kg
Battery Converter	98.0%	50 kW/kg	98.5%	100 kW/kg
Fuel Cells Converter	98.0%	50 kW/kg	98.0%	120 kW/kg

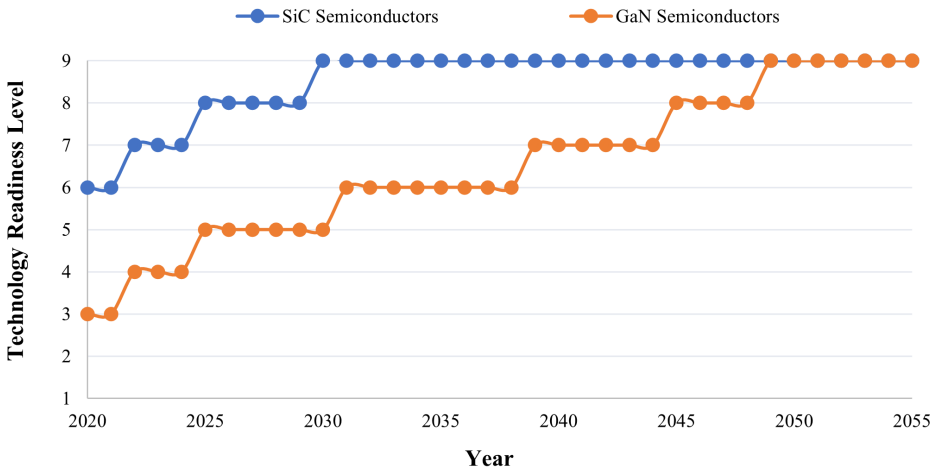

Figure 4.16: TRL forecasts for power electronics technologies (adapted from Ref. [239]).

4.3.7 Innovative Wing Design

When designing hybrid-electric aircraft, the possible adoption of DEP introduces the potential occurrence of propeller whirl flutter, a factor that must be considered in the structural design of wings. The mass distribution of a DEP wing is non-conventional, as typically small nacelles are distributed over the wingspan, possibly in addition to the larger primary nacelles. This leads to a non-conventional wing skin thickness distribution [136]. Furthermore, non-traditional vibration modes can be expected due to the non-conventional mass distribution, and finally, new instability mechanisms such as whirl flutter can be observed due to the gyroscopic nature of the spinning distributed propellers [136]. As whirl flutter is an aeroelastic effect, as well as the aeroelastic loads due to the increased wing flexibility, coupled structural-aerodynamic calculations need to be carried out to determine the internal static and dynamic strains to size the wing structural properly [136]. To face this problem, Wang et al. from TU Delft [273] developed an optimization method for the design of the load-carrying structure of a wing that is equipped with DEP [136]. The goal of their optimization algorithm was to quickly assess the structural mass of wing structures using physics-based models, that contrast with empirical models based on historic data [32], the latter being not available for DEP wing structures [136]. The dedicated aeroelastic analyzer, based on beam finite element model, was implemented in a nonlinear optimization algorithm to obtain optimal designs for a variety of wing configurations and materials [136]. The calculated value of the wing-box mass is finally corrected through a scaling factor to get the total wing mass [136, 274]. The method was implemented by Wang et al. into an in-house tool, named PROTEUS, capable of also dealing with non-conventional materials, such as carbon/epoxy composite materials and 100% recyclable biofibre composites [136]. In collaboration with the author, a parametric analysis was performed by TU Deft to evaluate the effect of main design parameters on the mass of the wing, while

implicitly taking into account dynamic stability constraints [137]. Maintaining the same planform of the ATR42 wing and defining reference positions for nacelles, a Latin hypercube sampling was used to combine different values of root chord, aspect ratio, primary and secondary nacelle masses, and fuel/distributed mass in a range of interest for the present study [137]. The set of design cases, kindly provided by TU Delft, allowed for the generation of a multidimensional response surface utilizing the MATLAB® Regression Learner tool [137, 275]. The model, suitable for a preliminary design application, was integrated into the analysis workflow, replacing semi-empirical data-based models. For this purpose, two innovative materials were selected as references by TU Delft, namely the *carbon/epoxy AS4/3501-6* and the *ampUD coPOM* composite, the latter featuring biodegradable fibers and re-processable matrix [137]. More information about the two materials and their mechanical properties is available in literature [276, 277]. Figure 4.17 displays some of the main trends associated with the set of design points. In particular, the use of biodegradable material is associated with masses that are approximately double compared to the carbon/epoxy composite. Nonetheless, in the following, biodegradable material will be taken into consideration for long-term scenarios, in light of its environmentally sustainable properties and the increasing importance of eco-friendly alternatives in the aerospace industry.

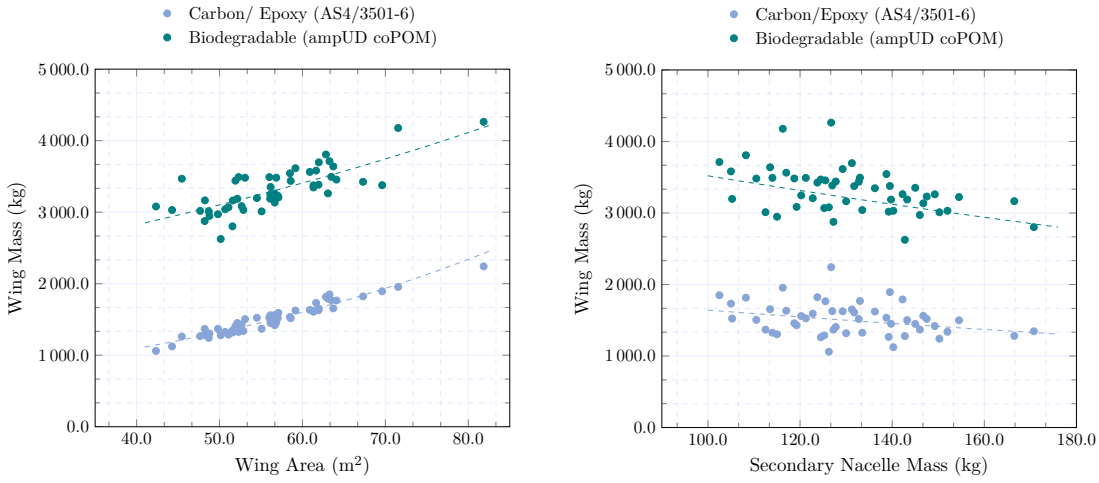

Figure 4.17: Wing masses resulting from the analyses conducted by TU Delft with the in-house PROTEUS software for different wing surface values, aspect ratio, distributed and concentrated masses [136, 137]. The data was integrated into the design workflow as a surrogate model generated with the MATLAB® Regression Learner tool [275]. (**a**) Detail of the trend of wing mass as the wing area varies. (**b**) Detail of the trend of wing mass as the mass of the secondary electric machine nacelle varies.

4.3.8 Aviation Fuels

Jet A-1

Conventional jet fuel for civil aircraft applications, *Jet A-1*, has long been the standard, serving as the go-to fuel for aircraft worldwide. Conventional Jet A-1 was selected as the reference kerosene fuel for the rubber engine model recalled in Subsection 4.3.2, as well as for the present application. An average value for the Jet A-1 LHV equal to 12.00 kWh/kg was considered [278]. The NO_x severity index associated with the combustion of jet fuel is calculated via the surrogate model discussed in Subsection 4.3.2, then corrected by a multiplicative correction factor equal to 23 to obtain the EI for NO_x [109, 247]. The simple methodology proposed by Filippone et al. was adopted to complement this workflow with fast and reasonable predictions of EIs for CO and HC for turboprop engines [111]. This methodology is based on emissions data collected in the ICAO emissions databank [279] (exclusively related to turbofan-powered aircraft), which were conveniently adapted by the same authors, through several correlations, to fit the emissions for a turboprop engine [111]. Since the estimating relationships proposed by Filippone et al. also depend on atmospheric conditions and average fuel flow, it is possible to differentiate the estimate based on the flight phase and the corresponding engine setting [111]. Regarding the EI for CO_2, H_2O, and SO_2, it is reasonable to assume constant values not explicitly related to the characteristics of the engine. Constant values suggested by Eurocontrol [160] and here reported in Tab. 4.8 were assumed for these species.

Table 4.8: Gas turbine EI values for CO_2, H_2O, and SO_2 associated with Jet A-1 [160].

Pollutant	Emission Index (g/kg)
CO_2	3 149.0
H_2O	1 230.0
SO_2	0.84

Sustainable Aviation Fuels

As environmental consciousness grows and the aviation industry seeks sustainable alternatives, the spotlight is shifting towards SAFs. Considered a promising short-term solution for mitigating the environmental impact of aviation, SAF will be taken into account as a viable option within the scenario analyses covered in this chapter. The impact of the percentage of SAF in the mixture will be evaluated by using a simplified approach. Hydro-processed esters and fatty acids synthetic paraffinic kerosene (HEFA-SPK), and synthetic paraffinic kerosene derived from the Fischer-Tropsch process (FT-SPK) were chosen among the set of biofuels certified for civil aviation use [280]. For both these biofuels, blending ratios up to 50 % with conventional jet fuel are already approved, and the experimental phase aimed at certifying higher percentages is already underway [281–284]. The reference blend

composition of HEFA-SPK and Fischer-Tropsch e-fuels may be assumed based on the expected market mix for each time horizon reported in Tab. 4.9 [280, 281].

Information on LHV and CO_2 EI, reasonably valid for both mixtures, was extrapolated from Wolters et al. [278] and reported in Tab. 4.10. The same table reports corrections for the EI of CO, SO_2 and H_2O [285, 286]. Reported corrections are valid in the case of HEFA-SPK, but the effect of variations in the chemical composition was considered negligible. However, it is also true that, even in the long term, the percentage of e-fuel on the total SAF remains below 30%, which reinforces the validity of the approximation.

Table 4.9: Sustainable aviation fuel market mix used for each time horizon [280, 281].

	Short-Term (2025–2035)	**Medium-Term (2035–2045)**	**Long-Term (2045–2050+)**
HEFA-SPK biofuel	100.0 %	92.0 %	72.0 %
FT-SPK e-fuel	0.0 %	8.0 %	28.0 %

Table 4.10: Corrections on some main properties for different SAF blending ratios: LHV [278], CO_2 EI [278], CO EI [285], SO_2 EI [286], H_2O EI [285].

	Jet A-1	**SPK 50 %**	**SPK 100 %**
LHV Correction (%)	+0.00	+1.01	+1.02
CO_2 EI Correction (%)	+0.00	−0.78	−1.56
CO EI Correction (%)	+0.00	−10.80	−21.70
H_2O EI Correction (%)	+0.00	+5.00	+10.00
SO_2 EI Correction (%)	+0.00	−37.50	−75.10

Hydrogen

The future of aviation is intrinsically tied to the pursuit of sustainable and eco-friendly solutions, and hydrogen emerges as a promising player in this transition process. Hydrogen stands as a beacon of innovation in the quest for a more sustainable and environmentally conscious aviation industry, from its potential to power zero-emission aircraft to its capacity for reducing carbon footprints. However, introducing hydrogen poses unique challenges that redefine the aviation paradigm. One of the main concerns is the technology scale-up and the knowledge transfer from laboratory to industrial processes. Being an example of non-drop-in fuel, hydrogen may not be compatible with the existing global fleet, requiring aircraft redesign and certification and new supply infrastructure [281]. Another problem is related to the production of hydrogen, which is still largely dependent on fossil fuels, undermining the potential environmental benefits of using hydrogen to decarbonize the aircraft industry. Currently, the main production routes for H_2 are based on natural gas (48%), oil (30%), coal (18%) and electrolysis (4%) [287]. Additionally,

the European energy crisis has highlighted the potential difficulties in achieving a surplus of energy in the short term necessary to produce hydrogen [288]. In the long term, the integration of novel hydrogen technologies necessitates a comprehensive European infrastructure overhaul, involving the interconnection of national energy grids, procurement of raw materials for energy storage, and fostering a favorable environment for the growing green hydrogen trend, all while considering the potential resurgence of nuclear power [288]. Last but not least, as already discussed in Subsection 4.3.4, the storage of hydrogen is complex and inefficient, requiring large volumes and adding significant weight penalties, especially for mobility applications. Despite the existing challenges, it is imperative to strategically invest in hydrogen for the future of aviation, acknowledging its pivotal role in advancing sustainable and environmentally friendly air travel. Europe is already moving in this direction by orienting research programs to introduce hydrogen-based regional aviation within the next 15 years [193]. For this reason, hydrogen will also be central to the main regional aircraft scenarios discussed in the next section. Given the absence of carbon in hydrogen, no pollutant emissions are expected from its use in FC systems other than water vapor. As anticipated in Chapter 2, a water EI equal to 8 936.0 g/kg for FC systems derives from the ratio between the molecular mass of water and that of molecular hydrogen, being the stoichiometric ratio associated with the chemical reaction reported in Eq. (2.22).

4.4 Definition of Future Scenarios

4.4.1 Future Scenarios

The imperative to scrutinize diverse technologies for hybrid-electric aircraft stems from the critical need to comprehensively assess their environmental impact, paving the way for sustainable advancements in aviation. For this reason, different major technologies for energy storage were considered for this work, including batteries, hydrogen-based FCs, and ICE generators. The most promising technologies available for the next decades were discussed in detail in the previous section. Considering possible combinations of the identified technology bricks, different innovative configurations were defined and analyzed with respect to three different time horizons, to represent the most promising technologies and their expected TRL. The technological levels were chosen assuming a representative reference year of EIS for each horizon, as already anticipated in Section 4.3.

The present section contains the definition of all scenarios that will be the subject of the study in the following sections. All configurations selected for this study are named and described below, and also visualized in Fig. 4.20:

- **Short-term (EIS 2030)**:
  - **Conventional\ICE**: Conventional aircraft with ICEs, using kerosene or SAF.
  - **ICE+bat**: Hybrid-electric configuration with ICEs, $Li-Ion$ batteries and DEP, using kerosene or SAF.

- **Medium-term (EIS 2040)**:
  - **Conventional\ICE**: Conventional aircraft with ICEs, using kerosene or SAF.
  - **ICE+bat**: Hybrid-electric aircraft with ICEs, $Li-S$ or SSB batteries and DEP, using kerosene or SAF.
  - **PEMFC+bat**: Hybrid-electric aircraft with PEMFCs, $Li-S$ or SSB batteries, pressurized H_2 tanks and DEP.
- **Long-term (EIS 2050)**:
  - **Conventional\ICE**: Conventional aircraft with ICEs, using kerosene or SAF.
  - **PEMFC+bat**: Hybrid-electric aircraft with PEMFCs, $Li-O_2$ batteries, cryogenic H_2 tanks and DEP.
  - **SOFC+bat**: Hybrid-electric aircraft with SOFC, $Li-O_2$ batteries, cryogenic H_2 tanks and DEP.

First, conventional configurations were considered for each time horizon, featuring ICE technologies evolving over the next decades [109]. These configurations also represent a reference for comparing the technical, economic, and environmental performance of more complex and innovative architectures. Then, a hybrid-electric configuration based on $Li-Ion$ batteries was defined for the short-term in light of this technology's current high level of maturity. Based on the TRLs forecast in Section 4.3, the use of hydrogen as an alternative primary energy source was reasonably limited to the medium-term and long-term scenarios. In this sense, the medium-term horizon is perceived as the transitional phase from a paradigm reliant on hydrocarbon fuels to one centered around hydrogen. This shift holds the potential to theoretically eliminate all direct pollutant emissions, except for water vapor. For this reason, two different hybrid configurations were considered for the medium term, one based on ICE and battery and the other based on PEMFCs systems and batteries. For the latter, energy is assumed to be extracted from hydrogen through FCs and converted into electric current, eventually powering electrically driven propellers. In the long term, the hybrid-electric configurations with ICE and battery were ditched in favor of those based on hydrogen, which benefits from general improvements in the mass and efficiency of the FCs and tanks.

All-electric and hybrid-electric architectures, featuring secondary energy storage systems, are usually associated with significant weight penalties compared to conventional configurations, which makes it unrealistic to certify the new aircraft concepts within the same MTOM values as conventional aircraft when the same set of TLARs is assumed. For this reason, DEP was also included in all hybrid-electric concepts, based on hydrocarbon fuel or hydrogen, to compensate for the increased mass. For hybrid-electric configurations featuring ICEs as a primary power source, a configuration with 8 (secondary) distributed propellers was considered. The total number of propellers was pre-selected as a compromise between the effectiveness of the associated aero-propulsive effects and the necessity to contain the cost and complexity of the powerplant. A schematic representation of hybrid-electric and hydrogen-based configurations is proposed in Fig. 4.18 and Fig. 4.19. The configurations represented in the figures are purely qualitative and aim to suggest one feasible solution for the location of the elements of a hybrid-electric powertrain, compliant with both aircraft stability constraints and accommodation requirements.

As seen in Fig. 4.18, in the case of hybrid-electric configurations with batteries, two primary propellers directly driven by ICEs are installed on the inner portion of the wing, and four electrically powered propellers per half-wing cover the remaining wing area. Batteries were qualitatively located in the lower deck of the fuselage and in the front of the cabin. A similar distribution was also considered for the aircraft concepts based on FCs, with five electrically driven propellers uniformly distributed along the wing half-span, as shown in Fig. 4.19.

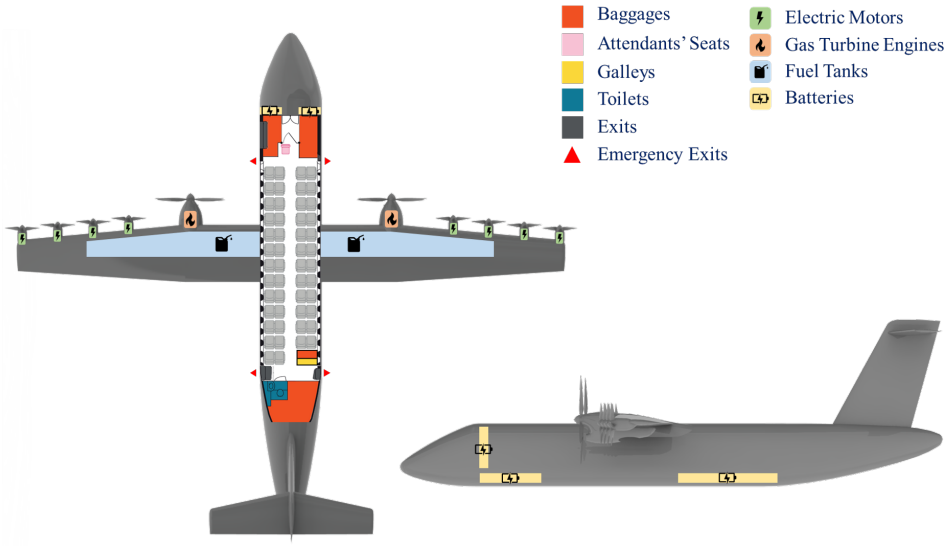

Figure 4.18: Schematic representation of the ICE-based hybrid-electric configurations considered (adapted from Ref. [94]).

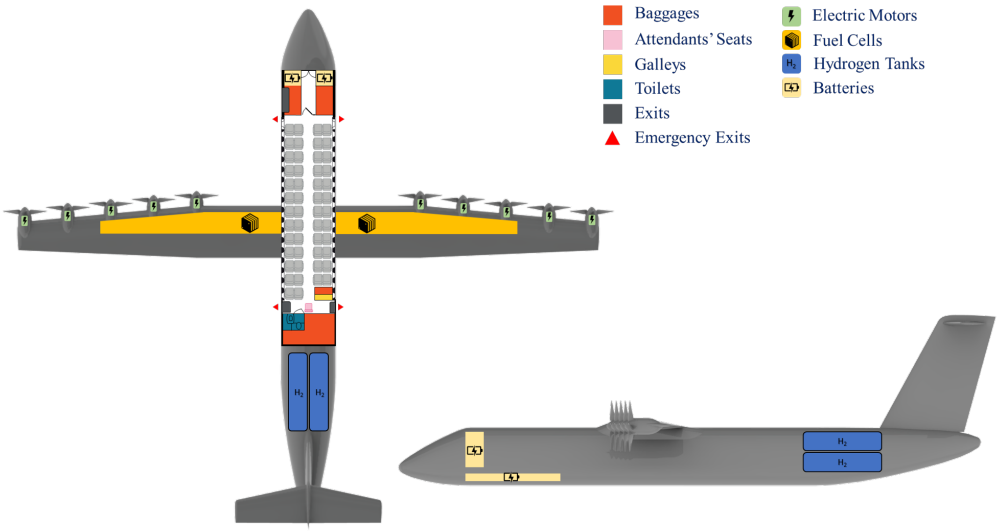

Figure 4.19: Schematic representation of the FC-based hybrid-electric configurations considered (adapted from Ref. [94]).

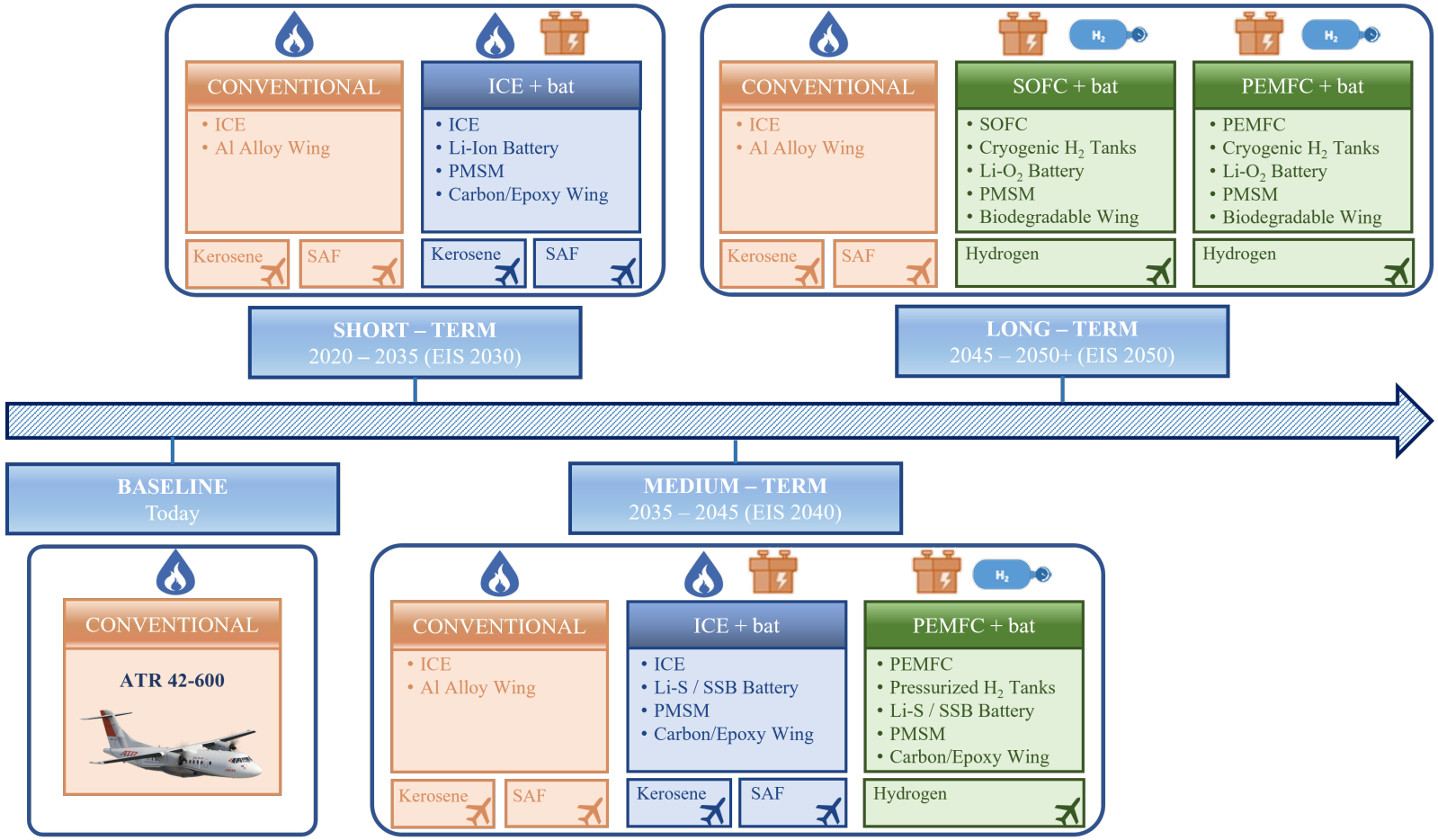

Figure 4.20: Future scenarios analyzed in the present study, concerning three different time horizons.

In the case of FC-based configurations, concerning the scheme in Fig. 2.3, the 10 electric motors were all modeled as secondary electric machines. The FC systems were placed in the vicinity of the wing, considering the option to house them inside the wing box in the place of the fuel tanks. The tanks were allocated in the rear of the fuselage. In this regard, the fuselage will be suitably stretched to provide enough space behind the passenger seats. As anticipated in Section 4.3 and shown here in Fig. 4.19, the necessary mass of gaseous/liquid hydrogen was split into four identical, longitudinally placed pressurized/cryogenic tanks. Although a detailed analysis of the mass distribution on board will not be performed, it is assumed that the presence of sufficient room for the batteries in front of the wing guarantees the possibility of keeping the CG of the airplane close to the 25% of the mean aerodynamic chord of the wing, ensuring a sufficient aircraft static stability margin.

In Tab. 4.11, the characteristics of the main technological building blocks employed for each scenario are specified in more detail. As explained in Section 4.3, the different technologies identified were translated into key performance indicators and mathematical models, and integrated into the aircraft design workflow. Each configuration will be designed in compliance with the same set of TLARs reported in Section 4.2, using an approach based on the analysis of the design mission as described in Section 2.4. The degree of hybridization and the geometry of each concept will be determined through extensive design explorations aimed at minimizing fuel consumption and direct pollutant emissions.

As discussed in Subsection 4.3.2, the performance of new turboprop engines will be evaluated thanks to the implementation of a rubber gas turbine engine model developed by Di Stasio [109]. Depending on the particular time frame, it will be possible to achieve reductions in fuel consumption ranging from 20% to 30% compared to today's reference baseline [109]. Kerosene was assumed to be the reference energy source for conventional aircraft, while 100% SAF will be used for hybrid-electric configurations based on ICE. Regarding the evaluation of the structural mass, a simple aluminum (Al) wing structure was considered for the conventional scenarios. For all future scenarios, innovative composite materials will be considered by using the model presented in Subsection 4.3.7. For the long-term scenario, a completely re-processable biomaterial was adopted. Concerning energy storage systems and electric components, anticipated values for the specific powers of the primary components, as informed by expert opinions, formed the basis for an iterative assessment of the masses of the powerplant components and their consequential impact on the aircraft's performance. $Li-Ion$ chemistry was considered for the short term. For the medium-term analyses at the aircraft level, both $Li-S$ and SSB will be considered as options to select the best one within the design process in accordance with the specific hybridization strategy adopted. Finally, $Li-O_2$ batteries were considered for the long-term only. Concerning hydrogen FCs, SOFC and PEMFC systems were both considered promising candidates, with the latter seen as a promising evolution of the former in the long term. Pressurized tanks were considered for the medium term, whereas cryogenic tanks were supposed to reach a sufficient TRL in the long term. PMSMs

Table 4.11: Summary table of the major technologies implemented for all of the concept models analyzed (adapted from Ref. [94]).

Scenario	**Short-Term (EIS 2030)**		**Medium-Term (EIS 2040)**			**Long-Term (EIS 2050)**		
Technology	**ICE**	**ICE + bat**	**ICE**	**ICE + bat**	**PEMFC + bat**	**ICE**	**SOFC + bat**	**PEMFC + bat**
Fuel	Kerosene (Jet A-1)	SAF (HEFA-SPK)	Kerosene (Jet A-1)	SAF (SPK Blend)	Hydrogen	Kerosene (Jet A-1)	Hydrogen	Hydrogen
ICE	3-spool TP OPR 18 Cooled HPT	3-spool TP OPR 18 Cooled HPT	3-spool TP OPR 19 Cooled H/LPT	3-spool TP OPR 19 Cooled H/LPT	-	3-spool TP OPR 19 Cooled H/LPT	-	-
Batteries	-	$Li-Ion$	-	$Li-S$ / SSB	$Li-S$ / SSB	-	$Li-O_2$ / SSB	$Li-O_2$ / SSB
Fuel Cells	-	-	-	-	PEMFC	-	SOFC	PEMFC
Hydrogen Tanks	-	-	-	-	Pressurized Tanks	-	Cryogenic Tanks	Cryogenic Tanks
Primary Electric Machines	-	Liquid Cooled PMSM	-	Halbach Array PMSM	Halbach Array PMSM	-	Halbach Array PMSM	Halbach Array PMSM
Secondary Electric Machines	-	Liquid Cooled PMSM	-	Liquid Cooled PMSM	Halbach Array PMSM	-	Halbach Array PMSM	Halbach Array PMSM
Power Electronics	-	SiC Converters	-	SiC Converters	SiC Converters	-	GaN Converters	GaN Converters
Wing Material	Al Alloy	Carbon/ Epoxy	Al Alloy	Carbon/ Epoxy	Carbon/ Epoxy	Al Alloy	Biodegradable Bio Fibres	Biodegradable Bio Fibres

were selected as the reference technology for all electric motors and generators, regardless of whether they will be used as motors or generators. Directly cooled stator windings and a Halbach magnet arrangement are proposed for the medium- and long-term horizons. The use of GaN converters was limited to the long-term horizon, while SiC converters were used in short- and medium-term scenarios.

In the following section, the outcomes of the exploratory analysis conducted to design the aforementioned concepts will be presented. The thoroughly examined configurations will serve as a representation of the potential that the regional segment holds for enhancing the sustainability of aviation in the coming decades.

4.4.2 Reference Aircraft

The exploration of innovative scenarios was preceded by modeling three distinct conventional airplanes for each of the three considered time horizons. These conventional concepts were modeled and analyzed to establish a reliable benchmark in terms of environmental performance and sustainability, particularly in comparison to new advanced concepts equipped with innovative propulsive solutions. The ATR 42-600 model [154, 155, 157, 231] served as the baseline for deriving the aforementioned reference models. The redesign of the baseline to create the three new conventional aircraft was based on the same TLARs outlined in Section 4.2.

Table 4.12 presents an overview of the block fuel consumption (i.e., encompassing the whole nominal mission except for reserves) for both the baseline airplane and the three conventional concepts. The performance of the baseline airplane was simulated for the 600 nmi design mission and the 200 nmi typical mission. Depending on the specific time frame considered, notable reductions in block fuel of up to 34% for the design mission and 31% for the typical mission are achieved compared to the reference ATR42-like airplane modeled. It is important to note that the primary modification made to the conventional future aircraft compared to the baseline involved the installation of more efficient and lighter gas turbine engines. New ICEs were designed within the design loop and tailored to each time horizon [109], revealing a progressive improvement in SFC and an enhanced power-to-weight ratio, reflecting the technological advancements assumed by the engine surrogate model (e.g., improved turbomachinery efficiencies, higher turbine operating temperatures, enhanced cooling technology). These enhancements have resulted in the design of more efficient conventional aircraft concepts than the reference baseline. Additionally, the designed conventional airplanes could benefit from a slightly lower MTOM than the baseline due to a different assumption regarding the design mission (600 nmi instead of the 726 nmi of the ATR 42-600).

Table 4.12: Reference conventional airplanes in three different future time horizons. Estimated fuel consumption and pollutant emissions are compared to the fuel consumed by today's reference airplane.

		Baseline (Today)	**Short-Term (EIS 2030)**		**Medium-Term (EIS 2040)**		**Long-Term (EIS 2050)**	
Parameter	**Unit**	**Value**	**Value**	**Diff.**	**Value**	**Diff.**	**Value**	**Diff.**
Primary Fuel	–	Jet A-1	Jet A-1		Jet A-1		Jet A-1	
Primary Power Source	–	ICE	ICE		ICE		ICE	
Design Range	nmi	726.0	600.0	−17.4%	600.0	−17.4%	600.0	−17.4%
Maximum Take-Off Mass	kg	18 600	17 812	−4.2%	17 421	−6.3%	17 366	−6.6%
				600 nmi Design Mission				
Block Fuel	kg	1 481.5	1 097.4	−26.0%	1 003.9	−32.2%	981.3	−33.8%
Block CO_2	kg	4 665.1	3 455.2	−26.0%	3 161.3	−32.2%	3090.1	−33.8%
Block NO_x	kg	17.91	12.59	−29.7%	12.08	−32.6%	11.71	−34.6%
Block CO	kg	5.54	4.28	−22.7%	3.91	−29.4%	3.81	−31.2%
Block HC	kg	0.734	0.402	−45.2%	0.331	−54.9%	0.319	−56.5%
Block SO_2	kg	1.244	0.922	−26.0%	0.843	−32.2%	0.824	−33.8%
Block H_2O	kg	1 822.2	1 349.7	−26.0%	1 234.8	−32.2%	1 207.0	−33.8%
				200 nmi Typical Mission				
Block Fuel	kg	610.7	473.1	−22.5%	431.5	−29.3%	421.0	−31.1%
Block CO_2	kg	1 923.2	1 489.9	−22.5%	1 358.9	−29.3%	1 325.8	−31.1%
Block NO_x	kg	6.14	4.90	−20.2%	4.67	−23.9%	4.52	−26.4%
Block CO	kg	4.77	3.76	−21.2%	3.44	−27.9%	3.35	−29.8%
Block HC	kg	0.611	0.339	−44.5%	0.278	−54.5%	0.267	−56.3%
Block SO_2	kg	0.513	0.397	−22.5%	0.362	−29.3%	0.354	−31.1%
Block H_2O	kg	751.2	581.9	−22.5%	530.8	−29.3%	517.9	−31.1%

4.5 Aircraft Design Exploration

4.5.1 Design of Experiments

For the purposes of the present study, the exploration of the optimal hybridization factors in terms of fuel consumption for different hybrid and electric concepts was conducted through DOE activities. Chapter 2 has already discussed the choice of employing a DOE approach over a methodological one. The rationale is essentially linked to the intent to perform the conceptual design using refined physics-based methods that size the aircraft based on the actual requirements from the design mission simulation. Forsaking more detailed full-factorial explorations to enhance computational efficiency [289], Latin hypercube sampling was used to generate around one thousand distinct aircraft for each investigated scenario. Each aircraft has undergone analysis and sizing through the process described in Section 2.4. In most instances, the DOE study also encompassed wing planform parameters to meet the entire set of TLARs, especially in cases of substantial increases in aircraft mass dictated by innovative propulsion technologies, or to potentially reduce the wing surface thanks to the beneficial effects provided by DEP in terms of the airplane's lifting capability. The design degrees of freedom chosen for exploration were streamlined to the following, deemed most relevant:

- *Shaft power ratio at take-off*, representing the shaft power associated with the secondary propulsive line over total shaft power (primary plus secondary line) in nominal take-off conditions.
- *Supplied power ratio at take-off*, representing the power supplied by the battery system over total source power (fuel plus battery), in nominal take-off conditions.
- *Supplied power ratio at climb*, representing the power supplied by the battery system over total source power (fuel plus battery), in nominal climb conditions.
- *Supplied power ratio at cruise*, representing the power supplied by the battery system over total source power (fuel plus battery), in nominal cruise conditions.
- *Wing planform surface*, which impacts the wing wetted area, influencing lift force, take-off and landing performance, and drag characteristics.
- *Wing aspect ratio*, which also directly affects the airplane's drag.

Although fuselage dimensions were not included among DOE variables, the fuselage length was automatically adjusted in case of hydrogen configurations, ensuring enough space for tanks positioned aft of the rear bulkhead. The battery was assumed to be inactive during the descent, landing, taxi, alternate, and holding phases. In this context, the secondary line of Figs. 2.2–2.3 represents the DEP, which is aimed at enhancing the aircraft's lifting capability on the ground. In the case of ICE-based hybrid-electric architectures, the shaft power ratio was set at 0.90 during the landing phase. During the cruise, given the distributed propellers' lower efficiency, all shaft power is routed through the primary line, redirecting energy from electric storage via electric machines working as motors, while the secondary propellers are assumed folded.

Figure 4.21 provides the results of the DOE performed to design airplanes corresponding to all the scenarios identified in the previous section. With reference to

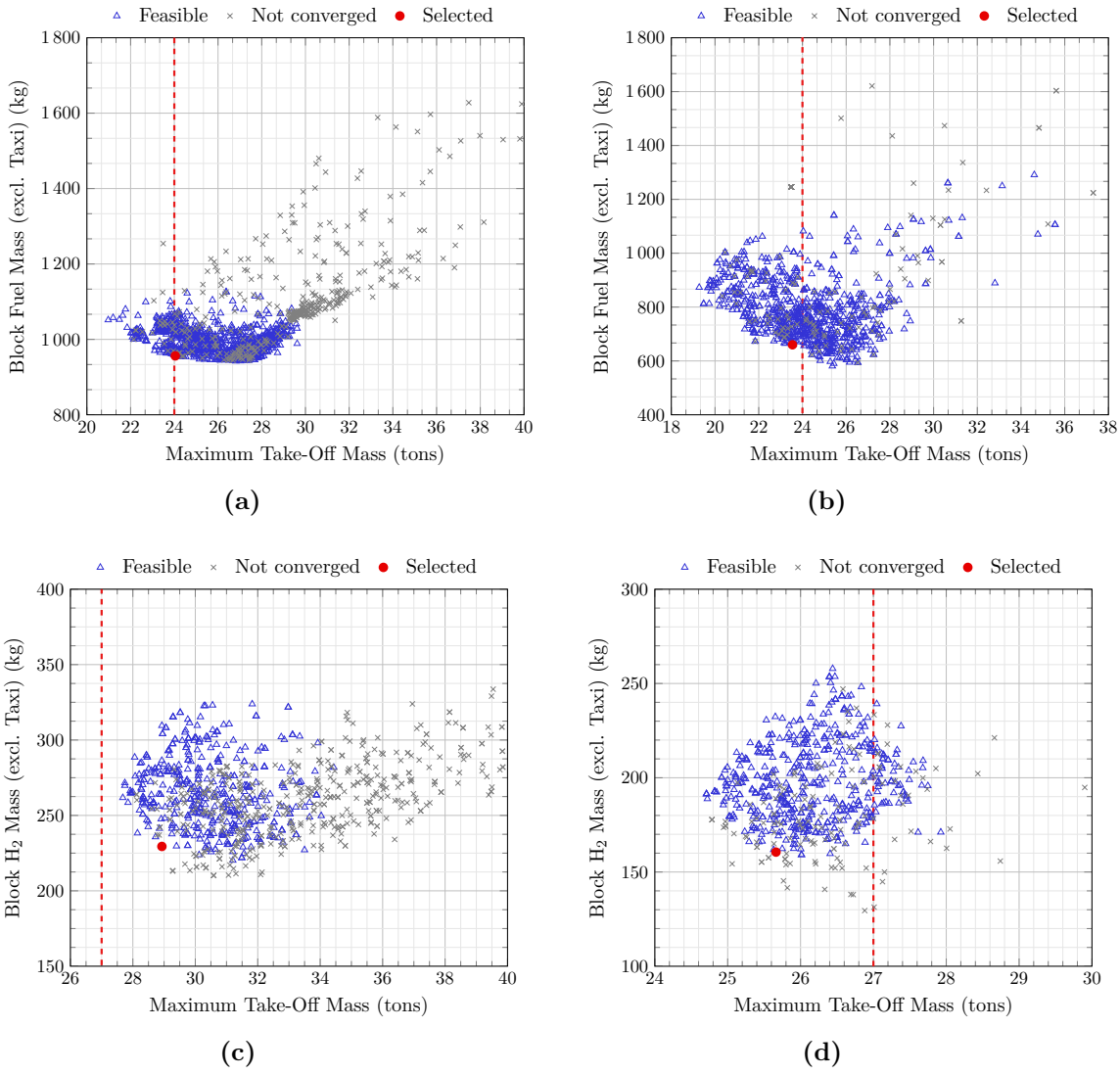

Figure 4.21: Results of the DOE activity, and selected solutions for different future scenarios. Red dotted lines indicate the recommended upper threshold of the MTOM for the different scenarios (adapted from Ref. [94]). (**a**) Short-term ICE+bat configuration. (**b**) Medium-term ICE+bat configuration. (**c**) Medium-term PEMFC+bat configuration. (**d**) Long-term SOFC+bat configuration.

the short-term hybrid-electric scenario, being interested in examining the feasibility of a hybrid-electric regional concept with a relatively near EIS, the decision was made to maintain the geometry identical to that of the baseline aircraft, leaving room for the possibility of retrofitting the latter. Consequently, adjustments to the wing area and wing aspect ratio were omitted during the design exploration for this scenario. A total of 1 500 DOE points, each representing a distinct hybridization strategy, underwent analysis for this scenario. Figure 4.21a presents the primary outcomes of this exploration, showcasing block fuel mass (excluding taxi phase contribution) and MTOM. It is worth underlying that each point in Fig. 4.21 represents an aircraft completely designed through the workflow of Fig. 2.14, based on the assigned

Table 4.13: Results of the DOE activities carried out for different scenarios and time horizons (reproduced from Ref. [94]).

		Short-Term (EIS 2030)	**Medium-Term (EIS 2040)**		**Long-Term (EIS 2050)**
Scenario		**ICE + bat**	**ICE + bat**	**PEMFC + bat**	**SOFC + bat**
Component	**Unit**	**Value**			
Wing Surface	m^2	54.5	59.1	70.8	58.6
Wing Aspect Ratio	-	11.1	12.3	12.9	12.2
Shaft Power Ratio at Take-Off	-	0.420	0.429	1.000	1.000
Supplied Power Ratio at Take-Off	-	0.172	0.341	0.390	0.379
Supplied Power Ratio at Climb	-	0.168	0.284	0.326	0.263
Supplied Power Ratio at Cruise	-	0.066	0.178	0.179	0.187

mission requirements. Notably, many points analyzed did not converge due to the challenging take-off mass and the inability to satisfy the specified set of TLARs. Specifically, the landing requirement proved to be demanding, given the absence of modifications to the baseline wing geometry, once again stressing the importance of imposing a cap on the MTOM. Moreover, a considerable increase in MTOM would probably mandate an extensive redesign of the landing gear system, contradicting the aim of maintaining the original geometry and architecture of the baseline airplane in the short-term horizon. Therefore, the design point was selected as the minimum block fuel solution that keeps the MTOM below 24 tons. Figure 4.21a also reveals the presence of a block fuel plateau for MTOM values ranging from 24 to 28 tons, indicating that relaxing or eliminating the MTOM constraint would not yield significantly different results in terms of fuel burn reduction. The first column of Tab. 4.13 reports the hybridization factors for take-off, climb, and cruise corresponding to the found solution.

For the medium term, two distinct DOE studies were conducted: one for the ICE+bat configuration based on ICEs and battery, and the other for the PEMFC+bat configuration featuring a FC system plus battery. Figure 4.21b illustrates the results for the ICE+bat scenario. In this case, given the more extended time horizon, the design exploration allowed for modifying the aircraft's geometry. Nearly 1 200 DOE points were analyzed in this scenario. As anticipated by Tab. 4.2, in the case of the medium-term ICE+bat configuration, it was decided to maintain the same MTOM limitation adopted for the short term. This decision stemmed from the consideration that a mass increase beyond 24 tons would result in relatively marginal additional fuel burn reductions while compromising ground performance and increasing manufacturing and operating costs. Consequently, as depicted in Fig. 4.21b, the final medium-term ICE+bat solution was selected, among those with an MTOM below 24 tons, as the feasible solution corresponding to the

minimum block fuel. The second column of Tab. 4.13 provides the design variable values for this solution, revealing a substantially higher utilization of electric power throughout all main flight phases compared to the short term. As will be seen later, this aspect has also led to a notable decrease in the rated power of the thermal engines, roughly two-thirds of that found in short-term ICE+bat configuration.

Figure 4.21c displays the outcomes of the DOE conducted for the medium-term PEMFC+bat aircraft. Once again, around 1 200 design points were scrutinized, with wing planform parameters included as design variables. Similar to previous scenarios involving hydrocarbon-based fuel, the objective was to identify the optimal hybridization strategy that minimizes hydrogen consumption while successfully fulfilling all technical constraints and requirements. As illustrated in Fig. 4.21c, no solution was found for MTOM values less than the upper limit of 27 tons. This is primarily attributed to the substantial mass penalty introduced by the pressurized hydrogen tanks installed in the rear of the fuselage. Consequently, it was decided to adjust the MTOM limitation to 30 tons, to avoid excessive increases in the wing planform area and mitigate the rise in the acquisition and operating costs. However, as depicted in Fig. 4.21c, the chosen solution corresponds to a hydrogen consumption mass slightly higher than the global minimum, the latter achievable for an MTOM value of around 32 tons. The third column in Tab. 4.13 presents the values of the design variables for this solution. Given the significantly higher MTOM compared to previous scenarios, a notable augmentation in the wing planform surface was necessary to continue meeting the same set of ground performance requirements.

Finally, a single DOE investigation was carried out with regard to the long-term horizon, focusing on the SOFC+bat hybrid-electric configuration based on SOFCs and batteries. Later, to ensure a fair assessment of FC technologies considered for the long-term horizon, the hybridization factors and wing planform parameters obtained from this DOE were utilized to evaluate the additional PEMFC+bat configuration incorporating PEMFCs. Figure 4.21d provides insights into the outcomes of this study, encompassing the analysis of nearly 600 DOE points. Similar to previous cases, the pursuit of minimal fuel consumption guided the final selection of the solution. In contrast to the medium-term counterpart, feasible solutions with an MTOM lower than 27 tons were identified in this case. This outcome is attributed, in part, to the higher power density and enhanced efficiency of SOFCs compared to medium-term PEMFCs. Furthermore, the significantly high GI of cryogenic hydrogen tanks, as opposed to pressurized tanks, contributes even more to a notable reduction in the powerplant system and aircraft empty masses. The last column of Tab. 4.13 presents the DOE design variables for the solution marked by a red dot in Fig. 4.21d. This solution showcases a substantially reduced wing planform area compared to the medium-term PEMFC+bat aircraft, thanks to the reduced MTOM.

4.5.2 Comparison of Scenarios

The selected, designed configurations are finally compared in Tabs. 4.14–4.17. Table 4.14 presents the sizing powers for all powertrain components in each analyzed scenario. Figures 4.22 and 4.23 show the power distribution associated with the short-term ICE+bat solution, in design take-off and cruise conditions respectively. The choice of a series/parallel partial hybrid architecture was functional to provide the possibility of splitting the power into two separated propulsive lines in take-off conditions, as exemplified by Fig. 4.22. However, it is more advantageous to redirect the propulsive power to the primary propellers in cruise, when the use of DEP to improve the aircraft's lift becomes superfluous. Figures 4.25–4.28 relate to the other configurations analyzed, where the take-off design condition is chosen as the most representative of the propulsion scheme. However, similar considerations made for the short term also apply to the ICE+bat configuration of the medium term. As for the hydrogen-based configurations, a simpler parallel architecture was adopted, by virtue of the full-electric nature of the power supplied.

Table 4.15 provides a detailed breakdown of masses for all analyzed scenarios. Except for the wing, the masses of airframe components were estimated using established literature methods [32]. The same approach was applied to systems, furnishings, operational items, and conventional powerplant components. Design fuel values in Tab. 4.15 refer to the total amount of fuel required onboard before take-off. Battery mass estimation assumed a minimum residual charge of 20%. In medium-term and long-term hybrid scenarios, the selection of the preferred chemistry ($Li-S$ or SSBs) was based on identifying which one corresponded to the smallest mass of the battery, in light of the mission requirements in terms of energy demand and maximum power (or C-Rate). Notably, SSBs have never been the preferable choice when compared to $Li-S$ batteries. Except for the medium-term PEMFC+bat scenario, the masses of all hybrid-electric configurations fall within a range between 24 and 27 tons. The criticality of the medium-term FC scenario is attributed to the technology performance level of FCs and the use of pressurized hydrogen tanks with a GI of 12.6 %. Conversely, the long-term configuration with PEMFCs utilizes cryogenic tanks with a GI that is more than three times higher. Despite variations, all MTOM values are considerably higher than those of conventional configurations, confirming the necessity of deploying DEP to prevent oversizing the lifting surfaces.

After completing the design process focusing only on the design mission, the off-design 200 nmi mission was also simulated. In the case of the short-term ICE+bat scenario, as it emerges from the comparison of Fig. 4.23 and Fig. 4.24, adjustments were made to increase the average battery power in cruise compared to the design mission, aiming to consume 80% of the battery energy capacity within the shorter mission duration. This was carried out in compliance with the power limitations of the battery and the other powertrain components, established during the design phase (see again Tab. 4.14). For medium-term and long-term hybrid configurations, only half of the consumable electrical energy was assumed to be

utilized in the typical mission. This assumption stems from the mission's brevity, making it impractical to entirely consume the available energy while adhering to the constraints on maximum powers. For these scenarios, it may be assumed that two flight legs can be completed before needing to recharge the battery.

Table 4.16 reports estimates of energy consumption and the main polluting species for the conventional and ICE+bat configurations. Two scenarios were considered for all ICE-based configurations depending on whether kerosene or a 100% SAF mixture was considered. The absence of intermediate scenarios, i.e., which consider mixtures with lower blend ratios, lies in the intention of considering the two extreme and most significant cases, especially in light of the current efforts to certify the use of 100% SAF [281–284]. However, as can be seen from the table, the differences in fuel consumption are limited, resulting significative only for some polluting species. Given the limited impact of the blend ratio at the aircraft level, it is believed quite reasonable to interpolate the values from Tab. 4.16 to obtain the emissions concerning any SAF blend ratio between 0% and 100%.

Table 4.17 proposes a final technical comparison of the innovative configurations, considering key performance indicators, energy consumption, and emissions for both the design and typical mission scenarios. At this stage, pollutant species, including CO_2, NO_x, and water vapor, are reported as key environmental factors. Table 4.17 also provides the same quantities expressed as a percentage difference with respect to the conventional ICE-based case corresponding to the same EIS year. Examining the short-term ICE+bat scenario, a limited advantage is observed for the design mission compared to the conventional case. The marginality of this impact is primarily attributed to the limited technological level of $Li-Ion$ batteries, wherein the increase in the aircraft's mass nullifies the partial replacement of thermal energy with electrical energy. However, leveraging the same amount of electricity for the shorter typical mission, a notable 23.6% reduction in block fuel is achieved. For the medium-term ICE+bat configuration, the benefits of hybridization become more pronounced, thanks to the higher specific energy of $Li-S$ batteries. In this case, the block fuel savings amount to 27.3% on the design mission and to a more substantial 45.1% on the typical mission. For medium-term and long-term hydrogen-based configurations, it is meaningful to assess the results in terms of the consumed fuel energy. In the case of PEMFC-based configurations, the resulting H_2 energy saving for the design mission is 36.6% in the medium term, and increases to 40.9% for the long-term scenario. As for the long-term SOFC-based configuration, the corresponding saving is 54.1%, reflecting the higher efficiency of SOFCs compared to PEMFCs. Across all ICE-based configurations, pollutant gas emissions decrease over time in correlation with fuel reduction. Hydrogen-based configurations theoretically exhibit zero direct emissions of CO_2 and NO_x, but further studies are necessary to reconsider this advantage from a long-life perspective. The next section, dealing with the LCA of the designed configurations, aims to validate or mitigate the expected advantages presented so far.

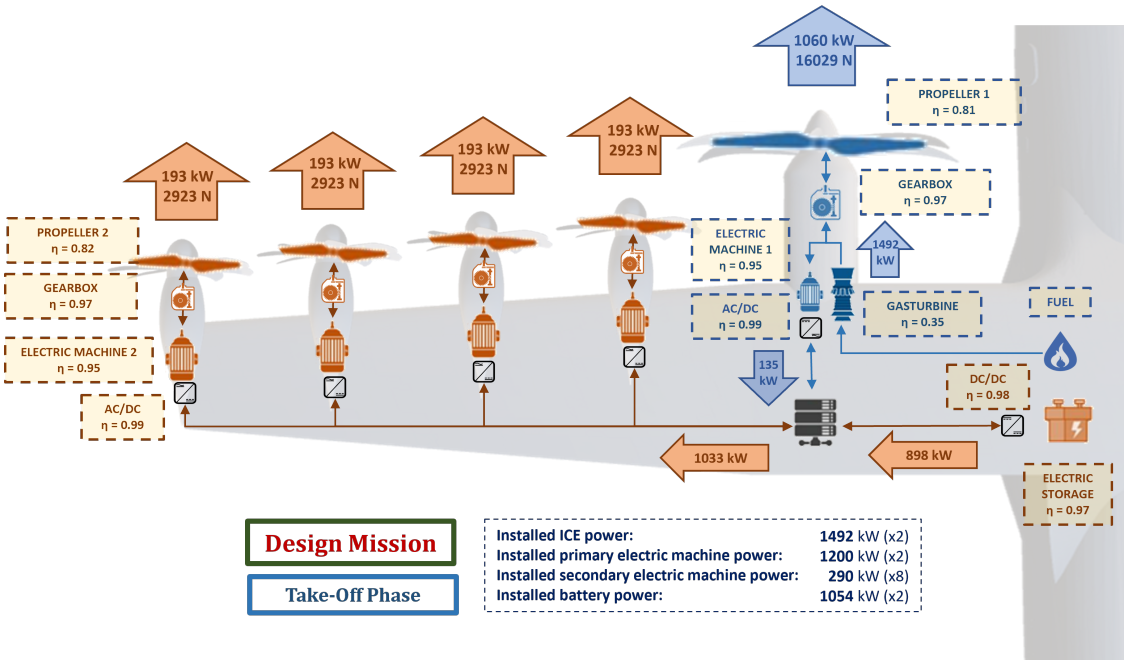

Figure 4.22: Power and thrust distribution for the short-term ICE+bat configuration in design take-off conditions.

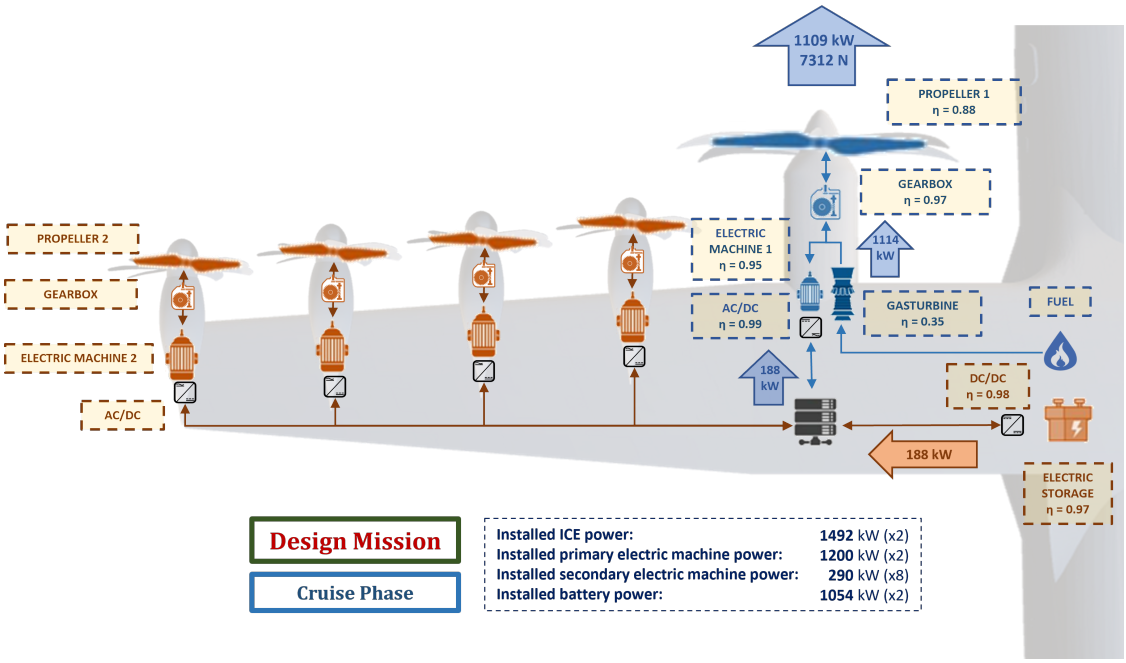

Figure 4.23: Peak power and thrust distribution for the short-term ICE+bat configuration in design cruise conditions.

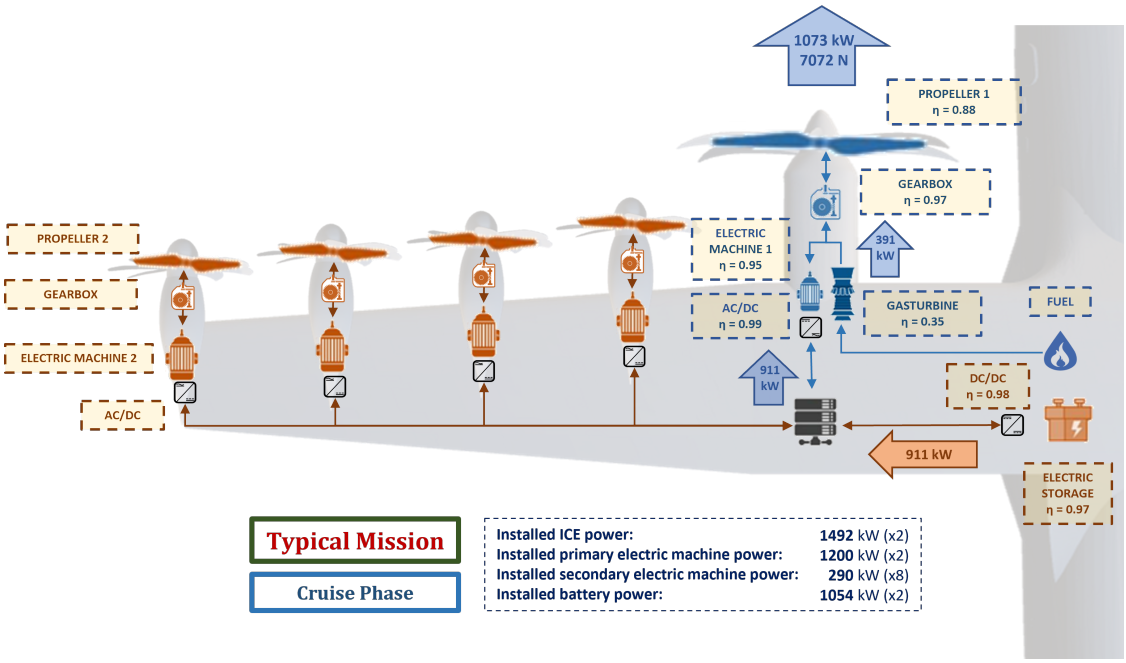

Figure 4.24: Peak power and thrust distribution for the short-term ICE+bat configuration in typical cruise conditions.

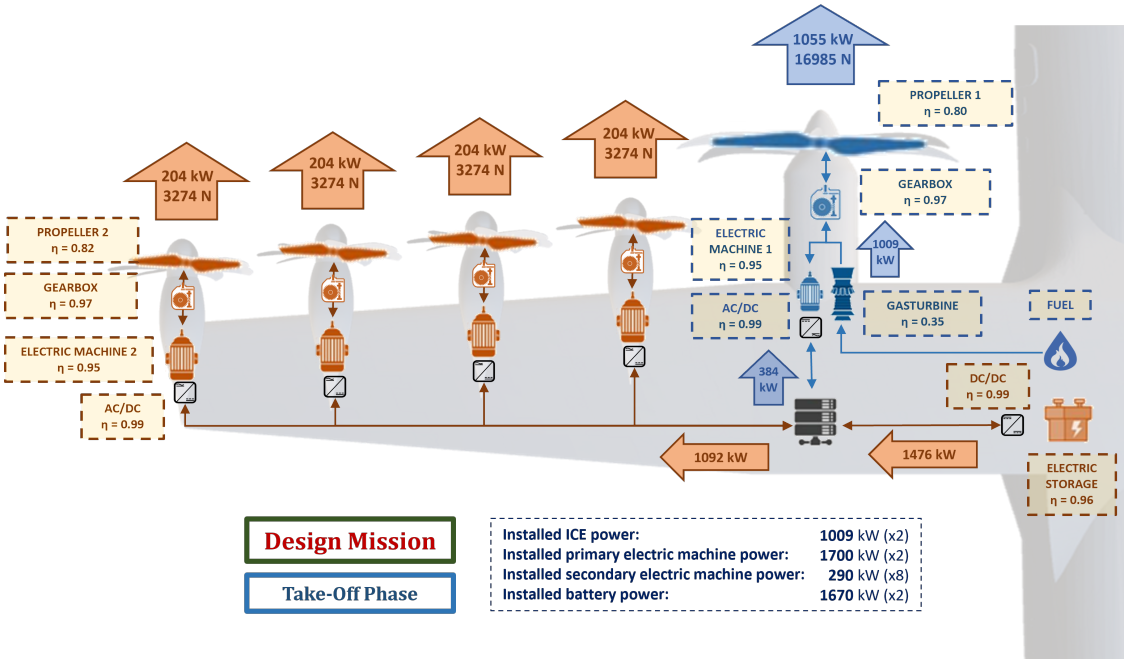

Figure 4.25: Power and thrust distribution for the medium-term ICE+bat configuration in design take-off conditions.

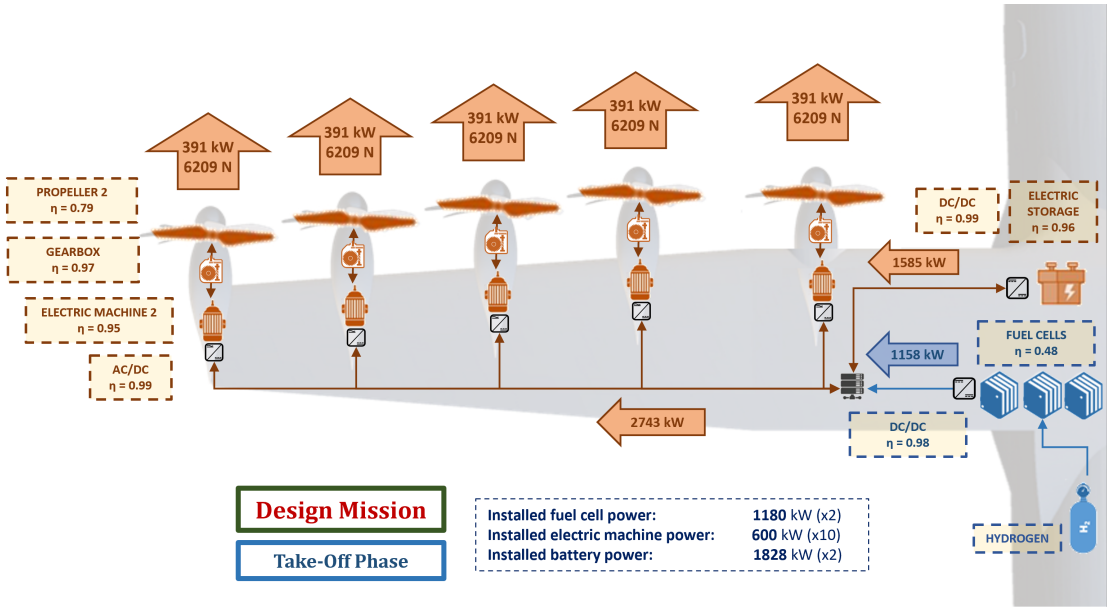

Figure 4.26: Power and thrust distribution for the medium-term PEMFC+bat configuration in design take-off conditions.

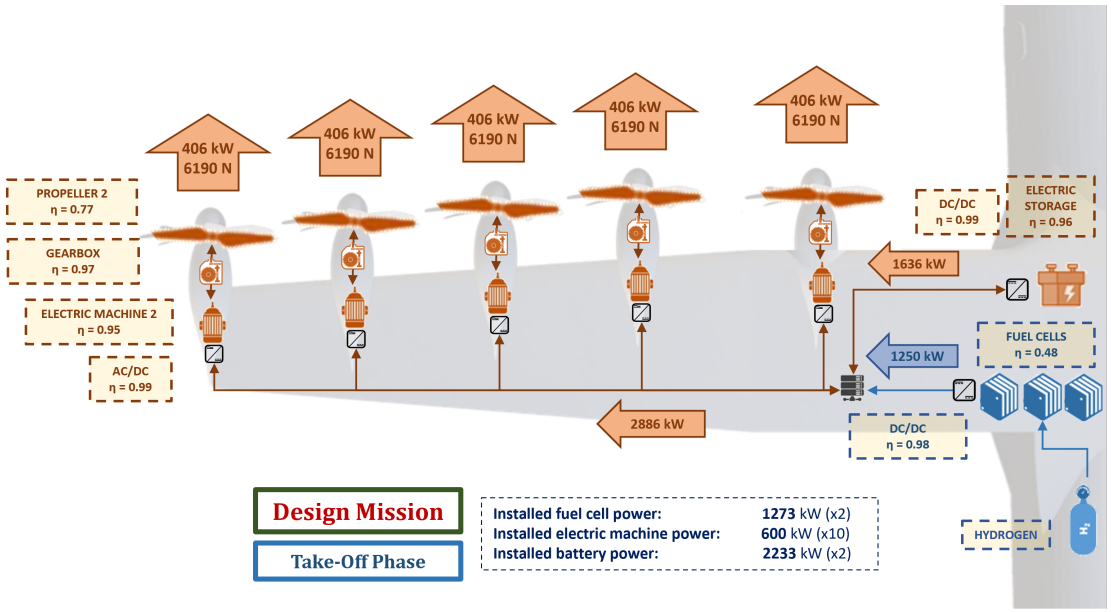

Figure 4.27: Power and thrust distribution for the long-term PEMFC+bat configuration in design take-off conditions.

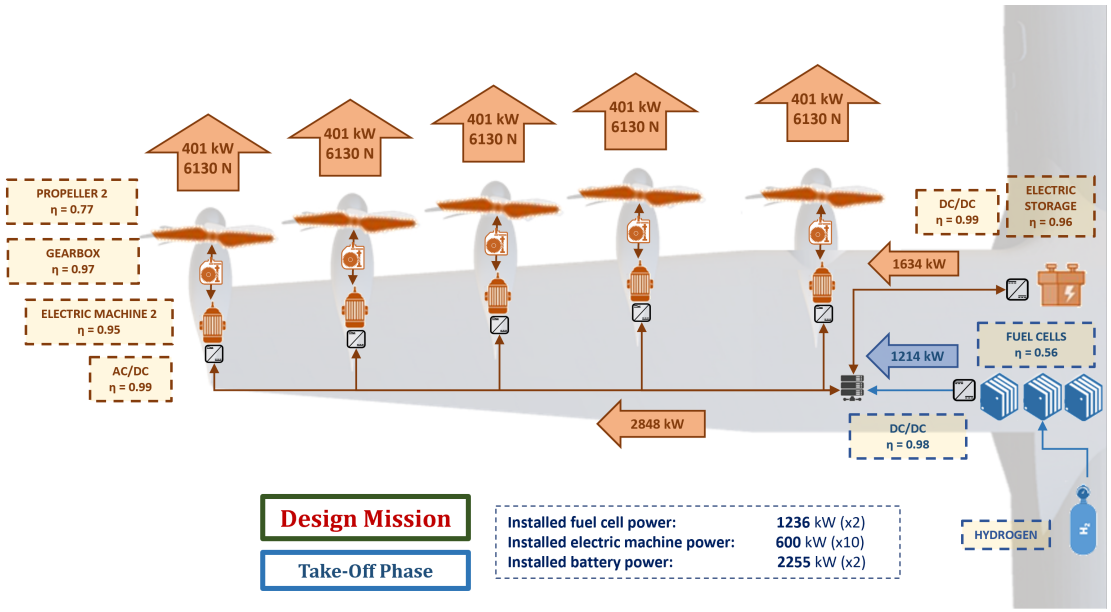

Figure 4.28: Power and thrust distribution for the long-term SOFC+bat configuration in design take-off conditions.

Table 4.14: Rated power of main powertrain components for all hybrid/electric configurations designed (adapted from Ref. [94]).

Scenario	**Short-Term (EIS 2030)**		**Medium-Term (EIS 2040)**				**Long-Term (EIS 2050)**			
	ICE + bat		**ICE + bat**		**PEMFC + bat**		**SOFC + bat**		**PEMFC + bat**	
Component	**Q.ty (–)**	**Rated Power (kW)**	**Q.ty (–)**	**Rated Power (kW)**	**Q.ty (–)**	**Rated Power (kW)**	**Q.ty (–)**	**Rated Power (kW)**	**Q.ty (–)**	**Rated Power (kW)**
Thermal Engine	2	1 492 (×2)	2	1 009 (×2)	–	–	–	–	—	-
Primary Electric Machine	2	1 200 (×2)	2	1 700 (×2)	–	–	–	–	–	–
Secondary Electric Machine	8	290 (×8)	8	290 (×8)	10	600 (×10)	10	600 (×10)	10	600 (×10)
Fuel Cell System	-	-	-	-	2	1 180 (×2)	2	1 236 (×2)	2	1 273 (×2)
Battery	1	2 108 (×1)	1	3 340 (×1)	1	3 656 (×1)	1	4 510 (×1)	1	4 466 (×1)

Table 4.15: Mass breakdown of all future configurations designed (adapted from Ref. [94]).

		Short-Term (EIS 2030)		**Medium-Term (EIS 2040)**			**Long-Term (EIS 2050)**		
Scenario		**ICE**	**ICE + bat**	**ICE**	**ICE + bat**	**PEMFC + bat**	**ICE**	**SOFC + bat**	**PEMFC + bat**
Component	**Unit**				**Mass**				
Wing	kg	1 504.4	1 450.8	1 484.1	1 580.2	1 790.8	1 481.3	3 821.3	3 818.3
Horizontal Tail	kg	201.0	201.0	201.0	210.9	241.3	201.0	187.8	182.8
Vertical Tail	kg	257.4	257.4	257.4	309.3	370.7	257.4	268.9	260.8
Fuselage	kg	2 374.3	2 374.3	2 374.3	2 397.5	3 183.6	2 374.3	2 969.6	3 129.6
Control Surfaces	kg	334.8	408.3	329.9	396.6	462.2	329.3	427.6	430.4
Main Undercarriage	kg	659.3	872.5	645.9	837.0	1 042.2	644.1	932.0	940.7
Nose Undercarriage	kg	153.8	192.2	151.3	185.9	221.5	151.0	202.6	204.1
Primary Nacelles	kg	384.9	398.5	377.1	403.6	0.0	372.7	0.0	0.0
Secondary Nacelles	kg	0.0	176.1	0.0	174.0	444.3	0.0	450.7	450.7
Structure	**kg**	**5 870.0**	**6 331.2**	**5 821.2**	**6 495.1**	**7 756.5**	**5 811.0**	**9 260.5**	**9 417.5**
Fuel System (Thermal)	kg	114.7	114.7	114.7	120.6	0.0	114.7	0.0	0.0
ICE (incl. Primary Gearboxes)	kg	699.5	641.8	505.6	330.1	0.0	499.3	0.0	0.0
Hydrogen Tanks	kg	0.0	0.0	0.0	0.0	2 685.6	0.0	410.2	529.3
Fuel Cell Systems	kg	0.0	0.0	0.0	0.0	1 963.1	0.0	1 318.0	1 162.2
Secondary Gearboxes	kg	0.0	145.1	0.0	184.4	349.5	0.0	311.2	311.2
Primary Electric Machines	kg	0.0	346.0	0.0	309.7	0.0	0.0	0.0	0.0
Secondary Electric Machines	kg	0.0	428.0	0.0	428.0	679.8	0.0	679.8	679.8
Primary Propellers	kg	667.7	576.6	657.2	582.4	0.0	0.0	0.0	0.0
Secondary Propellers	kg	0.0	437.3	0.0	475.8	1 126.4	651.2	1 035.1	1 035.1
Battery	kg	0.0	3 765.3	0.0	3 341.2	3 611.4	0.0	2 386.0	2 362.5
Cabling	kg	0.0	68.1	0.0	72.8	83.2	0.0	75.7	76.6
Power Electronics (incl. TMS)	kg	0.0	295.6	0.0	239.4	336.7	0.0	262.1	263.0
Powerplant	**kg**	**1 482.1**	**6 818.6**	**1 277.9**	**6 084.4**	**10 835.7**	**1 265.2**	**6 478.1**	**6 419.5**

Table 4.15: *Cont.*

Scenario		Short-Term (EIS 2030)		Medium-Term (EIS 2040)			Long-Term (EIS 2050)		
		ICE	**ICE + bat**	**ICE**	**ICE + bat**	**PEMFC + bat**	**ICE**	**SOFC + bat**	**PEMFC + bat**
Component	**Unit**	**Mass**							
Air Conditioning	kg	591.4	691.7	591.4	691.7	765.9	591.4	750.8	765.4
Electrical Systems	kg	741.6	881.9	741.6	881.9	1 024.2	741.6	995.6	1 023.4
Pneumatics/Hydraulics	kg	416.1	508.9	412.2	499.6	595.9	411.9	550.4	552.5
Instruments	kg	326.9	430.8	321.9	421.3	512.5	321.4	471.2	473.2
Auxiliary Power Unit	kg	181.6	181.6	181.6	181.6	181.6	181.6	181.6	181.6
Systems	**kg**	**2 257.7**	**2 694.9**	**2 248.8**	**2 676.1**	**3 080.1**	**2 248.0**	**2 949.6**	**2 996.1**
Furnishing	**kg**	**1 158.8**	**1 158.8**	**1 158.8**	**1 158.8**	**1 290.8**	**1 158.8**	**1 262.5**	**1 289.9**
Crew	kg	380.0	380.0	380.0	380.0	380.0	380.0	380.0	380.0
Operational Items	kg	430.9	430.9	430.9	430.9	430.9	430.9	430.9	430.9
Operative Equipment	**kg**	**810.9**	**810.9**	**810.9**	**810.9**	**810.9**	**810.9**	**810.9**	**810.9**
Operating Empty Mass	**kg**	**11 579.5**	**17 814.4**	**11 317.6**	**17 225.3**	**23 774.0**	**11 293.9**	**20 761**	**20 933.9**
Design Payload	kg	4 750.0	4 750.0	4 750.0	4 750.0	4 750.0	4 750.0	4 750.0	4 750.0
Design Fuel [1]	kg	1 482.1	1 462.8	1 353.7	1 045.7	0.0	1 322.0	0.0	0.0
Design H_2 [2]	kg	0.0	0.0	0.0	0.0	390.7	0.0	281.8	361.4
Maximum Take-Off Mass	**kg**	**17 811.6**	**24 027.2**	**17 421.3**	**23 021.0**	**28 914.7**	**17 365.8**	**25 793.3**	**26 045.3**

[1] Including fuel consumed during the nominal mission, excl. taxi-out, plus fuel for alternate and holding phases, and 5% reserve fuel.
[2] Including fuel consumed during the nominal mission, excl. taxi-out, plus fuel for alternate and holding phases, 5% reserve fuel, with a hydrogen utilization fraction of 0.85.

Table 4.16: Fuel, energy consumption, and pollutant emissions for all ICE-based solutions, referred to the nominal block mission.

		Short-Term (EIS 2030)				**Medium-Term (EIS 2040)**				**Long-Term (EIS 2050)**	
Scenario		**ICE**		**ICE + bat**		**ICE**		**ICE + bat**		**ICE**	
Parameter	**Unit**	**Value**									
Primary Fuel	–	Jet A-1	SPK	Jet A-1	SPK	Jet A-1	SPK	Jet A-1	SPK	Jet A-1	SPK
Primary Power Source	–	ICE		ICE		ICE		ICE		ICE	
Secondary Power Source	–	–		Li-Ion Battery		–		Li-S Battery		–	
Maximum Take-Off Mass	kg	17 812	17 785	24 054	24 027	17 421	17 398	23 040	23 021	17 366	17 342
600 nmi Design Mission											
Fuel	kg	1 097.4	1 077.9	1 069.9	1 051.0	1 003.9	986.2	743.1	730.0	981.3	963.9
Fuel Energy	MWh	13.19	13.19	12.86	12.86	12.07	12.07	8.93	8.93	11.80	11.80
Battery Energy	MWh	0.00	0.00	0.84	0.84	0.00	0.00	1.80	1.80	0.00	0.00
CO_2	kg	3 455.2	3 341.6	3 369.2	3 258.0	3 161.3	3 057.1	2 340.2	2 263.0	3 090.1	2 988.2
NO_x	kg	12.59	12.37	13.25	13.01	12.08	11.86	10.23	10.05	11.71	11.51
CO	kg	4.28	3.28	4.00	3.07	3.91	3.00	2.76	2.11	3.81	2.92
HC	kg	0.402	0.393	0.367	0.359	0.331	0.323	0.209	0.205	0.319	0.311
SO_2	kg	0.922	0.235	0.899	0.230	0.843	0.215	0.624	0.159	0.824	0.211
H_2O	kg	1 349.7	1 458.4	1 316.0	1 422.0	1 234.8	1 334.3	914.1	987.7	1 207.0	1 304.2
200 nmi Typical Mission											
Fuel	kg	473.1	464.7	368.1	361.6	431.5	423.9	241.4	237.1	421.0	413.6
Fuel Energy	MWh	5.69	5.69	4.42	4.42	5.19	5.19	2.90	2.90	5.06	5.06
Battery Energy	MWh	0.00	0.00	0.84	0.84	0.00	0.00	0.90	0.90	0.00	0.00
CO_2	kg	1 489.8	1 440.7	1 159.1	1 120.9	1 358.9	1 314.1	760.1	735.0	1 325.8	1 282.1
NO_x	kg	4.90	4.81	2.54	2.50	4.67	4.59	1.68	1.65	4.52	4.44
CO	kg	3.76	2.89	3.42	2.62	3.44	2.64	2.35	1.80	3.35	2.57
HC	kg	0.339	0.331	0.296	0.289	0.278	0.271	0.164	0.160	0.267	0.261
SO_2	kg	0.397	0.101	0.309	0.079	0.362	0.093	0.203	0.052	0.354	0.090
H_2O	kg	581.9	628.8	452.7	489.2	530.8	573.5	296.9	320.8	517.9	559.6

Table 4.17: Overview of the designed future scenarios, and comparison of hybrid/electric configurations with reference conventional aircraft using kerosene referred to the same EIS year. Fuel, energy consumption, and pollutant emissions are referred to the nominal block mission.

		Short-Term (EIS 2030)		**Medium-Term (EIS 2040)**				**Long-Term (EIS 2050)**			
Scenario		**ICE + bat**		**ICE + bat**		**PEMFC + bat**		**SOFC + bat**		**PEMFC + bat**	
Parameter	**Unit**	**Value**	**Diff.**	**Value**	**Diff.**	**Value**	**Diff.**	**Value**	**Diff.**	**Value**	**Diff.**
Primary Fuel	–	HEFA-SPK		SPK Blend		Pressurized H_2		Liquid H_2		Liquid H_2	
Primary Power Source	–	ICE		ICE		PEMFC		SOFC		PEMFC	
Secondary Power Source	–	Li-Ion Battery		Li-S Battery		Li-S Battery		Li-O_2 Battery		Li-O_2 Battery	
Design Range	nmi	600	0.0%	600	0.0%	600	0.0%	600	0.0%	600	0.0%
Cruise Altitude	ft	20 000	0.0%	20 000	0.0%	20 000	0.0%	20 000	0.0%	20 000	0.0%
Time to Climb	min	12.69	0.8%	12.68	0.7%	12.88	2.3%	12.83	0.5%	12.74	−0.2%
Balanced Field Length	m	1 145	12.5%	920	−7.0%	1 134	14.7%	1 101	11.1%	1 107	11.7%
Maximum Take-Off Mass	kg	24 027	34.9%	23 021	32.1%	28 915	66.0%	25 793	48.5%	26 045	50.0%
600 nmi Design Mission											
Fuel	kg	1 051.0	−4.2%	730.0	−27.3%	229.6	−77.1%	162.2	−83.5%	209.1	−78.7%
Fuel Energy	MWh	12.86	−2.5%	8.93	−26.0%	7.65	−36.6%	5.41	−54.1%	6.97	−40.9%
Battery Energy	MWh	0.84	100.0%	1.80	100.0%	1.95	100.0%	1.80	100.0%	1.79	100.0%
CO_2	kg	3 258.0	−5.7%	2 263.0	−28.4%	0.0	−100.0%	0.0	−100.0%	0.0	−100.0%
NO_x	kg	13.01	3.4%	10.05	−16.8%	0.00	−100.0%	0.00	−100.0%	0.00	−100.0%
H_2O	kg	1 422.0	5.4%	987.7	−20.0%	2 051.8	66.2%	1 450.1	20.1%	1 868.9	54.8%
200 nmi Typical Mission											
Fuel	kg	361.6	−23.6%	237.1	−45.1%	61.8	−85.7%	46.1	−89.0%	60.4	−85.7%
Fuel Energy	MWh	4.42	−22.2%	2.90	−44.1%	2.06	−60.2%	1.54	−69.6%	2.01	−60.2%
Battery Energy	MWh	0.84	100.0%	0.90	100.0%	0.97	100.0%	0.90	100.0%	0.89	100.0%
CO_2	kg	1 120.9	−24.8%	735.0	−45.9%	0.0	−100.0%	0.0	−100.0%	0.0	−100.0%
NO_x	kg	2.50	−49.0%	1.65	−64.7%	0.00	−100.0%	0.00	−100.0%	0.00	−100.0%
H_2O	kg	489.2	−15.9%	320.8	−39.6%	552.8	4.1%	412.3	−20.4%	539.7	4.2%

4.6 Life Cycle Analysis

4.6.1 Introduction

The pursuit of sustainable regional aviation necessitates a thorough understanding of the environmental implications of emerging technologies. In the previous section, scenarios representative of three future horizons were designed based on keeping direct polluting emissions as low as possible, and a comprehensive assessment of the latter was proposed. However, direct emissions, i.e., emissions connected only to the flight mission, cannot provide a complete picture of the environmental impact of the aircraft, given that numerous collateral contributions have not yet been taken into account. The need emerges for a holistic approach that considers the aircraft's production, management, and disposal phases, which is fundamental in confirming the expected advantages of the hybrid and electric solutions discussed above. To ensure that the shift to emerging technologies is truly environmentally beneficial, conducting comprehensive sustainability assessments, such as an LCA, is imperative. LCA offers a comprehensive framework, considering the entire life cycle of an aircraft from raw material extraction to end-of-life disposal [290]. By adopting a holistic perspective, LCA enables a nuanced examination of the environmental footprint associated with manufacturing, operation, and the eventual retirement of aircraft [62, 63]. According to the ISO standard, LCA methodology consists of four fundamental phases [62, 63]:

- *Goal and scope definition*, outlining the study's reasons, objectives, intended application, and audience.
- *LCI*, collecting and modeling data for all product life cycle processes.
- *LCIA*, elaborating LCI data and translating it into environmental impact indicators.
- *Interpretation* of results, drawing conclusions and recommendations based on the study's goal and scope.

The application of LCA to transportation systems involving batteries, FCs, and alternative fuels faces significant gaps within the current state-of-the-art prospective LCA framework [290, 291]. Firstly, there is a deficiency in LCI datasets specific to emerging technologies in aviation systems, leading to challenges in accurately assessing and comparing their environmental footprints. Existing databases do not adequately capture material needs, manufacturing processes, usage performance, and end-of-life treatments for technologies like batteries, hydrogen FCs, and alternative fuels [61, 210, 290, 292]. Additionally, the inconsistency and lack of transparency in available LCI data hinder reliable analysis and decision-making [61]. Finally, the absence of a prospective dimension in current LCI datasets limits the ability to anticipate and address potential environmental impacts, which is essential for ensuring the sustainability of emerging technologies in aviation systems.

Thanks to the collaboration of academic and industrial collaborators, and the coordination role of researchers from DTU [208], these gaps were addressed in an attempt to build a prospective LCI database for future regional aircraft [210]. The scenarios presented in the previous sections, designed and analyzed by the author,

provided a solid basis for the construction of the database, later supported by industries specialized in the design and production of the main innovative components and technologies. The purpose of Subsection 4.6.2 is to briefly present the work carried out to create prospective LCIs, to which the author has made a contribution. In Subsection 4.6.3, the work finally flows into the pLCA of the scenarios considered in the present study, conducted by DTU with the author's support. The results of the pLCA enrich the present discussion with deep insights on the environmental footprint of the configurations, evaluated in multiple impact categories, which allow for a more comprehensive comparison and trade-off considerations between the different technologies considered.

4.6.2 Life Cycle Inventory

During the LCI phase, each process in the aircraft's life cycle needs to be thoroughly analyzed, with extensive data collection and modeling. This data, detailing material and energy inputs and outputs for each process, is transformed into LCI building blocks, interconnected to create the product's life cycle model. A key characteristic of this phase is the need for a large amount of data, which, for the purposes of this application, was provided by various contributors for the characterization of future regional concepts and technologies. The Technical University of Delft [273] and UNINA took care of the airframe, the thermal engines, and the aircraft at a high level. Bern University of Applied Sciences [293] dealt with the characterization of batteries and SOFC systems, the Department of Electrical Engineering of the Friedrich-Alexander University [294] with electric drives and power electronics, Proton Motor Fuel Cell GmbH [262] with the characterization of PEMFCs, and Mahytec [266] with hydrogen storage systems. Finally, Rotterdam the Hague Airport [295] provided useful data to characterize airport operations and the possible impact of hybridization on future infrastructure. The data collection work, coordinated by DTU, has relied on the stepwise approach developed by Saavedra-Rubio et al., making use of an LCI data collection template [296]. The template was detailed for each aspect of the aircraft's production or operational life. Each contributor was provided with a variant of the template that could be filled in appropriately, thus ensuring harmonization and transparency across the different datasets. The technology specialists conducted a series of iterations to gradually populate the tailored LCI template with primary data, while also carrying out data verification and checks (as depicted in Fig. 4.29). A life-cycle perspective was adopted within each LCI dataset, covering all key processes from raw materials extraction, manufacturing, and use, up to the end-of-life. Material compositions and masses vary for each time horizon and configuration.

In this context, UNINA was involved in the particularization of the thermal propulsion system, the operation of the aircraft, and the airframe production. In this sense, the mass breakdown (Tab. 4.15), the sizing powers (Tab. 4.14 and Figs. 4.22–4.28), and the direct emissions (Tab. 4.16 and Tab. 4.17) estimated by the author constituted a valid starting point for filling the LCI dataset concerning

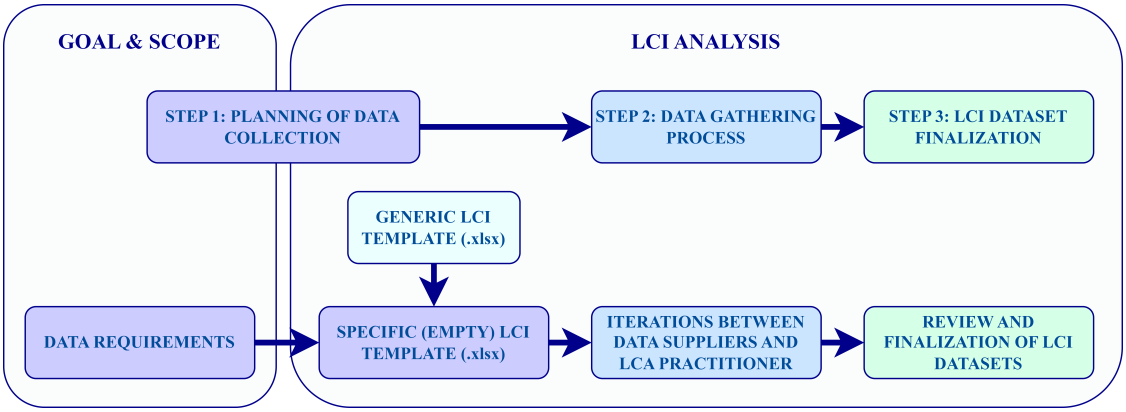

Figure 4.29: The LCI dataset-building methodology adopted (adapted from Refs. [210, 292, 296]).

airframe and conventional propulsion systems. Moreover, the definition of the scenarios has provided a solid basis for the detailed assessment of the specialized partners, responsible for describing the innovative technologies and components.

In addition to that, LCI data for materials and energy requirements were derived from literature sources. Some data provided by Lopes was used to detail the mass breakdown of the airframe [74], corrected to increase the material share of biodegradable or carbon-fiber reinforced plastics for the wing and fuselage parts of hybrid-electric configurations [74, 75, 137, 297]. For the air conditioning system, mass breakdowns provided by Yang et al. were used for the material composition based on steel, aluminum, copper, and plastics [298]. Electrical systems and instruments were assessed by using the dataset provided by Wernet et al. [299]. Fractions and materials used for pneumatic and hydraulic systems were characterized based on the assumptions of Annamalai et al. and Baroutian et al. [300, 301]. Data on the furnishing components and operational equipment was retrieved from Fabre et al. and Yang et al. [73, 298]. In the characterization of conventional powerplant materials and manufacturing, key assumptions included using GasTurb for gas turbine weight breakdown [247], selecting materials for engine components based on various sources [110, 248, 302, 303]. Assumptions on the material composition of engine nacelles and reduction gearboxes were based on Refs. [304, 305]. The use of innovative composite materials (like ASC-II [306]) for blades and forged aluminum for hubs was supposed, in order to derive information on the propellers' composition and manufacturing process. Buy-to-fly (BTF) ratios were determined for different parts, considering techniques like metal casting and precision die forging [307–311]. Energy consumption and emissions related to airframe manufacturing were estimated by multiplying the mass of the airframe components by the energy requirements and emissions per unit of component mass. The latter were estimated starting from the Airbus sustainability report [82], in the absence of other adequate public sources. A simplified approach was adopted to rescale the data provided by Airbus to the aircraft under analysis. The data on energy consumption (i.e., gas, steam, heat, electricity, and fuel) and emissions included in Ref. [82] were divided by the estimated

total mass of commercial aero parts produced by Airbus in the year 2021. This value was estimated by combining Airbus statements with the number of aircraft and helicopters delivered in 2021 according to Wikipedia [82, 312–314]. Finally, results were linearly extrapolated based on the data retrieved from sustainability reports of Airbus for the years 2019, 2020, and 2021, to obtain estimates for future time horizons. The final result is an estimate of the specific values (i.e., per kg of component produced) for energy consumption and emissions. The airframe was assumed to operate for 20 years, with an average of four 600 nmi design missions or six 200 nmi typical missions per day [162]. Information on the airframe's end-of-life, including dismantling and recycling of the structural components, was retrieved from the work of Lopes [74], which describes various waste treatment methods employed in different proportions depending on the specific material and component.

Although some notes were given here regarding the bibliographic research concerning UNINA's contribution, providing a detailed report of the generation of the LCI database goes beyond the scope of this dissertation. The interested reader may refer to the article by Thonemann et al. [210] for a detailed description of the prospective LCI datasets, their derivation, limitations, and potential applications. Moreover, the datasets are openly available in the Zenodo repository "Prospective Life Cycle Inventory Datasets for Conventional and Hybrid Electric Aircraft Technologies" [211]. Beyond forming the basis for the pLCA of the scenarios considered in this context, the performed generation of LCI database is believed to pave the way for several other relevant applications within the field of LCA, especially in light of the current shortage of aviation databases with the same level of detail [61, 290, 291]. One limitation is that the prospective LCI datasets are built on specific assumptions and forecasts, depending on the availability and thoroughness of trustworthy data, which could lead to uncertainty in the outcomes [210]. The LCI datasets can be incorporated into environmental databases like Ecoinvent, enabling practitioners to conduct more comprehensive LCAs of aviation systems [299]. In fact, the provided LCI datasets are believed to be adaptable for various aircraft models, at least in the regional class, and can inform prospective LCAs for alternative propulsion and fuel technologies in aviation, aiding sustainable technology decisions [210]. Additionally, these datasets can be modified for other heavy-duty transport systems like road and maritime, incorporating innovative elements like batteries and FCs [210].

4.6.3 Prospective Life Cycle Assessment

In LCA, the basis for analysis and comparison with different options is the *functional unit*, quantifying the performance requirements of the system [62]. The adopted functional unit in this analysis is the transportation of 50 passengers in a regional class aircraft over 200 nmi or 600 nmi, from and to a regional airport in Europe in the reference years 2030, 2040, and 2050. To facilitate comparison among all analyzed scenarios, the system boundaries included the same processes for each. In particular, the impact assessment included the life cycles of the airport, aircraft,

and fuels, spanning production, operation, and disposal. The LCI datasets discussed thus far served as the foreground data for the pLCAs to which this subsection is dedicated. The background processes, for which no primary data is available, were modeled using the *Premise* framework [291, 315], which allows for the creation of a prospective LCI database temporally specific for the three considered reference years. In particular, the database was built on the basis of a conservative model provided by the Premise framework, named SSP2-NDC [291, 315], in combination with the LCI unit process database Ecoinvent 3.8 with the cut-off system model [299, 315]. This additional prospective LCI database was primarily utilized for modeling the production of raw and intermediate materials, energy sources, transport processes, and waste treatment. In particular, biodiesel production via transesterification from palm oil from Latin America was selected as the best available process, although it does not seem to match the sustainability criteria mandated by the European Commission (i.e., -65% of the well-to-wake CO_2-eq./MJ in the case of biofuels, and -70% for e-fuels) [280, 281, 315]. For the medium and long term, e-fuels obtained by the Fischer-Tropsch process with hydrogen from wood gasification, and H_2 obtained from electrolysis, both passed the sustainability criteria [281, 315]. The carbon sequestration during the SAF production stage (by direct air capture and carbon intake in the biomass feedstock) was modeled separately from the CO_2 emitted during the SAF combustion [315].

The expression *environmental impact* generally means the potential impact on the environment, human health, or the depletion of natural resources, caused by the interventions between the ecosphere and the technosphere [316]. However, different impact categories exist that represent classes of environmental issues to which LCIA results may be assigned [316]. When approaching the environmental impact assessment of a system with respect to a specific impact category, various impact indicators are available for the practitioner to choose from. Choosing the impact categories of interest and their indicators is therefore preparatory to the LCA analysis, the latter consisting of the selection of process characterization models and associated characterization factors that convert LCI data into the single category indicators [63, 316]. In the analysis outlined in this subsection, the Environmental Footprint (EF) LCIA method was employed [317] as a reference collection of characterization models and impact categories. EF method focuses primarily on *midpoint-level* indicators [317], i.e., impact indicators positioned along the cause-effect chain but not at the damage level. Table 4.18 details the various impact categories utilized [316], facilitating the interpretation of the results that will be presented below. However, a particular focus will be placed on the GWI, representing the extent of climate change primarily due to the emission of GHGs like CO_2 or other gases with equivalent effects.

Table 4.18: Impact categories and indicators included in the EF3.0 LCIA methodology and considered for the present study [317].

Impact Category	Symbol	Impact Indicator	Unit
Global Warming Impact	GWI	Radiative forcing as Global Warming Potential (GWP100)	kg CO_2-eq.
Ozone Depletion	OD	Ozone depletion potential	kg CFC-11-eq.
Acidification	AC	Accumulated exceedance	mol H^+-eq.
Eutrophication (terrestrial)	EUTRO ter	Accumulated exceedance	mol N-eq.
Eutrophication (marine)	EUTRO marine	Fraction of nutrients reaching marine end compartment (N)	kg N-eq.
Eutrophication (freshwater)	EUTRO fresh	Fraction of nutrients reaching marine end compartment (P)	kg P-eq.
Photochemical Ozone Formation (human health)	POF	Tropospheric ozone concentration increase	kg NMVOC-eq.
Particulate Matter	PM	Disease incidence due to PM2.5 emitted	Incidence
Ionising Radiation (human health)	IR	Human exposure efficiency relative to U235	kBq U235-eq.
Ecotoxicity (freshwater)	ECOTOX fresh	Comparative Toxic Unit for ecosystems (CTUe)	CTUe
Human Toxicity (cancer)	HTc	Comparative Toxic Unit for human (CTUh)	CTUh
Human Toxicity (non-cancer)	HTnc	Comparative Toxic Unit for human (CTUh)	CTUh
Land Use	LU	Soil quality index	Point
Water Use	WU	User deprivation potential	m^3-world-eq.
Resource Use (fossils)	RE	Abiotic resource depletion of fossil fuels (ADP-fossil)	MJ
Resource Use (minerals and metals)	RM	Abiotic resource depletion (ADP ultimate reserve)	kg Sb-eq.

Short-Term Horizon

The total GWI associated to the different short-term aircraft configurations is given in Tab. 4.19. Moreover, Fig. 4.30 provides a more detailed breakdown showing the main contributions to the total GWI per unit mission. When considering the design mission, the GWI of both the conventional and the hybrid configurations were found to be very close to each other, regardless of the fuel type. In fact, the percentage difference is estimated to be below 1%, a value that is judged insignificant in light of the existing uncertainties. The reason for this lies in the high energy consumption of the ICE+bat configurations, in turn related to the increased mass of the aircraft, which almost completely nullifies the advantages of partial electrification. The advantage of the ICE+bat configuration in terms of direct emissions becomes more significant in the case of the typical mission, reaching a difference of 22.2% compared to conventional when kerosene is used as fuel. However, direct CO_2 emissions constitute only between 74% and 84% of total GWI, with important additional contributions coming from airport use and kerosene production (Fig. 4.30). This reduces the expected benefit for the ICE+bat scenario using kerosene to 16.4%. Other contributors to the total GWI include electricity production and aircraft production. It is notable that these contributions

Table 4.19: Results of the LCA analysis in the short-term, focusing on the GWI of the different scenarios analyzed (adapted from Ref. [315]). The table also reports the percentage differences referred to the kerosene-based conventional scenario.

Parameter	Unit	Conv. (Kerosene)	Conv. (SAF)	ICE+bat (Kerosene)	ICE+bat (SAF)
			600 nmi Design Mission		
Direct CO_2	kg CO_2	3 455.2 (+0.0 %)	3 341.6 (−3.3 %)	3 369.2 (−2.5 %)	3 258.0 (−5.7 %)
GWI (LCA)	kg CO_2-eq.	4 141.5 (+0.0 %)	1 904.4 (−54.0 %)	4 128.1 (−0.3 %)	1 947.0 (−53.0 %)
			200 nmi Typical Mission		
Direct CO_2	kg CO_2	1 489.8 (+0.0 %)	1 440.7 (−3.3 %)	1 159.1 (−22.2 %)	1 120.9 (−24.8 %)
GWI (LCA)	kg CO_2-eq.	1 879.2 (+0.0 %)	914.0 (−51.4 %)	1 570.7 (−16.4 %)	819.5 (−56.4 %)

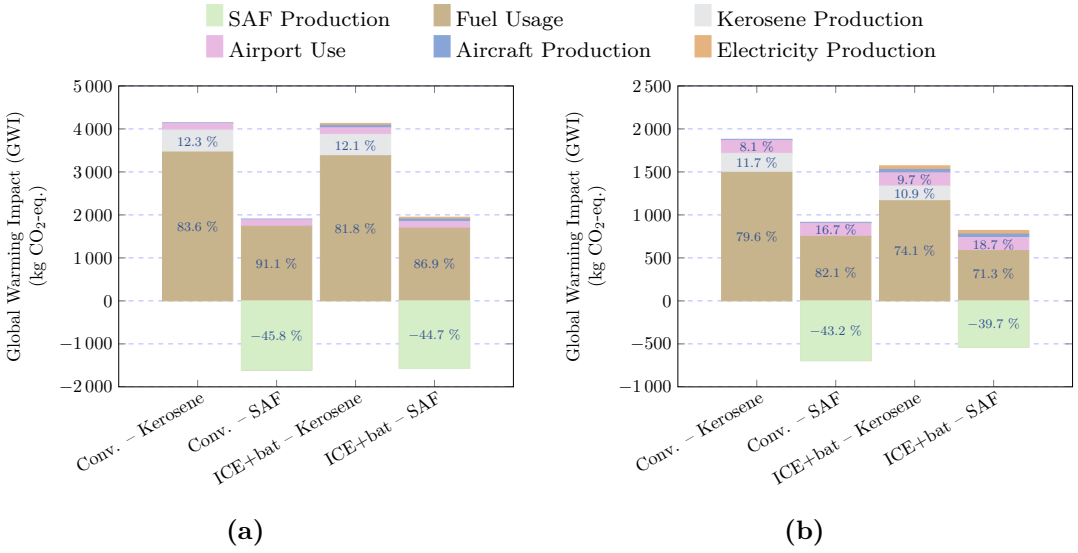

Figure 4.30: GWI contribution analysis of the different scenarios assessed in the short-term time horizon. (adapted from Ref. [315]). (**a**) 600 nmi design mission. (**b**) 200 nmi typical mission.

represent a small part of the total impact, never exceeding 5.0% even for the typical mission. As visible in Fig. 4.30, the fuel combustion is the dominant contributor to the overall GWI, regardless of the configuration and the fuel type. As a consequence, the relative increase in direct CO_2 emissions when transitioning from typical to design mission is lower in the case of the conventional configuration, because part of the required energy in the ICE+bat scenarios is supplied by electricity. Scenarios that utilize SAF show a lower environmental impact compared to those relying on kerosene, largely due to the diminished environmental effects during the production of SAF. This is attributed to the carbon sequestration benefits during biomass

cultivation for SAF production. However, it is crucial to acknowledge that the net GWI coming from producing and combusting SAF is still a positive value (represented by the brown section in Fig. 4.30), meaning that the use of SAF, while more sustainable, continues to contribute to climate change.

Finally, Tab. 4.20 gives some insight into the other impact categories considered in the study (and already described in Tab. 4.18). Being interested in a comparative analysis of innovative solutions compared to conventional configurations, the emphasis is placed on the differences compared to the reference conventional configuration using kerosene.

Table 4.20: Normalized environmental impacts per unit of flight of the short-term scenarios (adapted from Ref. [315]). The color scale reflects the differences with the reference conventional aircraft using kerosene, with the best option marked in light gray and the worst in dark gray.

(a) 600 nmi Design Mission.

Impact Category	Conv. (Kerosene)	Conv. (SAF)	ICE+bat (Kerosene)	ICE+bat (SAF)
GWI	+0.0 %	-54.0 %	-0.3 %	-53.0 %
OD	+0.0 %	-87.9 %	-1.7 %	-87.4 %
AC	+0.0 %	+58.7 %	+4.3 %	+61.4 %
EUTRO Ter	+0.0 %	+94.8 %	+5.7 %	+98.1 %
EUTRO Marine	+0.0 %	+480.0 %	+5.9 %	+473.7 %
EUTRO Fresh	+0.0 %	+1565.8 %	+33.2 %	+1559.8 %
POF	+0.0 %	+11.1 %	+5.0 %	+15.8 %
PM	+0.0 %	+144.3 %	+7.8 %	+148.5 %
IR	+0.0 %	-72.8 %	+17.7 %	-53.2 %
ECOTOX Fresh	+0.0 %	+238.8 %	+7.3 %	+240.1 %
HTc	+0.0 %	+9.0 %	+24.6 %	+33.4 %
HTnc	+0.0 %	+12.0 %	+14.5 %	+26.3 %
LU	+0.0 %	+901.3 %	+13.4 %	+892.2 %
WU	+0.0 %	+13.2 %	-2.3 %	+10.5 %
RE	+0.0 %	-72.2 %	+3.9 %	-66.5 %
RM	+0.0 %	+40.7 %	+13.2 %	+52.9 %

(b) 200 nmi Typical Mission.

Impact Category	Conv. (Kerosene)	Conv. (SAF)	ICE+bat (Kerosene)	ICE+bat (SAF)
GWI	+0.0 %	-51.4 %	-16.4 %	-56.4 %
OD	+0.0 %	-86.6 %	-20.2 %	-87.6 %
AC	+0.0 %	+53.9 %	-22.6 %	+19.5 %
EUTRO Ter	+0.0 %	+98.2 %	-36.4 %	+40.4 %
EUTRO Marine	+0.0 %	+499.0 %	-36.5 %	+352.0 %
EUTRO Fresh	+0.0 %	+795.8 %	+27.9 %	+647.0 %
POF	+0.0 %	+11.1 %	-33.2 %	-24.4 %
PM	+0.0 %	+115.9 %	-5.8 %	+84.5 %
IR	+0.0 %	-68.3 %	+23.3 %	-29.9 %
ECOTOX Fresh	+0.0 %	+159.4 %	+3.0 %	+127.1 %
HTc	+0.0 %	+4.7 %	+23.6 %	+27.3 %
HTnc	+0.0 %	+4.3 %	+11.6 %	+14.5 %
LU	+0.0 %	+593.7 %	+13.2 %	+475.1 %
WU	+0.0 %	+13.1 %	-21.8 %	-11.6 %
RE	+0.0 %	-69.0 %	-7.0 %	-60.8 %
RM	+0.0 %	+17.9 %	+11.9 %	+25.9 %

Table 4.20 also confirms that the differences for the same fuel are negligible on the design mission but become considerable on shorter missions. However, although there are evident advantages of the ICE+bat configuration compared to the conventional one, in GWI and in most of the other categories, some environmental trade-offs emerge. For instance, for the typical mission and when using kerosene, the conventional configuration performs even better than the ICE+bat configuration in several impact categories, including EUTRO Fresh, IR, and human toxicity. As for the use of SAF, although it contributes to reducing the GWI with respect to the kerosene-based conventional reference, it also leads to huge increases in several other categories. In particular, LU and eutrophication increase tremendously when using SAF due to palm fruit cultivation. Particularly concerning eutrophication, it may lead to an increased biomass production of planktonic algae, which degrades water quality and diminishes biodiversity [316]. However, the extent of these impacts is contingent upon several factors, including the scale at which the innovative technologies are implemented and the specific geographic areas they are applied to.

In conclusion, the adoption of ICE+bat configurations using SAF can be a valid temporary solution to reduce climate change in the short term. However, unless new methods of sustainable SAF production become established on a large scale, the non-CO_2-related impacts may soon become unsustainable, especially as demand grows.

Medium-Term Horizon

The GWI for the different medium-term scenarios is given in Tab. 4.21, and a more detailed breakdown is provided in Fig. 4.31. In addition, Tab. 4.22 provides a comparison between scenarios in terms of non-CO_2 related impact categories. Once again, fuel combustion is the largest contributor to GWI for the conventional and ICE+bat configurations. As already noted in Section 4.5, the hydrogen-based PEMFC+bat configuration does not emit GHG contributing to GWI during the flight; hence, the combustion contribution is null. However, non-negligible contributions to the total GWI come from hydrogen production and airport use, reducing the potential benefit from the theoretical value of -100.0% to a more realistic -84.3% / -81.8% with respect to the conventional reference. Interestingly, the aircraft production starts representing a non-negligible part of GWI (in terms of percentage) for the PEMFC+bat configuration, assessing between 9% and 17%.

As for the other impact categories, considerations similar to the ones proposed for the short term apply to the medium-term conventional and ICE+bat configurations, although the latter perform overall better in light of the technology improvements. The ICE+bat configuration using kerosene seems to offer an intermediary performance level for both missions but only a slight advantage compared to its conventional counterpart. As for the PEMFC+bat configuration, it shows lower GWI, AC, marine and terrestrial eutrophication, and POF than any other configurations for both missions, while it is associated with the worst impacts for HTc, HTnc, and RM. The impact in the HTc impact category can be explained by chromium emissions in ferrochromium production needed for

Table 4.21: Results of the LCA analysis in the medium-term, focusing on the GWI of the different scenarios analyzed (adapted from Ref. [315]). The table also reports the percentage differences referred to the kerosene-based conventional scenario.

Parameter	Unit	Conv. (Kerosene)	Conv. (SAF)	ICE+bat (Kerosene)	ICE+bat (SAF)	PEMFC+bat (H_2)
				600 nmi Design Mission		
Direct CO_2	kg CO_2	3 161.3 (+0.0 %)	3 057.1 (−3.3 %)	2 340.2 (−26.0 %)	2 263.0 (−28.4 %)	0.0 (−100.0 %)
GWI (LCA)	kg CO_2-eq.	3 766.8 (+0.0 %)	1 584.5 (−57.9 %)	2 902.2 (−23.0 %)	1 286.8 (−65.8 %)	592.8 (−84.3 %)
				200 nmi Typical Mission		
Direct CO_2	kg CO_2	1 358.9 (+0.0 %)	1 314.1 (−3.3 %)	760.1 (−44.1 %)	735.0 (−45.9 %)	0.0 (−100.0 %)
GWI (LCA)	kg CO_2-eq.	1 707.2 (+0.0 %)	768.5 (−55.0 %)	1 076.3 (−37.0 %)	551.0 (−67.7 %)	311.0 (−81.8 %)

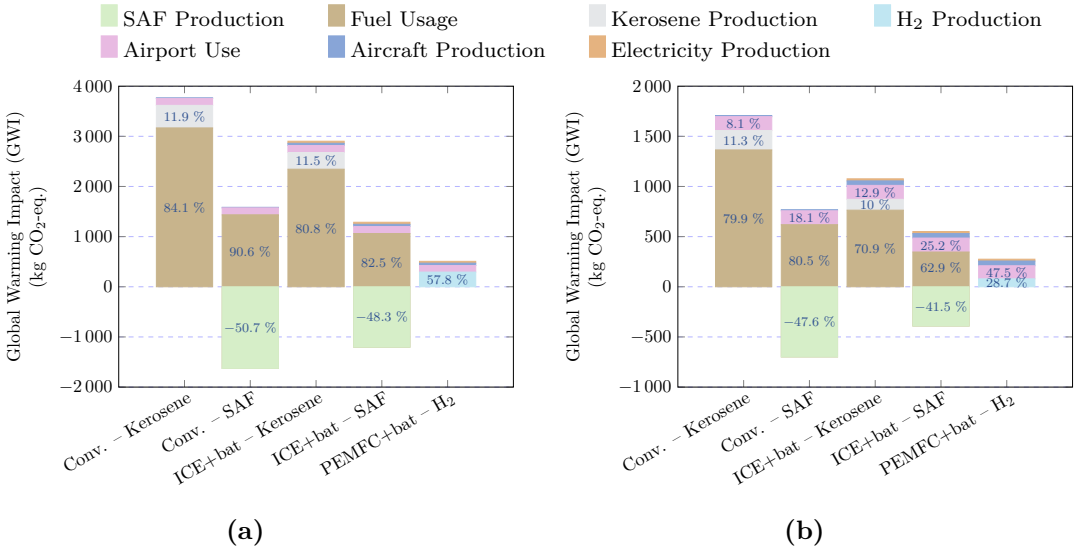

Figure 4.31: GWI contribution analysis of the different scenarios assessed in the medium-term time horizon. (adapted from Ref. [315]). (**a**) 600 nmi design mission. (**b**) 200 nmi typical mission.

the housing of the electrolyzer [315], and the ones in HTnc and RM by the production of copper necessary for electricity production via photovoltaics and wind power [315]. Overall, the PEMFC+bat scenario demonstrates superior environmental performance compared to other alternatives across most impact categories. However, it is important to address the impacts on human toxicity, mineral resource utilization, water usage, and freshwater eutrophication, e.g., by focusing on using less chromium and copper, and optimizing water and energy use in hydrogen production. This is crucial to prevent the transference of environmental burdens from climate change to these categories.

Table 4.22: Normalized environmental impacts per unit of flight of the medium-term scenarios (adapted from Ref. [315]). The color scale reflects the differences with the reference conventional aircraft using kerosene, with the best option marked in light gray and the worst in dark gray.

(a) 600 nmi Design Mission.

Impact Category	Conv. (Kerosene)	Conv. (SAF)	ICE+bat (Kerosene)	ICE+bat (SAF)	PEMFC+bat (H_2)
GWI	+0.0 %	-57.9 %	-23.0 %	-65.8 %	-84.3 %
OD	+0.0 %	-88.8 %	-24.8 %	-90.5 %	-93.4 %
AC	+0.0 %	+50.5 %	-11.9 %	+25.4 %	-57.9 %
EUTRO Ter	+0.0 %	+83.4 %	-13.7 %	+47.8 %	-82.5 %
EUTRO Marine	+0.0 %	+424.2 %	-13.8 %	+300.0 %	-83.1 %
EUTRO Fresh	+0.0 %	+1497.7 %	+34.6 %	+1143.3 %	+1066.4 %
POF	+0.0 %	+8.9 %	-14.6 %	-8.2 %	-81.9 %
PM	+0.0 %	+130.6 %	-4.3 %	+92.3 %	-7.7 %
IR	+0.0 %	-67.3 %	+0.2 %	-49.6 %	-4.2 %
ECOTOX Fresh	+0.0 %	+215.0 %	-0.7 %	+158.5 %	+59.8 %
HTc	+0.0 %	+25.9 %	+34.4 %	+53.6 %	+883.6 %
HTnc	+0.0 %	+16.4 %	+13.3 %	+25.5 %	+128.9 %
LU	+0.0 %	+918.0 %	+16.2 %	+695.7 %	+173.4 %
WU	+0.0 %	+1402.0 %	+59.7 %	+1097.6 %	+457.4 %
RE	+0.0 %	-72.8 %	-17.7 %	-71.6 %	-67.8 %
RM	+0.0 %	+44.5 %	+26.2 %	+59.1 %	+216.2 %

(b) 200 nmi Typical Mission.

Impact Category	Conv. (Kerosene)	Conv. (SAF)	ICE+bat (Kerosene)	ICE+bat (SAF)	PEMFC+bat (H_2)
GWI	+0.0 %	-55.0 %	-37.0 %	-67.7 %	-81.8 %
OD	+0.0 %	-87.7 %	-41.5 %	-90.6 %	-93.3 %
AC	+0.0 %	+46.3 %	-32.9 %	-6.9 %	-51.8 %
EUTRO Ter	+0.0 %	+86.6 %	-52.5 %	-3.8 %	-80.4 %
EUTRO Marine	+0.0 %	+442.3 %	-52.7 %	+194.9 %	-81.4 %
EUTRO Fresh	+0.0 %	+729.3 %	+28.2 %	+436.2 %	+341.6 %
POF	+0.0 %	+8.9 %	-49.7 %	-44.6 %	-79.7 %
PM	+0.0 %	+103.5 %	-13.2 %	+44.7 %	-13.5 %
IR	+0.0 %	-63.8 %	-11.2 %	-46.8 %	-30.4 %
ECOTOX Fresh	+0.0 %	+140.0 %	-3.4 %	+74.9 %	+23.9 %
HTc	+0.0 %	+13.4 %	+23.4 %	+30.9 %	+300.1 %
HTnc	+0.0 %	+6.5 %	+7.7 %	+11.0 %	+37.1 %
LU	+0.0 %	+593.3 %	+8.5 %	+340.3 %	+69.6 %
WU	+0.0 %	+1003.9 %	+49.4 %	+611.0 %	+208.0 %
RE	+0.0 %	-69.8 %	-31.8 %	-70.8 %	-72.8 %
RM	+0.0 %	+19.5 %	+16.7 %	+27.6 %	+72.0 %

Long-Term Horizon

Table 4.23, Fig. 4.32 and Tab. 4.24 provide the overview of the environmental performance of all long-term scenarios. The GWI of the conventional configuration remains dominated by the contributions of fuel combustion and production. When SAF is used, the overall impact is reduced by more than 50% thanks to the direct air capture and the carbon intake in the biomass feedstock. The GWI of the hydrogen-based configurations is up to 9 times lower than the reference.

Table 4.23: Results of the LCA analysis in the long-term, focusing on the GWI of the different scenarios analyzed (adapted from Ref. [315]). The table also reports the percentage differences referred to the kerosene-based conventional scenario.

Parameter	Unit	Conv. (Kerosene)	Conv. (SAF)	PEMFC+bat (H_2)	SOFC+bat (H_2)
			600 nmi Design Mission		
Direct CO_2	kg CO_2	3 090.1 (+0.0 %)	2 988.2 (−3.3 %)	0.0 (−100.0 %)	0.0 (−100.0 %)
GWI (LCA)	kg CO_2-eq.	3 667.0 (+0.0 %)	1 253.6 (−65.8 %)	468.1 (−87.2 %)	407.9 (−88.9 %)
			200 nmi Typical Mission		
Direct CO_2	kg CO_2	1 325.8 (+0.0 %)	1 282.1 (−3.3 %)	0.0 (−100.0 %)	0.0 (−100.0 %)
GWI (LCA)	kg CO_2-eq.	1 658.4 (+0.0 %)	622.3 (−62.5 %)	261.7 (−84.2 %)	242.9 (−85.4 %)

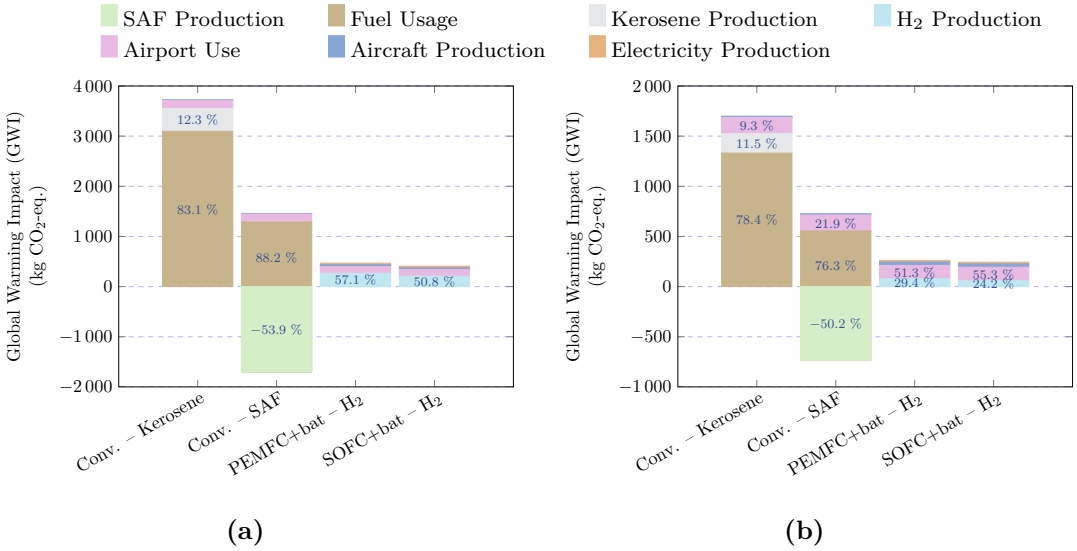

Figure 4.32: GWI contribution analysis of the different scenarios assessed in the long-term time horizon. (adapted from Ref. [315]). (**a**) 600 nmi design mission. (**b**) 200 nmi typical mission.

Moreover, no significant difference in the GWI of the PEMFC+bat and SOFC+bat configurations is found as the range varies, due to the absence of contributions from direct GHG emissions. Again, the highest contributors to both the PEMFC and SOFC configurations are airport use and hydrogen supply. The impact of aircraft production of massive hydrogen-based configurations is mitigated by the use of biodegradable materials, although its contribution is still limited (from less than 1% for conventional aircraft to 13% for hydrogen-based configurations). The better GWI performance of the configurations based on FCs becomes more nuanced when observed along with results in other impact categories. As a matter of fact, these configurations present the worst performance in terms of human toxicity and RM.

Table 4.24: Normalized environmental impacts per unit of flight of the long-term scenarios (adapted from Ref. [315]). The color scale reflects the differences with the reference conventional aircraft using kerosene, with the best option marked in light gray and the worst in dark gray.

(a) 600 nmi Design Mission.

Impact Category	Conv. (Kerosene)	Conv. (SAF)	PEMFC+bat (H_2)	SOFC+bat (H_2)
GWI	+0.0 %	-65.8 %	-87.2 %	-88.9 %
OD	+0.0 %	-88.3 %	-91.3 %	-92.9 %
AC	+0.0 %	+37.2 %	-62.1 %	-67.4 %
EUTRO Ter	+0.0 %	+66.9 %	-83.5 %	-86.0 %
EUTRO Marine	+0.0 %	+334.4 %	-84.1 %	-86.5 %
EUTRO Fresh	+0.0 %	+1105.9 %	+877.0 %	+681.5 %
POF	+0.0 %	+7.4 %	-83.1 %	-85.7 %
PM	+0.0 %	+109.2 %	-16.1 %	-28.0 %
IR	+0.0 %	-14.6 %	-12.3 %	-28.7 %
ECOTOX Fresh	+0.0 %	+175.1 %	+47.0 %	+25.3 %
HTc	+0.0 %	+70.5 %	+805.8 %	+629.0 %
HTnc	+0.0 %	+29.9 %	+118.6 %	+90.3 %
LU	+0.0 %	+1075.7 %	+161.0 %	+118.8 %
WU	+0.0 %	+1181.5 %	+405.6 %	+312.8 %
RE	+0.0 %	-59.6 %	-70.2 %	-75.3 %
RM	+0.0 %	+55.2 %	+200.5 %	+161.9 %

(b) 200 nmi Typical Mission.

Impact Category	Conv. (Kerosene)	Conv. (SAF)	PEMFC+bat (H_2)	SOFC+bat (H_2)
GWI	+0.0 %	-62.5 %	-84.2 %	-85.4 %
OD	+0.0 %	-87.0 %	-87.7 %	-89.7 %
AC	+0.0 %	+33.9 %	-57.0 %	-60.9 %
EUTRO Ter	+0.0 %	+69.2 %	-80.9 %	-82.9 %
EUTRO Marine	+0.0 %	+347.0 %	-81.7 %	-83.6 %
EUTRO Fresh	+0.0 %	+544.3 %	+299.8 %	+231.2 %
POF	+0.0 %	+7.4 %	-80.5 %	-82.5 %
PM	+0.0 %	+85.7 %	-21.1 %	-28.1 %
IR	+0.0 %	-13.6 %	-34.4 %	-45.2 %
ECOTOX Fresh	+0.0 %	+112.7 %	+16.6 %	+5.2 %
HTc	+0.0 %	+36.2 %	+289.9 %	+225.8 %
HTnc	+0.0 %	+13.0 %	+37.9 %	+28.0 %
LU	+0.0 %	+689.5 %	+68.8 %	+49.5 %
WU	+0.0 %	+829.1 %	+201.4 %	+154.3 %
RE	+0.0 %	-56.7 %	-73.8 %	-77.3 %
RM	+0.0 %	+24.0 %	+71.0 %	+58.7 %

In conclusion, the FC configurations seem to have the best environmental performance in most of the categories, with the SOFC+bat configuration showing slightly better performance. Nevertheless, the high impacts of FCs in some critical categories, like HTc and HTnc, should be addressed to avoid transferring the burden from climate change to these areas.

4.6.4 Discussion of Results

This section has illustrated the work of LCI and pLCA conducted for the purpose of studying promising future technologies for future regional aviation. The analysis was conducted in collaboration with experts across different fields of aviation research, leading to an extensive and detailed inventory of the configurations studied. The published inventory addresses the lack of publicly available environmental databases for aeronautical applications and is adaptable for future regional transportation applications. However, the data was manually mapped to prospective LCI datasets by LCA practitioners, a process that introduces potential errors. Additionally, a further limitation is intrinsic to the prospective nature of information on emerging technologies.

The key findings of the LCA highlighted the promising effect of hybridization on the environmental performance of future regional aircraft. The results show that hybrid-electric configurations based on ICE and batteries, and even more the utilization of hydrogen FCs, prove highly advantageous for decarbonization. As time progresses, the GWI of the various configurations decreases, especially thanks to efficiency improvements. The impact of aircraft production acquires relative importance only for hydrogen-based scenarios, for which the predominant effect of fuel combustion becomes absent. However, some trade-offs emerge in non-CO_2-related environmental impact categories, preventing a definitive recommendation for any single configuration. Assuming that these trade-offs will be addressed by research and industrial efforts, FC options will dominate in the long term in light of their extreme advantages in most of the impact categories. On the other hand, the use of SAF in combination with conventional or hybrid architectures is recommendable as a short-term, temporary solution.

4.7 Cost Analysis

4.7.1 Introduction

Decisions made in the conceptual and preliminary design stages significantly impact both the initial costs and subsequent operational expenses of an aircraft. Gudmundsson [40] underscores the importance of persuading potential customers to choose one's aircraft over competitors. To achieve this, manufacturers often maintain dedicated sales departments, offering transparent ownership cost comparisons. This focus on DOC, evident in marketing materials like ATR's brochure for the ATR42 aircraft [174], highlights operating costs' crucial role in airline and operator decision-making. This underscores the continual need for aircraft manufacturers to enhance design and operational efficiency for sustained competitiveness in the aviation industry. In this context of intense economic competition, finding space for innovative solutions not primarily focused on reducing operating costs is challenging. While the imperative to address environmental concerns and enhance fuel efficiency has triggered a shift toward innovative propulsion technologies,

assessing their economic feasibility and operational viability is crucial as well. Macro-economic scenarios, especially uncertainties in energy source prices and possible incentives, may significantly impact the success of hybrid or electric concepts [318–323]. Concurrently, the European ETS is expected to play a pivotal role in achieving ACARE's objectives, regulating limits on GHG emissions in aviation. By encouraging emissions reduction through a market-driven approach, ETS translates into a surcharge on carbon emissions [6, 7, 20]. In parallel, incentive policies, such as low-carbon electricity and carbon taxes, are essential for the success of cost-effective all-electric narrow-body aircraft, particularly if jet fuel prices will remain below 100 USD per barrel [324]. Similar considerations apply to taxation policies for conventional and hybrid/electric aircraft, where some European airports individually adopt charging systems tied to emissions but remain far from a standardized approach [172].

Guided by the previous considerations, this section aims to evaluate the economic feasibility of the analyzed concepts by exploring various economic scenarios, with also a focus on uncertainties in economic assumptions, particularly regarding energy sources. This aircraft-based study intends to complement the sustainability considerations of innovative solutions for regional aviation. In light of the diversity of the effects considered in the assessment, its prospective nature, and the variety of concepts analyzed, the study aims to provide a reference point for assessing economic feasibility in this field, in the absence of equally detailed literature studies. Subsection 4.7.2 will outline the key assumptions covering capital costs and operating expenses. Subsection 4.7.3 will provide the author's estimates for short-term, medium-term, and long-term scenarios, utilizing the analysis tool presented in Section 2.5, and already validated on an aircraft similar to the reference baseline (see Subsection 2.5.6). Later, the impact of uncertainties in economic assumptions will be scrutinized, and a specific application concerning the estimation of air ticket prices for a 200 nmi mission will be carried out. Subsection 4.7.4 will concisely summarize the section's key findings.

4.7.2 Economic Assumption

Distinct economic scenarios were developed for the three time horizons. When focusing on conventional or hybrid-electric configurations with ICEs, scenarios vary based on using pure kerosene or a 100% SAF blend, with SAF composition and expected costs linked to the time horizon (see Tab. 4.9 again). All values will be reported in US dollars, maintaining a fixed reference level for inflation related to the year 2020. The adopted reference metric is the DOC per flight unit.

For the purposes of cost estimation, several economic assumptions were necessary. The analysis considered specifically DOC rather than TOC, focusing solely on costs directly associated with aircraft operation. In addition, ground handling charges were not considered. However, they are usually proportional to the number of passengers, ensuring that neglecting their contribution should have a consistent impact across configurations, thus preserving their comparability. The number

Table 4.25: Main economic assumptions for the analysis of future aircraft scenarios (adapted from Ref. [97]).

Parameter	Value	Unit
Depreciation time	20 years	–
Financing	85% of investment over 10 years	–
Insurance	1% of aircraft price per year	–
Interests on loans	5% of initial investment per year	–
Profit on sale	10% of aircraft price	–
Spares (airframe & systems)	10% airframe price	–
Pilot annual salary	74 730	2020USD/year
Crew annual salary	47 730	2020USD/year
Engineering labor rate	43.56	2020USD/h
Manufacture labor rate	24.80	2020USD/h
Maintenance labor rate	31.30	2020USD/h
Maintenance frequency	every 500 flights	–

of flights per year was set at 4 per day for the 600 nmi mission and 6 per day for a typical 200 nmi mission, based on a statistical relationship provided by the AEA for short-medium range aircraft [162]. The assumption on the number of flights remained constant across configurations to maintain homogeneity in the interpretation of the results. Capital cost estimation necessitated defining some general economic assumptions, which are detailed in Tab. 4.25. These assumptions included the residual value of aircraft and spares, financing costs, interest rates, insurance premiums, and a 10% profit margin for new aircraft sales. Additional information, drawn from Roskam's suggestions for preliminary evaluations across different aircraft categories [34], served as calibration parameters, ensuring alignment with the case study in Subsection 2.5.6. Finally, a uniform 20-year lifetime was assumed for all analyzed aircraft, with no residual value for airframes and systems.

Pilot and cabin crew salaries were derived from publicly available statistics [325–327]. Captain and first officer salaries were determined by averaging the salaries of 12-year experienced pilots from various regional airlines, updated to 2022 [325]. For the analyzed configurations, the salary of one flight attendant was considered based on information reported by Ref. [326]. Other relevant labor rates were obtained from Ref. [327], where the US Bureau of Labor Statistics provided wage estimates for aerospace occupations. Specifically, engineering, manufacturing, and maintenance labor rates were assumed as the median hourly wages for "industrial engineers", "production occupations", and "installation, maintenance, and repair occupations", respectively [327]. These values, adjusted for inflation, were considered constant for all time horizons. For this application, it was assumed that one maintenance check in the hangar occurs every 500 flight hours [328].

The capital cost related to ICEs was assessed by using the approach discussed in Chapter 2. A residual value of 20% and spares cost equal to 30% of the nominal price were assumed [35].

Information on the price of innovative technology components for future time horizons was sourced from the LCI database [210], therefore relying on the opinion of experts in each technology sector. Main assumptions related to electric storage systems are detailed in Tab. 4.26. An expected battery lifespan between 2 and 3 years was considered [210, 329]. While this assumption might appear optimistic compared to current battery technologies, it was deemed plausible given the swift advancements in developing durable lithium batteries for electric vehicle applications [330].

Battery unit prices were derived from current values and trends based on expert assumptions [210, 257, 331]. The cost of replacing the component, treated as maintenance cost, was evaluated considering the estimated market price, including the effect of depreciation over time. The residual value at the end of life was assessed considering a yearly depreciation rate of 40% [329]. Installation costs were assumed to be equal to 10% of the battery price based on expert assumptions [210].

The FC unit cost was derived from data provided by Ref. [332], as detailed in Tab.4.27. Although the source primarily addresses FCs for heavy-duty vehicles, it was assumed that similar stacks and systems are also applicable to aircraft. The estimation of maintenance cost involved planning for a complete stack replacement once in the product's lifespan, along with a provision for routine maintenance intervals covering the replacement of minor components (e.g., filters, cooling liquid, sensors, hoses, etc.) [210, 264]. The cost of FCs was complemented with the cost of hydrogen storage, estimated based on the breakdowns reported by Alves et al. [333]. Additionally, an assumed unit price of approximately 60.0 USD/kW was applied for electric machines, while power electronics were assigned a unit price in the range of 250–280 USD/kW for all time horizons, with slight variations based on the specific component [210, 271].

Several predictive studies were consulted to gather data on the pricing of energy sources. Estimates for kerosene, electricity, SAF, and H_2 costs were derived from the literature, with average, low, and high estimates identified for each fuel and time horizon. The kerosene price was determined using the global oil price forecast from the International Energy Outlook 2021, adjusted by the estimated difference between the global oil price and Jet-A price during the years 2016 to 2019 [165, 334]. The period from 2019 to 2023 was excluded due to the impact of the COVID-19 pandemic and the war in Ukraine. Moreover, these events were assumed to have only residual effects on prices between 2030 and 2050. Electricity price ranges

Table 4.26: Main economic assumptions for electric storage systems (adapted from Ref. [97]).

Parameter	**Unit**	**Short-Term (EIS 2030)**	**Medium-Term (EIS 2040)**	**Long-Term (EIS 2050)**
Technology	–	$Li-Ion$	$Li-S$	$Li-O_2$
Unit Price	2020USD/kWh	100.0	79.0	61.0
Lifespan	years	3.0	2.0	2.0
Residual Value	%	21.6	28.4	22.0

Table 4.27: Unit prices assumed for FC systems [210, 332] (adapted from Ref. [97]).

Parameter	Unit	Medium-Term (EIS 2040)	Long-Term (EIS 2050)	
Technology	–	*PEMFC*	*PEMFC*	*SOFC*
Unit Price	2020USD/kW	356.4	151.2	830.0

were sourced from simulations presented by Capros et al. [318], which assumed a reduction of 80% to 100% in the EU's GHG emissions by 2050, using the PRIMES energy-economics model [318]. The low electricity price scenario involved a mix of technologies and incentives (electrification, hydrogen, carbon-neutral e-fuels, energy efficiency measures, circular economy, and biofuels) in 2040, with the emergence of carbon-neutral e-fuels in 2050. The high electricity price scenario focused on energy efficiency in 2040 and a mix of technologies in 2050.

The SAF price was assumed to be equivalent to the production cost due to the absence of robust market price forecasts. The cost of HEFA-SPK and Fischer-Tropsch e-fuels was retrieved, with the average cost of HEFA-SPK for 2030 obtained from Bullerdiek et al. [319]. Low and high values were assigned based on different feedstock options. Costs for 2040 and 2050 were extrapolated, assuming a 15% reduction in production costs per decade [320], reflecting the expected impact of increasing TRL and supportive public policies. The average e-fuel prices for 2030 and 2050 were derived from Gonzalez-Garay et al. [321], assuming that the production costs of Fischer-Tropsch e-fuel in Spain were representative of European costs. Additionally, the cost in 2040 was linearly interpolated between 2030 and 2050. The SAF price used in the cost analysis considers the blend of HEFA-SPK and e-fuels based on the expected market mix for each time horizon as reported in Tab. 4.9 [280, 281].

In the absence of price forecasts, the production and distribution costs of hydrogen were considered reliable proxies for market prices. The average, low, and high hydrogen prices in 2050 were obtained from simulations by Blanco et al. using the JRC-EU-TIMES model [322]. The lower value corresponds to a scenario with an 80% reduction in GHG emissions, while the higher value represents a scenario with a 95% reduction in GHG emissions incorporating carbon capture and storage in the EU [322]. Projections for 2030 and 2040 factor in an approximate 10% reduction per decade [323].

To facilitate comparison, all prices were converted to 2020USD using an average inflation rate of 2% (except for kerosene, where no specific inflation rate was provided in the references). The exchange rate used for calculations was the average euro to USD rate of 1.142 in 2020 [335]. Figure 4.33 summarizes the assumptions regarding the unit prices of energy sources for the three considered time horizons. It is important to note that the visualized values relating to fuels do not reflect the price per unit of mass, as they rather refer to the unit of energy theoretically extractable from them.

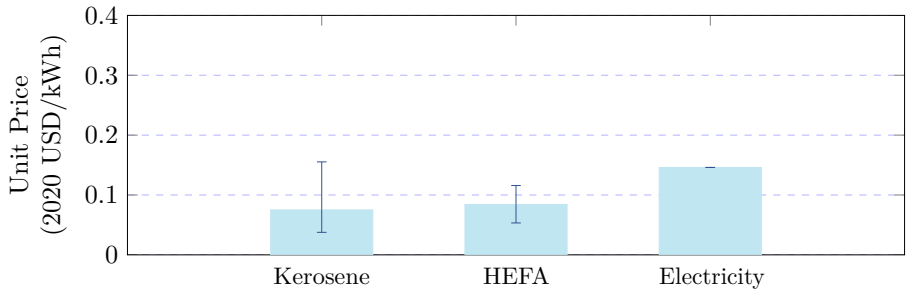

(a) Short-Term (2030)

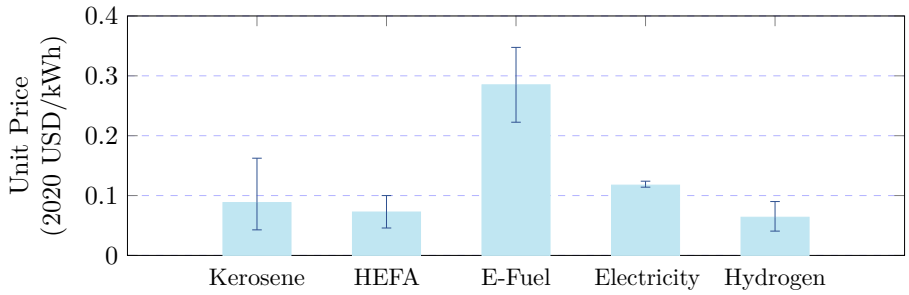

(b) Medium-Term (2040)

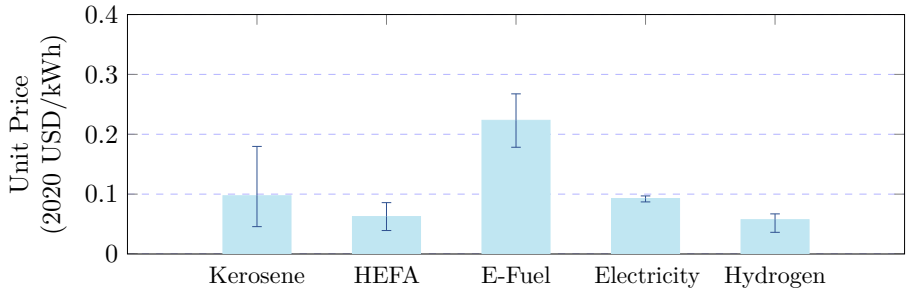

(c) Long-Term (2050)

Figure 4.33: Range of unit prices for each energy source and time horizon: kerosene [165, 334], HEFA-SPK [319, 320], e-fuel [321], hydrogen [322], electricity [318]. A reference value for the specific energy of 33.3 kWh/kg is considered for hydrogen, while 12 kWh/kg is considered for kerosene and SAF (adapted from Ref. [97]).

Regarding carbon permits, as of 1st May 2023, the carbon price stood at 90 USD per metric ton of CO_2-eq. emitted [7]. Anticipated increases aim to favor the achievement of a 55% reduction in GHG emissions by 2030 [6, 20]. Future values were estimated based on BloombergNEF forecasts, reflecting the hybrid market scenario considered by the source [336]. This has resulted in projected prices of 200 USD/ton CO_2-eq. for 2030, 150 USD/ton CO_2-eq. for 2040, and 100 USD/ton CO_2-eq. for 2050. The uncertainty range, as proposed by BloombergNEF, spans from -95%/+8% in the short-term to -53%/+20% for the long term, contingent on possible market behaviors. Additionally, there is uncertainty regarding the potential intervention of the European Commission to raise the carbon price further. In July 2021, the Commission announced a 2.2% annual reduction in emission allowances from 2021 onward to expedite emissions cuts [7]. However, in this context, the

carbon price will only be applied to kerosene-powered aircraft, as SAF and hydrogen were assumed exempt from surrendering allowances [337].

4.7.3 Results

Short-Term Horizon

Figure 4.34 presents the estimated DOC breakdown for various scenarios in the short-term horizon, considering a 200 nmi typical mission. The four scenarios presented involve two alternatives for fossil fuels (kerosene or SAF) for both conventional and hybrid-electric configurations. Based on recent regulatory actions by the European Commission, it was assumed that free allowances for the aviation sector will be phased out by 2030; additionally, the use of sustainable aviation fuel is expected to accelerate, financed with twenty million free allowances [20, 338]. Standard charges were considered unaffected by incentive policies. The results highlight a significantly higher cost for hybrid-electric aircraft compared to conventional ones. This is not solely attributed to the development costs of such an unconventional configuration, but also to the greater mass of the aircraft. This substantial increase in aircraft price translates to a 57.1% higher capital cost per unit flight compared to the conventional case. Charges and airframe maintenance costs also see a considerable rise due to the larger size of the aircraft. It is noteworthy that, despite electricity being less expensive than fuel according to the forecasts for the year 2030, the price of energy sources for hybrid-electric aircraft results to be higher than for conventional configurations. This is due to the significantly higher energy requirements of hybrid-electric configurations owing to their increased weight. In scenarios where SAF is used instead of kerosene, the higher price of SAF compared to kerosene also results in higher energy source costs. However, configurations with SAF prove overall advantageous due to the exemption from additional charges associated with the ETS. The DOC of the conventional configuration with SAF is 7.5% lower than the same configuration using kerosene. The hybrid-electric configuration could only be economically advantageous by including specific taxation policies that discourage conventional configurations. Under the assumption that navigation taxes and landing fees remain consistent for all aircraft, the hybrid-electric configuration with SAF could become advantageous only if the price of carbon permits reaches 580 USD/ton CO_2-eq., compared to the 200 USD/ton CO_2-eq. forecast for 2030. Without such an increase, the economically preferable solution in the short term would be a conventional configuration making substantial use of SAF. However, it is essential to note that these results do not consider uncertainties affecting the major economic assumptions, particularly regarding the energy source prices discussed in Subsection 4.7.2. Anticipating the discussion on uncertainties presented later in this subsection, even with uncertainties considered, conventional aircraft using SAF emerge as strong contenders against kerosene-based alternatives in the short term. However, the latter could still be economically more favorable in the most pessimistic projections.

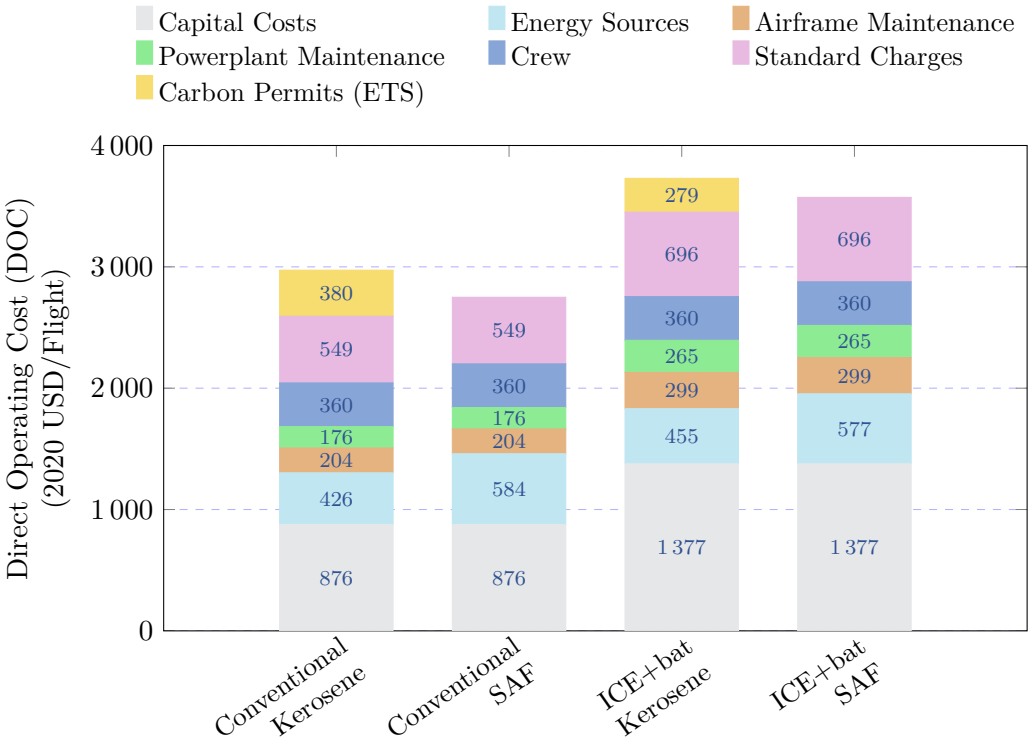

Figure 4.34: Comparison between direct operating costs of the short-term scenarios considered for the 200 nmi typical mission (adapted from Ref. [97]).

Medium-Term Horizon

Figure 4.35 illustrates the breakdown of estimated DOC for the five scenarios examined in the medium term. Four of these scenarios align with those considered for the short term, while the fifth is represented by the hydrogen-based PEMFC+bat configuration. In the medium term, the ICE+bat configuration is more costly than the conventional one, with a price exceeding 35 million USD. The PEMFC+bat configuration, due to its technological complexity and greater mass, is even more expensive. Similar considerations regarding charges and maintenance costs apply in this case. However, enhanced energy efficiency resulting from technological advancements allows for a slight reduction in the cost associated with energy sources, bringing it below the energy cost of conventional aircraft. In scenarios where SAF is used instead of kerosene, the energy source costs are higher than in the conventional kerosene-based case due to SAF's higher price compared to kerosene. Nevertheless, scenarios based on SAF prove more cost-effective than their kerosene-based counterparts, thanks to the exemption from additional charges outlined by the ETS. The DOC of the conventional configuration when using SAF is 5.3% lower than the corresponding kerosene-based scenario. The configuration with PEMFC+bat has an overall DOC comparable to that of the ICE+bat configuration with SAF. Both configurations cost more than the conventional scenario with the same EIS year and could only be economically advantageous if the price of carbon permits rises

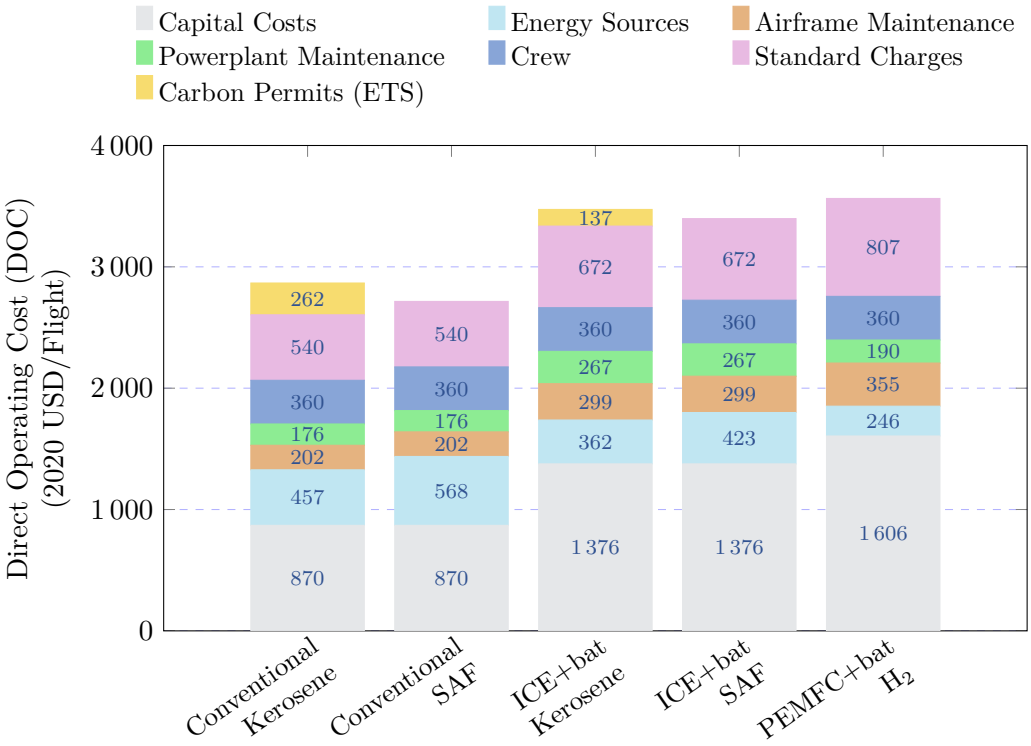

Figure 4.35: Comparison between direct operating costs of the medium-term scenarios considered for the 200 nmi typical mission (adapted from Ref. [97]).

to around 500 USD/ton CO_2-eq., compared to the 150 USD/ton CO_2-eq. forecast for 2040. Consequently, even in the medium term, the most economically favorable solution seems to be a conventional configuration using SAF. This conclusion is based solely on a best estimate and does not account for uncertainties, with the same considerations made for the short term being also applicable here.

Long-Term Horizon

The outcomes for the long-term horizon are presented in Fig. 4.36. In this case, aside from the two conventional scenarios also considered in the previous time frames, two distinct hydrogen-based configurations were examined, differing solely in the FC technology. Hydrogen-based configurations are reaffirmed to be the most expensive, even in the long term, with prices hovering around 45 million USD. Their DOC is approximately 25% to 27% higher when compared to conventional aircraft of the same time horizon. Both hydrogen-based configurations could only prove economically advantageous over conventional ones if the carbon permit price rises to approximately 240 USD/ton CO_2-eq. Otherwise, the most viable solution would again be the conventional configuration using SAF. Even when accounting for uncertainties, as detailed below, the economic disadvantage of hydrogen seems highly likely. Nonetheless, it is interesting to note that the utilization of hydrogen entails a substantial reduction in operational expenditure, reaching -8.62% for the SOFC+bat

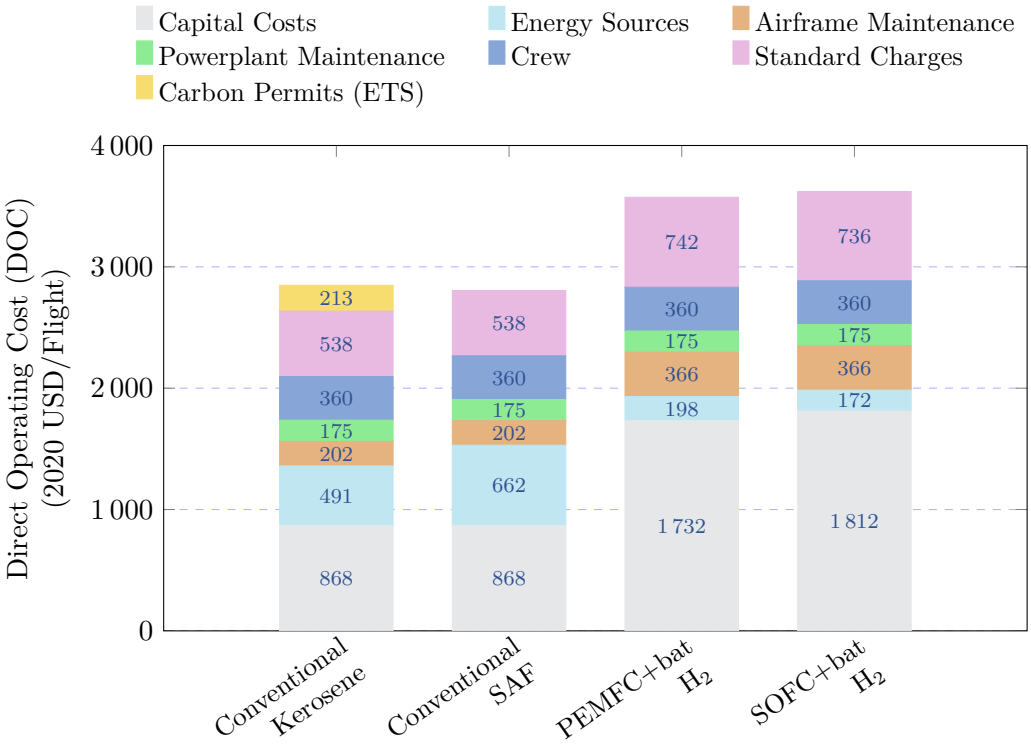

Figure 4.36: Comparison between direct operating costs of the long-term scenarios considered for the 200 nmi typical mission (adapted from Ref. [97]).

scenario. Therefore, hydrogen configurations remain promising, especially because if large-scale production brings down capital expenditures, they could become even more cost-effective than a suitably penalized kerosene-based alternative.

Uncertainties and Limitations

The breakdowns presented in Figs. 4.34, 4.35, and 4.36 were based on the best estimate, relying on certain primary assumptions. First of all, the unit costs of energy sources were projected based on the most reliable forecasts for each time horizon (refer to Subsection 4.7.2). Consequently, uncertainties associated with these assumptions have not been considered thus far. A similar uncertainty is also applicable to the future trajectory of carbon prices. Except for carbon pricing, thus far no incentives were factored into standard charges depending on the utilization of environmentally sustainable technologies. As proposed by Scholz et al. [164], one potential option is to incentivize hybrid-electric aircraft operation by reducing navigation charges proportionally to their degree of hybridization.

To incorporate uncertainties into the study, optimistic and pessimistic scenarios were introduced for each analyzed case. Pessimistic scenarios are designed to make hybrid and electric solutions less economically viable, while optimistic scenarios envision hybrid and electric solutions as more competitive with conventional alternatives. All these scenarios are summarized in Fig. 4.37. Alongside the

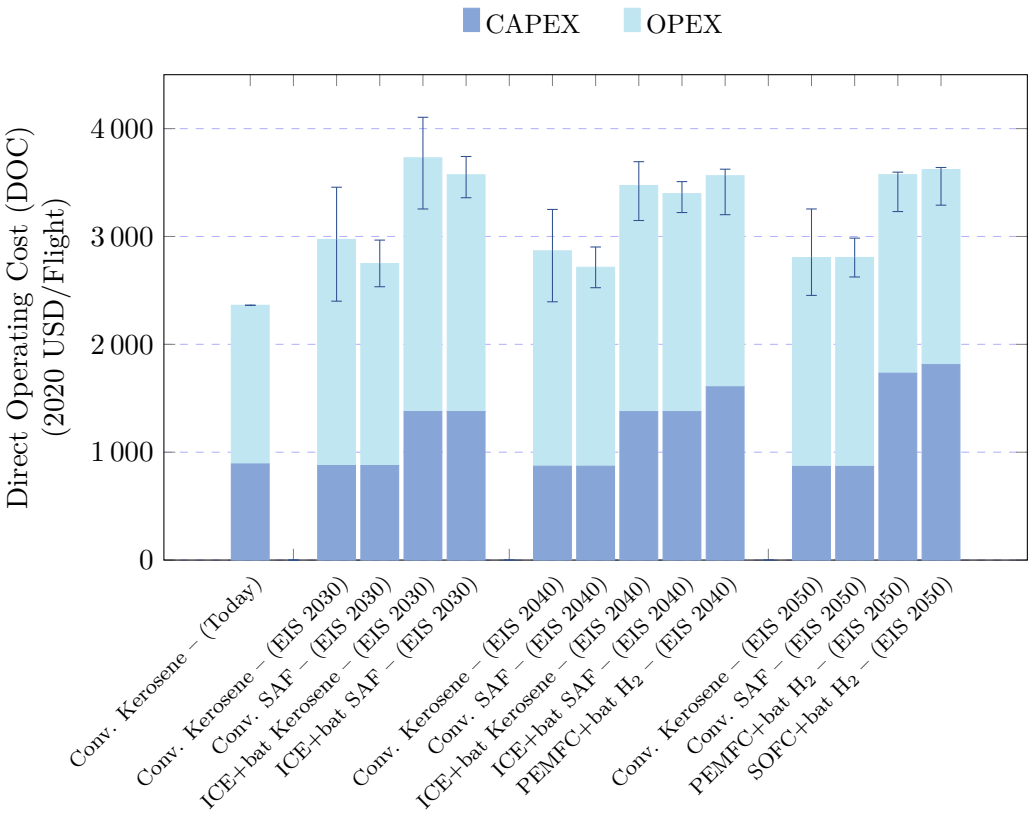

Figure 4.37: Comparison between the direct operating cost of all scenarios considered in three different time horizons, plus an additional today's reference, for a 200 nmi typical mission. The error bars represent the uncertainty associated with the price of energy sources, the air navigation charges, and the carbon price (adapted from Ref. [97]).

configurations previously examined, today's conventional aircraft, reflecting the 2020 technology levels, was included for comparative purposes. The error bars in the figure represent the range of uncertainty between the most optimistic and pessimistic cases. The width of the bars results from uncertainties surrounding fuel, electricity, and carbon prices, as well as potential reductions in airport charges modeled as suggested by Scholz et al. [164]. These reductions, tied to the degree of hybridization, are conceived as incentives for the adoption of environmentally friendly technologies.

In summary, despite existing uncertainties, direct operating costs for aircraft are predicted to rise over time, regardless of the propulsion system. Hybrid/electric scenarios are found to be less economically attractive than conventional cases across all three future time horizons. The most significant difference occurs in the short-term horizon for a hybrid-electric configuration, where the direct operating costs could surpass conventional ones by up to 71.0%. However, on average, this difference is mitigated by increases in the price of kerosene and carbon. Moreover, under the most pessimistic scenario for conventional aircraft (i.e., highest carbon price and fuel cost) and the best scenario for hybrid/electric aircraft (i.e., reduced navigation charges, low price of alternative energy sources), the DOCs of the latter align closely with those of conventional configurations using kerosene, across

each time horizon. This suggests that the planned evolution of carbon prices aligns with the need for technological transition, but only under the most optimistic scenario and with accompanying tax relief policies. A more economically competitive alternative emerges with the use of SAF on conventional architectures. On average, scenarios employing SAF outperform those using kerosene, with potential savings despite the higher price of SAF, which is attributable to the exemption from carbon permits. Opting for SAF over electrification appears to be a means of stabilizing the economic viability of future regional aviation, albeit with smaller environmental impact savings.

Table 4.28 reports the results underlying Fig. 4.37 in more detail. In addition, Tab. 4.29 reports cost estimates for a 600 nmi design mission, although the latter is not considered representative of actual average aircraft operation. Given the existing uncertainties, it is challenging to arrive at universal conclusions. Therefore, further research is essential to alleviate uncertainties, particularly in relation to energy and carbon prices, as these factors exert the most profound impact on determining the cost hierarchy among the various scenarios under consideration.

Table 4.28: Direct operating cost of all scenarios considered in three different time horizons, plus an additional today's reference, for the 200 nmi typical mission.

	DOC (2020USD/Flight)		
Scenario	**Optimistic**	**Nominal**	**Pessimistic**
		Today	
Conventional – Kerosene	2 362 (−0.0 %)	2 362	2 362 (+0.0 %)
		Short-Term (EIS 2030)	
Conventional – Kerosene	2 400 (−19.3 %)	2 973	3 457 (+16.3 %)
Conventional – SAF	2 534 (−7.8 %)	2 749	2 967 (+7.9 %)
ICE+bat – Kerosene	3 254 (−12.8 %)	3 730	4 106 (+10.1 %)
ICE+bat – SAF	3 359 (−6.0 %)	3 572	3 742 (+4.8 %)
		Medium-Term (EIS 2040)	
Conventional – Kerosene	2 394 (−16.5 %)	2 867	3 251 (+13.4 %)
Conventional – SAF	2 525 (−7.0 %)	2 715	2 903 (+6.9 %)
ICE+bat – Kerosene	3 148 (−9.4 %)	3 473	3 694 (+6.4 %)
ICE+bat – SAF	3 222 (−5.2 %)	3 398	3 509 (+3.3 %)
PEMFC+bat – H_2	3 202 (−10.1 %)	3 563	3 624 (+1.7 %)
		Long-Term (EIS 2050)	
Conventional – Kerosene	2 453 (-12.5 %)	2 805	3 256 (+16.1 %)
Conventional – SAF	2 624 (-6.5 %)	2 805	2 985 (+6.4 %)
PEMFC+bat – H_2	3 231 (-9.6 %)	3 573	3 596 (+0.6 %)
SOFC+bat – H_2	3 290 (-9.1 %)	3 621	3 640 (+0.5 %)

Table 4.29: Direct operating cost of all scenarios considered in three different time horizons, plus an additional today's reference, for the 600 nmi design mission.

	DOC (2020USD/Flight)		
Scenario	**Optimistic**	**Nominal**	**Pessimistic**
		Today	
Conventional – Kerosene	4 188 (−0.0 %)	4 188	4 188 (+0.0 %)
		Short-Term (EIS 2030)	
Conventional – Kerosene	4 162 (−20.4%)	5 503	6 628 (+20.4%)
Conventional – SAF	4 473 (−10.0 %)	4 972	5 477 (+10.2 %)
ICE+bat – Kerosene	5 484 (−20.0 %)	6 856	7 954 (+16.0 %)
ICE+bat – SAF	5 786 (−8.5 %)	6 325	6 817 (+7.8 %)
		Medium-Term (EIS 2040)	
Conventional – Kerosene	4 166 (−21.0 %)	5 275	6 168 (+16.9 %)
Conventional – SAF	4 470 (−9.0 %)	4 911	5 348 (+8.9 %)
ICE+bat – Kerosene	5 338 (−15.5 %)	6 316	6 989 (+10.7 %)
ICE+bat – SAF	5 561 (−7.9 %)	6 035	6 371 (+5.6 %)
PEMFC+bat – H_2	4 941 (−18.4 %)	6 056	6 270 (+3.5 %)
		Long-Term (EIS 2050)	
Conventional – Kerosene	4 310 (−16.0 %)	5 132	6 185 (+20.5 %)
Conventional – SAF	4 705 (−8.2 %)	5 127	5 546 (+8.2 %)
PEMFC+bat – H_2	4 950 (−17.4 %)	5 991	6 067 (+1.3 %)
SOFC+bat – H_2	5 010 (−16.7 %)	6 014	6 075 (+1.0 %)

Estimation of Ticket Prices

A final application pertains to estimating the ticket price for the 200 nmi typical flight. To achieve a comprehensive estimate of the ticket price, it is not only necessary to incorporate the IOC but also consider ground handling charges and include a profit margin on the sale. In 2022, Rotterdam The Hague Airport [339] charged 17.37€ per passenger for ground handling operations, along with an 11.06€ security surcharge. These values, converted into 2020 USD dollars, were adopted as a reference for the purposes of this work. A profit margin of 10% was assumed on the ticket price, corresponding to a passenger load factor of 80%. The results are summarized in Fig. 4.38 and Fig. 4.39. For hybrid-electric configurations in the short term, the increase compared to today's reference aircraft ranges between 17% and 33% on the typical mission, gradually decreasing over time until it stabilizes between 17% and 25% for long-term hydrogen-based configurations. Although evaluating the social impact of this rise in the cost of flying is beyond the scope of this work, the results suggest that the impact of hybridization on the final consumer is relatively limited. Therefore, the consequences on the overall regional aviation market do not appear to be overly dramatic.

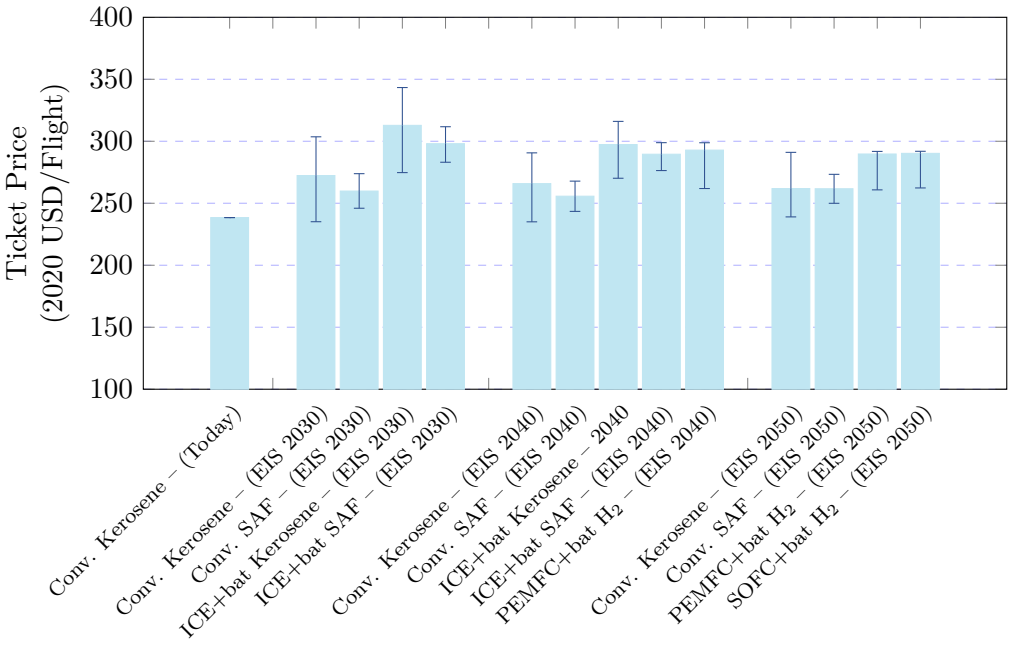

Figure 4.38: Comparison between predicted ticket prices for the 600 nmi design mission, for all scenarios considered in three different time horizons, plus an additional today's reference. The error bars represent the uncertainty associated with the price of energy sources, the air navigation charges and the carbon price (adapted from Ref. [97])).

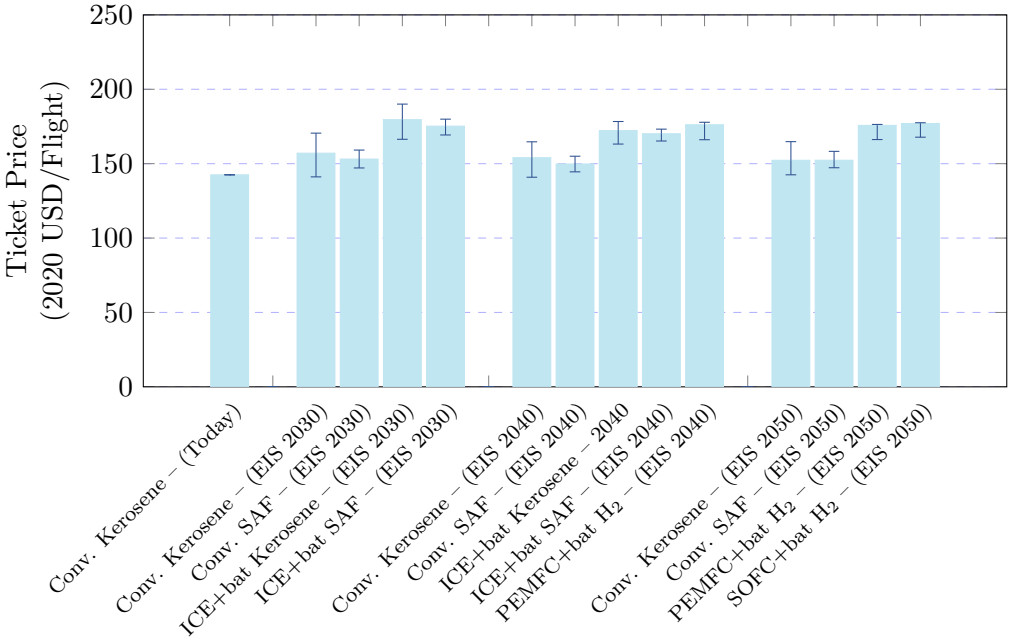

Figure 4.39: Comparison between predicted ticket prices for a 200 nmi typical mission, for all scenarios considered in three different time horizons, plus an additional today's reference. The error bars represent the uncertainty associated with the price of energy sources, the air navigation charges and the carbon price (adapted from Ref. [97])).

4.7.4 Discussion of Results

This section has provided an overview of the operational costs associated with innovative aircraft in the 50-passenger regional class. The analysis encompassed diverse configurations, spanning various propulsion architectures, energy sources, and time horizons. The results indicate that, despite their environmental promise, hybrid/electric solutions are linked to significantly higher DOC, reaching up to 71.0% for a typical mission compared to conventional alternatives entering service in the same year. This underscores the necessity for targeted tax policies and strategies aimed at promoting environmentally sustainable alternatives. While discouraging the use of kerosene-based aircraft might be a potential solution, it is contingent on public acceptance of a potential ticket price increase of up to 33% over the forthcoming decades. In this context, the adoption of SAF in conjunction with conventional propulsion emerges as a promising interim solution, offering potential cost advantages provided that a secure and large-scale supply of sustainable fuel can be ensured.

Although these insights are specific to the analyzed aircraft category, they offer valuable considerations for industry stakeholders, guiding strategic decisions toward a more sustainable and economically viable future for aviation. Future developments may involve refining economic assumptions based on evolving technological and macroeconomic trends. In particular, the limited availability of resources for the production of alternative fuels, which appears to be particularly critical for the SAF, could result in estimates outside the range of values that is considered plausible today. On the one hand, the growing demand for alternative fuels could encounter a limited supply of raw materials, leading to higher prices. On the other hand, investments in research could increase the efficiency of SAF production, making it less dependent on limited feedstocks, and eventually leading to economies of scale. Despite the uncertainty surrounding the numerical estimates presented in this section, the results of this comparative economic analysis will be useful for the purposes of determining a possible transitional roadmap toward future aviation, which is the subject of the next section. The results of the economic analysis, combined with the technical and environmental performances already presented in the previous sections, will form the basis for drawing up a technological roadmap and a set of recommendations for future aviation that reflect the author's vision.

4.8 Technology Roadmap

4.8.1 Short-Term Vision

Table 4.30 summarizes some of the main key indicators of flight, environmental and economic performance of all short-term scenarios discussed in the previous sections. All configurations were designed starting from the same set of TLARs, in order to guarantee minimum technical performance and market attractiveness. On the other hand, they show very different energy requirements due to the much

Table 4.30: Summary of the main performance indicators of the short-term scenarios.

Parameter	Unit	Conv. (Kerosene)	Conv. (SAF)	ICE+bat (Kerosene)	ICE+bat (SAF)
MTOM	kg	17 812	17 785	24 054	24 027
			600 nmi Design Mission		
Energy Demand	MWh	13.19	13.19	13.70	13.70
GWI	kg CO_2-eq.	4 141.5	1 904.4	4 128.1	1 947.0
DOC	USD/flight[1]	4 162–6 628	4 473–5 477	5 484–7 954	5 786–6 817
			200 nmi Typical Mission		
Energy Demand	MWh	5.69	5.69	5.27	5.27
GWI	kg CO_2-eq.	1 879.2	914.0	1 570.7	819.5
DOC	USD/flight[1]	2 400–3 457	2 534–2 967	3 254–4 106	3 359–3 742

[1] The reference inflation year is 2020.

greater mass of the ICE+bat aircraft, for which $Li-Ion$ batteries are responsible. Considering that the short-term configurations were designed assuming that the geometry (including the wing area) remains unchanged compared to the reference baseline, it was possible to justify the same ground performance even for the heavier configurations only through exploiting aero-propulsive effects due to DEP. However, the effectiveness of these systems in this aircraft category remains to be demonstrated via targeted experimental campaigns and could reveal critical. As for the environmental impact, the pLCA has demonstrated how it is possible to reduce the global warming impact through all the alternatives considered for the short-term. However, the reduction in CO_2-eq. of ICE+bat configurations is limited, especially for longer missions, compared to using SAF. The reason lies in the higher energy demand for the mission, directly correlated with the increase in weight of the aircraft due to the installation of batteries. Furthermore, the attainable degree of hybridization remains limited. The significant increase in their direct operating cost makes them unattractive, as the flight and environmental performance are insufficient to justify the investment. On the other hand, the conventional configuration remains the most economically competitive in its simplicity of realization.

The main advantages and disadvantages discussed so far for each of the short-term scenarios are summarized in Tab. 4.31. In the short term, the conventional configuration is still seen as the one most likely to succeed on the market, embodying an aviation paradigm that has been established for decades. However, using SAF appears to be the most promising short-term solution, especially if the ETS will continue to encourage its development and use. As a matter of fact, the EU's ETS provides an incentive to aircraft operators to use SAF that complies with the sustainability criteria (i.e., -65% of the well-to-wake CO_2-eq./MJ in the case of biofuels) by attributing them zero emissions under the scheme [20, 280, 281].

Table 4.31: Overview of the scenarios considered for the short-term horizon. The main advantages and disadvantages of each scenario are qualitatively summarized concerning technological feasibility, environmental impact, performance, and cost. The color scale reflects the ranking of scenarios with good performance marked in light green and poor performance marked in dark green.

		Technical Performance		Environmental Impact		Cost		Feasibility
Conventional (Kerosene)	↑	• Good performance compliant with TLARs.	↑		↑	• Low aircraft price. • Low DOC.	↑	• Well-established technologies.
	↓		↓	• High GWI. • High OD, IR, RE. • Does not meet ACARE goals.	↓	• (Potentially) high carbon price. • Uncertain fuel cost.	↓	
Conventional (SAF)	↑	• Good performance compliant with TLARs.	↑	• Low GWI. • Low OD, IR, RE.	↑	• Low aircraft price. • Exemption from carbon permits. • Low DOC.	↑	• Well-established technologies.
	↓		↓	• High impact in most of the categories.	↓	• Uncertain fuel cost.	↓	• Limited availability of feedstock for SAF production.
ICE+bat (Kerosene)	↑		↑	• Slight reduction in GWI.	↑	• (Potential) reduction in development costs due to scale-up effects.	↑	
	↓	• Degraded ground performance due to increased mass. • High power and energy demand.	↓	• High GWI. • High EUTRO Fresh, IR, HT. • Hardly meets ACARE goals.	↓	• High aircraft price. • (Potentially) high carbon price. • Uncertain fuel cost. • High DOC.	↓	• Uncertainty about the expected TRLs for this timeframe. • (Potential) unique challenges during integration and certification. • Remarkable impact on ground infrastructures and operations.
ICE+bat (SAF)	↑		↑	• Low GWI. • Low OD, IR, RE. • Potentially meets ACARE goals.	↑	• (Potential) reduction in development costs due to scale-up effects. • Exemption from carbon permits.	↑	
	↓	• Degraded ground performance due to increased mass. • High power and energy demand.	↓	• High impact in most of the categories (including HTc and HTnc).	↓	• High aircraft price. • Uncertain fuel cost. • High DOC.	↓	• Limited availability of feedstock for SAF production. • Uncertainty about the expected TRLs for this timeframe. • (Potential) unique challenges during integration and certification. • Remarkable impact on ground infrastructures and operations.

Operating costs benefit from this, making the overall cost of the required energy lower and less uncertain. SAF can potentially reduce life cycle GHG emissions, representing the fastest way to achieve short-term environmental objectives. On the other hand, SAF has no real environmental advantage over kerosene when looking at the deterioration in the other impact categories, such as land use and water use (see Section 4.6). While forecasts suggest improvements in the efficiency of kerosene-based ICEs, these advancements fall short of meeting short-term goals.

The utilization of a 100% HEFA-SPK blend, incorporating carbon capture

during palm fruit cultivation, could, however, achieve over 50% reduction in the global warming impact compared to a 2030 kerosene-based configuration. Based on this result, it is possible to infer a significantly higher percentage when referring to aircraft based on 1990 technologies, indicating alignment with ACARE goals [6]. Despite these benefits, challenges arise, such as competition with food systems for feedstock and potential deforestation from feedstock expansion [340]. For this reason, different types of biofuel production processes should be identified that can meet the sustainability criteria specified by the EU [281]. To avoid first-generation biofuels, second-generation options derived from residues or waste materials emerge as a rapid and cost-effective solution for short-term climate impact mitigation in regional aviation. However, the scale of SAF usage hinges on concurrent advancements in biofuels and e-fuels to meet rising flight demands while ensuring the absence of environmental trade-offs [61, 340, 341]. At present, the availability of SAF for 2030 is expected to be limited to about 3.4 million tons per year [342], which makes it difficult to imagine a complete transition from kerosene for the entire regional aviation. Instead, in light of feedstock considerations, SAF may be the most appropriate solution for long-haul flights, where alternatives to kerosene are scarce [343].

In parallel, it will be worth investing in developing hybrid-electric aircraft configurations based on $Li-Ion$ batteries, with a forward-looking approach that looks at medium- and long-term benefits. Hybridization, in conjunction with reduced kerosene use, holds promise for decarbonizing short-haul flights. Thus, a hybrid-electric architecture featuring lithium batteries and SAF-fueled ICEs embodies key *transitioning technologies*, paving the way for a progressive shift in aviation paradigms, while addressing short-term objectives and waiting for better alternatives (such as hydrogen) to reach sufficient maturity. Furthermore, implementing these technologies in the short term initiates a process of efficiency improvement and reduction of development and production costs, thanks to large-scale production. Research plays a pivotal role in evaluating SAF options and expediting critical technologies' development for aircraft electrification, establishing a robust foundation for the imminent transition. Therefore, the vision for the short-term is mixed, seeing hybrid-electric configurations side by side with conventional configurations, promoting for both an increase in the use of SAF compared to today's scenario.

4.8.2 Medium-Term Vision

Table 4.32 summarizes some of the main outputs relating to all medium-term scenarios. Due to the significant increase in mass of the aircraft, the power demands for unconventional configurations are much higher. The energy demand is lower only thanks to the improved efficiency of the electrical components. In this sense, the high specific energy of $Li-S$ batteries matches well with the high energy requirement of heavy unconventional configurations, which allows to aspire to higher degrees of hybridization and decarbonization. Thanks to that, the estimated reduction in CO_2-eq. of ICE+bat configurations using kerosene was more significant than for the short-term. Preserving ground performance remains a critical aspect due to

Table 4.32: Summary of the main performance indicators of the medium-term scenarios.

Parameter	Unit	Conv. (Kerosene)	Conv. (SAF)	ICE+bat (Kerosene)	ICE+bat (SAF)	PEMFC+bat (H_2)
MTOM	kg	17 421	17 398	23 040	23 021	28 915
				600 nmi Design Mission		
Energy Demand	MWh	12.07	12.07	10.73	10.73	9.60
GWI	kg CO_2-eq.	3 766.8	1 584.5	2 902.2	1 286.8	592.8
DOC	USD/flight[1]	4 166–6 168	4 470–5 348	5 338–6 989	5 561–6 371	4 941–6 270
				200 nmi Typical Mission		
Energy Demand	MWh	5.19	5.19	3.80	3.80	3.03
GWI	kg CO_2-eq.	1 707.2	768.5	1 076.3	551.0	311.0
DOC	USD/flight[1]	2 394–3 251	2 525–2 903	3 148–3 694	3 222–3 509	3 202–3 624

[1] The reference inflation year is 2020.

the weight of the aircraft, but the analyses have shown how a careful redesign of the wing and of the geometry may help to overcome this problem without affecting too much the substantial reduction in environmental impact provided by $Li - S$ batteries and/or the use of hydrogen. On the other hand, DOC of unconventional configurations still remains very high due to production costs and charges. However, it should be specified that the development and production costs could actually be lower than the estimated ones, provided that in the short term the tendency will have been to invest in facing the main technological challenges related to the integration of an electric powertrain on regional aircraft. For both conventional and ICE+bat configurations, the SAF mixture assumed for the medium-term was partially made up of e-fuels (see Tab. 4.9). Such a SAF blend has shown the potential to reduce GWI significantly but at the expense of most of the other impact categories. If adequate incentives are applied, the use of SAF could also be economically advantageous compared to kerosene also in the medium term.

The main advantages and disadvantages discussed so far for the medium-term scenarios are summarized in Tab. 4.33. The vision presented for the short term evolves into a very varied scenario in the medium term, seen as a crucial moment of transition towards a totally new aviation paradigm. In the medium term, the conventional configuration is still seen as the more economically attractive one unless the use of kerosene is sufficiently penalized. Although the use of SAF has proved crucial to contribute to the achievement of short-term objectives, its exclusive use does not seem sustainable over an extended period of time [342]. Moreover, the current long-term objectives of ACARE make it imperative to invest in solutions capable of allowing for net-zero emissions by 2050 [6]. As already discussed in Subsection 4.8.1, the use of SAF may still be useful to support an increasingly sharp reduction in the use of kerosene long-haul flights, if accompanied by an intensification of the search for carbon-neutral solutions for its production. On the other hand, this is associated with the risk that the use of carbon-intensive SAF

Table 4.33: Overview of the scenarios considered for the medium-term horizon. The main advantages and disadvantages of each scenario are qualitatively summarized concerning technological feasibility, environmental impact, performance, and cost. The color scale reflects the ranking of scenarios with good performance marked in light green and poor performance marked in dark green.

	Technical Performance		Environmental Impact		Cost		Feasibility	
Conventional (Kerosene)	↑	• Good performance compliant with TLARs.	↑		↑	• Low aircraft price. • Low DOC.	↑	• Well-established technologies.
	↓		↓	• High GWI, RE, OD. • Does not meet ACARE goals.	↓	• (Potentially) high carbon price. • Uncertain fuel cost.	↓	
Conventional (SAF)	↑	• Good performance compliant with TLARs.	↑	• Low OD, IR, RE.	↑	• Low aircraft price. • Exemption from carbon permits. • Low DOC.	↑	• Well-established technologies.
	↓		↓	• High impact in most of the categories. • Hardly meets ACARE goals.	↓	• Uncertain fuel cost.	↓	• Limited availability of feedstock for SAF production.
ICE+bat (Kerosene)	↑		↑	• Low PM, ECOTOX freshwater.	↑	• (Potential) reduction in development costs due to scale-up effects.	↑	• Experience gained during the short-term.
	↓	• Degraded ground performance due to increased mass. • High power demand.	↓	• High impact in most of the categories. • Hardly meets ACARE goals.	↓	• High aircraft price. • (Potentially) high carbon price. • Uncertain fuel cost. • High DOC.	↓	• Uncertainty about the expected TRLs for this timeframe. • (Potential) unique challenges during integration and certification. • Remarkable impact on ground infrastructures and operations.
ICE+bat (SAF)	↑		↑	• Low OD, IR, RE • (Potentially) meets ACARE goals.	↑	• (Potential) reduction in development costs due to scale-up effects. • Exemption from carbon permits.	↑	• Experience gained during the short-term.
	↓	• Degraded ground performance due to increased mass. • High power demand.	↓	• High impact in most of the categories.	↓	• High aircraft price. • Uncertain fuel cost. • High DOC.	↓	• Limited availability of feedstock for SAF production. • Uncertainty about the expected TRLs for this timeframe. • (Potential) unique challenges during integration and certification. • Remarkable impact on ground infrastructures and operations.
PEMFC+bat (H_2)	↑		↑	• Lowest GWI, OD, AC, eutrophication, POF • Meets ACARE goals.	↑	• (Potential) reduction in development costs due to scale-up effects. • Exemption from carbon permits.	↑	• Experience gained during the short-term regarding batteries and electric drives.
	↓	• Degraded ground performance due to increased mass. • High power demand.	↓	• Highest HTc, HTnc, RM.	↓	• High aircraft price. • Low OPEX. • High DOC.	↓	• Uncertainty about the expected TRLs for this timeframe. • Need to ensure low carbon H_2 supply. • (Potential) unique challenges during integration and certification. • Remarkable impact on ground infrastructures and operations.

could still be economically competitive, preventing medium-term investments in more environmentally sustainable solutions such as hydrogen.

Conventional configurations are unlikely to be completely phased out by 2040, but they will hopefully be joined by hybrid-electric configurations with high-performance batteries capable of supporting the EU's environmental targets. ICE+bat configurations show encouraging results, especially if their adoption since the short term will have provided enough time to overcome the implementation difficulties and all safety and certification barriers. Nevertheless, these solutions are intrinsically unable to achieve the net-zero emissions target. The long-term point of arrival, in this sense, is aviation entirely based on low-carbon hydrogen (e.g., produced by electrolysis with renewable energy and water).

An entirely battery-based solution is not technically feasible for aircraft of this class due to their energy requirements. For this reason, it is essential to invest in the development and application of hydrogen FCs, to be coupled to batteries in order to approach the net-zero emissions target. The analysis of the PEMFC+bat configuration has revealed a high potential reduction in carbon footprint. However, the LCA results suggested a remarkable effect of the hydrogen-based configuration in other impact categories, particularly on human toxicity. It is for this reason that it is essential, as well as in line with the objectives of ACARE, that all non-CO_2 climate effects are fully understood, managed, and monitored within the next decade, in order to identify the available mitigation solutions in time for their application in the medium-term. In conclusion, the deployment of electric drivers and systems over the next 20 years, i.e., in the short and medium term, will pave the way for developing hydrogen-powered aircraft in the long term, progressively increasing their economic feasibility. However, actions will be necessary at first to promote investment in hydrogen-based configurations, as well as for the production of low-carbon hydrogen, by virtue of their long-term importance as permanent replacements for carbon-based solutions. Reducing fossil fuel use drastically (e.g., through the ETS or by promoting lower air navigation charges for full-electric configurations) has the potential to make this solution competitive already in the medium term. If policies in this sense are not adopted, conventional configurations will always remain the most economically convenient by virtue of their consolidated reliability and simplicity of realization due to the use of conventional technologies.

4.8.3 Long-Term Vision

Table 4.34 summarizes some of the main outputs relating to all long-term scenarios. As for the conventional configuration using SAF, the same considerations already made for the previous time horizons apply also for the long-term. A good reduction of costs and CO_2 emissions is expected from SAF, which however collides with an increase in other impact categories and with the low availability of feedstocks for large-scale use [342]. More important, the reduction in environmental impact provided by the use of SAF only, however promising, is not compatible with the long-term objectives foreseen in the ACARE agenda [6]. One possibility

Table 4.34: Summary of the main performance indicators of the long-term scenarios.

Parameter	Unit	Conv. (Kerosene)	Conv. (SAF)	PEMFC+bat (H_2)	SOFC+bat (H_2)
MTOM	kg	17 366	17 342	26 045	25 793
			600 nmi Design Mission		
Energy Demand	MWh	11.80	11.80	8.76	7.21
GWI	kg CO_2-eq.	3667.0	1 253.6	468.1	407.9
DOC	USD/flight[1]	4 310–6 185	4 705–5 546	4 950–6 067	5 010–6 075
			200 nmi Typical Mission		
Energy Demand	MWh	5.06	5.06	2.91	2.44
GWI	kg CO_2-eq.	1 658.4	622.3	261.7	242.9
DOC	USD/flight[1]	2 453–3 256	2 624–2 985	3 231–3 596	3 290–3 640

[1] The reference inflation year is 2020.

is to invest in the development of more advanced SAF blends, for example fully composed of e-fuels produced via direct air capture [344], but hydrogen-based solutions are seen as the most promising and viable solution in light of their drastic reduction in carbon footprint.

As already discussed for the medium term, hydrogen-based solutions feature very low energy demand thanks to the excellent efficiency of hydrogen FCs. The reduced mass of the cryogenic hydrogen storage systems further improves both performance and energy demand with respect to the medium-term PEMFC+bat configuration. A free redesign of the geometry combined with the use of DEP allowed to mitigate the effects of mass penalties, without affecting too much the substantial reduction in carbon footprint provided by the use of hydrogen and $Li-O_2$ batteries. However, it should be noted that the LCA results suggested a high impact of the hydrogen-based configuration in other impact categories, in particular on human toxicity and ecotoxicity. Therefore, PEMFC and SOFC technology developments should integrate an eco-design dimension focused on mitigating these other impacts. The main advantages and disadvantages discussed so far for each of the long-term scenarios are summarized in Tab. 4.35.

In the long term, configurations based on hydrogen-powered FC systems are desired to dominate the regional aviation scenario. They represent the preferential path towards achieving the complete decarbonization of regional flights by 2050, at least with reference to the 50-passenger regional class [6]. In this vision, conventional configurations could be completely phased out by the year 2050. The widespread diffusion of this new type of aircraft must be carefully guided through regulations and incentives aimed at the complete phase-out of fossil fuels and any other unsustainable energy source. This vision is based on the premise that the electricity grid is shifting toward low-carbon energy sources, industries are getting more efficient and electrified, and low-carbon hydrogen is abundant. Without these conditions, the comparative

Table 4.35: Overview of the scenarios considered for the long-term horizon. The main advantages and disadvantages of each scenario are qualitatively summarized concerning technological feasibility, environmental impact, performance, and cost. The color scale reflects the ranking of scenarios with good performance marked in light green and poor performance marked in dark green.

		Technical Performance		Environmental Impact		Cost		Feasibility
Conventional (Kerosene)	↑	• Good performance compliant with TLARs.	↑		↑	• Low aircraft price. • Low DOC.	↑	• Well-established technologies.
	↓		↓	• High GWI. • High OD, IR, RE. • Does not meet ACARE goals.	↓	• (Potentially) high carbon price. • Uncertain fuel cost.	↓	
Conventional (SAF)	↑	• Good performance compliant with TLARs.	↑	• Low GWI. • Low OD, IR, RE.	↑	• Low aircraft price. • Exemption from carbon permits. • Low DOC.	↑	• Well-established technologies.
	↓		↓	• High impact in most of the categories. • Hardly meets ACARE goals.	↓	• Uncertain fuel cost.	↓	• Limited availability of feedstock for SAF production.
PEMFC+bat (H_2)	↑		↑	• Very low GWI. • Low impact in most of the impact categories. • Meets the ACARE goals.	↑	• (Potential) reduction in development costs due to scale-up effects. • Exemption from carbon permits.	↑	• Experience gained during the previous time horizons regarding batteries, electric drives, and fuel cells. • Experience gained during the medium-term in the specific use of PEMFC systems.
	↓	• Degraded ground performance due to increased mass. • High power and energy demand.	↓	• High HT, RM.	↓	• High aircraft price. • Low OPEX. • High DOC.	↓	• Uncertainty about the expected TRLs for this timeframe. • Need to ensure low carbon H_2 supply. • (Potential) unique challenges during integration and certification.
SOFC+bat (H_2)	↑		↑	• Very low GWI. • Very low impact in most of the impact categories. • Meets the ACARE goals.	↑	• (Potential) reduction in development costs due to scale-up effects. • Exemption from carbon permits.	↑	• Experience gained during the previous time horizons regarding batteries, electric drives, and fuel cells.
	↓	• Degraded ground performance due to increased mass. • High power and energy demand.	↓	• High HT, RM.	↓	• High aircraft price. • Low OPEX. • High DOC.	↓	• Uncertainty about the expected TRLs for this timeframe. • Need to ensure low carbon H_2 supply. • (Potential) unique challenges during integration and certification. • Remarkable impact on ground infrastructures and operations.

environmental benefits of hybridization may be significantly reduced due to a higher energy and material demand. However, the search for new innovative solutions will

never cease, aimed at the continuous will to reduce the environmental impact and operating costs of aircraft. The development and use of SOFCs can be already seen as one of these secondary objectives, as well as structural batteries, innovative structural solutions, and materials that are increasingly reliable, well-performing, and environmentally sustainable.

4.8.4 Roadmap to Sustainable Regional Aircraft

The previous subsections have offered a comparative analysis of the different scenarios analyzed for the short-term, the medium-term, and the long-term time horizons. The environmental impact of each scenario was commensurate with the extent of the environmental objectives set by the EU's ACARE, necessary for achieving climate-neutral air mobility [6]. A roadmap, outlined in Fig. 4.40, was derived from the main outcomes of this study. The purpose of this roadmap is to provide indications of how the environmental objectives of the EU can be pursued based on potentially available instruments. The considerations proposed below aim to propose technical solutions to reduce the environmental impacts of short-haul aviation, which is critical. The reader should be cautious in interpreting the conclusions, as they are valid only for the class of aircraft under analysis and for short-haul flights unless differently specified. The outlined roadmap introduces several needed actions that lay the foundations for recommendations to various stakeholders, i.e., the aviation industry, policymakers, and research in general. Table 4.36 summarizes the main ones that reflect the author's vision.

SAF, particularly HEFA-SPK, has emerged as a promising short-term transition technology for meeting EU objectives by 2030. However, challenges exist, such as limited feedstock for 1st generation SAF and certification limitations on SAF blending ratios. In this sense, there is a need for rapid and large-scale commercial mobilization of sustainable feedstock. In parallel, accelerated research is crucial to certify 100% SAF use in aircraft engines by 2030. Long-term sustainability requires exploration of SAF and feedstock compliant with EU criteria, particularly from waste feedstock, as the industry transitions to hydrogen and e-fuels. While, on the one hand, the technology roadmap outlined supports the progressive transition to hydrogen and the phase-out of ICEs for regional turboprop aircraft, the development of e-fuels and 2nd generation SAF remains a wise long-term investment, especially for long-haul flights.

Policy measures are also recommended, such as a tax system favoring SAF over kerosene and improved traceability. Attention must be paid to avoid discouraging investment in hybridization or hydrogen. Technologies for electrification, including hybrid-electric solutions, need immediate development and implementation efforts. Ground infrastructures will have to adapt progressively with charging stations and, later, hydrogen supply. This presupposes the immediate need for incentives to conduct research in this direction, having as an intermediate target the development of hybrid-electric solutions (with conventional engines coupled with batteries) already within the short term. The operators should be eventually encouraged to purchase

Table 4.36: Main recommendations to different stakeholders.

Recommendation	Description
Policy Makers	
Government funding for research, development, demonstration and deployment of innovative aviation fuels and solutions	– Government-funded research may accelerate the learning curve for production processes, contributing to scaling up production of alternative fuels that meet sustainability criteria. – Research should also be funded to integrate innovative solutions (e.g., hybrid/electric architectures) on aircraft, focusing on safety.
Green hydrogen and SAF development policy to secure low-carbon fuel supply	– Secure the supply of low-carbon SAF and H_2 by including market demand forecasts in the development policy. – Mandate increasing SAF and H_2 volumes and reduction in carbon intensity of transportation fuel supply.
Targeted incentives and tax relief to expand the use of sustainable solutions	– Create incentives for H_2 aircraft operations when commercial models are launched, if their environmental performance meets the expected levels. – Apply taxation strategies (e.g., under the ETS) to incentivize SAF use in the short-term and H_2 use in the medium- and long-term. – Refine the carbon market, e.g., by increasing traceability of SAFs and differentiating ETS credits according to their environmental performance. – Encourage investment in hybrid-electric solutions for short-haul flights, e.g., through a reduction in charges proportional to the hybridization level.
Research	
Research, development, demonstration and deployment of H_2 and SAFs	– Research is needed to demonstrate all environmental effects of different processes and feedstocks used to produce SAFs, identifying the most sustainable solutions and increasing their availability on the market. – Research must be accelerated to evaluate options for certifying 100% SAF use in aircraft engines in the short term.
Investigate eco-sustainability of innovative systems to solve environmental trade-offs	– A careful eco-design of such systems is necessary to solve the environmental trade-offs and reduce the non-CO_2 effects related to hydrogen FCs and batteries, such as increases in human toxicity.
Research, development and demonstration of hybridization technologies to pave the way to hydrogen-based aircraft	– Research is needed to accelerate the maturation of several key technologies within timescales for their aeronautical application. – Applied research has to demonstrate all the effects of integrating electrical systems and innovative materials on board, under typical flight conditions. This includes batteries, FCs, electrical systems, and hydrogen tanks.
Aviation Industry	
Increased environmental responsibility	– Being open to innovation, and proactive in developing sustainable solutions. – Invest in renewing fleets with hybrid/electric and hydrogen-based aircraft. – Accurately analyze its internal processes to identify all opportunities for reducing the environmental impact. – Provide transparent reports of internal processes, to support the development of environmental databases that allow for the understanding of all environmental effects and the search for mitigation solutions.
Dialogue with policy makers and certification entities	– Embrace funding opportunities offered by governments. – Include environmental sustainability targets in design and optimization processes, manufacturing, use, and decommissioning of the aircraft. – Engage in dialogue with certification entities to incorporate evolving regulations into the design process.

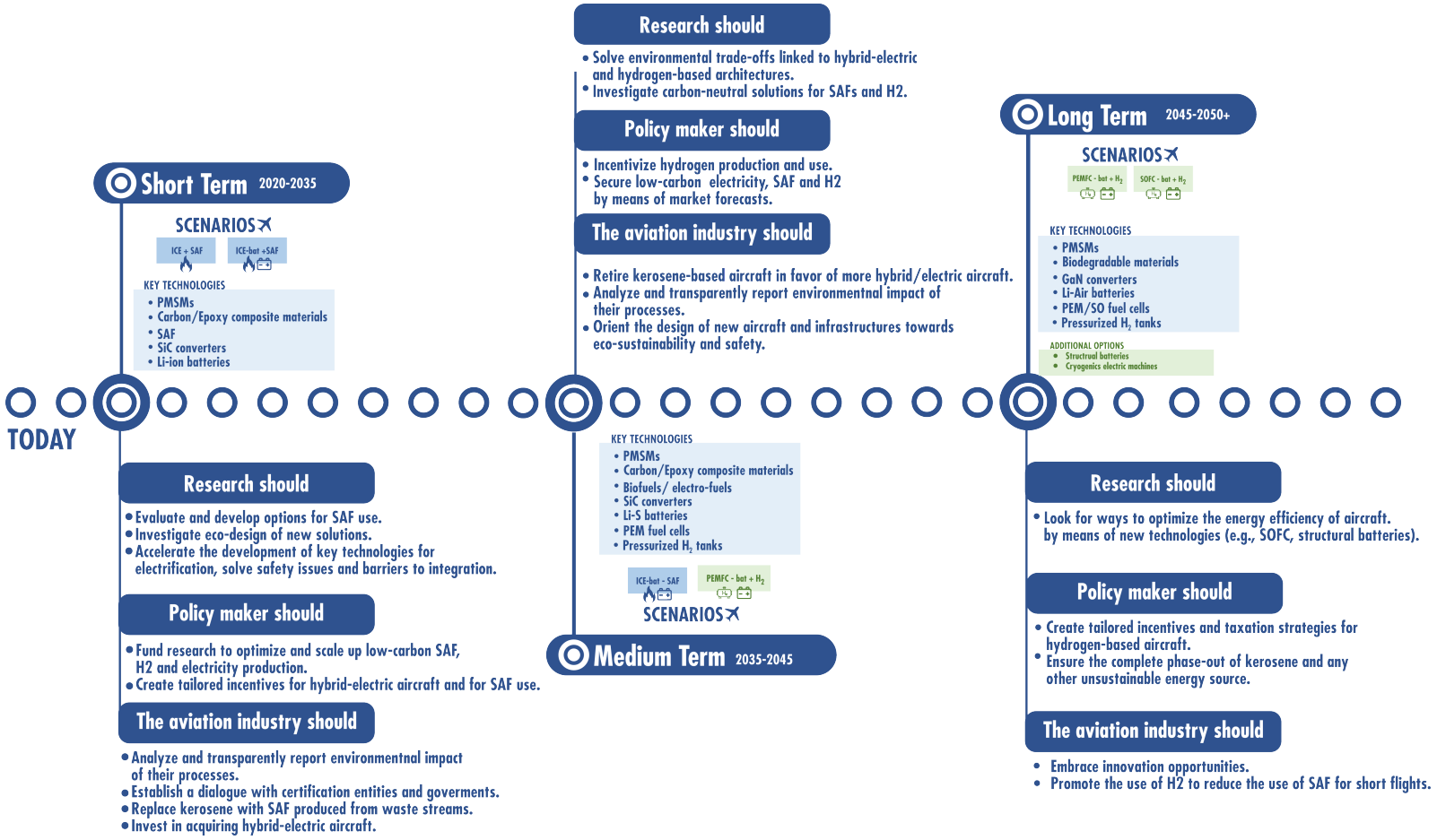

Figure 4.40: Technology roadmap towards a sustainable regional aircraft and recommendations for main stakeholders [215].

hybrid-electric aircraft by means of incentives to reduce operating expenses, e.g., by decreasing charges in proportion to the hybridization level. In this way, it would be possible to have greater control over the commercial development of the different technologies over the years, causing the progressive phase-out of kerosene first, and then of all carbon-based fuels that are not fully compliant with sustainability targets. The use of sustainable fuels in the long term should be encouraged only concerning low-carbon SAF and should, in any case, be reserved for longer-haul flights.

Europe needs to define its level of ambition for H_2, outline a pathway, and provide a reference point for private investment [345]. Being in its infancy, the green hydrogen sector requires dedicated industrial policymaking to meet increasing demand, necessitating a rapid scale-up of electrolyzer capacity. In this sense, a balance between short- and long-term strategies is vital to achieve net-zero emissions. The roadmap described in IRENA's 2022 World Energy Transitions Outlook foresees a total installed electrolyzer capacity of 5 TW by 2050, up from today's 300 MW [345].

The development and diffusion of hydrogen-based solutions require incentives for hybrid and electric aircraft since the next decade, accompanied by continuous efforts to mitigate environmental trade-offs through careful eco-design. Applied research is crucial to accelerate the development of key technology bricks and to understand the effects of integrating electrical systems in flight conditions. Even if innovative technologies reach a state of maturity where they are considered technologically ready, they still have to go through the certification process. This process requires thorough testing, evaluation, and documentation to ensure compliance with stringent safety, performance, and regulatory standards. The complexity and novelty of these new technologies often pose unique challenges during certification, with potentially significant delays before new aircraft implementing these technologies can enter service. In the end, close collaboration between industry, policymakers, and certification entities will be crucial. More in general, the aeronautical industry has the responsibility of being ready and open to innovation, proving to be proactive in the development of eco-sustainable solutions. Accurately analyzing their internal processes can be important to identify all opportunities for reducing the environmental impact. Furthermore, providing transparent reports of their processes and emissions would support the development of wider environmental databases that allow for the understanding of all the environmental effects involved and the search for mitigation solutions.

Conclusions and Future Developments

The present thesis work has explored the frontiers of regional aviation, focusing on the opportunities offered by innovative technologies such as hybrid-electric architectures and alternative aviation fuels. Due to their smaller size and shorter route profiles, regional turboprop airplanes have been identified as the ideal test bed for the integration of cutting-edge technologies that potentially respond to the need to decarbonize aviation. In light of the major impact of design choices on the technical, economic, and environmental performance of new aircraft, emphasis was placed on the role that the preliminary designer may have in supporting the transition toward sustainable aviation. In this regard, the following research question was posed in the Introduction chapter:

How can preliminary aircraft designers support the transition to a future sustainable regional aviation, with a specific focus on hybrid-electric and hydrogen-based technologies, while including life-cycle considerations?

To answer this multifaceted question, it was further detailed by identifying more specific needs, which the various chapters of the thesis have tried to address.

First, as emerging from the existing literature, the variety of viable solutions for decarbonization raises the need to provide the preliminary designer with a unique tool that can grasp all options available, in order to evaluate and compare their possible benefits at the aircraft level. In this sense, an attempt was made to answer this question:

How can traditional preliminary design methodologies be generalized and adapted into a flexible, multidisciplinary workflow to address the diversity of hybrid-electric propulsion architectures in regional aircraft?

In Chapter 2, innovative approaches to aircraft design have been proposed. The presented design workflow started from state-of-the-art methodologies, adapting and generalizing them to manage innovative propulsion architectures as well as conventional aircraft. In particular, the author has proposed a general mathematical model to describe a huge variety of propulsion systems involving alternative energy sources. The model is able to degenerate into specific architectures based on thermal engines, batteries, hydrogen FC systems, or any combination of them, and it is also able to include DEP and model the aero-propulsive effects associated with it. Furthermore, the model robustness is supported by consistency checks, which pass through the analysis of the operating modes and of the direction of energy flows exchanged between the powertrain components. Overall, the model is believed to provide important added value compared to the state of the art. Its remarkable generality and replicability, combined with the simplicity of the linear algebraic equations it relies on, make it suitable for preliminary aircraft design applications. Leaving room for future development, the model is also easy to generalize further, to include even more systems and degrees of freedom. The model

was included in a design chain under development by UNINA's DAF research group, to which the author also contributed directly in terms of continuous improvement and maintenance. Combining the generalized powertrain description with II-class methods for mass estimation and with a design approach based on mission analysis, the workflow presented in Chapter 2 allows for a consistent and complete design of new concepts, with an improved level of accuracy compared to methods based on point performance evaluation. Unfortunately, the scarcity of enough public data relating to flying electric prototypes did not allow for an exhaustive verification of the tool. As research in the field of electric regional aviation advances, and statistics become available for innovative aircraft in this category, further testing and improvement of the presented design methodologies will become possible.

The development of the tool was also the result of the author's active participation in research projects of international relevance, most notably the CS2 ELICA project, to which Chapter 3 was dedicated. Focusing on a 19-passenger regional aircraft, the project's results, contingent on technological assumptions for a close EIS, suggested that the advantages of hybridization based on batteries would be limited by the current certification constraints, leading to unsatisfactory reductions in environmental impact. In this sense, investing directly in hydrogen FCs could represent a more efficient solution for this class of aircraft, although various safety and certification challenges of the new systems still need to be addressed. More important, the activities carried out within the ELICA project have contributed to increasing the author's knowledge on this research topic and to highlighting even more the need for a reliable, automatic, and flexible tool to effectively fulfill the role of the preliminary designer. In light of its generality and relative ease of use, the developed workflow responded to this research need, providing a tool suitable for exploring a diversity of innovative solutions for aviation.

Founded on this methodological basis, the core of this thesis was later focused on the meticulous evaluation of the potential benefits of alternative fuels and hybrid-electric technologies for regional aviation. Past studies on hybrid-electric regional aircraft have shown the marked sensitivity of the expected advantages to the assumed technological levels. This stresses the importance of careful technology foresight, when the purpose is to provide a prospective analysis of the benefits expected from innovative technologies in a specified time horizon. Furthermore, increasing sensitivity to the environmental problem imposes holistic considerations, which do not neglect life-cycle and cost considerations even in the preliminary design phases. In fact, only in this way can the designer's choices be guided by a sufficient awareness of the existing trade-offs between economic viability and long-term sustainability. Given the paucity of similar prospective studies within the context of regional aviation, the following additional question was asked:

How can integrating life-cycle and cost considerations into the preliminary design of a 50-passenger regional aircraft, with either conventional or hybrid-electric architecture, assess the real impacts of the most promising technologies over time?

In this sense, the study proposed in Chapter 4 tried to respond to this need, by offering an overview of the most promising technologies available in three different future time horizons, and by defining representative aircraft scenarios to be analyzed from a multidisciplinary perspective. A parallel intent was to use the lessons learned from this study to formulate recommendations for aviation stakeholders in response to a third, last research question:

How can this study inform the development of an environmental database and provide actionable recommendations for technology selection to policymakers, aviation stakeholders, and aircraft designers?

Therefore, the study of Chapter 4 has focused on the design of several regional aircraft concepts in the 50-passenger class. After identifying a probable evolution of the maturity levels of different alternative propulsion technologies, several scenarios were defined as representing the most promising solutions. Starting from market-driven top-level requirements, a wide design exploration was performed for each scenario, using an accurate approach based on surrogate models and mission analysis, and being guided by the principle of minimum fuel consumption. This assessment has shed light on the challenges to be faced before it is possible to realize these advanced aircraft, as well as the trade-offs that emerge compared to more conventional choices. In particular, hybrid-electric solutions appear to have limited advantages with short-term technology levels, while entailing important penalties on the total mass of the aircraft. Medium- and long-term hydrogen-based solutions, although theoretically free of direct pollutant emissions, were associated with the highest MTOM values. However, the accuracy of the results obtained is intrinsically limited by the semi-empirical nature of the methods used, and by the uncertainty associated with the prospective nature of the technological assumptions. Future work may involve refining assumptions, especially as technological progress advances and uncertainty fades. Furthermore, it should be underlined that the concepts obtained were the result of design explorations but, although the minimization of fuel consumed was a driving factor, a rigorous optimization was not performed. This is justified by underlining that the aim of the study was to provide comparative analyses between different solutions and highlight the main characteristics of each, rather than refine the concepts in detail. However, future investigations may concern sensitivity analyses on the TLARs, on the number and arrangement of propellers, and on other design parameters. Last but not least, the study could be extended to further configurations that have not been considered here, such as ICEs burning hydrogen directly, or hybrid architectures combining ICEs and FC systems together.

After designing the concepts, the analysis extended beyond mere technical capabilities, providing an assessment of their economic viability. The analysis encompassed several economic scenarios, and the results indicated that, despite their environmental promise, hybrid-electric solutions are linked to significantly higher DOC. This underscores the necessity for targeted tax policies and strategies aimed at promoting environmentally sustainable alternatives. While discouraging the use of kerosene-based aircraft might be a potential solution, it is contingent on

public acceptance of a limited but significant ticket price increase. In this context, the adoption of SAF in conjunction with conventional propulsion emerges as a promising interim solution, offering potential cost advantages provided that a secure and large-scale supply of sustainable fuel can be ensured. Future developments may involve refining economic assumptions based on evolving technological and macroeconomic trends.

The designed aircraft concepts also provided a basis for a pLCA, which was carried out in collaboration with expert collaborators and coordinated by DTU researchers. As a first product of this activity, extensive and scalable LCI datasets were created and published, describing the analyzed aircraft scenarios from a life-cycle perspective. The datasets cover all key processes from raw materials extraction, manufacturing, and use, up to the end-of-life. The generated LCI datasets are believed to pave the way for several other relevant applications within the field of LCA, especially in light of the current shortage of aviation data sources with the same level of detail. The LCI datasets can be incorporated into environmental databases like Ecoinvent, enabling practitioners to conduct more comprehensive LCAs of aviation systems. They represent a first step toward the integration of sustainability considerations at the preliminary design level. In fact, the provided datasets are adaptable for various aircraft models in the regional class, allowing for pLCAs of alternative propulsion and fuel technologies in aviation. One limitation is that the prospective LCI datasets are built on specific assumptions and forecasts, depending on the availability and thoroughness of trustworthy data, which could lead to uncertainty in the outcomes.

Furthermore, an extensive LCIA was conducted, highlighting the actual environmental footprints of each solution across multiple environmental categories. The key findings highlighted the promising effect of hybridization on the environmental performance of future regional aircraft. As time progresses, the GWI of the various configurations decreases, thanks to efficiency improvements. However, some trade-offs emerge in non-CO_2-related environmental impact categories, preventing a definitive recommendation for any single configuration. Assuming that these trade-offs will be addressed by research and industrial efforts, FC options will dominate in the long term in light of their extreme advantages in most of the impact categories. On the other hand, the use of SAF in combination with conventional or hybrid architectures is recommendable as a short-term, temporary solution.

In this context, cost and environmental analyses were carried out downstream of the design activity, using the selected concepts as a starting point. The design of the concepts was guided by the desire to minimize the fuel consumed, while costs and LCA impacts were subsequently evaluated as figures of merit. However, the integration of cost and LCA analyses within the design loop could have led to the selection of different design parameters in light of the trade-offs encountered. Hence, future activity will consist of integrating the cost and environmental analyses into a more holistic aircraft design workflow. In particular, a future collaboration between the UNINA and DTU research groups is already planned, which aims to use the developed LCI datasets to integrate the LCIA directly into the design workflow even

more. In this sense, the study presented here, which culminated in the development of scalable LCI datasets, represents a significant initial stride towards incorporating LCA considerations into the preliminary design of innovative regional aircraft. This integration aims to capture all relevant trade-offs at the design stage, in order to achieve improved compromises between ecological and economic considerations compared to optimization based solely on direct pollutant emissions.

All in all, the study has demonstrated that, although challenges remain, integrating hybrid and electric propulsion systems into regional aircraft seems to represent a viable path toward the decarbonization of the sector. The technical, economic, and environmental results of the study were critically compared, electing the most promising scenarios for each time horizon. In building a roadmap toward future regional aviation, this thesis has outlined a strategic timeline for the development and deployment of hybrid and electric aircraft in the regional sector.

SAFs and battery systems, capable of supporting the EU's environmental targets, were identified as valid transition technologies in the short and medium terms, while waiting for hydrogen-based propulsive systems to mature sufficiently. In the long term, configurations based on hydrogen-powered FC systems are desired to dominate the regional aviation scenario, since they represent the preferential path towards achieving the complete decarbonization of regional flights by 2050. In parallel, the use of SAF may still be useful to support an increasingly sharp reduction in the use of kerosene for long-haul flights, but only if accompanied by intensified research for carbon-neutral production solutions.

The roadmap also implied recommendations for stakeholders, from manufacturers to policymakers, helping them navigate the complexities of this transformation journey. In particular, reflecting the gap in comprehensive research found in existing literature, it was found essential for key players in aviation to expand their environmental sustainability goals for future aircraft. In fact, as the significance of environmental impacts from aircraft flight operations diminishes over time, the focus shifts towards the predominance of other life-cycle activities, especially those related to airport operations and aircraft manufacturing. More research is needed to fully understand and manage all non-CO_2 climate effects related to the new technologies and alternative fuels, in order to identify the available mitigation solutions in time for their implementation. This is especially true in relation to expected increases in human toxicity. One additional concern about FC's water vapor emissions is the possible indirect effects on the formation of contrails.

The widespread diffusion of this new type of aircraft must be carefully guided through regulations and incentives aimed at the complete phase-out of fossil fuels and any other unsustainable energy source. This vision is based on the premise that the electricity grid is shifting toward low-carbon energy sources, industries are getting more efficient and electrified, and low-carbon hydrogen is abundant. Without these conditions, the comparative environmental benefits of hybridization may be significantly reduced due to a higher energy and material demand.

All of the recommendations gathered have been tailored for the 50-passenger regional turboprop aircraft analyzed, but having identified all of the major key

technologies, they are deemed scalable for aircraft with more passengers and medium-haul flights. Currently, European research is already active, in the context of Clean Aviation, in the investigation of aircraft with up to 100 passengers [18]. Dedicated studies will try to demonstrate if it is possible to aspire to the same benefits also for that class of aircraft. Only by embracing the funding opportunities offered by governments and including environmental sustainability targets in the design of new aircraft and infrastructure, will it be possible to achieve the set goals. In conclusion, preliminary designers have a pivotal role in reshaping the aviation paradigm, but cannot succeed without engaging in dialogue with technical experts, certification entities, policymakers, aircraft operators, and all other stakeholders involved. Such close collaboration is seen as a fundamental element for a successful transition towards environmentally and economically sustainable aviation, ultimately leading to the genesis of a greener and more prosperous future.

Appendices

A

Appendix A: Generalized Model of a Hybrid-Electric Powertrain

Contents

A.1 Powertrain Scheme

In this appendix, the general hybrid-electric powertrain model introduced in Chapter 2 will be discussed in more detail. The mathematical model represents a generalization of the approach originally proposed by de Vries et al. [26], based on sets of linear powertrain equations that reflect the operating mode of the versatile components of the system. The model is suitable for integration into preliminary design chains for hybrid-electric aircraft, flexibly allowing for any combination of conventional or alternative energy sources. Figure A.1 represents a slightly more detailed version of the diagram shown in Chapter 2. The model allows for the integration of up to 5 energy sources, including two groups of electric storage systems, two thermal engines, and an FC system. The fuel used by thermal machines (and FCs) may also differ from that suggested by the figure, without any loss of generality. In this sense, the fuel used for thermal machines can be kerosene, hydrogen, or any mixture of SAF. Up to 3 propeller lines can be included, representing conventional propellers or DEP. Accompanied by an adequate mass estimation model, the powertrain model enables the description of any conventional, hybrid-electric, or full-electric architecture. Some of the nodes present in Fig. A.1 may be absent, causing the general model to degenerate into more specific schemes. These include parallel, serial, turbo-electric, and hybrid-electric architectures with a variable number of power sources. Furthermore, each group of components in the figure is representative of an arbitrary number of units. In the figure, it is also assumed that power offtakes can be taken indiscriminately from each power source or directly from the bus (PMAD) in order to supply power to secondary systems onboard.

Related Publications

This chapter represents an anticipation of a future publication currently in preparation, which will be submitted to an internationally respected journal (e.g., Aerospace Science and Technology). The article will offer a more in-depth description of the model accompanied by appropriate case studies. Provisional authors and title are presented below:

[94] **Valerio Marciello**, Giuseppe Grazioso, Vittorio Trifari, Mario Di Stasio, Michele Tuccillo, Manuela Ruocco, Fabrizio Nicolosi. *A General and Robust Powertrain Equations Model for Preliminary Design of Hybrid-Electric Aircraft.*

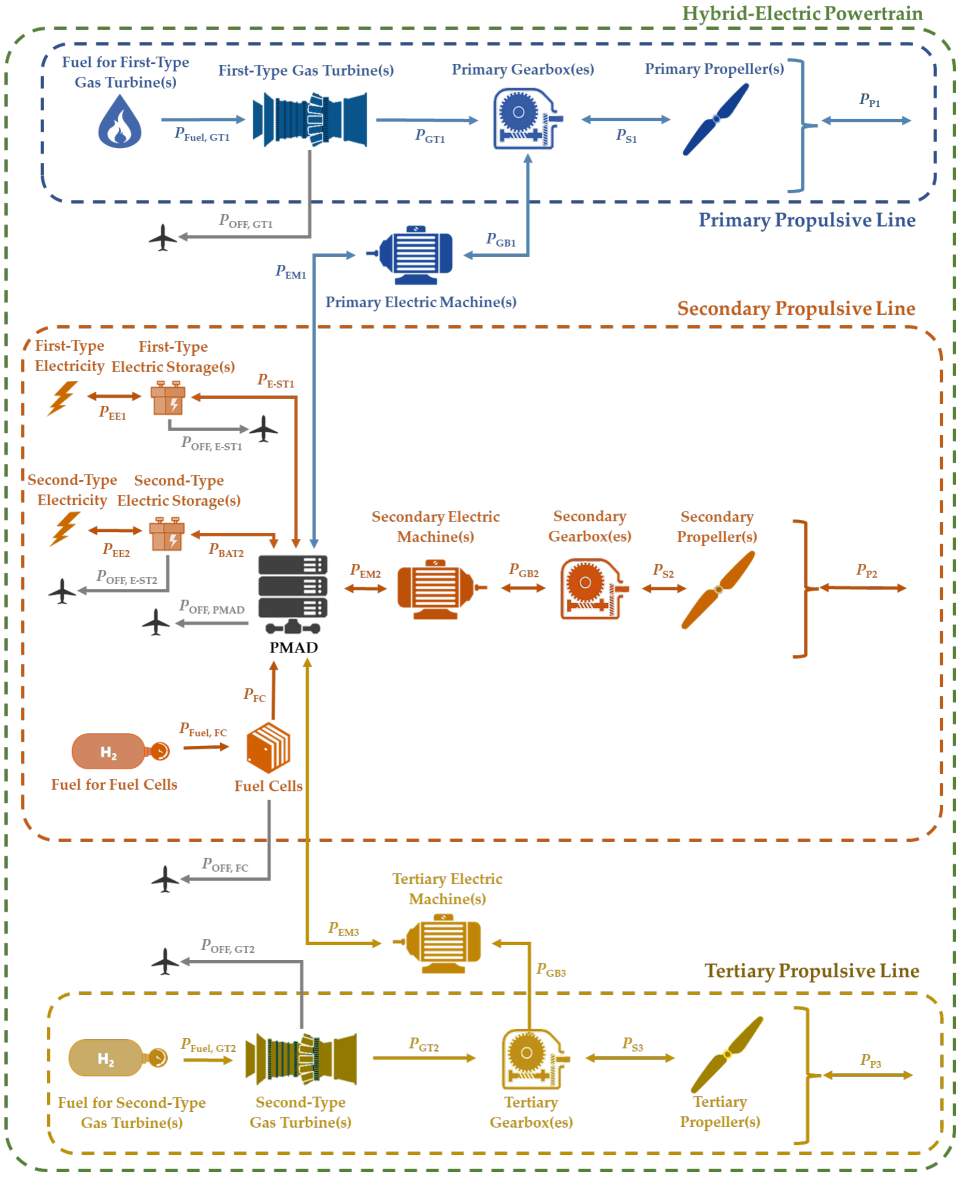

Figure A.1: The most general propulsive architecture model, featuring up to five energy sources, supplying power to up to three propeller lines. The scheme also includes power offtakes from the energy sources and the PMAD.

A.2 Generalized Powertrain Equations

Equations (A.1) propose a generalization of the powertrain equations designed to describe the model in Fig. A.1 in any of its operating modes. The system of equations may be solved iteratively, starting from the knowledge of the total propulsive power given by the sum of the contributions of all the propulsion lines. However, the system can be conveniently inverted as a function of non-zero power related to any other power node. The coefficients Φ_{i} represent the supplied power ratios, defined by Eq. (2.2), relating to the five power sources numbered as follows:

1. First-Type Thermal Engine.
2. First-Type Electric Storage.
3. Second-Type Electric Storage.
4. Fuel Cell System.
5. Second-Type Thermal Engines.

Slightly different from the definition provided in Chapter 2, supplied power ratios in this context are defined as the ratio of the output power of each power supplier, divided by the total power, thus excluding the effect of the source efficiencies on their values. As for the shaft power ratios φ_{i}, they are defined by Eq. (2.3) as the fraction of shaft power referred, respectively, to:

1. Primary Propulsive Line.
2. Secondary Propulsive Line.
3. Tertiary Propulsive Line.

Finally, the power offtakes referring to the energy sources and the PMAD appear in the vector of known terms of Eqs. (A.1).

A.3 Operating Modes

The coefficients $K_{\mathrm{i,j}}$ that appear in the system matrix of Eqs. (A.1) vary depending on the operating mode of the system. Table A.1 reports the values of the coefficients for each combination of the behaviors of the versatile components. Seven components with versatile behavior are identified in the system, including the primary and tertiary electrical machines, the three propeller types, and the two electrical storage systems. Although secondary electric machines can also work as motors and generators, the choice of their operating mode has not been considered free as it is constrained by the behavior of the secondary propellers. In this sense, the secondary electric machines will work as motors when the associated propellers generate thrust, or as generators to convert the energy harvested from the external airflow. In total, of the $2^7 = 128$ combinations of operating modes of the other seven versatile components, only 68 are recognized as logically valid, and are listed in Tab. A.2. As already discussed in Chapter 2 regarding simpler propulsion schemes, the feasibility of an operating mode may depend on the specific circumstance, i.e., on the specific combination of efficiencies and hybridization ratios. In this sense, the author suggests that Eqs. (A.1) are coupled with an algorithm for dynamically

$$
\begin{bmatrix}
-\Phi_1 & 0 & 1 & 0 & 0 & 0 & 0 & 0 & 0 & 0 & 0 & 0 & 0 & 0 & 0 & 0 & 0 & 0 & 0 & 0 & 0 & 0 & 0 \\
0 & -\eta_{\mathrm{GT1}} & 1 & 0 & 0 & 0 & 0 & 0 & 0 & 0 & 0 & 0 & 0 & 0 & 0 & 0 & 0 & 0 & 0 & 0 & 0 & 0 & 0 \\
0 & 0 & 0 & K_{3,4} & K_{3,5} & 0 & 0 & 0 & 0 & 0 & 0 & 0 & 0 & 0 & 0 & 0 & 0 & 0 & 0 & 0 & 0 & 0 & 0 \\
0 & 0 & 0 & 0 & K_{4,5} & K_{4,6} & 0 & K_{4,8} & 0 & K_{4,10} & 0 & 0 & -\eta_{\mathrm{PMAD}} & K_{4,14} & 0 & 0 & 0 & 0 & 0 & 0 & 0 & 0 & 0 \\
0 & 0 & 0 & 0 & 0 & K_{5,6} & K_{5,7} & 0 & 0 & 0 & 0 & 0 & 0 & 0 & 0 & 0 & 0 & 0 & 0 & 0 & 0 & 0 & 0 \\
-\Phi_2 & 0 & 0 & 0 & 0 & 1 & 0 & 0 & 0 & 0 & 0 & 0 & 0 & 0 & 0 & 0 & 0 & 0 & 0 & 0 & 0 & 0 & 0 \\
0 & 0 & 0 & 0 & 0 & 0 & 0 & K_{7,8} & K_{7,9} & 0 & 0 & 0 & 0 & 0 & 0 & 0 & 0 & 0 & 0 & 0 & 0 & 0 & 0 \\
-\Phi_3 & 0 & 0 & 0 & 0 & 0 & 0 & 1 & 0 & 0 & 0 & 0 & 0 & 0 & 0 & 0 & 0 & 0 & 0 & 0 & 0 & 0 & 0 \\
0 & 0 & 0 & 0 & 0 & 0 & 0 & 0 & 0 & 0 & 0 & 0 & 0 & 0 & 0 & 0 & (1-\varphi_1) & -\varphi_1 & -\varphi_1 & 0 & 0 & 0 & 0 \\
0 & 0 & 0 & 0 & 0 & 0 & 0 & 0 & 0 & K_{10,10} & K_{10,11} & 0 & 0 & 0 & 0 & 0 & 0 & 0 & 0 & 0 & 0 & 0 & 0 \\
-\Phi_4 & 0 & 0 & 0 & 0 & 0 & 0 & 0 & 0 & 0 & 0 & 0 & 1 & 0 & 0 & 0 & 0 & 0 & 0 & 0 & 0 & 0 & 0 \\
0 & 0 & 0 & 0 & 0 & 0 & 0 & 0 & 0 & 0 & 0 & -\eta_{\mathrm{FC}} & 1 & 0 & 0 & 0 & 0 & 0 & 0 & 0 & 0 & 0 & 0 \\
0 & 0 & 0 & 0 & 0 & 0 & 0 & 0 & 0 & 0 & 0 & 0 & 0 & 0 & 0 & 0 & -\varphi_2 & (1-\varphi_2) & -\varphi_2 & 0 & 0 & 0 & 0 \\
-\Phi_5 & 0 & 0 & 0 & 0 & 0 & 0 & 0 & 0 & 0 & 0 & 0 & 0 & 0 & 0 & 1 & 0 & 0 & 0 & 0 & 0 & 0 & 0 \\
0 & 0 & 0 & 0 & 0 & 0 & 0 & 0 & 0 & 0 & 0 & 0 & 0 & -\eta_{\mathrm{GT2}} & 1 & 0 & 0 & 0 & 0 & 0 & 0 & 0 & 0 \\
0 & 0 & 0 & 0 & 0 & 0 & 0 & 0 & 0 & 0 & 0 & 0 & K_{16,14} & 0 & 0 & K_{16,17} & 0 & 0 & 0 & 0 & 0 & 0 & 0 \\
0 & 0 & -\eta_{\mathrm{GB1}} & K_{17,4} & 0 & 0 & 0 & 0 & 0 & 0 & 0 & 0 & 0 & 0 & 0 & 0 & K_{17,18} & 0 & 0 & 0 & 0 & 0 & 0 \\
0 & 0 & 0 & 0 & 0 & 0 & 0 & 0 & 0 & 0 & K_{18,11} & 0 & 0 & 0 & 0 & 0 & 0 & K_{18,19} & 0 & 0 & 0 & 0 & 0 \\
0 & 0 & 0 & 0 & 0 & 0 & 0 & 0 & 0 & 0 & 0 & 0 & 0 & 0 & 0 & -\eta_{\mathrm{GB3}} & K_{19,17} & 0 & K_{19,20} & 0 & 0 & 0 & 0 \\
0 & 0 & 0 & 0 & 0 & 0 & 0 & 0 & 0 & 0 & 0 & 0 & 0 & 0 & 0 & 0 & 0 & K_{20,18} & 0 & 0 & K_{20,21} & 0 & 0 \\
0 & 0 & 0 & 0 & 0 & 0 & 0 & 0 & 0 & 0 & 0 & 0 & 0 & 0 & 0 & 0 & 0 & 0 & K_{21,19} & 0 & 0 & K_{21,22} & 0 \\
0 & 0 & 0 & 0 & 0 & 0 & 0 & 0 & 0 & 0 & 0 & 0 & 0 & 0 & 0 & 0 & 0 & 0 & 0 & K_{22,20} & 0 & 0 & K_{22,23} \\
0 & 0 & 0 & 0 & 0 & 0 & 0 & 0 & 0 & 0 & 0 & 0 & 0 & 0 & 0 & 0 & 0 & 0 & 0 & 0 & 1 & 1 & 1
\end{bmatrix}
\begin{bmatrix}
P_{\mathrm{Supplied}} \\
P_{\mathrm{Fuel,\ GT1}} \\
P_{\mathrm{GT1}} \\
P_{\mathrm{GB1}} \\
P_{\mathrm{EM1}} \\
P_{\mathrm{E\text{-}ST1}} \\
P_{\mathrm{EE1}} \\
P_{\mathrm{E\text{-}ST2}} \\
P_{\mathrm{EE2}} \\
P_{\mathrm{EM2}} \\
P_{\mathrm{GB2}} \\
P_{\mathrm{Fuel,\ FC}} \\
P_{\mathrm{FC}} \\
P_{\mathrm{EM3}} \\
P_{\mathrm{Fuel,\ GT2}} \\
P_{\mathrm{GT2}} \\
P_{\mathrm{GB3}} \\
P_{\mathrm{S1}} \\
P_{\mathrm{S2}} \\
P_{\mathrm{S3}} \\
P_{\mathrm{P1}} \\
P_{\mathrm{P2}} \\
P_{\mathrm{P3}}
\end{bmatrix}
=
\begin{bmatrix}
0 \\
-P_{\mathrm{OFF,\ GT1}} \\
0 \\
-P_{\mathrm{OFF,\ PMAD}} \\
-P_{\mathrm{OFF,\ E\text{-}ST1}} \\
0 \\
-P_{\mathrm{OFF,\ E\text{-}ST2}} \\
0 \\
0 \\
0 \\
0 \\
-P_{\mathrm{OFF,\ FC}} \\
0 \\
0 \\
-P_{\mathrm{OFF,\ GT2}} \\
0 \\
0 \\
0 \\
0 \\
0 \\
0 \\
P_{\mathrm{P}}
\end{bmatrix}
\tag{A.1}
$$

verifying the feasibility of the mode. The latter can be verified by checking the sign of each power of the resulting power vector. Since the powers in all nodes are defined as positive, even a single negative value is indicative of a solution without physical meaning and, therefore, of an infeasible operating mode. Analysts are free to implement the strategy they prefer for managing such an eventuality, but an automatic switch to an alternative operating mode is recommended. In this sense, a possible logic consists in defining a preferential order of destination modes, which minimizes the differences compared to the original mode. Solving the powertrain equations will occur sequentially for each suggested operating mode, until a feasible (if any) operating mode is found.

Table A.1: Values of the coefficients $K_{\mathrm{i,j}}$ appearing in Eqs. (A.1) as a function of the operating mode of the versatile components of the propulsive scheme in Fig. A.1.

Parameter	**Operating Mode**	
	Primary Propeller	
	Thrust	**Harvest**
$K_{\mathbf{17,18}}$	1	$-\eta_{\mathrm{GB1}}$
$K_{\mathbf{20,18}}$	$-\eta_{\mathrm{P1}}$	1
$K_{\mathbf{20,21}}$	1	$-\eta_{\mathrm{P1}}$
	Secondary Propeller	
	Thrust	**Harvest**
$K_{\mathbf{4,10}}$	1	$-\eta_{\mathrm{PMAD}}$
$K_{\mathbf{10,10}}$	$-\eta_{\mathrm{EM2}}$	1
$K_{\mathbf{10,11}}$	1	$-\eta_{\mathrm{EM2}}$
$K_{\mathbf{18,11}}$	$-\eta_{\mathrm{GB2}}$	1
$K_{\mathbf{18,19}}$	1	$-\eta_{\mathrm{GB2}}$
$K_{\mathbf{21,19}}$	$-\eta_{\mathrm{P2}}$	1
$K_{\mathbf{21,22}}$	1	$-\eta_{\mathrm{P2}}$
	Tertiary Propeller	
	Thrust	**Harvest**
$K_{\mathbf{19,20}}$	1	$-\eta_{\mathrm{GB3}}$
$K_{\mathbf{22,20}}$	$-\eta_{\mathrm{P3}}$	1
$K_{\mathbf{22,23}}$	1	$-\eta_{\mathrm{P3}}$
	Primary Electric Machine	
	Motor	**Generator**
$K_{\mathbf{3,4}}$	1	$-\eta_{\mathrm{EM1}}$
$K_{\mathbf{3,5}}$	$-\eta_{\mathrm{EM1}}$	1
$K_{\mathbf{4,5}}$	1	$-\eta_{\mathrm{PMAD}}$
$K_{\mathbf{17,4}}$	$-\eta_{\mathrm{GB1}}$	1
	Tertiary Electric Machine	
	Motor	**Generator**
$K_{\mathbf{4,14}}$	1	$-\eta_{\mathrm{PMAD}}$
$K_{\mathbf{16,14}}$	$-\eta_{\mathrm{EM3}}$	1
$K_{\mathbf{16,17}}$	1	$-\eta_{\mathrm{EM3}}$
$K_{\mathbf{19,17}}$	$-\eta_{\mathrm{GB3}}$	1
	First-Type Electric Storage	
	Discharge	**Charge**
$K_{\mathbf{4,6}}$	$-\eta_{\mathrm{PMAD}}$	1
$K_{\mathbf{5,6}}$	1	$-\eta_{\mathrm{E\text{-}ST1}}$
$K_{\mathbf{5,7}}$	$-\eta_{\mathrm{E\text{-}ST1}}$	1
	Second-Type Electric Storage	
	Discharge	**Charge**
$K_{\mathbf{4,8}}$	$-\eta_{\mathrm{PMAD}}$	1
$K_{\mathbf{7,8}}$	1	$-\eta_{\mathrm{E\text{-}ST2}}$
$K_{\mathbf{7,9}}$	$-\eta_{\mathrm{E\text{-}ST2}}$	1

Table A.2: List of feasible operating modes for the propulsive architecture represented in Fig. A.1.

Index	Primary Propeller	Secondary Propeller	Tertiary Propeller	First-Type Electric Storage	Second-Type Electric Storage	Primary Electric Machine	Tertiary Electric Machine
1	Thrust	Thrust	Thrust	Discharge	Discharge	Motor	Motor
2	Thrust	Thrust	Thrust	Discharge	Discharge	Motor	Generator
3	Thrust	Thrust	Thrust	Discharge	Discharge	Generator	Motor
4	Thrust	Thrust	Thrust	Discharge	Discharge	Generator	Generator
5	Thrust	Thrust	Thrust	Discharge	Charge	Motor	Motor
6	Thrust	Thrust	Thrust	Discharge	Charge	Motor	Generator
7	Thrust	Thrust	Thrust	Discharge	Charge	Generator	Motor
8	Thrust	Thrust	Thrust	Discharge	Charge	Generator	Generator
9	Thrust	Thrust	Thrust	Charge	Discharge	Motor	Motor
10	Thrust	Thrust	Thrust	Charge	Discharge	Motor	Generator
11	Thrust	Thrust	Thrust	Charge	Discharge	Generator	Motor
12	Thrust	Thrust	Thrust	Charge	Discharge	Generator	Generator
13	Thrust	Thrust	Thrust	Charge	Charge	Motor	Motor
14	Thrust	Thrust	Thrust	Charge	Charge	Motor	Generator
15	Thrust	Thrust	Thrust	Charge	Charge	Generator	Motor
16	Thrust	Thrust	Thrust	Charge	Charge	Generator	Generator
17	Thrust	Thrust	Harvest	Discharge	Discharge	Motor	Generator
18	Thrust	Thrust	Harvest	Discharge	Discharge	Generator	Generator
19	Thrust	Thrust	Harvest	Discharge	Charge	Motor	Generator
20	Thrust	Thrust	Harvest	Discharge	Charge	Generator	Generator
21	Thrust	Thrust	Harvest	Charge	Discharge	Motor	Generator
22	Thrust	Thrust	Harvest	Charge	Discharge	Generator	Generator
23	Thrust	Thrust	Harvest	Charge	Charge	Motor	Generator
24	Thrust	Thrust	Harvest	Charge	Charge	Generator	Generator
25	Thrust	Harvest	Thrust	Discharge	Discharge	Motor	Motor
26	Thrust	Harvest	Thrust	Discharge	Discharge	Motor	Generator
27	Thrust	Harvest	Thrust	Discharge	Discharge	Generator	Motor
28	Thrust	Harvest	Thrust	Discharge	Charge	Motor	Motor
29	Thrust	Harvest	Thrust	Discharge	Charge	Motor	Generator
30	Thrust	Harvest	Thrust	Discharge	Charge	Generator	Motor
31	Thrust	Harvest	Thrust	Discharge	Charge	Generator	Generator
32	Thrust	Harvest	Thrust	Charge	Discharge	Motor	Motor
33	Thrust	Harvest	Thrust	Charge	Discharge	Motor	Generator
34	Thrust	Harvest	Thrust	Charge	Discharge	Generator	Motor
35	Thrust	Harvest	Thrust	Charge	Discharge	Generator	Generator
36	Thrust	Harvest	Thrust	Charge	Charge	Motor	Motor
37	Thrust	Harvest	Thrust	Charge	Charge	Motor	Generator
38	Thrust	Harvest	Thrust	Charge	Charge	Generator	Motor
39	Thrust	Harvest	Thrust	Charge	Charge	Generator	Generator
40	Thrust	Harvest	Harvest	Discharge	Discharge	Motor	Generator
41	Thrust	Harvest	Harvest	Discharge	Charge	Motor	Generator
42	Thrust	Harvest	Harvest	Discharge	Charge	Generator	Generator
43	Thrust	Harvest	Harvest	Charge	Discharge	Motor	Generator
44	Thrust	Harvest	Harvest	Charge	Discharge	Generator	Generator
45	Thrust	Harvest	Harvest	Charge	Charge	Motor	Generator
46	Thrust	Harvest	Harvest	Charge	Charge	Generator	Generator
47	Harvest	Thrust	Thrust	Discharge	Discharge	Generator	Motor
48	Harvest	Thrust	Thrust	Discharge	Discharge	Generator	Generator
49	Harvest	Thrust	Thrust	Discharge	Charge	Generator	Motor
50	Harvest	Thrust	Thrust	Discharge	Charge	Generator	Generator
51	Harvest	Thrust	Thrust	Charge	Discharge	Generator	Motor
52	Harvest	Thrust	Thrust	Charge	Discharge	Generator	Generator
53	Harvest	Thrust	Thrust	Charge	Charge	Generator	Motor
54	Harvest	Thrust	Thrust	Charge	Charge	Generator	Generator
55	Harvest	Thrust	Harvest	Discharge	Discharge	Generator	Generator
56	Harvest	Thrust	Harvest	Discharge	Charge	Generator	Generator
57	Harvest	Thrust	Harvest	Charge	Discharge	Generator	Generator
58	Harvest	Thrust	Harvest	Charge	Charge	Generator	Generator
59	Harvest	Thrust	Thrust	Discharge	Discharge	Generator	Motor
60	Harvest	Harvest	Thrust	Discharge	Charge	Generator	Motor
61	Harvest	Harvest	Thrust	Discharge	Charge	Generator	Generator
62	Harvest	Harvest	Thrust	Charge	Discharge	Generator	Motor
63	Harvest	Harvest	Thrust	Charge	Discharge	Generator	Generator
64	Harvest	Harvest	Thrust	Charge	Charge	Generator	Motor
65	Harvest	Harvest	Thrust	Charge	Charge	Generator	Generator
66	Harvest	Harvest	Harvest	Discharge	Charge	Generator	Generator
67	Harvest	Harvest	Harvest	Charge	Discharge	Generator	Generator
68	Harvest	Harvest	Harvest	Charge	Charge	Generator	Generator

B

Appendix B: Fault-Tolerance Considerations for Hybrid-Electric Aircraft

Contents

B.1 Introduction

This appendix reports a parallel study conducted by the author in the field of failure management for hybrid-electric architectures. Inspired by the candidate's participation in the ELICA project [16], this work was originally published in the Chinese Journal of Aeronautics [93], and is referenced here to complement the discussion of Chapter 3.

According to Farokhi, the use of hybrid-electric powerplants with a large number of propulsion elements has the potential to mitigate the risk of thrust loss compared to conventional aircraft with 2-4 engines [346]. At the same time, as the number of failure points increases, adequate considerations about safety management need to be pursued. An accurate estimation of benefits related to hybrid-electric architectures is only possible provided that the adopted design chain integrates aerodynamics, structures, propulsion, mission, and performance analysis in optimal synergy [347, 348]. When a failure occurs, hybrid architectures, composed of a multitude of interconnected electric and thermal units, can manifest very different behaviours with respect to conventional architectures. The probability of failure of new components, such as electric machines and battery packs, must also be taken into consideration.

In fact, it cannot be determined a priori whether the worst-case scenario is associated with the failure of an electric or conventional component. Therefore, a simulation-based approach becomes of fundamental importance when analyzing critical flight phases. In literature, there is a lack of methodologies suitable for the early design phases of a new aircraft, when the powertrain architecture and its operating characteristics are not yet well defined. Accurate deductive fault-tolerance analysis approaches, including fault-tree analysis, exist to accomplish risk assessment, but would require a level of system definition that is too advanced for the purposes of the conceptual design. For example, refined studies of Clarke et al. [52] are not suitable for the early stages of a project, when the definition of the propulsive architecture is far from being complete, and the rate of failure of the components could be a mirage for the designer. While certification specifications for hybrid-electric aircraft have not been defined yet, some key hazards have been identified by Courtin and Hansman [349], strongly depending on the number of propulsors, powered lift, as well as on the altitude of operations. When investigating a new concept, it is only possible to quantitatively assess the probability of failure through a risk matrix, while assuming that the aircraft will be certified with a regulation code similar to Part 23 [138]. A more detailed analysis can be carried out only once the aircraft configuration is frozen in every single sub-component, which is not usually the case in preliminary design stages. During the preliminary design of a new airplane, the emphasis is rather on its performance and on the design of the overall architecture. In this sense, the present work focuses on the evaluation of the benefits deriving from hybrid-electric propulsion featuring DEP related to the design of the vertical tailplane. Klunk et al. [350] suggest that DEP can enable significant reductions in the required vertical tail size. Nguyen et al. [351] analyzed the influence of an engine failure, highlighting that aircraft using differential thrust have the potential for reducing the vertical tail surface area up to 45%. However, they did not focus on the multiple possible failure scenarios characterizing hybrid-electric powertrains. Bendarkar et al. [352] focused on the failure rate compliance of powertrain architecture components without any considerations on power redistribution or operating modes of the powertrain.

The systematic approach proposed in this appendix tries to fill this gap, covering the analysis of multiple failure scenarios, regardless of the adopted powertrain architecture and the number and type of its components. An overview of a mathematical model for failure simulation will be presented, including notes on the redefinition of the classic idea of *critical engine*. The model described in the next section allows for a preliminary evaluation of the effects of a failure of any element of the hybrid-electric powertrain, in terms of maximum thrust loss or maximum yaw moment. The proposed method aims to be easy to implement, general, and accurate at the same time, trying to fill a gap in the literature due to the almost infinite multitude of possible hybrid-electric architectures. The definition of the OEI condition will be generalized, after which a strategy will be proposed to simulate the failure for any architecture, degree of hybridization, and operating mode. The calculation of thrust and propulsive power distribution will be coupled with the

estimation of the minimum control speed when airborne, including certification considerations and aerodynamic effects. Due to the computational burden of the method, implemented in MATLAB® language, it was not directly integrated into the design workflow but rather used for a subsequent evaluation of the controllability of the aircraft. The case study of Section B.3 will concern an intermediate assessment of the hybrid-electric 19-seat aircraft concept designed for the ELICA project [16], and will aim to demonstrate the potential advantages that a DEP architecture offers in terms of thrust redistribution and controllability.

Related Publications

The content of this appendix reflects the original content of the following journal article by the same author:

[93] **Valerio Marciello**, Francesco Orefice, Fabrizio Nicolosi, Danilo Ciliberti, and Pierluigi Della Vecchia. *Design of Hybrid-Electric Aircraft with Fault-Tolerance Considerations*. Chinese Journal of Aeronautics, 36(2):160–178, 2023.

B.2 Failure Occurrence and Risk Management

B.2.1 Failure Scenarios

The development of aircraft is closely tied to compliance with ever-evolving airworthiness standards. These standards, which integrate new technologies with heightened safety measures, are pivotal in guiding aircraft design. On the other hand, regulatory bodies adapt and update standards based on these novel designs. In this context, *aircraft controllability* is defined as the aircraft's ability to respond to the pilot' control regarding flight path and attitude. According to regulations CS-23 §23.143 and CS-25 §25.143 [138, 139], an airplane must be controllable and maneuverable throughout all flight phases, including maintaining lateral-directional control under nominal and OEI conditions. These regulatory demands can restrict design options, particularly impacting the development of hybrid-electric aircraft [353]. In situations like propulsion system failure, lateral-directional controllability is linked to the *minimum control speed*, defined in CS-23 §23.149 and CS-25 §25.149 [138, 139]. This speed is the lowest at which an aircraft can be controlled with a non-operational engine, maintaining a bank angle below 5 degrees. For CS-23 and CS-25 certified aircraft, this speed must not exceed 1.2 and 1.13 times the stall speed, respectively [138, 139]. Hybrid-electric aircraft require extensive optimization in the early design stages. Unlike conventional aircraft, where yaw moment assessment and vertical tailplane sizing are based on the engine contributing most to yaw, hybrid aircraft with multiple power sources necessitate a new definition of the OEI condition. As a matter of fact, the failure of a single component in these interconnected systems can variably affect the remaining units. In highly hybridized systems with the architecture depicted in Fig. 2.2, the critical

condition may stem from a battery pack or an electric motor rather than a thermal engine. Thus, the analysis shifts from identifying the critical engine to determining the critical unit in the system, meaning one of the following:

- One thermal engine inoperative.
- One primary electric machine inoperative.
- One secondary electric machine inoperative.
- One battery pack inoperative.

In this context, electric buses will not be considered significant failure points in light of their high mean time to failure [354]. The methodology discussed in the following aims to simulate the scenarios mentioned above. More complex scenarios will be neglected as their probability is not considered a major risk at the preliminary design level. Farhoki estimates the failure rate of modern gas turbine engines to be very low, around 5×10^{-5} per flight hour [346]. When distributed propulsion is achieved with 10 small-sized thermal engines, the probability that two or more of them fail simultaneously is in the order of 10^{-7}, or even lower if gas turbines are replaced with more reliable electric motors, making multiple-failure scenarios extremely rare and categorizable as "extremely remote" or "extremely improbable" [355, 356]. Additionally, since power distribution aids in mitigating the impact of thrust loss during a failure, such events are unlikely to result in catastrophic outcomes. For these reasons, in the interest of simplicity and due to the low likelihood of such events, complex scenarios involving multiple independent failures will be neglected from the discussion. The powertrain model based on powertrain equations, already discussed in Section 2.2.1, considers the overall powers associated with electric motors, thermal engines, and battery systems, under the hypothesis that the power is homogeneously distributed on similar parts. This means that the power exchanged by the isolated physical unit is obtainable by dividing the overall power of the group by the number of units. In this sense, the presented powertrain equations do not allow to capture the effects of the asymmetry produced by the occurrence of a failure.

B.2.2 Powertrain Subsystems

To address this problem, an initial step consists of detailing the definition of the propulsion architecture. To this end, it is convenient to subdivide the propulsion system into an arbitrary number of *subsystems*, where one subsystem is a generic set of units capable of electrical or mechanical energy exchanges with each other. The designer is let free to define the configuration, specifying subsystems containing different combinations of thermal engines, electric motors, and battery packs, and that can be symmetrical or asymmetrical relative to the aircraft's centerline. Units may also belong to multiple subsystems, sharing power accordingly. The choice of the best architecture may take into account factors like safety, reliability, maintenance, cabling weight, and optimizing performance in emergency conditions. The example proposed in Fig. B.1 shows a solution that consists of a division into two subsystems, the first including all the propulsive units installed on the left wing, the other for the right wing, with one battery pack connected to each group.

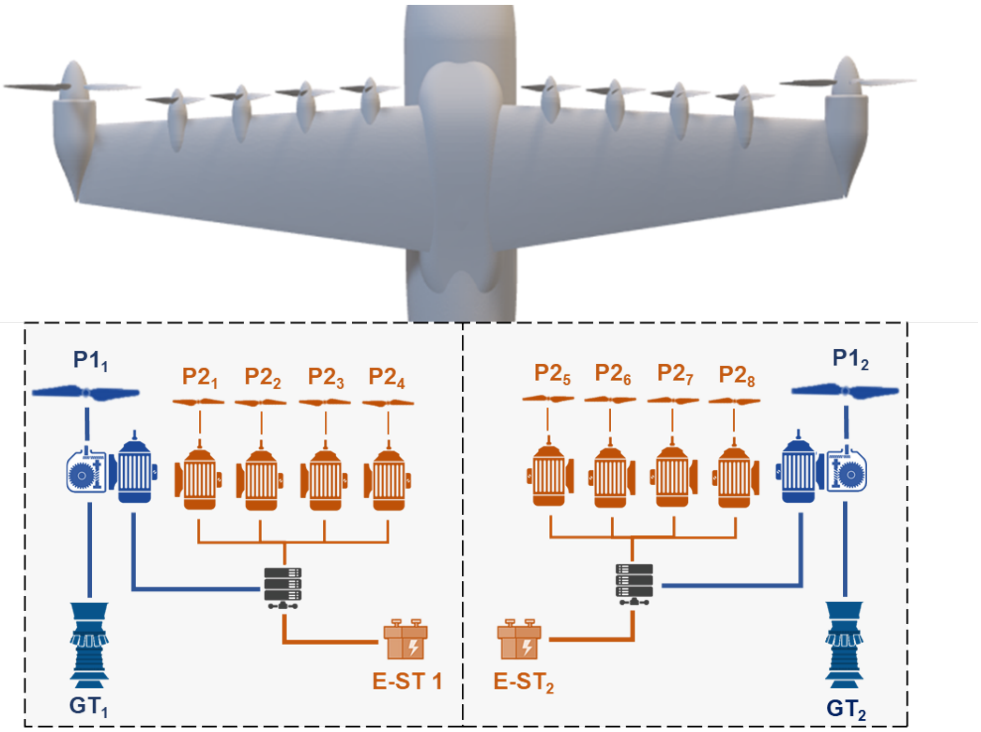

Figure B.1: An example of subdivision of the propulsion system into two subsystems (adapted from Ref. [93]).

In the example of Fig. B.1, as a first approximation, the designer could assume that the worst-case scenario is characterized by the failure of the thermal engine, inducing a loss of power and thrust also on the secondary propellers in the case that the primary electric machine was working as a generator. A conservative assumption could be to consider a thrust loss factor of 50%, as in the case of a conventional architecture with two engines. However, this assumption may be too approximate and simplistic in the case of high levels of hybridization. First, the most critical condition may not be linked to the thermal engine, especially in the presence of high hybridization or secondary propellers generating significant yawing moments. Also, the impact of a failure varies based on the operating mode prior to the failure occurrence. For instance, if secondary electric machines are partly powered by a battery and a thermal engine, a failure of the latter only partially reduces the secondary thrust. Moreover, advanced architectures offer benefits like cabling weight reduction, redundancies, and enhanced directional controllability, influencing factors like the number of propulsion elements, their rated power, the length of cables, and even tailplane size. Therefore, accurately modeling hybrid propulsion networks early in the design process is crucial to exploit these potentials. Additionally, risk management should consider how the PMAD is designed, with strategies to handle excess power through redistribution of the residual energy or by battery power modulation.

B.2.3 Failure Occurrence

In the event of a failure, evaluating the power loss in each affected power node is crucial. This involves using modified powertrain equations tailored to the specific operating mode and damaged element. Considering the nine operating modes of Tab. 2.1 and the four types of damageable elements listed above, 36 unique failure scenarios emerge. An additional nine scenarios account for the possibility of a primary electric machine non-decoupling from the corresponding thermal engine, for a total of 45 cases. However, the number of scenarios can be reduced for simpler implementation, depending on the relevance of the associated risk. The initial step is to divide the propulsion system into subsystems, which can be done through a user interface allowing to select the connected elements. Elements can belong to multiple subsystems, and there are no limits on the number or type of elements in each subsystem. A hybrid-electric subsystem may include a varying number of battery packs, thermal engines, electric motors, and generators, while a full-electric system could be broken down into several subsystems with at least one battery pack and one electric machine each. A conventional setup simply involves a non-zero number of thermal engines.

Determining the worst-case scenario requires simulating each element's failure to identify the most critical case. Two criteria can guide this identification:

- The minimum power or thrust criterion.
- The maximum yaw moment criterion.

The first criterion is particularly relevant for climb and take-off certification constraints, while the second one is crucial for directional control and vertical tailplane sizing. The two criteria might not coincide with the same failure scenario due to the different distances of the involved propulsive units from the aircraft's CG. The analysis of the power distribution immediately after a failure involves specific equations to redirect energy flow, either automatically or controlled. For instance, for the particular architecture described in Fig. B.1 and operating in mode 1 of Tab. 2.1, the failure of a right-wing thermal engine affects not only its primary propulsion unit but also the corresponding secondary half-system, with significant implications if the battery usage is low. Conversely, in mode 4, failure of the thermal engine does not completely disable the primary propeller thanks to the battery backup, allowing for less conservative design considerations.

For operating mode 1, Eqs. (2.7) are solved as many times as the number of subsystems, starting from the fraction of power associated with the thermal machines belonging to it. In Eq. (B.1), $p_{\mathrm{GT,AEO}}$ is the power related to the gas turbine of a specific subsystem in AEO conditions, $P_{\mathrm{GT,AEO}}$ is related to the complete system, N_1 is the total number of thermal engines in the system, and n_1 is the number of thermal engines in the subsystem only.

$$p_{\mathrm{GT,AEO}} = P_{\mathrm{GT,AEO}} \cdot \left(\frac{n_1}{N_1}\right) \tag{B.1}$$

Total powers at the system level can be obtained by summing all single subsystem contributions by virtue of the linearity of the powertrain equations. In the event

of failure of a thermal engine, while the system is operating in mode 1, Eqs. (B.2) can be applied to all subsystems containing the damaged element.

$$\begin{bmatrix} p_{\text{Fuel,OEI}} \\ p_{\text{GT,OEI}} \\ p_{\text{GB1,OEI}} \\ p_{\text{S1,OEI}} \\ p_{\text{EM1,OEI}} \\ p_{\text{E-ST,OEI}} \\ p_{\text{EM2,OEI}} \\ p_{\text{S2,OEI}} \\ p_{\text{P1,OEI}} \\ p_{\text{P2,OEI}} \\ p_{\text{P,OEI}} \end{bmatrix} = \begin{bmatrix} f_1 & 0 & 0 & 0 & 0 & 0 & 0 & 0 & 0 & 0 \\ 0 & f_1 & 0 & 0 & 0 & 0 & 0 & 0 & 0 & 0 \\ 0 & 0 & f_1 & 0 & 0 & 0 & 0 & 0 & 0 & 0 \\ 0 & 0 & 0 & f_1 & 0 & 0 & 0 & 0 & 0 & 0 \\ 0 & 0 & 0 & 0 & f_1 & 0 & 0 & 0 & 0 & 0 \\ 0 & 0 & 0 & 0 & 0 & 1 & 0 & 0 & 0 & 0 \\ 0 & 0 & 0 & 0 & \eta_{\text{PMAD}}\, f_1 & \eta_{\text{PMAD}} & 0 & 0 & 0 & 0 \\ 0 & 0 & 0 & 0 & \eta_{\text{EM2}}\, \eta_{\text{PMAD}}\, f_1 & \eta_{\text{EM2}} \eta_{\text{PMAD}} & 0 & 0 & 0 & 0 \\ 0 & 0 & 0 & 0 & 0 & 0 & 0 & f_1 & 0 & 0 \\ 0 & 0 & 0 & 0 & \eta_{\text{P2}}\, \eta_{\text{EM2}}\, \eta_{\text{PMAD}}\, f_1 & \eta_{\text{P2}}\, \eta_{\text{EM2}}\, \eta_{\text{PMAD}} & 0 & 0 & 0 & 0 \\ 0 & 0 & 0 & 0 & \eta_{\text{P2}}\, \eta_{\text{EM2}}\, \eta_{\text{PMAD}}\, f_1 & \eta_{\text{P2}}\, \eta_{\text{EM2}}\, \eta_{\text{PMAD}} & 0 & f_1 & 0 & 0 \end{bmatrix} \begin{bmatrix} p_{\text{Fuel,AEO}} \\ p_{\text{GT,AEO}} \\ p_{\text{GB1,AEO}} \\ p_{\text{S1,AEO}} \\ p_{\text{EM1,AEO}} \\ p_{\text{E-ST,AEO}} \\ 0 \\ 0 \\ p_{\text{P1,AEO}} \\ 0 \\ 0 \end{bmatrix} \tag{B.2}$$

In Eqs. (B.2), f_1 represents the fraction of residual primary units. The number of residual primary propulsion units is trivially equal to $n_1 - 1$ when the failed engine is not shared with any other subsystem. The definition given in Eq. (B.3) generalizes the residual fraction to the case of elements that are shared with (i.e., belong only partially to) the subsystem affected by the failure.

$$f_1 = \left(\sum_{i=1}^{n_1} \alpha_{1,i} \right) - \alpha_{1,\text{Failed}} \tag{B.3}$$

In Eq. (B.3), α_1 represents the share percentages of the single primary propulsion unit belonging to the subsystem. The value of $\alpha_{1,i}$ is 1 if the engine is connected only to the subsystem under analysis, and it is 0 when it does not belong to it. If the same thermal engine powers two distinct subsystems, it will be associated with a value of $\alpha_{1,i}$ equal to 0.5, and its failure will consequently determine for both subsystems a power loss equal to half the power of one engine. While the propulsive power produced by the primary propeller must be zero, the propulsive power of the primary propellers not affected by the failure is given by Eq. (B.4).

$$p_{\text{P1},i \neq \text{Failed}} = \frac{p_{\text{P1,OEI}}}{n_1 \cdot f_1} \tag{B.4}$$

Previous equations only apply to subsystems directly affected by the failure, i.e., those including the damaged element. Finally, the overall system powers are obtained as the sum of the powers of all subsystems. Each failure scenario requires the implementation of a specific version of Eqs. (B.2) and an ad-hoc procedure for each operating mode. For the purposes of the present work, the implementation has been realized for the 45 scenarios already discussed above.

To keep the discussion concise, it would be impractical to delve into every possible combination of operating mode and failure type. Thus, this subsection will be concluded with a final example concerning the failure of a secondary electric motor in operating mode 4. The corresponding algorithm is schematized in Fig. B.2. In the first place, the loss of one secondary electric machine does not alter the power output of the thermal engine or the primary electric motors belonging to the same subsystem. Analysts may then consider various scenarios. One possibility is

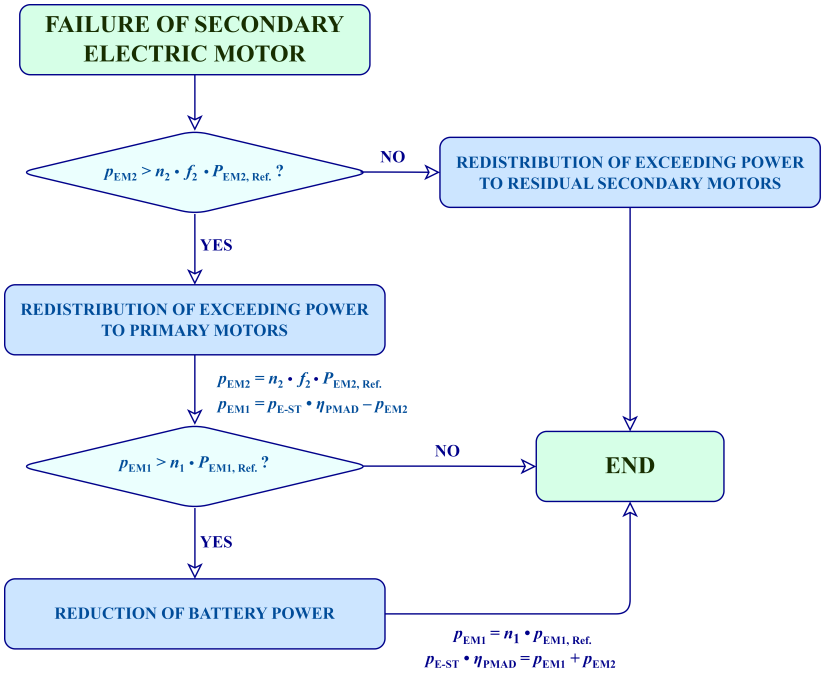

Figure B.2: Algorithm for the simulation of secondary electric motor failure in operating mode 4 (adapted from Ref. [93]).

to hypothesize that the exchange of electric power between the battery and the primary line remains unchanged, assuming either the failed motor still runs idle consuming the same battery power, or that this power is redistributed to the $n_2 \cdot f_2$ residual secondary motors by the PMAD system. Alternatively, the battery power might be reduced to prevent waste, particularly if the failed motor was the only one in its subsystem. To prevent power overload, a change in operating mode also takes place automatically when needed. The approach preferred in this context is to redistribute excess battery power among all motors in the same (secondary) propulsion line. The first attempt involves distributing the power demand of the failed motor (denoted as p_{EM2}) among the remaining secondary engines. This aims to maintain the same shaft power, up to the individual motors' power limits. If this limit is reached, the PMAD system then redirects excess power to the primary electric motors in respect of their maximum power (indicated with subscript *Ref.*). Finally, if no solutions are found to continue producing the same power as before the failure, the battery power is appropriately reduced.

B.2.4 Analysis of Lateral-Directional Controllability

In general, it is not possible to disengage the fault-tolerance analysis from a multidisciplinary approach that also keeps the aerodynamics and performance of the aircraft under control. In particular, the design of the vertical tailplane is driven by the need to balance the maximum yaw moment that may result from a failure. Therefore, the criterion to be taken into account, in this case, is the maximum yaw

moment. Once the worst-case scenario is identified (i.e., the critical unit is known), the thrust distribution immediately after the failure can be determined. Minimum control speed when airborne, V_{MC}, is defined as the minimum calibrated airspeed at which the aircraft is controllable. Regulation for CS-23 aircraft requires that V_{MC} does not exceed $1.2\,V_{\mathrm{Stall,1}}$, where $V_{\mathrm{Stall,1}}$ is the stall speed at MTOM. At this speed, it is necessary that lateral, directional, and longitudinal controls are still effective, and the aircraft should sustain straight flight while maintaining an equilibrium bank angle ϕ of no more than 5 degrees [138, 139]. Achieving this condition requires specific aileron (δ_a) and rudder (δ_r) deflections, making the control systems' maximum deflection angles crucial in the determination of V_{MC}. The bank angle is essential to counterbalance the intense force from the vertical plane with a component of the aircraft's weight in the same direction. Equations (B.5) are instrumental in solving this problem in the unknowns δ_a, V_{MC}, and the sideslip angle β.

$$\begin{bmatrix} C_{\mathrm{Y}_\beta} & C_{\mathrm{Y}_{\delta_a}} & \dfrac{2\,\mathrm{MTOM}\,g}{\rho_\infty S_{\mathrm{w}}}\tan\phi \\ C_{\mathcal{N}_\beta} & C_{\mathcal{N}_{\delta_a}} & \dfrac{2\,\mathcal{N}_{\mathrm{Eng}}}{\rho_\infty S_{\mathrm{w}}\, b_{\mathrm{w}}} \\ C_{\mathcal{L}_\beta} & C_{\mathcal{L}_{\delta_a}} & 0 \end{bmatrix} \begin{bmatrix} \beta \\ \delta_a \\ {V_{\mathrm{MC}}}^{-2} \end{bmatrix} = \begin{bmatrix} -\,C_{\mathrm{Y}_{\delta_r}} \cdot \delta_r \\ -\,C_{\mathcal{N}_{\delta_r}} \cdot \delta_r \,-\, C_{\mathcal{N}_{\mathrm{Eng}}} \\ -\,C_{\mathcal{L}_{\delta_r}} \cdot \delta_r \end{bmatrix} \tag{B.5}$$

The system is modeled with three equations involving three unknowns, with the bank angle set at 5 degrees or adjusted as needed, based on the yaw moment direction. Setting the rudder deflection angle to its maximum value helps lower the minimum control speed. For this reason, it is not considered an unknown in the equations but rather an input value. While ϕ aids in countering lateral forces due to the use of side-directional controls, less than 5 degrees may be sufficient for equilibrium. The crucial aspect is ensuring that ϕ stays within its limit and that the aileron's deflection angle does not surpass the maximum value set by the designer. In Eqs. (B.5), g is the gravitational acceleration, $C_{\mathcal{N}_{\mathrm{Eng}}}$ is the yawing moment coefficient due to drag asymmetry from windmilling propellers, $\mathcal{N}_{\mathrm{Eng}}$ is the propulsive yawing moment, $C_{\mathcal{L}}$ is the rolling moment coefficient, $C_{\mathcal{N}}$ is the yawing moment coefficient, and C_{Y} is the side force coefficient. Their derivatives with respect to δ_{a}, δ_{r}, and β are also involved in the equilibrium equations along lateral, roll, and yaw axes. All coefficients should be evaluated in take-off conditions. If the aerodynamic derivatives are non-linearly dependent on the control surfaces' deflection angles, these equations might require iterative solutions.

The failure tolerance analysis consists of several steps shown in Fig. B.3. Initially, the minimum control speed is set equal to the regulatory limit, which helps determine thrust distribution for the most critical failure scenario. Aerodynamic coefficients are calculated based on the specified flight condition. Subsequently, Eqs. (B.5) are solved to update V_{MC}. The failure occurrence can be followed by a redistribution of the power among the still functioning units, in order to mitigate the yawing moment. This involves redirecting the power flow towards propellers that are closer to the CG. In cases of thermal engine or electric machine failures, the supplied power ratio of the subsystems is adjusted to reduce the yawing moment. In case of

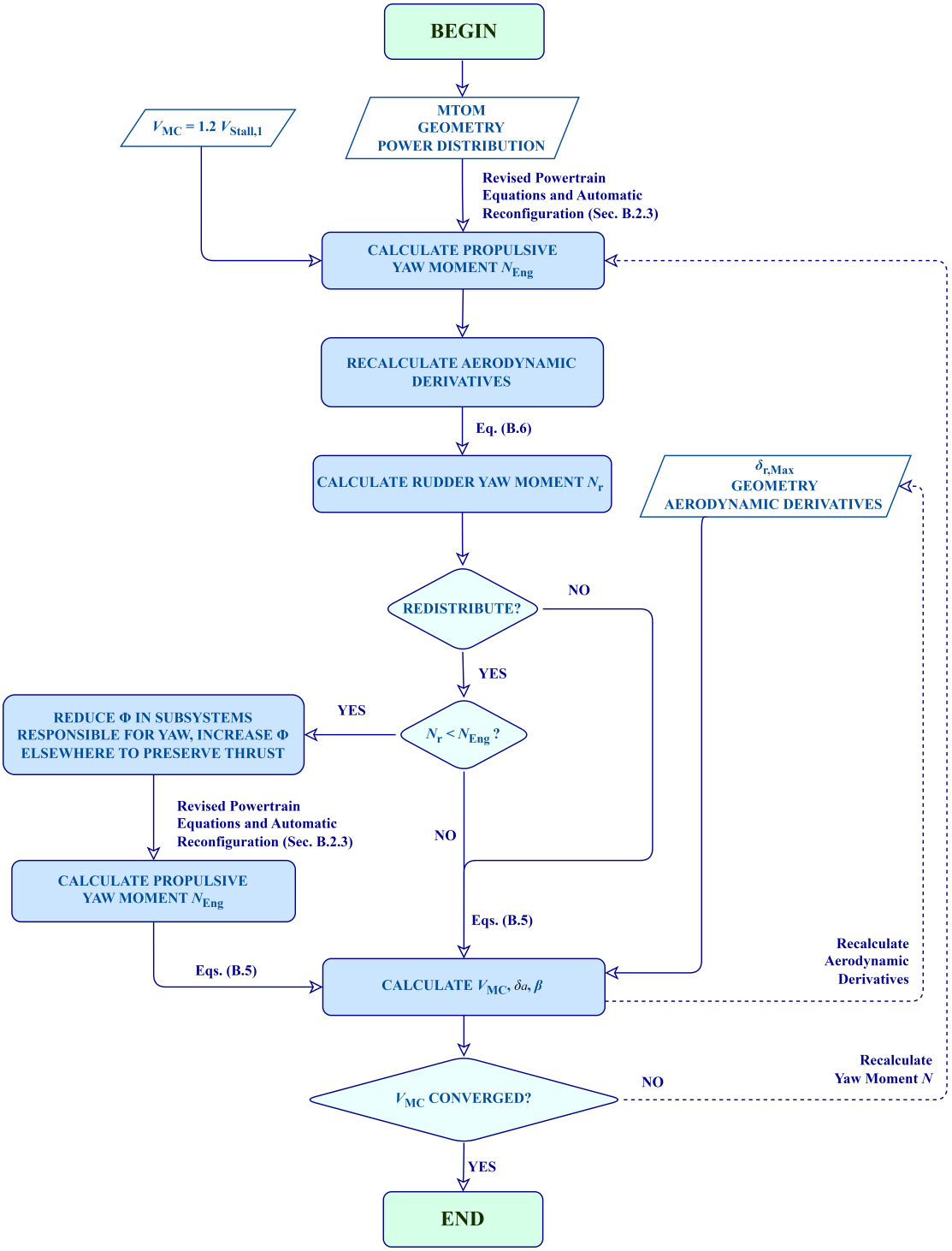

Figure B.3: Algorithm for the calculation of the minimum control speed for a single failure scenario (adapted from Ref. [93]).

battery pack failures, the power directed to the subsystems that are responsible for the yaw moment is decreased. However, in the latter case, the redistribution might lead to an additional thrust penalty. Splitting the battery into multiple battery packs can minimize this issue. In general, the redistribution aims to lower the

yawing moment to an acceptable level, possibly matching the rudder's effectiveness at the same speed, given by Eq. (B.6). In the equation, S_{w} is the wing area, b_{w} is the wing span, and ρ_∞ is the air density.

$$\mathcal{N}_r = \frac{1}{2}\,\rho_\infty\, V_{\mathrm{MC}}^2\, S_{\mathrm{w}}\, b_{\mathrm{w}}\, C_{\mathcal{N}_{\delta_r}}\, \delta_r \tag{B.6}$$

The process is repeated iteratively until convergence, with each iteration re-evaluating aero-propulsive interactions, especially significant in the presence of disruptive technologies like DEP. When the worst-case scenario is unpredictable, the algorithm simulates each failure scenario sequentially, considering the highest V_{MC} obtained. When the resulting minimum control speed is higher than the limit certification value, designers can opt for different strategies, like automatically adjusting the vertical tailplane size to enhance directional control. This change requires recalculating the aircraft's aerodynamics from scratch. Adjustments to the propulsive architecture or mission strategy might also be necessary to meet requirements. Failure analysis is completed by the verification that the residual thrust is still sufficient to meet requirements, assessing BFL and ceiling altitude in the worst-case scenario with minimal residual thrust. Climb performance is checked against certification limits for the rate of climb and climb gradient, referring to sections §CS 23.65, §CS 23.67, §CS 23.77 of Part 23 and §CS 25.111, §CS 25.119, §CS 25.121 for Part 25 regulations [138, 139]. The entire procedure, integrated into the design chain, may necessitate an increase in installed power (electric or thermal) if any constraints are not met.

To summarize, the whole procedure can be described by the following main steps:

1. Definition of TLARs and selection of the propulsive architecture.
2. Aircraft sizing with initialization of geometry, installed powers, masses, and aerodynamics.
3. Subdivision of the propulsion system into subsystems.
4. Selection of the failure point to be simulated.
5. Determination of propulsive efficiencies and available power (e.g., from efficiency maps) in take-off conditions.
6. Calculation of power distribution in all subsystems by means of powertrain equations.
7. Recalculation of power distribution in the subsystems affected by the failure, e.g., by means of Eqs. (B.2).
8. If the operating mode and the scenario require it, application of further redistribution logics (e.g., Fig. B.2 in case of failed secondary electric machine operating in mode 4).
9. Calculation of the total residual thrust, and of the propulsive yaw moment as the sum of the cross products of the distances from the CG and the thrusts.
10. Repetition of steps 4–9 for each failure scenario considered.
11. Identification of worst-case scenario according to the maximum yaw moment criterion.

12. Calculation of the rudder yaw moment by means of Eq. (B.6), based on a first-attempt value of V_{MC}.
13. If no redistribution is applied after the failure occurrence, the minimum control speed, and sideslip and aileron deflection angles are calculated by means of Eqs. (B.5).
14. If a redistribution strategy based on supplied battery power is implemented, the supplied power is increased for subsystems affected by the failure, and reduced elsewhere. Hence, V_{MC} is calculated via Eqs. (B.5).
15. In case of redistribution, repetition of steps 4–12 and 14 until the maximum propulsive yaw moment falls below the available rudder moment, or until no further redistribution is possible.
16. Repetition of steps 4–15 until convergence of the V_{MC}.
17. If the minimum control speed exceeds the certification limit, the vertical tailplane is enlarged to improve directional controllability, and aerodynamic coefficients and masses are updated accordingly. Alternatively, the safety margin with respect to the certification limit is reduced. Hence, repetition of steps 4–16.
18. Repetition of steps 4–10 in climb conditions and identification of the worst-case scenario based on the minimum residual thrust criterion, for the verification of the prescriptions on climb gradient.
19. If one or more requirements are not met, the propulsion system is resized. Hence, repetition of steps 4–18.
20. If the result is not considered satisfactory by the designer, the whole procedure is repeated, choosing a different propulsive architecture or partitioning into subsystems.

For the present application, steps No. 1 and No. 2 are carried out by means of HEAD, but any other design chain is suitable for the purpose, provided that it is capable of characterizing the geometry, masses, and aerodynamics of the aircraft and that hybrid-electric propulsion is modeled by means of powertrain equations. The algorithm's computational time can vary up to a few minutes, depending on the chosen convergence thresholds as well as on the characteristics of the workstation. A linear complexity has been inferred for the algorithm, justified by the fact that each scenario is simulated at each iterative step [93]. In light of the linear complexity of the algorithm, for an efficient implementation into a preliminary design chain, it is recommended to restrict the number of failure scenarios to the most likely ones.

The next section will present a sample application whose purpose is to demonstrate how including failure-tolerance and lateral-directional controllability considerations at the preliminary design level may benefit the final result.

B.3 Application

B.3.1 Case Study

This last section presents the results of an application on a hybrid-electric commuter aircraft with 19 seats, designed for the purposes of the ELICA project [16]. The application concerns the EIS 2025 concept featuring a series/parallel partial hybrid architecture with 8 DEPs. In particular, the analysis was conducted on an intermediate assessment of the concept, slightly different from the second-loop results discussed in Section 3.4. The assumed propulsive architecture is similar to the one visualized in Fig. B.1, characterized by 4 distributed electrically-driven propellers per each half-wing, uniquely associated with one battery pack and one gas turbine, for a total of two thermal engines and two battery packs in the system. The reference geometry is described in Tab. B.1. The two primary propellers are located at 33% of the wingspan, while the 4 DEPs are distributed between 52% and 100% of the span. Values of $\Phi = 0.05$ and $\varphi = 0.8$ were selected for take-off. Table B.2 lists the rated powers, i.e., the maximum powers that can be exchanged by every single element of the propulsion system. Table B.3 reports the aerodynamic derivatives useful for the calculation of V_{MC} by means of Eqs. (B.5).

B.3.2 Results and Discussion

Table B.4 presents the results of the simulation for all possible failure scenarios, detailing both yaw moments and propulsive power losses. The most critical scenario is visibly associated with the failure of a gas turbine. Battery failures appear less critical in this case, given the low value of the supplied power ratio. When dealing with the failure of secondary electric motors, the scenario gets complex due to the potential worst-case scenario linked to distributed propellers located far from the CG. Nevertheless, this imbalance can be significantly reduced by redirecting the power originally intended for the failed motor toward the remaining electric motors in the same subsystem. This process can continue until the electric motors reach their reference power capacity. At this point, any remaining power is diverted to the primary propulsion line, forcing the primary electric machine to change its behavior from generator to motor. This translates into a change in the subsystem's operating mode (from 1 to 4), as previously explained in Fig. B.2. This procedure not only helped balance the system but also enhanced the overall efficiency of the system, leading to a slight increase in thrust post-failure. A similar approach is applied in the event of a generator failure, where the gas turbine's output is rerouted to primary propellers.

As already highlighted above, gas turbines represent the most critical elements, also due to the fact that their failure entails a loss of power on both propulsion lines. Therefore, the minimum control speed must be deduced from the simulation of this scenario. Figure B.4 represents both propulsive and aerodynamic yawing moments as the flight speed varies, where V_{MC} is localized by the intersection of the two

Table B.1: Main geometric parameters of a 19-passenger hybrid-electric concept (ELICA EIS 2025 concept; intermediate assessment).

Parameter	Value	Unit
Wing		
Wing Surface	33.94	m^2
Wing Span	22.58	m
Mean Aerodynamic Chord	1.78	m
Horizontal Tail		
Surface	10.60	m^2
Span	7.00	m
Mean Aerodynamic Chord	1.53	m
Distance from Aftmost CG	7.89	m
Vertical Tail		
Surface	8.63	m^2
Span	3.76	m
Mean Aerodynamic Chord	2.46	m
Distance from Aftmost CG	7.51	m
Fuselage		
Fuselage Length	16.25	m
Cross Section Diameter	2.15	m
Propellers		
Number of Primary Propellers	2	-
Primary Propeller Diameter	2.54	m
Primary Propeller No. 1 Y-Coordinate	−3.75	m
Primary Propeller No. 2 Y-Coordinate	3.75	m
Number of Secondary Propellers (DEP)	8	-
Secondary Propeller Diameter	1.77	m
Secondary Propeller No. 1 Y-Coordinate	−11.29	m
Secondary Propeller No. 2 Y-Coordinate	−9.51	m
Secondary Propeller No. 3 Y-Coordinate	−7.72	m
Secondary Propeller No. 4 Y-Coordinate	−5.94	m
Secondary Propeller No. 5 Y-Coordinate	5.94	m
Secondary Propeller No. 6 Y-Coordinate	7.72	m
Secondary Propeller No. 7 Y-Coordinate	9.51	m
Secondary Propeller No. 8 Y-Coordinate	11.29	m

Table B.2: Reference power of the main powerplant components.

Element	Power	Unit
Gas Turbine	782.4	kW
Primary Electric Generator	645.8	kW
Secondary Electric Motor	184.5	kW
Battery Pack	267.0	kW

curves. The aerodynamic yaw moment is produced by both the contribution of the sideslip angle and that of the control surfaces. The stall speed, which benefits from the aero-propulsive effects, is 43.1 m/s. The maximum take-off mass is 7 982 kg.

Figure B.4 demonstrates that a single gas turbine failure leads to a yawing moment surpassing the aerodynamic moment, resulting in a minimum control speed exceeding the regulatory limit. Consequently, the system was reconfigured to adhere to power limits and OEI performance standards for climb and take-off.

Table B.3: Aerodynamic parameters for the calculation of minimum control speed.

Parameter	Value	Unit
$\delta_{r,\mathrm{Max}}$	30.0	deg
$\delta_{a,\mathrm{Max}}$	20.0	deg
$C_{\mathcal{L}_\beta}$	−0.0033	deg^{-1}
$C_{\mathcal{L}_{\delta_r}}$	0.0043	deg^{-1}
$C_{\mathcal{L}_{\delta_a}}$	−0.0024	deg^{-1}
$C_{\mathcal{N}_\beta}$	0.0030	deg^{-1}
$C_{\mathcal{N}_{\delta_r}}$	−0.0011	deg^{-1}
$C_{\mathcal{N}_{\delta_a}}$	0.0000	deg^{-1}
C_{Y_β}	−0.0162	deg^{-1}
$C_{Y_{\delta_r}}$	0.0043	deg^{-1}
$C_{Y_{\delta_a}}$	0.0000	deg^{-1}

Table B.4: Total propulsive power loss and yaw moment resulting from the simulation of each failure scenario, without power redistribution. Propulsive power in AEO condition is 1 255.5 kW.

Failure Case	Yaw Moment (N m)	Diff. Propulsive Power (%)
Gas Turbine No. 1	−54 370.6	−41.6
Gas Turbine No. 2	+54 370.6	−41.6
Primary Electric Generator No. 1	−26 232.7	+4.1
Primary Electric Generator No. 2	+26 232.7	+4.1
Secondary Electric Motor No. 1	−27 281.4	+4.1
Secondary Electric Motor No. 2	−26 582.1	+4.1
Secondary Electric Motor No. 3	−25 883.2	+4.1
Secondary Electric Motor No. 4	−25 183.9	+4.1
Secondary Electric Motor No. 5	+25 183.9	+4.1
Secondary Electric Motor No. 6	+25 883.2	+4.1
Secondary Electric Motor No. 7	+26 582.1	+4.1
Secondary Electric Motor No. 8	+27 281.4	+4.1
Battery Pack No. 1	−10 123.2	−4.7
Battery Pack No. 2	+10 123.2	−4.7

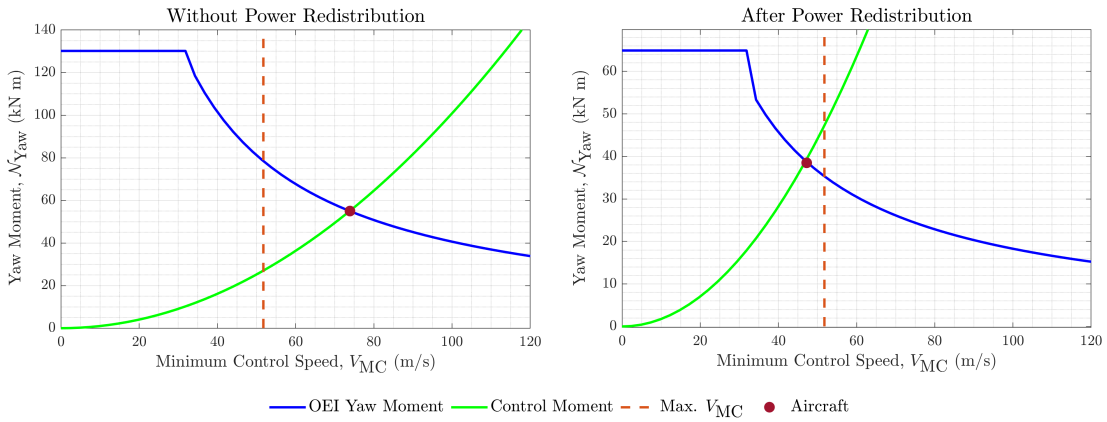

Figure B.4: Analysis of lateral-directional controllability, with and without power redistribution (adapted from Ref. [93]).

Specifically, in the case of a thermal engine failure, the power was redistributed by increasing the power supplied by the battery on the affected (right) half-wing, while proportionally increasing it on the other (left) side in order to preserve the same propulsive power. Table B.5 provides a detailed analysis of the effects of the left half-wing gas turbine failure, examining the power exchanged among propulsion elements before and after the failure. Table B.6 also includes minimum control speed values before and after this power redistribution. In particular, redistribution results in a notable decrease in both the net yawing moment and minimum control speed. The analysis reveals that, without any power redistribution strategy immediately after failure occurrence, V_{MC} would be higher than the certification limit. For this reason, it would be necessary to enlarge the vertical tailplane, or to opt for major changes in the aircraft configurations. However, the flexibility and the redundancy of hybrid-electric propulsion represent indeed two of their main advantages, so it is appropriate to fully exploit it by considering similar redistribution strategies that aim to minimize the required control moment.

Table B.5: Power distribution consequent to failure of gas turbine No. 1 (left half-wing).

Element	Unit	AEO Condition	Before Redistribution	After Redistribution
Primary Propeller No. 1	kW	121.2	0.0	0.0
Primary Propeller No. 2	kW	121.2	121.2	75.7
Primary Electric Generator No. 1	kW	632.1	0.0	0.0
Primary Electric Generator No. 2	kW	632.1	632.1	645.0
Secondary Propellers No. 1–4	kW	126.6	21.9	34.2
Secondary Propellers No. 5–8	kW	126.6	126.6	79.1
Secondary Electric Motors No. 1–4	kW	184.5	32.0	66.7
Secondary Electric Motors No. 5–8	kW	184.5	184.5	155.7
Battery Pack No. 1	kW	127.9	127.9	267.0
Battery Pack No. 2	kW	127.9	127.9	0.0

Table B.6: Main results from failure simulation of gas turbine No. 1, with and without power redistribution. The bank angle was conveniently set to -5 degrees for the resolution of Eqs. (B.5).

Parameter	Unit	Without Redistribution	With Redistribution
Yawing Moment	N m	−54 370.6	−38 721.7
Propulsive Power Loss	%	−41.6	−42.1
Minimum Control Speed	m/s	74.7	47.2
Aileron Deflection Angle	deg	1.19	8.61
Sideslip Angle	deg	4.29	−1.17
Bank Angle	deg	−5.00	−5.00

B.4 Conclusions

The present appendix wished to introduce an innovative method for evaluating the effects of a failure on an aircraft's controllability and design that is suitable for hybrid-electric aircraft. The definition of the OEI condition was generalized, after which a strategy was proposed to simulate the failure for a wide variety of hybrid-electric architectures, for any combination of operating mode and degree of hybridization. The proposed method can be integrated into the aircraft design workflow to support the conceptual design of the vertical tailplane in the case of hybrid aircraft with distributed electric propulsion. Future developments may consist of implementing the simulation of more complex powertrain systems and scenarios, including also multiple, stochastically independent failures. Considerations on failure rates may also be integrated into the algorithm by preliminarily and automatically selecting the most probable failure scenarios to be investigated. The application presented in the last section has highlighted the importance of properly considering fault-tolerance aspects to fully exploit the potential of hybrid-electric platforms. The worst-case scenario, identified as the failure of a thermal engine, led to a minimum control speed below the regulatory limit, but only if the battery power is redistributed to reduce the yawing moment. On the contrary, minimum control speed would result in being excessively high when no redistribution strategy is adopted, requiring a redesign of the vertical tailplane. This confirms both the advantageous flexibility of hybrid-electric architectures and the need for an accurate fault-tolerance analysis approach, suitable for the preliminary design stages.

Bibliography

[1] United Nations. The Paris Agreement. URL https://unfccc.int/process-and-meetings/the-paris-agreement. Accessed on 08/01/2024.

[2] Copernicus Climate Change Service, European Centre for Medium-Range Weather Forecasts. Global Temperature Trend Monitor, 2024. URL https://cds.climate.copernicus.eu/cdsapp#!/software/app-c3s-global-temperature-trend-monitor?tab=app. Accessed on 08/01/2024.

[3] International Civil Aviation Organization (ICAO). Innovation for a Green Transition – 2022 Environmental Report Aviation and Environment 2022, 2022. URL https://www.icao.int/environmental-protection/Documents/EnvironmentalReports/2022/ICAO%20ENV%20Report%202022%20F4.pdf. Accessed on 15/12/2023.

[4] Hannah Ritchie. Cars, planes, trains: where do CO2 emissions from transport come from?, 2020. URL https://ourworldindata.org/co2-emissions-from-transport. Accessed on 02/12/2023.

[5] Volker Grewe, Arvind Gangoli Rao, Tomas C. Grönstedt, Xisto, Florian Linke, Joris Melkert, Jan Middel, Barbara Ohlenforst, Simon Blakey, Simon Christie, Sigrun Matthes, and Katrin Dahlmann. Evaluating the Climate Impact of Aviation Emission Scenarios Towards the Paris Agreement Including COVID-19 Effects. *Nature Communications*, 12:3841, 2021. doi:10.1038/s41467-021-24091-y.

[6] Advisory Council for Aviation Research and Innovation in Europe (ACARE). *Fly the Green Deal*. 2022. URL https://www.acare4europe.org/wp-content/uploads/2022/06/20220815_Fly-the-green-deal_LR-1.pdf. Accessed on 25/05/2023.

[7] European Commission. EU Emissions Trading System (EU ETS), 2023. URL https://climate.ec.europa.eu/eu-action/eu-emissions-trading-system-eu-ets_en. Accessed on 25/05/2023.

[8] International Civil Aviation Organization (ICAO). Carbon Offsetting and Reduction Scheme for International Aviation (CORSIA). URL https://www.icao.int/environmental-protection/CORSIA/Pages/default.aspx. Accessed on 08/01/2024.

[9] Office for Official Publications of the European Communities. European Aeronautics: a Vision for 2020, 2001. URL https://www.acare4europe.org/sites/acare4europe.org/files/document/Vision%202020_0.pdf. Accessed on 21/10/2012.

[10] Air Transport Action Group (ATAG). Climate Change, 2008. URL https://www.atag.org/our-activities/climate-change.html. Accessed on 22/07/2011.

[11] BBC News. Europe push for greener aviation, 2008. URL http://news.bbc.co.uk/2/hi/europe/7228054.stm. Accessed on 13/01/2024.

[12] Clean Aviation. Clean Aviation – History, 2024. URL https://www.clean-aviation.eu/about-us/history. Accessed on 13/01/2024.

[13] European Commission. *Flightpath 2050. Europe's Vision for Aviation - Maintaining Global Leadership & Serving Society's Needs*. Publications Office of the European Union, 2011.

[14] Advisory Council for Aviation Research and Innovation in Europe (ACARE). Strategic Research & Innovation Agenda 2017 Update, 2017. URL https://open4aviation.at/resources/pdf/ACARE-Strategic-Research-Innovation-Volume-1.pdf. Accessed on 13/01/2024.

[15] Clean Sky 2 GENESIS Project. Project GENESIS – Gauging the ENvironmEntal Sustainability of electrIc aircraft Systems, Official Website, . URL https://www.genesis-cleansky.eu/. Accessed on 15/12/2023.

[16] Clean Sky 2 ELICA Project. Project ELICA – ELectric Innovative Commuter Aircraft, Official Website. URL https://www.elica-cleansky-project.eu/. Accessed on 15/12/2023.

[17] Emma Powell. The IRON project: The Future of Regional Aviation, 2022. URL https://dowty.com/innovation-news/the-iron-project-the-future-of-regional-aviation/. Accessed on 13/01/2024.

[18] Clean Sky 2 GENESIS Project. Project HERA – Hybrid Electric Regional Architecture, . URL https://project-hera.eu/home. Accessed on 13/01/2024.

[19] Council of the European Union. Fit for 55. URL https://www.consilium.europa.eu/en/policies/green-deal/fit-for-55-the-eu-plan-for-a-green-transition/. Accessed on 13/01/2024.

[20] European Commission. European Green Deal: new rules agreed on applying the EU emissions trading system in the aviation sector, 2022. URL https://ec.europa.eu/commission/presscorner/detail/en/ip_22_7609. Accessed on 27/06/2023.

[21] International Air Transport Association (IATA). Aircraft Technology Roadmap to 2050. Technical report, International Air Transport Association (IATA), 2019. URL `https://www.sipotra.it/wp-content/uploads/2020/03/Aircraft-Technology-Roadmap-to-2050.pdf`. Accessed on 13/01/2024.

[22] International Air Transport Association (IATA). Net Zero Roadmaps. URL `https://www.iata.org/en/programs/environment/roadmaps/`. Accessed on 13/01/2024.

[23] ATR. Delivering Sustainable Connections. Turboprop Market Forecast 2022-2041, 2022. URL `https://www.atr-aircraft.com/wp-content/uploads/2022/07/ATR_Market-Forecast_2022_Digital_HD.pdf`. Accessed on 14/01/2024.

[24] International Council on Clean Transportation (ICCT). *CO2 Emissions From Commercial Aviation: 2013, 2018, and 2019*. 2020.

[25] Karim Abu Salem, Giuseppe Palaia, and Alessandro A. Quarta. Review of hybrid-electric aircraft technologies and designs: Critical analysis and novel solutions. *Progress in Aerospace Sciences*, 141:100924, 2023. doi:10.1016/j.paerosci.2023.100924.

[26] Reynard de Vries, Malcom T. Brown, and Roelof Vos. Preliminary Sizing Method for Hybrid-Electric Distributed-Propulsion Aircraft. *Journal of Aircraft*, 56(6), 2019. doi:10.2514/1.C035388.

[27] Mark Voskuijl, Joris van Bogaert, and Arvind G. Rao. Analysis and Design of Hybrid Electric Regional Turboprop Aircraft. *CEAS Aeronautical Journal*, 9(1):15–25, 2018. ISSN 18695590. doi:10.1007/s13272-017-0272-1.

[28] Kevin R. Antcliff, Mark D. Guynn, Ty Marien, Douglas P. Wells, Steven J. Schneider, and Mike J. Tong. Mission analysis and aircraft sizing of a hybrid-electric regional aircraft. In *54th AIAA Aerospace Sciences Meeting*, San Diego, California, 2016. doi:10.2514/6.2016-1028.

[29] Felix D. Finger, Cees Bil, and Carsten Braun. Comparative Assessment of Parallel-Hybrid-Electric Propulsion Systems for Four Different Aircraft. *Journal of Aircraft*, 57(5), 2020. doi:10.2514/1.C035897.

[30] Vincenzo Palladino, Arnaud Jordan, Nathalie Bartoli, Peter Schmollgruber, Valérie Pommier-Budinger, and Emmanuel Benard. Preliminary studies of a regional aircraft with hydrogen-based hybrid propulsion. In *AIAA Aviation 2021 Forum*, Virtual event, 2021. doi:10.2514/6.2021-2411.

[31] Jona Eissele, Stefan Lafer, Cristian Mejía Burbano, Julian Schließus, Tristan Wiedmann, Jonas Mangold, and Andreas Strohmayer. Hydrogen-Powered Aviation - Design of a Hybrid-Electric Regional Aircraft for Entry into Service in 2040. *Aerospace*, 10(3):277, 2020. doi:10.3390/aerospace10030277.

[32] Egbert Torenbeek. *Syntesis of Subsonic Airplane Design*. 1976.

[33] Barnes W. McCormick. *Aerodynamics, Aeronautics, and Flight Mechanics*. John Wiley & Sons Ltd., 1979.

[34] Jan Roskam. *Airplane Design. Part VIII: Airplane Cost Estimation: Design, Development, Manufacturing and Operating*. 1990.

[35] Lloyd Jenkinson, Paul Simpkin, and Darren Rhodes. *Civil Jet Aircraft Design*. 1999. doi:10.2514/4.473500.

[36] Leland M. Nicolai and Grant E. Carichner. *Fundamentals of Aircraft and Airship Design. Volume I – Aircraft Design*. American Institute of Aeronautics and Astronautic, Inc., 2010.

[37] Ajoy Kumar Kundu. *Aircraft Design*. 2012. ISBN 9780521885164.

[38] Antonio Filippone. *Advanced Aircraft Flight Performance*. Cambridge University, 2012. doi:10.1017/CBO9781139161893.

[39] Egbert Torenbeek. *Advanced Aircraft Design*. John Wiley & Sons, Ltd., 2013.

[40] Snorri Gudmundsson. *General Aviation Aircraft Design: Applied Methods and Procedures*. Elsevier Inc., 2013. ISBN 9780123973085. doi:10.1016/C2011-0-06824-2.

[41] Pasquale M. Sforza. *Commercial Airplane Design Principles*. 2014. ISBN 9780124199538. doi:10.1016/C2012-0-00332-8.

[42] Ed Obert. *Aerodynamic Design of Transport Aircraft*. IOS press, 2009.

[43] Trevor M. Young. *Performance of the Jet Transport Airplane: Analysis Methods, Flight Operations and Regulations*. John Wiley & Sons, 2017. doi:10.1002/9781118534786.

[44] NASA Langley Research Center. Flight Optimization System (FLOPS) Software v.9. URL `https://software.nasa.gov/software/LAR-18934-1`. Accessed on 20/01/2024.

[45] ALR Aerospace, DARcorporation, and RUAG. Aircraft Performance Program (APP). URL `https://www.darcorp.com/aircraft-performance-program-software/`. Accessed on 20/01/2024.

[46] Lyssys Ltd. Piano, Official Website. URL `http://www.piano.aero`. Accessed on 20/01/2024.

[47] Reynard De Vries, Maurice F.M. Hoogreef, and Roelof Vos. Range equation for hybrid-electric aircraft with constant power split. *Journal of Aircraft*, 57 (3), 2023. doi:10.2514/1.C035734.

[48] Aman Batra, Reiko Raute, and Robert Camilleri. On the Range Equation for Hybrid-Electric Aircraft. *Aerospace*, 10(8):687, 2023. doi:10.3390/aerospace10080687.

[49] Nicholas K. Borer and Michael D. Patterson. X-57 High-Lift Propeller Control Schedule Development. In *AIAA Aviation 2020 Forum*, Virtual event, 2016. doi:10.2514/6.2020-3091.

[50] Michael D. Patterson and Nicholas K. Borer. Approach considerations in aircraft with high-lift propeller systems. *Proceedings of the 17th AIAA Aviation Technology, Integration, and Operations Conference*, 2017. doi:10.2514/6.2017-3782.

[51] Karen A. Deere, Jeffrey K. Viken, Melissa B. Viken, Sally A. Carter, Michael R. Wiese, and Norma Farr. Computational analysis of a wing designed for the X-57 distributed electric propulsion aircraft. In *35th AIAA Applied Aerodynamics Conference*, Denver, Colorado, 2017. doi:10.2514/MAPA17.

[52] Sean Clarke, Matthew Redifer, Kurt Papathakis, Aamod Samuel, and Trevor Foster. X-57 Power and Command System Design. *2017 IEEE Transportation and Electrification Conference and Expo, ITEC 2017*, pages 393–400, 2017. doi:10.1109/ITEC.2017.7993303.

[53] Giuseppe Palaia, Davide Zanetti, Karim Abu Salem, Vittorio Cipolla, and Vincenzo Binante. THEA-CODE: a design tool for the conceptual design of hybrid-electric aircraft with conventional or unconventional airframe configurations. *Mechanics & Industry*, 22(19), 2021. doi:10.1051/meca/2021012.

[54] Benedikt Aigner, Philipp Strathoff, and Eike Stumpf. MICADO: Recent Developments of Models for Design and Evaluation of Electric Aircraft Propulsion Systems. In *Deutscher Luft- und Raumfahrtkongress 2020*, Virtual event, 2021. doi:10.25967/530051.

[55] PACE Aerospace & IT. Pacelab APD & SysArc. URL `https://pace.txtgroup.com/products/preliminary-design/pacelab-apd-for-engineers-by-engineers`. Accessed on 16/01/2024.

[56] Jonas Mangold, Dominik Eisenhut, Felix Brenner, Nicolas Moebs, and Andreas Strohmayer. Preliminary hybrid-electric aircraft design with advancements on the open-source tool SUAVE. *Journal of Physics: Conference Series*, 2526: 012022, 2023. doi:10.1088/1742-6596/2526/1/012022.

[57] Dominik Eisenhut, Jonas Mangold, Nicolas Moebs, Felix Brenner, and Andreas Strohmayer. Case study on hybrid-electric aircraft designs enabled by an enhanced SUAVE version. *Journal of Physics: Conference Series*, 2526:012019, 2022. doi:10.1088/1742-6596/2526/1/012019.

[58] Stanford Aerospace Design Lab. SUAVE 2.5: Design Dreams Come Alive. URL `https://suave.stanford.edu/`. Accessed on 20/01/2024.

[59] Jacopo Zamboni, Roelof Vos, Mathias Emeneth, and Alexander Schneegans. A method for the conceptual design of hybrid electric aircraft. In *AIAA Scitech 2019 Forum*, San Diego, California, 2019. ISBN 9781624105784. doi:10.2514/6.2019-1587.

[60] Felix D. Finger, Reynard de Vries, Roelof Vos, Carsten Braun, and Cees Bil. A Comparison of Hybrid-Electric Aircraft Sizing Methods. In *AIAA Scitech 2020 Forum*, Orlando, Florida, 2020. doi:10.2514/6.2020-1006.

[61] Lea Rupcic, Eleonore Pierrat, Karen Saavedra-Rubio, Nils Thonemann, Chizoba Ogugua, and Alexis Laurent. Environmental impacts in the civil aviation sector: Current state and guidance. *Transportation Research Part D: Transport and Environment*, 119:103717, 2023. doi:10.1016/j.trd.2023.103717.

[62] International Organization for Standardization (ISO). ISO 14044:2006. Environmental management -– Life Cycle Assessment – Requirements and Guidelines, 2006.

[63] International Organization for Standardization (ISO). ISO 14040:2006. Environmental management -– Life Cycle Assessment – Principles and Framework, 2006.

[64] Duran Calisir, Selcuk Ekici, Adnan Midilli, and Tahir Hikmet Karakoc. A review on environmental impacts from aviation sector in terms of life cycle assessment. *International Journal of Global Warming*, 22:211–234, 2020. doi:10.1504/IJGW.2020.110299.

[65] Patrick Schmidt, Valentin Batteiger, Arne Roth, Werner Weindorf, and Tetyana Raksha. Power-to-Liquids as Renewable Fuel Option for Aviation: A Review. *Chemie Ingenieur Technik*, 90(1-2):127–140, 2018. doi:10.1002/cite.201700129.

[66] Ben W. Kolosz, Yang Luo, Bing Xu, M. Mercedes Maroto-Valer, and John M. Andresen. Life cycle environmental analysis of 'drop in' alternative aviation fuels: a review. *Sustainable Energy & Fuels*, 4:3229–3263, 2020. doi:10.1039/c9se00788a.

[67] Fiona Greer, Jasenka Rakas, and Arpad Horvath. Airports and environmental sustainability: a comprehensive review. *Environmental Research Letters*, 15: 103007, 2020. doi:10.1088/1748-9326/abb42a.

[68] Cristiano Facanha and Arpad Horvath. Evaluation of life-cycle air emission factors of freight transportation. *Environmental Science & Technology*, 41: 7138–7144, 2007. doi:10.1021/es070989q.

[69] Mikhail V. Chester and Arpad Horvath. Environmental assessment of passenger transportation should include infrastructure and supply chains. *Environmental Research Letters*, 4:024008, 2009. doi:10.1088/1748-9326/4/2/024008.

[70] Lucile Trevisan and Mélanie Bordignon. Screening life cycle assessment to compare CO2 and greenhouse gases emissions of air, road, and rail transport: an exploratory study. *Procedia CIRP*, 90:303–309, 2020. doi:10.1016/j.procir.2020.01.100.

[71] Eleonore Pierrat, Lea Rupcic, Michael Z. Hauschild, and Alexis Laurent. Global environmental mapping of the aeronautics manufacturing sector. *Journal of Cleaner Production*, 297:126603, 2021. doi:10.1016/j.jclepro.2021.126603.

[72] Brian Cox, Wojciech Jemiolo, and Chris Mutel. Life cycle assessment of air transportation and the Swiss commercial air transport fleet. *Transportation Research Part D: Transport and Environment*, 58:1–13, 2018. doi:10.1016/j.trd.2017.10.017.

[73] Alice Fabre, Thomas Planès, Scott Delbecq, Valérie Budinger, and Gilles Lafforgue. Life Cycle Assessment models for overall aircraft design. In *AIAA Scitech 2022 Forum*, Reston, Virginia, 2022. doi:10.2514/6.2022-1028.

[74] João Vasco de Oliveira Fernandes Lopes. Life Cycle Assessment of the Airbus A330-200 Aircraft, M.Sc. Thesis, Universidade Técnica de Lisboa, 2010.

[75] Andreas Johanning and Dieter Scholz. A First Step Towards the Integration of Life Cycle Assessment into Conceptual Aircraft Design. In *Deutscher Luft- und Raumfahrtkongress 2013*, Stuttgart, Germany, 2013. URL `https://www.fzt.haw-hamburg.de/pers/Scholz/Airport2030/Airport2030_PUB_DLRK_13-09-10.pdf`. Accessed on 30/01/2024.

[76] Andreas Johanning and Dieter Scholz. Adapting Life Cycle Impact Assessment Methods for Application in Aircraft Design. In *Deutscher Luft- und Raumfahrtkongress 2014*, Augsburg, Germany, 2014. URL `https://www.fzt.haw-hamburg.de/pers/Scholz/Airport2030/Airport2030_PUB_DLRK_14-09-16.pdf`. Accessed on 30/01/2024.

[77] Lino Scelsi, Michael Bonner, Alma Hodzic, Constantinos Soutis, C. Wilson, Richard J. Scaife, and Keith Ridgway. Potential emissions savings of lightweight composite aircraft components evaluated through life cycle assessment. *Express Polymer Letters*, 5:209–217, 2011. doi:10.3144/expresspolymlett.2011.20.

[78] Xiang Li, Ruibin Bai, and Jon McKechnie. Environmental and financial performance of mechanical recycling of carbon fibre reinforced polymers and comparison with conventional disposal routes. *Journal of Cleaner Production*, 127:451–460, 2016. doi:10.1016/j.jclepro.2016.03.139.

[79] Pernelle Nunez and Sammy Jones. Cradle to gate: life cycle impact of primary aluminium production. *International Journal of Life Cycle Assessment*, 21: 1594–1604, 2016. doi:10.1007/s11367-015-1003-7.

[80] Lea Rupcic, Eleonore Pierrat, Kilian Fricke, Torsten Moll, Michael Z. Hauschild, and Alexis Laurent. Improving environmental performances of integrated bladed rotors for aircraft. *CIRP Annals*, 71:13–16, 2022. doi:10.1016/J.CIRP.2022.04.047.

[81] Dennis Keiser, Lars Henrik Schnoor, Birte Pupkes, and Michael Freitag. Life cycle assessment in aviation: A systematic literature review of applications, methodological approaches and challenges. *Journal of Air Transport Management*, 110:102418, 2023. doi:10.1016/j.jairtraman.2023.102418.

[82] Airbus. Airbus Annual Report 2021, Connecting and protecting, 2022.

[83] Andreas Johanning and Dieter Scholz. Comparison of the Potential Environmental Impact Improvements of Future Aircraft Concepts Using Life Cycle Assessment. In *5th CEAS Air & Space Conference*, Delft, Netherlands, 2015. URL `https://www.fzt.haw-hamburg.de/pers/Scholz/Airport2030/Airport2030_PUB_CEAS_15-09-07.pdf`. Accessed on 30/01/2024.

[84] Andreas Johanning. Life Cycle Assessment in Conceptual Aircraft Design, 2016.

[85] Kristina Kossarev, Anna Elena Scholz, and Mirko Hornung. Comparative environmental life cycle assessment and operating cost analysis of long-range hydrogen and biofuel-fueled transport aircraft. *CEAS Aeronautical Journal*, 14:3–28, 2022. doi:10.1007/s13272-022-00627-w.

[86] Francesco Orefice. *Conceptual Design of Hybrid-Electric Aircraft*. PhD thesis, Department of Industrial Engineering, University of Naples "Federico II", 2022.

[87] Francesco Orefice, Pierluigi Della Vecchia, Danilo Ciliberti, and Fabrizio Nicolosi. Aircraft conceptual design including powertrain system architecture and distributed propulsion. In *AIAA Propulsion and Energy 2019 Forum*, Indianapolis, Indiana, 2019. doi:10.2514/6.2019-4465.

[88] Francesco Orefice, Fabrizio Nicolosi, Pierluigi Della Vecchia, and Danilo Ciliberti. Conceptual Design of Commuter Aircraft including Distributed Electric Propulsion. In *AIAA Aviation 2020 Forum*, Virtual event, 2020. doi:10.2514/6.2020-2627.

[89] Francesco Orefice, Fabrizio Nicolosi, Danilo Ciliberti, and Giuseppe De Rosa. Performance Calculation for Hybrid-Electric Aircraft integrating Aero-Propulsive Interactions. In *AIAA Scitech 2021 Forum*, Virtual event, 2021. doi:10.2514/6.2021-1640.

[90] Francesco Orefice, Fabrizio Nicolosi, Salvatore Corcione, and Pierluigi Della Vecchia. Hybridization and Mission Analysis of a Regional Turboprop. In *AIAA Aviation 2021 Forum*, Virtual event, 2021. doi:10.2514/6.2021-2421.

[91] Francesco Orefice, Valerio Marciello, Qinyin Zhang, Guido Wortmann, Jonathan Menu, and Vincenzo Cusati. Design of Hybrid-Electric Small Air Transports. *IOP Conference Series: Materials Science and Engineering*, 1226:012075, 2022. doi:10.1088/1757-899X/1226/1/012075.

[92] Francesco Orefice, Valerio Marciello, Vincenzo Cusati, and Fabrizio Nicolosi. Powertrain Model Improvement for Hybrid-Electric Regional Aircraft. In *AIAA Scitech 2022 Forum*, San Diego, California, 2022. doi:10.2514/6.2022-0886.

[93] Valerio Marciello, Francesco Orefice, Fabrizio Nicolosi, Danilo Ciliberti, and Pierluigi Della Vecchia. Design of Hybrid-Electric Aircraft with Fault-Tolerance Considerations. *Chinese Journal of Aeronautics*, 36(2):160–178, 2023. doi:10.1016/j.cja.2022.05.014.

[94] Valerio Marciello, Mario Di Stasio, Manuela Ruocco, Vittorio Trifari, Fabrizio Nicolosi, Markus Meindl, Bruno Lemoine, and Priscilla Caliandro. Design Exploration for Sustainable Regional Hybrid-Electric Aircraft: A Study Based on Technology Forecasts. *Aerospace*, 10(2):165, 2023. doi:10.3390/aerospace10020165.

[95] Salvatore Corcione, Gennaro Di Mauro, Vincenzo Cusati, Valerio Marciello, Michele Guida, and Fabrizio Nicolosi. *Dynamic Response and Failure of Composite Materials*, chapter Preliminary Sizing of a Hybrid-Electric Aircraft with Structural Batteries. Springer, 2023.

[96] Gennaro Di Mauro, Salvatore Corcione, Vincenzo Cusati, Valerio Marciello, Michele Guida, and Fabrizio Nicolosi. The Potential of Structural Batteries for Commuter Aircraft Hybridization. *Journal of Materials Engineering and Performance*, 32(1):3871–3880, 2023. doi:10.1007/s11665-023-07856-y.

[97] Valerio Marciello, Vincenzo Cusati, Fabrizio Nicolosi, Karen Saavedra-Rubio, Eleonore Pierrat, Nils Thonemann, and Alexis Laurent. Evaluating the Economic Landscape of Hybrid-Electric Regional Aircraft: A Cost Analysis Across Three Time Horizons. Submitted to Energy Conversion and Management.

[98] Matthias Strack, Gabriel P. Chiozzotto, Michael Iwanizki, Martin Plohr, and Martin Kuhn. Conceptual Design Assessment of Advanced Hybrid Electric Turboprop Aircraft Configurations. *17th AIAA Aviation Technology, Integration, and Operations Conference, 2017*, pages 1–20, 2017. doi:10.2514/6.2017-3068.

[99] Askin T. Isikveren, S. Kaiser, Clément Pornet, and Patrick C. Vratny. Predesign strategies and sizing techniques for dual-energy aircraft. *Aircraft Engineering and Aerospace Technology*, 86(6):525–542, 2014. doi:10.1108/AEAT-08-2014-0122.

[100] Hans-Jörg Steiner, Patrick C. Vratny, Corin Gologan, Kerstin Wieczorek, Askin T. Isikveren, and Mirko Hornung. Performance and Sizing of Transport Aircraft Employing Electrically-Powered Distributed Propulsion. In *Deutscher Luft- und Raumfahrtkongress 2012*, Berlin, Germany, 2012.

[101] Carlo E. D. Riboldi and Federico Gualdoni. An integrated approach to the preliminary weight sizing of small electric aircraft. *Aerospace Science and Technology*, 58:134–149, 2016. ISSN 12709638. doi:10.1016/j.ast.2016.07.014.

[102] Benjamin J. Brelje and Joaquim R. R. A. Martins. Electric, hybrid, and turboelectric fixed-wing aircraft: A review of concepts, models, and design approaches. *Progress in Aerospace Sciences*, 104:1–19, 2019. ISSN 03760421. doi:10.1016/j.paerosci.2018.06.004.

[103] Gabrielle E. Wroblewski and Phillip J. Ansell. Mission analysis and emissions for conventional and hybrid-electric commercial transport aircraft. *AIAA Aerospace Sciences Meeting, 2018*, 2018. doi:10.2514/6.2018-2028.

[104] Tyler S. Dean, Gabrielle E. Wroblewski, and Phillip J. Ansell. Mission analysis and component-level sensitivity study of hybrid-electric general aviation propulsion systems. In *AIAA Aerospace Sciences Meeting, 2018*, Kissimmee, Florida, 2018. ISBN 9781624105241. doi:10.2514/6.2018-1749.

[105] Gokcin Cinar, Dimitri N. Mavris, Mathias Emeneth, Alexander Schneegans, Carsten Riedige, Yann Fefermann, and Askin T. Isikveren. Sizing, integration and performance evaluation of hybrid electric propulsion subsystem architectures. In *AIAA SciTech Forum - 55th AIAA Aerospace Sciences Meeting*, Grapevine, Texas, 2017. ISBN 9781624104473. doi:10.2514/6.2017-1183.

[106] Taewoo Nam, Danielle S. Soban, and Dimitri N. Mavris. Power based sizing method for aircraft consuming unconventional energy. In *43rd AIAA Aerospace Sciences Meeting and Exhibit - Meeting Papers*, Reno, Nevada, 2005. doi:10.2514/6.2005-818.

[107] James L. Felder. *Commercial Aircraft Propulsion and Energy Systems Research: Reducing Global Carbon Emissions*. The National Academies Press, 2016. doi:10.17226/23490.

[108] Trevor M. Young. *Performance of the Jet Transport Airplane: Analysis Methods and Regulations*, chapter International Standard Atmosphere (ISA) Table. John Wiley & Sons Ltd., 2017.

[109] Mario Di Stasio. *Efficient Gas Turbine Modeling for Low Emissions Aircraft Preliminary Design Workflows*. PhD thesis, Department of Industrial Engineering, University of Naples "Federico II", 2022.

[110] Feijia Yin and Arvind Gangoli Rao. Performance analysis of an aero engine with inter-stage turbine burner. *The Aeronautical Journal*, 121(1245): 1605–1626, 2017. doi:10.1017/aer.2017.93.

[111] Antonio Filippone and Nicholas Bojdo. Statistical model for gas turbine engines exhaust emissions. *Transportation Research Part D: Transport and Environment*, 59:451–463, 2018. doi:10.1016/j.trd.2018.01.019.

[112] Pratt & Withney. PW100/150 Engines, 2023. URL `https://www.prattwhitney.com/en/products/regional-aviation-engines/pw100-150`. Accessed on 29/11/2023.

[113] Pratt & Withney. PW127XT Engine Series – Regional Aviation's New Standard for Operating Economics and Sustainability, 2023. URL `https://www.prattwhitney.com/en/products/regional-aviation-engines/pw127xt`. Accessed on 29/11/2023.

[114] Michael D. Patterson. *Conceptual Design of High-Lift Propeller Systems for Small Electric Aircraft*. PhD thesis, Georgia Institute of Technology, 2016.

[115] Patrick C. Vratny, Corin Gologan, Clément Pornet Pornet, Askin T. Isikveren, and Mirko Hornung. Battery Pack Modeling Methods for Universally-Electric Aircraft. In *4th CEAS Air & Space Conference*, Link"oping, Sweden, 2013.

[116] Hubert Rubenbauer and Stefan Henninger. Definitions and reference values for battery systems in electrical power grids. *Journal of Energy Storage*, 12: 87–107, 2017. doi:https://doi.org/10.1016/j.est.2017.04.004.

[117] Tianyuan Zhao. Propulsive Battery Packs Sizing for Aviation Applications, 2017.

[118] Samsung SDI – Energy Business Division. Introduction of INR18650-30Q, 2014. URL `https://eu.nkon.nl/sk/k/30q.pdf`. Accessed on 19/12/2023.

[119] Ian Cotton, Richard Gardner, Daniel Schweickart, Dennis Grosean, and Christopher Severns. Design considerations for higher electrical power system voltages in aerospace vehicles. In *2016 IEEE International Power Modulator and High Voltage Conference (IPMHVC 2016)*, San Francisco, California, 2016. doi:10.1109/IPMHVC.2016.8012771.

[120] Sandy Munro. The Future of Electric Vehicles: Exploring 800V Architectures, 2023.

[121] Frano Barbir. *PEM Fuel Cells: Theory and Practice*. 2013. doi:10.1016/C2011-0-06706-6.

[122] James Larminie and Andrew Disck. *Fuel Cell Systems Explained, Second Edition*. 2003.

[123] Sebastian Nicolay, Stanislav Karpuk, and Ali Elham. Conceptual design and optimization of a general aviation aircraft with fuel cells and hydrogen as propulsion system. In *Aerospace Europe Conference 2020*, Bordeaux, France, 2020.

[124] Marie-Cécile Péra, Daniel Hissel, Hamid Gualous, and Christophe Turpin. *Electrochemical Components*. John Wiley & Sons Ltd., 2013. ISBN 9781848214019. doi:10.1002/9781118576892.

[125] Patrick T. Moseley. Fuel Cell Systems Explained. *Journal of Power Sources*, 93: 285, 2001. URL `https://api.semanticscholar.org/CorpusID:96541125`. Accessed on 19/12/2023.

[126] Souleman M. Njoya, Olivier Tremblay, and Louis A. Dessaint. A generic fuel cell model for the simulation of fuel cell vehicles. In *2009 IEEE Vehicle Power and Propulsion Conference*, Dearborn, Michigan, 2009. doi:10.1109/VPPC.2009.5289692.

[127] Mojtaba Baghban Yousefkhani, Hossein Ghadamian, Keyvan Daneshvar, Nima Alizadeh, and Brendy C. Rincon Troconis. Investigation of the Fuel Utilization Factor in PEM Fuel Cell Considering the Effect of Relative Humidity at the Cathode. *Energies*, 13(22):6117, 2020. doi:10.3390/en13226117.

[128] Bruno Lemoine, Priscilla Caliandro, Nils Baumann, Wannemacher; Thomas, and Benjamin Sala. Deliverable 2.4 – Fuel Cell Technology Analysis. Technical report, Clean Sky 2 GENESIS Project, 2023. URL `https://www.genesis-cleansky.eu/deliverables/`. Awaiting publication.

[129] Siemens. SINAVY PEM Fuel Cells For Submarines, 2016.

[130] Fabrizio Nicolosi, Valerio Marciello, and Francesco Orefice. Conceptual Design of a Hydrogen-Propelled Aircraft with Distributed Electric Propulsion. In *AIAA Aviation Forum 2022*, Chicago, Illinois, 2022. doi:10.2514/6.2022-3205.

[131] Lars Eriksson and Lars Nielsen. *Modeling and Control of Engines and Drivelines*. John Wiley & Sons Ltd., 2014. doi:10.1002/9781118536186.

[132] Robert McMullen and Yirot Pino. Conditioning Turbocharger Compressor Map Data for Use in Engine Performance Simulation. *SAE International Journal of Engines*, 11(4), 2018. doi:10.4271/03-11-04-0033.

[133] Neil E. Anderson, Stuart H. Loewenthal, and Joseph D. Black. An Analytical Method To Predict Efficiency of Aircraft Gearboxes. In *Twentieth Joint Propulsion Conference*, Cincinnati, Ohio, 1984.

[134] Amin Mahmoudi, Wen L. Soong, Gianmario Luigi Pellegrino, and Eric Giacomo Armando. Efficiency maps of electrical machines. In *Energy Conversion Congress and Exposition (ECCE), 2015 IEEE*, Montreal, Canada, 2015. doi:10.1109/ECCE.2015.7310051.

[135] Emad Roshandel, Amin Mahmoudi, Solmaz Kahourzade, Amirmehdi Yazdani, and GM Shafiullah. Losses in Efficiency Maps of Electric Vehicles: An Overview. *Energies*, 14(22):7805, 2021. doi:10.3390/en14227805.

[136] Zhijun Wang, Vanessa Q. Liu Xu, and Roeland De Breuker. Preliminary Aeroelastic Design of Composite Wings with Distributed Electric Propulsion. In *International Forum on Aeroelasticity and Structural Dynamics (IFASD 2022)*, Madrid, Spain, 2022. URL `https://research.tudelft.nl/en/publications/preliminary-aeroelastic-design-of-composite-wings-with-distribute`. Accessed on 05/12/2023.

[137] Zhijun Wang and Roeland De Breuker (TU Delft). Personal communication, 2023.

[138] European Union Aviation Safety Agency (EASA). Certification Specifications for Normal-Category Aeroplanes (CS-23), Amendment 5, 2017.

[139] European Union Aviation Safety Agency (EASA). Certification Specifications for Large Aeroplanes (CS-25), Amendment 28, 2023.

[140] Peter Phillip Edwards, Vladimir L. Kuznetsov, William I.F. David, and Nigel P. Brandon. Hydrogen and fuel cells: Towards a sustainable energy future. *Energy Policy*, 36:4356–4362, 2008. doi:10.1016/j.enpol.2008.09.036.

[141] Daniel P. Raymer. *Aircraft Design: A Conceptual Approach*. AIAA education series. American Institute of Aeronautics and Astronautics, Reston, 5th edition, 2012. ISBN 978-1-60086-921-1.

[142] Eric S. Hendricks and Michael T. Tong. Performance and Weight Estimates for an Advanced Open Rotor Engine, 2012. URL `https://ntrs.nasa.gov/api/citations/20120014381/downloads/20120014381.pdf`. Accessed on 21/12/2023.

[143] Ira H. A. Abbott and Albert E. Von Doenhoff. *Theory of Wing Sections*. Dover Publications Inc., 2009.

[144] Fabrizio Nicolosi, Pierluigi Della Vecchia, Danilo Ciliberti, and Vincenzo Cusati. Fuselage Aerodynamic Prediction Methods. *Aerospace Science and Technology*, 55:322–343, 2016. doi:10.1016/j.ast.2016.06.01.

[145] Courtland D. Perkins and Robert E. Hage. *Airplane Performance Stability and Control*. John Wiley and Sons, Inc., 1949.

[146] Michael D. Patterson, Matthew J. Daskilewicz, and Brian German. Simplified aerodynamics models to predict the effects of upstream propellers on wing lift. *Proceedings of the 53rd AIAA Aerospace Sciences Meeting*, 2015. doi:10.2514/6.2015-1673.

[147] Pierluigi Della Vecchia, Daniele Malgieri, Fabrizio Nicolosi, and Agostino De Marco. Numerical analysis of propeller effects on wing aerodynamic: tip mounted and distributed propulsion. *Transportation Research Procedia*, 29: 106–115, 2018. doi:10.1016/j.trpro.2018.02.010.

[148] Danilo Ciliberti, Francesco Orefice, Pierluigi Della Vecchia, Fabrizio Nicolosi, and Salvatore Corcione. An approach to preliminary sizing of turbo-electric aircraft with distributed propulsion. *Proceedings of the AIDAA XXV International Congress, Rome, Italy*, 2019.

[149] Danilo Ciliberti, Pierluigi Della Vecchia, Vittorio Memmolo, Fabrizio Nicolosi, Guido Wortmann, and Fabrizio Ricci. The Enabling Technologies for a Quasi-Zero Emissions Commuter Aircraft. *Aerospace*, 9(6):319, 2022. doi:10.3390/aerospace9060319.

[150] James F. Manwell, Jon G. McGowan, and Anthony L. Rogers. *Wind Energy Explained - Theory, Design and Application, Second Edition*. John Wiley and Sons, Ltd., 2009.

[151] Carlo E. D. Riboldi, Federico Gualdoni, and Lorenzo Trainelli. Preliminary weight sizing of light pure-electric and hybrid-electric aircraft. *Transportation Research Procedia*, 29:346–389, 2018. doi:10.1016/j.trpro.2018.02.034.

[152] RUAG. Dornier 228 NG – Benefit from a New Generation, 2017. URL `https://aviationdoctor.files.wordpress.com/2017/03/ruag-do228ng-1.pdf`. Accessed on 27/12/2023.

[153] Valerio Marciello, Manuela Ruocco, Fabrizio Nicolosi, and Mario Di Stasio. Market Analysis, TLARs Selection and Preliminary Design Investigations for a Regional Hybrid-Electric Aircraft. In *33rd Congress of the International Council of the Aeronautical Sciences (ICAS 2022)*, Stockholm, Sweden, 2022. URL `https://www.icas.org/ICAS_ARCHIVE/ICAS2022/data/preview/ICAS2022_0649.htm`. Accessed on 30/01/2024.

[154] ATR. ATR42-600 - The ideal local commuter, 2023. URL https://www.atr-aircraft.com/wp-content/uploads/2022/06/ATR_Fiche42-600-3.pdf. Accessed on 13/11/2023.

[155] European Union Aviation Safety Agency (EASA). Type-Certificate Data Sheet No. EASA.A.084, Issue 12, 2023.

[156] ATR. ATR72-600 - The first choice for operators, 2023. URL https://www.atr-aircraft.com/wp-content/uploads/2022/06/ATR_Fiche72-600-3.pdf. Accessed on 13/11/2023.

[157] ATR. ATR Family, 2014. URL ttp://www.atraircraft.com/products_app/media/pdf/FAMILY_septembre2014.pdf. Accessed on 08/05/2018.

[158] ATR. ATR - Cabin Crew Operating Manual, 2012.

[159] Eurocontrol. Taxi times - Summer 2022, 2022. URL https://www.eurocontrol.int/publication/taxi-times-summer-2022. Accessed on 07/12/2023.

[160] Eurocontrol. Forecasting civil aviation fuel burn and emissions in Europe - Interim Report, 2001.

[161] Air Transport Association of America. *Standard method of estimating comparative direct operating costs of turbine powered transport airplanes*. Number December. ATA, 1967.

[162] Association of European Airliners. AEA requirements - short range aircraft, 1989.

[163] Association of European Airlines. Long range aircraft - AEA requirements, 1987.

[164] Anna Elena Scholz, Dimitar Trifonov, and Mirko Hornung. Environmental life cycle assessment and operating cost analysis of a conceptual battery hybrid-electric transport aircraft. *CEAS Aeronautical Journal*, 13(1):215–235, 2022. doi:10.1007/s13272-021-00556-0.

[165] International Air Transport Association (IATA). Jet Fuel Price Monitor, 2023. URL https://www.iata.org/en/publications/economics/fuel-monitor/. Accessed on 25/05/2023.

[166] European Commision. Commission Regulation (EU) No. 83/2014, 2014. URL https://eur-lex.europa.eu/LexUriServ/LexUriServ.do?uri=OJ:L:2014:028:0017:0029:EN:PDF. Accessed on 25/05/2023.

[167] Jinning Zhang, Ioannis Roumeliotis, Xin Zhang, and Argyrios Zolotas. Techno-economic-environmental evaluation of aircraft propulsion electrification: Surrogate-based multi-mission optimal design approach . *Renewable and Sustainable Energy Reviews*, 175:113168, 2023. doi:10.1016/j.rser.2023.113168.

[168] Luis Arévalo Villa. Economic Feasibility Study of New Electric Commuter Aircraft. M.Sc. Thesis, Wissenschaftliche Arbeit zur Erlangung des Grades M.Sc. Luft- und Raumfahrttechnik an der Fakultät für Maschinenwesen, Technischen Universität München, 2017.

[169] Marco Fioriti, Nicole Viola, Davide Ferretto, Valeria Vercella, Sara Cresto Aleina, Fabrizio Nicolosi, and Vincenzo Cusati. Parametric approach to operating costs estimation for an innovative regional aircraft. In *31st Congress of the International Council of the Aeronautical Sciences, ICAS 2018*, 2018. ISBN 9783932182884.

[170] Kay Plötner, Michael Schmidt, Marcin Baranowski, Askin Isikveren, and Mirko Hornung. Operating Cost Estimation for Electric-Powered Transport Aircraft. In *2013 Aviation Technology, Integration, and Operations Conference*, 2013. doi:10.2514/6.2013-4281.

[171] Eurocontrol. Customer Guide to Charges, 2023. URL `https://www.eurocontrol.int/publication/customer-guide-route-charges`. Accessed on 13/11/2023.

[172] Nick Harper. How Many Airports Have Emissions-Based Charges? *AirportCharges*, 2022. URL `https://rdcaviation.com/news/q-how-many-airports-have-emissions-based-charges/#:~:text=At%20the%20end%20of%20October,pre%2Dpandemic%20levels%20October%202019.andtext=What%20do%20these%20airports%20currently,are%20all%20in%20Western%20Europe.` Accessed on 25/05/2023.

[173] CoinNews. US Inflation Calculator, 2023. URL `https://www.usinflationcalculator.com/`. Accessed on 13/11/2023.

[174] ATR. ATR 42-500: A new standard of excellence, 2007. URL `www.aerocontact.com/en/virtual-aviation-exhibition/catalog/76-atr-42-500-a-new-standard-of-excellence#lg=1andslide=5`. Accessed on 25/05/2023.

[175] Paul Jackson, Kenneth Munson, and Lindsay Peacock. *Jane's all the world's aircraft 2007-2008, 98th ed.* Cambridge University Press, 2008.

[176] Rolls-Royce. Rolls-Royce, Official Website. URL `https://www.rolls-royce.com/products-and-services/electrical.aspx`. Accessed on 30/12/2023.

[177] Piaggio Aerospace. Piaggio Aerospace, Official Website. URL `https://www.piaggioaerospace.it/it`. Accessed on 02/01/2024.

[178] Air s.Pace. Air s.Pace, Official Website. URL `https://airspace-aachen.de/`. Accessed on 30/12/2023.

[179] Siemens Digital Industries Software. Siemens Digital Industries Software, Official Website. URL `https://www.sw.siemens.com/en-US/`. Accessed on 30/12/2023.

[180] Smartup Engineering s.r.l. Smartup Engineering s.r.l., Official Website. URL `https://www.smartup-engineering.com/`. Accessed on 30/12/2023.

[181] Günther Schuh, Maximilian Spangenberg, Qinyin Zhang, Benedikt Dannbeck, and Johann Stürken. Economic Feasibility Study of a Hybrid-Electric 19-Passenger Commuter Aircraft. In *Deutscher Luft- und Raumfahrtkongress 2020*, Virtual event, 2021. URL `https://www.dglr.de/publikationen/2021/530307.pdf`. Accessed on 05/01/2024.

[182] Günther Schuh, Maximilian Spangenberg, and Qinyin Zhang. Economically driven requirements for a hybrid-electric 19-passenger commuter aircraft. *IOP Conference Series: Materials Science and Engineering*, 1024:012079, 2021. doi:10.1088/1757-899X/1024/1/012079.

[183] Emre Öngüt, Vincenzo cusati, Vittorio Memmolo, Fabrizio Nicolosi, Francesco Orefice, Danyu Qiao, and Yves Lemmens. A Design Chain for Distributed Electric Propulsion with Increased Fidelity Structural Strength Assessment and Mass Estimation. In *AIAA Scitech 2022 Forum*, San Diego, California, 2022. doi:10.2514/6.2022-0169.

[184] Fabrizio Nicolosi, Valerio Marciello, Vincenzo Cusati, and Francesco Orefice. Technology Roadmap and Conceptual Design of Hybrid and Electric Configurations in the Commuter Class. In *33rd Congress of the International Council of the Aeronautical Sciences (ICAS 2022)*, Stockholm, Sweden, 2022. URL `https://www.icas.org/ICAS_ARCHIVE/ICAS2022/data/preview/ICAS2022_0641.htm`. Accessed on 30/01/2024.

[185] Qinyin Zhang, Fabrizio Nicolosi, Valerio Marciello, Vincenzo Cusati, Jonathan Menu, Emre Öngüt, and Maximilian Spangenberg. Concept Designs of Hybrid-Electric Passenger Commuter Aircraft with Potential to Enable Zero-Emission Regional Air Transport. In *12th EASN International Conference*, Barcelona, Spain, 2022. Presentation only.

[186] Qinyin Zhang and Valerio Marciello. The ELICA Project. In *Workshop on Commuter and Regional Hybrid-Electric Aircraft Design: Transition from Clean Sky 2 to Clean Aviation*, Naples, Italy, 2022. Presentation only.

[187] Simon Calder. Electric planes coming to Scotland's islands, 2021. URL `https://www.independent.co.uk/travel/news-and-advice/electric-planes-scotland-islands-orkney-b1790617.html`. Accessed on 30/12/2023.

[188] Stephen Dowling. Norway's plan for a fleet of electric planes, 2018. URL https://www.bbc.com/future/article/20180814-norways-plan-for-a-fleet-of-electric-planes. Accessed on 30/12/2023.

[189] Rolls-Royce. Rolls-Royce and Tecnam join forces with Widerøe to deliver an all-electric passenger aircraft ready for service in 2026, 2021. URL https://www.rolls-royce.com/media/press-releases/2021/11-03-2021-rr-and-tecnam-join-forces.aspx. Accessed on 30/12/2023.

[190] Thomas Kadyk, Christopher Winnefeld, Richard Hanke-Rauschenbach, and Ulrike Krewer. Analysis and Design of Fuel Cell Systems for Aviation. *Energies*, 11(2):375, 2018. doi:10.3390/en11020375.

[191] Thomas Kadyk, René Schenkendorf, Sebastian Hawner, Bekir Yildiz, and Ulrich Römer. Design of Fuel Cell Systems for Aviation: Representative Mission Profiles and Sensitivity Analyses. *Frontiers in Energy Research*, 7:35, 2019. doi:10.3389/fenrg.2019.00035.

[192] Anthony J. Colozza. Hydrogen Storage for Aircraft Applications Overview, 2002. URL https://ntrs.nasa.gov/citations/20020085127. Accessed on 03/01/2024.

[193] Clean Sky 2 JU. *Hydrogen-powered aviation, A fact-based study of hydrogen technology, economics, and climate impact by 2050.* 2020.

[194] Diego Giuseppe Romano, Gianvito Apuleo, and Jiri Duda. Affordable and Environmental Friendly Small Commuter Aircraft Improving European Mobility. *International Journal of Aerospace and Mechanical Engineering*, 14 (9), 2020.

[195] Wikipedia contributors. Pratt & Whitney Canada PT6, 2024. URL https://en.wikipedia.org/wiki/Pratt_%26_Whitney_Canada_PT6#Specifications_(PT6A-6). Accessed on 03/01/2024.

[196] Till Lennart Kösters, Xi Liu, Dragan Kožulović, Shaofan Wang, Jens Friedrichs, and Xin Gao. Comparison of phase-change-heat-pump cooling and liquid cooling for PEM fuel cells for MW-level aviation propulsion. *International Journal of Hydrogen Energy*, 47(68):29399–29412, 2022. doi:10.1016/j.ijhydene.2022.06.235.

[197] International Civil Aviation Organization (ICAO). Annex 16 Environmental Protection - Volume I Aircraft Noise, 2011.

[198] Valerio Marciello. Design Methodologies for Aircraft Noise Estimation with Parametric Analysis. M.Sc. Thesis, University of Naples "Federico II", 2020.

[199] Engineering Sciences Data Unit (ESDU). Engineering Sciences Data Unit (ESDU), Official Website. URL `https://www.esdu.com`. Accessed on 05/01/2024.

[200] Engineering Sciences Data Unit (ESDU). *Airframe Noise Prediction, Item No. 90023*. ESDU International, 1990.

[201] Engineering Sciences Data Unit (ESDU). *Evaluation of the Attenuation of Sound by a Uniform Atmosphere, Item No. 78002*. ESDU International, 1990.

[202] Engineering Sciences Data Unit (ESDU). *Estimation of Lateral Attenuation of Air-to-Ground Jet or Turbofan Aircraft Noise in One-Third Octave Bands, Item No. 82027*. ESDU International, 1993.

[203] Engineering Sciences Data Unit (ESDU). *Estimation of Noise Shielding by Barriers, Item No. 79011*. ESDU International, 1993.

[204] Engineering Sciences Data Unit (ESDU). *Prediction of Near-Field and Far-Field Harmonic Noise from Subsonic Propellers with Non-Axial Inflow, Item No. 95029*. ESDU International, 1996.

[205] Engineering Sciences Data Unit (ESDU). *Prediction of Noise Generated by Fans and Compressors in Turbojet and Turbofan Engines, Item No. 98008*. ESDU International, 1998.

[206] Robert D. Bruce, Charles T. Moritz, and Arno S. Bommer. *Handbook of Noise and Vibration Control*, chapter Sound Power Level Predictions for Industrial Machinery. John Wiley & Sons, Inc., 2007.

[207] European Environment Agency. Greenhouse gas emission intensity of electricity generation by country, 2021. URL `https://www.eea.europa.eu/data-and-maps/daviz/co2-emission-intensity-9/#tab-chart_2`. Accessed on 29/07/2021.

[208] Technical University of Denmark (DTU). Technical University of Denmark, Official Website. URL `https://www.dtu.dk/english/`. Accessed on 05/12/2023.

[209] Markus Meindl, Cor De Ruiter, Valerio Marciello, Mario Di Stasio, Florian Hilpert, Manuela Ruocco, Fabrizio Nicolosi, Nils Thonemann, Karen Saavedra-Rubio, Louis Locqueville, Alexis Laurent, and Martin März. Decarbonised Future Regional Airport Infrastructure. *Aerospace*, 10(3):283, 2023. doi:10.3390/aerospace10030283.

[210] Nils Thonemann, Karen Saavedra-Rubio, Eleonore Pierrat, Katarzyna Dudka, Mathilde Bangoura, Nils Baumann, Christian Bentheimer, Priscilla Caliandro, Roeland De Breuker, Cor De Ruiter, Mario Di Stasio, Julie Elleby, Alexe Guiguemde, Bruno Lemoine, Martin Maerz, Valerio Marciello, Markus Meindl, Fabrizio Nicolosi, Manuela Ruocco, Benjamin Sala, Anna Lia Scharling Tromer Dragsdahl, Andrea Vezzini, Zhangqi Wang, Thomas Wannemacher, Julius Zettelmeier, and Alexis Laurent. Prospective Life Cycle Inventory Datasets for Conventional and Hybrid-Electric Aircraft Technologies. *Journal of Cleaner Production*, 434(3):140314, 2023. doi:10.1016/j.jclepro.2023.140314.

[211] Nils Thonemann, Karen Saavedra-Rubio, Eleonore Pierrat, Katarzyna Dudka, Mathilde Bangoura, Nils Baumann, Christian Bentheimer, Priscilla Caliandro, Roeland De Breuker, Cor De Ruiter, Mario Di Stasio, Julie Elleby, Alexe Guiguemde, Bruno Lemoine, Martin Maerz, Valerio Marciello, Markus Meindl, Nicolosi Fabrizio, Manuela Ruocco, Benjamin Sala, Anna Lia Scharling Tromer Dragsdahl, Andrea Vezzini, Zhangqi Wang, Thomas Wannemacher, Julius Zettelmeier, and Alexis Laurent. Prospective Life Cycle Inventory Datasets for Conventional and Hybrid-Electric Aircraft Technologies, 2023. URL `https://doi.org/10.5281/zenodo.8155003`. Accessed on 12/12/2023.

[212] Valerio Marciello, Mario Di Stasio, Manuela Ruocco, and Fabrizio Nicolosi. Design Exploration for Sustainable and Innovative Regional Aircraft. In *12th EASN International Conference*, Barcelona, Spain, 2022. Presentation only.

[213] Fabrizio Nicolosi, Valerio Marciello, Mario Di Stasio, and Manuela Ruocco. Design of Sustainable and Innovative Regional Aircraft for Three Time Horizons. In *13th EASN International Conference*, Salerno, Italy, 2023. Presentation only.

[214] Valerio Marciello, Vincenzo Cusati, Manuela Ruocco, Mario Di Stasio, and Fabrizio Nicolosi. Technology Roadmap for a Transition to Sustainable and Competitive Electric Aircraft Systems. In *13th EASN International Conference*, Salerno, Italy, 2023. Presentation only.

[215] Fabrizio Nicolosi, Valerio Marciello, Mario Di Stasio, and Manuela Ruocco. Technology Roadmap for a Transition to Sustainable and Competitive Hybrid-Electric Regional Aircraft. To be presented at the AIAA Aviation Forum 2024. Extended abstract submitted, 2024.

[216] ATR. Discover our Legacy and -500 families, 2023. URL `https://www.atr-aircraft.com/our-aircraft/previous-generations/`. Accessed on 13/11/2023.

[217] European Union Aviation Safety Agency (EASA). Type-Certificate Data Sheet No. EASA.IM.A.673, Issue 3.0, 2023.

[218] Canadair Regional Jet. Model CL-600-2B19, Series 100/200/440, Airport Planning Manual Volume 1, 2016.

[219] Bombardier. CRJ Series, 2017. URL https://mhirj.com/themes/bca/pdf/Bombardier_CRJ_Series_Brochure.pdf. Accessed on 13/11/2023.

[220] Canadair Regional Jet. Model CL-600-2C10, Series 700, Airport Planning Manual Volume 1, 2016.

[221] Aircraft Commerce. Owner's & Operator's Guide: CRJ Family, Aircraft Commerce, Issue No. 66, 2009. URL https://www.aircraft-commerce.com/wp-content/uploads/aircraft-commerce-docs/Aircraft%20guides/CRJ%20FAMILY%20CF34%20FAMILY/ISSUE66_CRJGUIDE.pdf. Accessed on 13/11/2023.

[222] Bombardier Aerospace. Bombardier Q300, 2006. URL https://web.archive.org/web/20161005085657/https://www2.bombardier.com/Used_Aircraft/pdf/Q300_EN.pdf. Accessed on 13/11/2023.

[223] Bombardier Aerospace. PSM 1-83-13, Dash 8 Q-300, Airport Planning Manual, 2001.

[224] Embraer. Embraer ERJ145. URL https://www.embraercommercialaviation.com/wp-content/uploads/2017/02/Embraer_spec_145_web.pdf. Accessed on 13/11/2023.

[225] Embraer. EMB145 Airport Planning Manual, 1997.

[226] Fokker Services. Fokker 50 Information Booklet. URL https://www.fokkerservices.com/media/z05j5mhx/fokker50_informationbooklet.pdf. Accessed on 13/11/2023.

[227] European Union Aviation Safety Agency (EASA). Type-Certificate Data Sheet No. EASA.A.069, Issue 12, 2022.

[228] SAAB. SAAB 2000. URL https://www.saab.com/products/saab2000. Accessed on 13/11/2023.

[229] Jetstream Aviation Capital. SAAB 2000 Cargo, 2022. URL https://www.jetstreamavcap.com/wp-content/uploads/2022/01/JAC-SAAB-2000-Cargo-Data-Sheet-2022-01-27-A.pdf. Accessed on 13/11/2023.

[230] SeatGuru. Find your seat map, 2016. URL https://www.seatguru.com/findseatmap. Accessed on 13/11/2023.

[231] AIN Media Group: Newark. ATR Upgrades Turboprops with New Pratt Engines, 2021. URL https://www.ainonline.com/aviation-news/air-transport/2021-11-15/atr-upgrades-turboprops-new-pratt-whitney-engine. Accessed on 20/11/2023.

[232] Lukas Brink, Ryan Brown, Sarina Carter, Axel Esqué, Benjamin Meigs, and Robin Riedel. Short-haul flying redefined: The promise of regional air mobility, 2023. URL https://www.mckinsey.com/industries/aerospace-and-defense/our-insights/short-haul-flying-redefined-the-promise-of-regional-air-mobility. Accessed on 13/11/2023.

[233] Steer Davies Gleave. *High speed rail: international comparison, Final Report.* 2004.

[234] Our Airports. Open data downloads, 2023. URL https://ourairports.com/data/. Accessed on 13/11/2023.

[235] Bruno Lemoine, Thomas Wannemacher, Nils Baumann, Alexe Guiguemde, Zhangqi Wang, Mario Di Stasio, Manuela Ruocco, and Christian Bentheimer. Deliverable 2.1 – Short-term technology analysis covering all main technologies. Technical report, Clean Sky 2 GENESIS Project, 2021. URL https://www.genesis-cleansky.eu/deliverables/. Accessed on 30/01/2024.

[236] Markus Meindl, Bruno Lemoine, Priscilla Caliandro, Thomas Wannemacher, Nils Baumann, Alexe Guiguemde, Zhangqi Wang, Mario Di Stasio, Manuela Ruocco, Erdem Akay, Sergio Turteltaub, Fabrizio Nicolosi, Agostino De Marco, and Pierluigi Della Vecchia. Deliverable 2.2 – Short-term technology analysis covering all main technologies. Technical report, Clean Sky 2 GENESIS Project, 2021. URL https://www.genesis-cleansky.eu/deliverables/. Accessed on 30/01/2024.

[237] Bruno Lemoine, Priscilla Caliandro, Erdem Akay, Sergio Turteltaub, and Zhangqi Wang. Deliverable 2.3 – Battery Technology Analysis. Technical report, Clean Sky 2 GENESIS Project, 2023. URL https://www.genesis-cleansky.eu/deliverables/. Awaiting publication.

[238] Mario Di Stasio, Manuela Ruocco, Valerio Marciello, Fabrizio Nicolosi, Vittorio Trifari, Pierluigi Della Vecchia, and Agostino De Marco. Deliverable 2.5 – Turbine/ICE Generator Set Technology Analysis. Technical report, Clean Sky 2 GENESIS Project, 2023. URL https://www.genesis-cleansky.eu/deliverables/. Awaiting publication.

[239] Markus Meindl and Christian Bentheimer. Deliverable 2.6 – Full Power Electronics Technology Analysis. Technical report, Clean Sky 2 GENESIS Project, 2023. URL `https://www.genesis-cleansky.eu/deliverables/`. Awaiting publication.

[240] Markus Meindl and Christian Bentheimer. Deliverable 2.7 – Electric Drives Technology Analysis. Technical report, Clean Sky 2 GENESIS Project, 2023. URL `https://www.genesis-cleansky.eu/deliverables/`. Awaiting publication.

[241] Markus Meindl, Cor de Ruiter, Bruno Lemoine, Julius Zettelmeier, and Benjamin Sala. Deliverable 2.8 – Full On Ground Energy Supply Technology Analysis. Technical report, Clean Sky 2 GENESIS Project, 2023. URL `https://www.genesis-cleansky.eu/deliverables/`. Awaiting publication.

[242] Wikipedia contributors. Pratt & Whitney Canada PW100, 2023. URL `https://en.wikipedia.org/wiki/Pratt_%26_Whitney_Canada_PW100`. Accessed on 28/06/2023.

[243] Eric John Hosking, David P. Kenny, Rodney I. McCormick, S. Hany Moustapha, Parthasarathy Sampath, and Arvydas A. Smailys. The PW100 engine : 20 years of gas turbine technology evolution. In *RTO AVT Symposium*, 1999. URL `https://api.semanticscholar.org/CorpusID:115072515`. Accessed on 29/11/2023.

[244] Bill Gunston. *Jane's Aero Engines*. 2002.

[245] Gobierno de España. *Report IN-052/2019 Incident involving an ATR 72-212 A aircraft, registration EC-MPI, operated by Canarias Airlines at the Tenerife North Airport (GCXO) on 15 October 2019*. 2004.

[246] European Union Aviation Safety Agency (EASA). Type-Certificate Data Sheet No. IM.E.041, Issue 06, 2023.

[247] GasTurb GmbH. GasTurb Official Website. URL `https://www.gasturb.com/`. Accessed on 30/01/2023.

[248] Philip P. Walsh and Paul Fletcher. *Gas Turbine Performance, 2nd ed.* John Wiley & Sons, 2004.

[249] Hubert Grieb. *Projektierung von Turboflugtriebwerken*. Springer Basel, 2004.

[250] Jack D. Mattingly, William H. Heiser, and David T. Pratt. *Aircraft Engine Design, Second Edition*. AIAA Education Series, 2001. doi:10.2514/4.861444.

[251] Taehoon Kim, Wentao Song, Dae-Yong Son, Luis K. Ono, and Yabing Qi. Lithium-ion batteries: outlook on present, future, and hybridized technologies. *Journal of Material Chemistry A*, 7:2942–2964, 2019. doi:10.1039/C8TA10513H.

[252] European Technology and Innovation Platform on Batteries - Batteries Europe. D3.6 – Strategic Research Agenda for batteries 2020. Technical report, Batteries Europe, 2020.

[253] Dong-Won Park, Jin Won Kim, and Jaeyoung Lee. Physicochemical Behaviors of Oxygen and Sulfur in Li Batteries. *Applied Chemistry for Engineering*, 23 (3):247–252, 2012.

[254] Chen-Xi Bi, Meng Zhao, Li-Peng Hou, Zi-Xian Chen, Xue-Qiang Zhang, Bo-Quan Li, Hong Yuan, and Jia-Qi Huang. Anode Material Options Toward 500 Wh/kg Lithium–Sulfur Batteries. *Advanced Science*, 9:2103910, 2021. doi:10.1002/advs.202103910.

[255] Oxis Energy. Li-S, UAV, Bus, Truck, EV and Marine Batteries, 2022. URL `https://oxisenergy.com/products/`. Accessed on 20/04/2022.

[256] Jianmin Ma, Yutao Li, Nicholas S. Grundish, John B. Goodenough, Yuhui Chen, Limin Guo, Zhangquan Peng, Xiaoqun Qi, Fengyi Yang, Long Qie, Chang-An Wang, Bing Huang, Zeya Huang, Linhui Chen, Dawei Su, Guoxiu Wang, Xinwen Peng, Zehong Chen, Junliang Yang, Shiman He, Xu Zhang, Haijun Yu, Chaopeng Fu, Min Jiang, Wenzhuo Deng, Chuan-Fu Sun, Qingguang Pan, Yongbing Tang, Xianfeng Li, Xiulei Ji, Fang Wan, Zhiqiang Niu, Fang Lian, Caiyun Wang, Gordon G. Wallace, Min Fan, Qinghai Meng, Sen Xin, Yu-Guo Guo, and Li-Jun Wan. The 2021 battery technology roadmap. *Journal of Physics D: Applied Physics*, 54(18):183001, 2021. doi:10.1088/1361-6463/abd353.

[257] Chen Yang, Peng Li, Jia Yu, Li-Da Zhao, and Long Kong. Approaching energy-dense and cost-effective lithium–sulfur batteries: From materials chemistry and price considerations. *Energy*, 201:117718, 2020. doi:10.1016/j.energy.2020.117718.

[258] Bright Appiah Adu-Gyamfi and Clara Good. Electric aviation: A review of concepts and enabling technologies. *Transportation Engineering*, 9:100134, 2022. doi:10.1016/j.treng.2022.100134.

[259] Girish Girishkumar, Brian McCloskey, Alan C. Luntz, Sally A. Swanson, and Winfried W. Wilcke. Lithium-Air Battery: Promise and Challenges. *Journal of Physical Chemistry Letters*, 1(14):2193–2203, 2010. doi:10.1021/jz1005384.

[260] Stefan Stückl, Jan van Toor, and Hans Lobentanzer. VoltAir - The All Electric Propulsion Concept Platform - A Vision for Atmosperic Friendly Flight. In *28th International Congress of the Aeronautical Sciences (ICAS 2012)*, Brisbane, Australia, 2012. URL `https://www.icas.org/ICAS_ARCHIVE/ICAS2012/PAPERS/521.PDF`. Accessed on 30/01/2024.

[261] Kerry-Ann Adamson. *Stationary Fuel Cells: An Overview, 1st Edition*. 2007. ISBN 9780080554709.

[262] PMFC GmgH. Proton Motor Hydrogen Fuel Cells, Official Website. URL `https://www.proton-motor.com/en/`. Accessed on 04/12/2023.

[263] Green Car Congress. New On-Board Solid Oxide Fuel Cell Delivers 50 % Efficiency, 2005.

[264] Thomas Wannemacher and Nils Baumann (Proton Motor Fuel Cell GmbH). Personal communication, 2023.

[265] Advanced Structural Technologies, Inc. AST: Hydrogen Storage Tanks - Materials, Types & Uses, 2023. URL `https://astforgetech.com/ast-hydrogen-storage-tanks-materials-types-uses/`. Accessed on 05/12/2023.

[266] Mahytec. Mahytec, Official Website. URL `https://www.mahytec.com/en/`. Accessed on 05/12/2023.

[267] Clemens Müller, Ulrich Schwarzer, Fang Qi, Daniel Scharfenstein, and Claude Weiss. *Motor Handbook*. 2019.

[268] Andy Yoon, Xuan Yi, Yuanshan Chen, and Kiruba Haran. A high-speed, high-frequency, air-core PM machine for aircraft application. In *2016 IEEE Power and Energy Conference at Illinois (PECI)*, Urbana, Illinois, 2016. doi:10.1109/PECI.2016.7459221.

[269] Bouloukza Ibtissam, Mordjaoui Mourad, Medoued Ammar, and Guerboussa Fouzi. Magnetic Field Analysis of Halbach Permanent Magnetic Synchronous Machine. In *International Conference on Control, Engineering & Information Technology (CEIT'14)*, 2014. URL `https://api.semanticscholar.org/CorpusID:15436261`. Accessed on 04/12/2023.

[270] Hilltop Products. Technical Information, Shielded Cable for Automotive Electric Powertrain, 2023. URL `https://www.hilltop-products.co.uk/media/Electric_Vehicle_Cable_70mm.pdf`. Accessed on 04/12/2023.

[271] Markus Meindl (Friedrich-Alexander-University of Erlangen-Nürnberg). Personal communication, 2023.

[272] Lubin Han, Lin Liang, Yong Kang, and Yufeng Qiu. A Review of SiC IGBT: Models, Fabrications, Characteristics, and Applications. *IEEE Transactions on Power Electronics*, 36(2):2080–2093, 2021. doi:10.1109/TPEL.2020.3005940.

[273] Delft University of Technology (TUD). Delft University of Technology, Official Website. URL `https://www.tudelft.nl/en/`. Accessed on 05/12/2023.

[274] Mark D. Ardema, Mark C. Chambers, Anthony P. Patron, Andrew S. Hahn, Hirokazu Miura, and Mark D. Moore. Analytical fuselage and wing weight estimation of transport aircraft. Technical report, NASA report, 1996.

[275] MathWorks. MATLAB® Regression Learner, 2023. URL `https://it.mathworks.com/help/stats/regressionlearner-app.html`. Accessed on 05/12/2023.

[276] Chao Liu and Yaoyao Shi. An Improved Analytical Solution for Process-Induced Residual Stresses and Deformations in Flat Composite Laminates Considering Thermo-Viscoelastic Effects. *Materials*, 11:2506, 2018. doi:10.3390/ma11122506.

[277] Kunal Masania, Wilhelm Woigk, Julien Rion, and Clemens Dransfeld. Effect of Fibre Volume Content on the Mechanical Performance of Natural Fibre Reinforced Thermoplastic Composites. In *17th European Conference on Composite Materials (ECCM17)*, Munich, Germany, 2016. URL `https://www.researchgate.net/publication/304659433_EFFECT_OF_FIBRE_VOLUME_CONTENT_ON_THE_MECHANICAL_PERFORMANCE_OF_NATURAL_FIBRE_REINFORCED_THERMOPLASTIC_COMPOSITES`. Accessed on 07/12/2023.

[278] Florian Wolters, Richard-Gregor Becker, and Martin Schaefer. Impact of Alternative Fuels on Engine Performance and CO2 Emissions. In *28th International Congress of the Aeronautical Sciences (ICAS 2012)*, Brisbane, Australia, 2012. URL `https://www.icas.org/ICAS_ARCHIVE/ICAS2012/PAPERS/737.PDF`. Accessed on 14/01/2023.

[279] European Union Aviation Safety Agency (EASA). ICAO Aircraft Engine Emissions Databank, 2023. URL `https://www.easa.europa.eu/en/domains/environment/icao-aircraft-engine-emissions-databank`. Accessed on 14/01/2023.

[280] European Commission. *ANNEXES to the proposal for a regulation of the european parliamant and of the council on ensuring a level playing field for sustainable air transport.* 2021.

[281] European Union Aviation Safety Agency (EASA) - EASA Eco. What are Sustainable Aviation Fuels?, 2023. URL `https://www.easa.europa.eu/eco/eaer/topics/sustainable-aviation-fuels/what-are-sustainable-aviation-fuels`. Accessed on 25/05/2023.

[282] Air Transport Action Group (ATAG). Aviation: Benefits Beyond Borders, 2020.

[283] Airbus. Airbus A330MRTT completes first 100 % SAF test flight on both engines, 2022.

[284] Emirates. Emirates operates milestone demonstration flight powered with 100 % Sustainable Aviation Fuel, 2023.

[285] Airport Cooperative Research Program (ACRP). Alternative Jet Fuels Emissions: Quantification Methods Creation and Validation Report. URL `https://nap.nationalacademies.org/read/25548/chapter/1`. Accessed on 30/01/2023.

[286] Mafalda Narciso and João M. Melo de Sousa. Influence of Sustainable Aviation Fuels on the Formation of Contrails and Their Properties. *Energies*, 14(17): 5557, 2021. doi:10.3390/en14175557.

[287] Véronique Dias, Maxime Pochet, Francesco Contino, and Hervé Jeanmart. Energy and Economic Costs of Chemical Storage. *Frontiers in Mechanical Engineering*, 6:21, 2020. doi:10.3389/fmech.2020.00021.

[288] Paola Testa. *The energy crisis in the EU: an updated outlook on underway actions and proposals to limit the impact on Citizens*. Ernst & Young, 2023.

[289] Younhee Choi, Doosam Song, Sungmin Yoon, and Junemo Koo. Comparison of Factorial and Latin Hypercube Sampling Designs for Meta-Models of Building Heating and Cooling Loads. *Energies*, 14:512, 2021. doi:10.3390/en14020512.

[290] Nils Thonemann, Anna Schulte, and Daniel Maga. How to Conduct Prospective Life Cycle Assessment for Emerging Technologies? A Systematic Review and Methodological Guidance. *Sustainability*, 12(3):1192, 2018. doi:10.3390/su12031192.

[291] Romain Sacchi, Tom Terlouw, Kais Siala, Alois Dirnaichner, Christian Bauer, Brian L. Cox, Christopher Mutel, Vassilis Daioglou, and Gunnar Luderer. PRospective EnvironMental Impact asSEment (premise): A streamlined approach to producing databases for prospective life cycle assessment using integrated assessment models. *Renewable and Sustainable Energy Reviews*, 160:112311, 2022. doi:10.1016/j.rser.2022.112311.

[292] Nils Thonemann, Karen Saavedra-Rubio, Eleonore Pierrat, Katarzyna Dudka, Mathilde Bangoura, Nils Baumann, Christian Bentheimer, Priscilla Caliandro, Roeland De Breuker, Cor De Ruiter, Mario Di Stasio, Julie Elleby, Alexe Guiguemde, Bruno Lemoine, Martin Maerz, Valerio Marciello, Markus Meindl, Fabrizio Nicolosi, Manuela Ruocco, Benjamin Sala, Anna Lia Scharling Tromer Dragsdahl, Andrea Vezzini, Zhangqi Wang, Thomas Wannemacher, Julius Zettelmeier, and Alexis Laurent. Prospective Life Cycle Inventory Datasets for Conventional and Hybrid-Electric Aircraft Technologies. *SSRN Electronic Journal*, 2023. doi:10.2139/ssrn.4537185.

[293] Bern University of Applied Sciences (BFH). Bern University of Applied Sciences, Official Website. URL `https://www.bfh.ch/en/`. Accessed on 05/12/2023.

[294] Friedrich-Alexander-Universität, Department Elektrotechnik-Elektronik-Informationstechnik (FAU-LEE). Department Elektrotechnik-Elektronik-Informationstechnik, Official Website. URL `https://www.lee.tf.fau.de/`. Accessed on 05/12/2023.

[295] Rotterdam The Hague Airport. Rotterdam The Hague Airport, Official Website. URL `https://www.rotterdamthehagueairport.nl/en/`. Accessed on 05/12/2023.

[296] Karen Saavedra-Rubio, Nils Thonemann, Eleonora Crenna, Bruno Lemoine, Priscilla Caliandro, and Alexis Laurent. Stepwise guidance for data collection in the life cycle inventory (LCI) phase: Building technology-related LCI blocks. *Journal of Cleaner Production*, 366:132903, 2023. doi:10.1016/j.jclepro.2022.132903.

[297] Karthikeyan Ramachandran, Constance L. Gnanasagaran, and Ashish Vekariya. Life cycle assessment of carbon fiber and bio-fiber composites prepared via vacuum bagging technique. *Journal of Manufacturing Progresses*, 89:124–131, 2023. doi:10.1016/j.jmapro.2023.01.068.

[298] Changru Yang, Sangwon Seo, Nobuo Takata, Kyaw Thu, and Takahiko Miyazaki. The life cycle climate performance evaluation of low-GWP refrigerants for domestic heat pumps. *Renewable and Sustainable Energy Reviews*, 121:33–42, 2021. doi:10.1016/j.ijrefrig.2020.09.020.

[299] Gregor Wernet, Christian Bauer, Bernhard Steubing, Jürgen Reinhard, Emilia Moreno-Ruiz, and Bo Weidema. The Ecoinvent Database Version 3 (Part I): Overview and Methodology. *The International Journal of Life Cycle Assessment*, 21:1218–1230, 2016. doi:10.1007/s11367-016-1087-8.

[300] Kalyan Annamalai and Ishwar K. Puri. *Combustion Science and Engineering*. CRC press, 2006. doi:10.1201/9781420003789.

[301] Baroutian Saeid, Shafie Azzahra, Ismail Adeliza, Hamdan Hartini, and Abdul Aziz Abdul Raman. Blended aviation biofuel from esterified Jatropha curcas and waste vegetable oils. *Journal of the Taiwan Institute of Chemical Engineers*, 44(6), 2013. doi:10.1016/j.jtice.2013.02.007.

[302] Edward M. Greitzer, Philippe A. Bonnefoy, Elena De la Rosa Blanco, Chris S. Dorbian, Mark Drela, Dorothy K. Hall, R. John Hansman, James I. Hileman, Robert H. Liebeck, Jonathan Lovegren, Pritesh Mody, Julio A. Pertuze, Shun Sato, Zoltán S. Spakovszky, Choon S. Tan, Jeremy S. Hollman, Jessica E. Duda, Nathan Fitzgerald, James Houghton, Jack L. Kerrebrock, George F. Kiwada,

David Kordonowy, Joe C. Parrish, John Tylko, Ed A. Wen, and Wesley K. Lord. N+3 Aircraft Concept Designs and Trade Studies, Final Report Volume 2: Appendices - Design Methodologies for Aerodynamics, Structures, Weight, and Thermodynamic Cycles, 2010. URL `https://ntrs.nasa.gov/api/citations/20100042398/downloads/20100042398.pdf`. Accessed on 12/12/2023.

[303] Konstantinos G. Kyprianidis. *Advances in Gas Turbine Technology*, chapter Future Aero Engine Designs: An Evolving Vision. IntechOpen, 2011.

[304] Konrad Kozaczuk. Engine nacelles design – Problems and challenges. *Proceedings of the Institution of Mechanical Engineers, Part G: Journal of Aerospace Engineering*, 231(12):2259–2265, 2017. doi:10.1177/0954410017706993.

[305] Anaheim Automation. Gearbox Guide, 2021. URL `https://www.anaheimautomation.com/manuals/forms/gearbox-guide.php`. Accessed on 13/01/2023.

[306] Hartzell Propeller Inc. Composite Propellers: Turboprop Engine Aircraft, 2023. URL `https://hartzellprop.com/products/propeller-systems/composite-propellers-turboprop-engineaircraft/`. Accessed on 26/06/2023.

[307] Egoitz Artetxe, Haizea González, Amaia Calleja, Asier Fernández Valdivielso, Roberto Polvorosa, Aitzol Lamikiz, and L. Norberto López de Lacalle. Optimised methodology for aircraft engine IBRs five-axis machining process. *International Journal of Mechatronics and Manufacturing Systems*, 9(4):385, 2016. doi:10.1504/IJMMS.2016.10003806.

[308] Ginger Gardiner. Commercialization of CMCs and developments for next-gen performance, 2017. URL `https://www.compositesworld.com/articles/the-next-generation-of-ceramic-matrix-composites`. Accessed on 12/12/2023.

[309] Balaji Viswanadhapalli, Nagari Sateesh, and M. Manjoor Manzoor Hussain. Manufacture of Aluminium Metal Matrix Composite (Al7075-SiC) by Stir Casting Technique. *Materials Today: Proceedings*, 2(4-5):3403–3408, 2015. doi:10.1016/j.matpr.2015.07.315.

[310] Debashis Mishra and Tirupati Tulasi. Experimental Investigation on Stir Casting Processing and Properties of Al 6082/SiC Metal Matrix Composites. In *Recent Trends in Mechanical Engineering*, 2020. doi:10.1007/978-981-15-1124-0_14.

[311] Pamela A. Kobryn, Neal R. Ontko, Larry P. Perkins, and Jaimie S. Tiley. Additive Manufacturing of Aerospace Alloys for Aircraft Structures. In *Meeting Proceedings RTO-MP-AVT-139, Paper 3. Cost Effective Manufacture via Net-Shape Processing*, Neuilly-sur-Seine, France, 2006.

[312] Wikipedia contributors. Lists of Airbus aircraft orders and deliveries, 2020. URL `https://en.wikipedia.org/wiki/Category:Lists_of_Airbus_aircraft_orders_and_deliveries`. Accessed on 28/06/2023.

[313] Wikipedia contributors. ATR 42, 2023. URL `https://en.wikipedia.org/wiki/ATR_42`. Accessed on 28/06/2023.

[314] Wikipedia contributors. ATR 72, 2023. URL `https://en.wikipedia.org/wiki/ATR_72`. Accessed on 28/06/2023.

[315] Nils Thonemann, Karen Saavedra-Rubio, Eleonore Pierrat, Katarzyna Dudka, Julie Elleby, Anna Lia S. Tromer Dragsdahl, and Alexis Laurent. Deliverable 3.3 – Report on prospective LCA. Technical report, Clean Sky 2 GENESIS Project, 2023. URL `https://www.genesis-cleansky.eu/deliverables/`. Awaiting publication.

[316] Michael Z. Hauschild, Ralph K. Rosenbaum, and Stig Irving Olsen. *Life Cycle Assessment Theory and Practice*. Springer, 2018. doi:10.1007/978-3-319-56475-3.

[317] European Commission – Joint Research Center (EC-JRC). Supporting information to the characterisation factors of recommended EF Life Cycle Impact Assessment methods: Version 2 from ILCD to EF 3.0, Ispra, 2018. URL `https://eplca.jrc.ec.europa.eu/permalink/TR_SupportingCF_FINAL.pdf`. Accessed on 26/06/2023.

[318] Pantelis Capros, Georgios Zazias, Stavroula Evangelopoulou, Maria Kannavou, Theofano Fotiou, Pelopidas Siskos, Alessia De Vita, and Konstantinos Sakellaris. Energy-system modelling of the EU strategy towards climate-neutrality. *Energy Policy*, 134:110960, 2020. doi:10.1016/j.enpol.2019.110960.

[319] Nils Bullerdiek, Ulf Neuling, and Martin Kaltschmitt. A GHG reduction obligation for sustainable aviation fuels (SAF) in the EU and in Germany. *Journal of Air Transport Management*, 92:102020, 2021. doi:10.1016/j.jairtraman.2021.102020.

[320] Samarth Jain, Hsun Chao, Muharrem Mane, William A. Crossley, and Daniel A. DeLaurentis. Estimating the Reduction in Future Fleet-Level CO2 Emissions From Sustainable Aviation Fuel. *Frontiers in Energy Research*, 9, 2021. doi:10.3389/fenrg.2021.771705.

[321] Andres Gonzalez-Garay, Clara Heuberger-Austin, Xiao Fu Fu, Mark Klokkenburg, Di Zhang, Alexander van der Made, and Nilay Shah. Unravelling the potential of sustainable aviation fuels to decarbonise the aviation sector. *Energy & Environmental Science*, 15:3291–3309, 2022. doi:10.1039/D1EE03437E.

[322] Herib Blanco, Wouter Nijs, Johannes Ruf, and André Faaij. Potential for hydrogen and Power-to-Liquid in a low-carbon EU energy system using cost optimization. *Applied Energy*, 232:617—639, 2018. doi:10.1016/j.apenergy.2018.09.216.

[323] Gregor Brändle, Max Schönfisch, and Simon Schulte. Estimating long-term global supply costs for low-carbon hydrogen. *Applied Energy*, 302:117481, 2021. doi:10.1016/j.apenergy.2021.117481.

[324] Andreas W. Schäfer, Steven R. H. Barrett, Khan Doyme, Lynnette M. Dray, Albert R. Gnadt, Rod Self, Aidan O'Sullivan, Athanasios P. Synodinos, and Antonio J. Torija. Technological, economic and environmental prospects of all-electric aircraft. *Nature Energy*, 4:160–166, 2019. doi:10.1038/s41560-018-0294-x.

[325] Liz Brassaw. Airline Pilot Salary – How Much Do Pilots Make?, 2022. URL `https://www.thrustflight.com/how-much-do-pilots-make/`. Accessed on 25/05/2023.

[326] Bureau Of Labor Statistics, U.S. Department of Labor. Occupational Employment and Wages - May 2012, 2013. URL `https://www.bls.gov/news.release/archives/ocwage_03292013.pdf`. Accessed on 27/11/2023.

[327] U.S. Bureau of Labor Statistics. NAICS 336400 - Aerospace Product and Parts Manufacturing, 2023. URL `https://www.bls.gov/oes/current/naics4_336400.htm`. Accessed on 25/05/2023.

[328] André Orban. ATR extends A-checks intervals from 500 to 750 hours, 2019. URL `https://www.aviation24.be/manufacturers/atr/atr-extends-a-checks-intervals-from-500-to-750-hours/`. Accessed on 25/05/2023.

[329] Australian Taxation Office. ATO Depreciation Rates 2023, 2023. URL `https://www.depreciationrates.net.au/batteries`. Accessed on 25/10/2023.

[330] Joey Klender. Tesla and Jeff Dahn's million-mile battery needs a name upgrade, 2023. URL `https://www.teslarati.com/tesla-jeff-dahn-s-million-mile-battery-four-million-miles/`. Accessed on 01/03/2024.

[331] BloombergNEF. Battery Pack Prices Cited Below $ 100/kWh for the First Time in 2020, While Market Average Sits at $ 137/kWh, 2020. URL `https://about.bnef.com/blog/battery-pack-prices-cited-below-100-kwh`. Accessed on 25/10/2023.

[332] Battelle Memorial Institute. *Manufacturing Cost Analysis of 100 and 250 kW Fuel Cell Systems for Primary Power and Combined Heat and Power Applications*. 2016.

[333] Mariana Pimenta Alves, Waseem Gul, Carlos Alberto Cimini Junior, and Sung Kyu Ha. A Review on Industrial Perspectives and Challenges on Material, Manufacturing, Design and Development of Compressed Hydrogen Storage Tanks for the Transportation Sector. *Energies*, 15:5152, 2022. doi:10.3390/en15145152.

[334] U.S. Energy Information and Administration. *International Energy Outlook 2021: Macroeconomics and assumptions*. 2021.

[335] Exchange Rates UK. Euro to US Dollar Spot Exchange Rates for 2020, 2023. URL `https://www.exchangerates.org.uk/EUR-USD-spot-exchange-rates-history-2020.html`. Accessed on 25/05/2023.

[336] BloombergNEF. Carbon Offset Prices Could Increase Fifty-Fold by 2050, 2022. URL `https://about.bnef.com/blog/carbon-offset-prices-could-increase-fifty-fold-by-2050/`. Accessed on 25/05/2023.

[337] International Civil Aviation Organization (ICAO). *Guidance on potential policies and coordinated approaches for the deployment of sustainable aviation fuels*. 2022.

[338] Eduardo Mariz. ESG Extra: EU agrees ETS reform but SAF rules slip into 2023. *Ishka*, 2023. URL `https://www.ishkaglobal.com/News/Article/6851/ESG-Extra-EU-agrees-ETS-reform-but-SAF-rules-slip-into-2023`. Accessed on 30/01/2024.

[339] Rotterdam the Hague Airport. *Airport Charges Regulation April 2022 Summary*. 2022.

[340] Xin Zhao, Farzad Taheripour, Robert Malina, Mark D. Staples, and Wallace E. Tyner. Estimating induced land use change emissions for sustainable aviation biofuel pathways. *Science of The Total Environment*, 779:146238, 2021. doi:10.1016/j.scitotenv.2021.146238.

[341] Matteo Prussi, Uisung Lee, Michael Wang, Robert Malina, Hugo Valin, Farzad Taheripour, César Velarde, Mark D. Staples, Laura Lonza, and James I. Hileman. CORSIA: The first internationally adopted approach to calculate life-cycle GHG emissions for aviation fuels. *Renewable and Sustainable Energy Reviews*, 150:111398, 2021. doi:10.1016/j.rser.2021.111398.

[342] International Council on Clean Transportation. *Estimating sustainable aviation fuel feedstock availability to meet growing European Union demand*. 2021.

[343] Peggy Hollinger. Airportwatch - Hydrogen very unlikely to be used in long-haul planes; huge problems even for short-haul, 2021.

[344] International Energy Agency (IEA). *Direct Air Capture - A key technology for net zero*. IEA Publications, 2021.

[345] International Renewable Energy Agency (IRENA). Policies for green hydrogen, 2023. URL `https://www.irena.org/Energy-Transition/Policy/Policies-for-green-hydrogen#Current-policy-status`. Accessed on 02/12/2023.

[346] Saeed Farokhi. *Future Propulsion Systems and Energy Sources in Sustainable Aviation*. 2019. ISBN 9781119414995. doi:10.1002/9781119415077.

[347] Carlo E. D. Riboldi. An optimal approach to the preliminary design of small hybrid-electric aircraft. *Aerospace Science and Technology*, 81:14–31, 2018. doi:10.1016/j.ast.2018.07.042.

[348] Carlo E. D. Riboldi. Energy-optimal off-design power management for hybrid-electric aircraft. *Aerospace Science and Technology*, 95:105507, 2019. doi:10.1016/j.ast.2019.105507.

[349] Christopher Courtin and John R. Hansman. Safety considerations in emerging electric aircraft architectures. In *2018 Aviation Technology, Integration, and Operations Conference*, Atlanta, Georgia, 2018. doi:10.2514/6.2018-4149.

[350] Garrett Klunk and Jeffrey Freeman. Vertical tail area reduction for aircraft with spanwise distributed electric propulsion. In *2018 AIAA/IEEE Electric Aircraft Technologies Symposium*, Cincinnati, Ohio, 2018. doi:10.2514/6.2018-5022.

[351] Eric Nguyen, Pierre Troillard, Joël Jézégou, Daniel Alazard, Philippe Pastor, and Carsten Döll. Reduction of vertical tail using differential thrust: Influence on flight control and certification. In *AEGATS 2018*, Toulouse, France, 2018. URL `https://hal.science/hal-02183315`. Accessed on 07/01/2024.

[352] Mayank Bendarkar, Darshan Sarojini, Evan Harrison, and Dimitri Mavris. Evaluation of off-nominal performance and reliability of a distributed electric propulsion aircraft during early design. In *AIAA Scitech 2021 Forum*, Virtual event, 2021. doi:10.2514/6.2021-1723.

[353] Felix D. Finger, Carsten Braun, and Cees Bil. Impact of engine failure constraints on the initial sizing of hybrid-electric ga aircraft. In *AIAA Scitech 2019 Forum*, 2019. doi:10.2514/6.2019-1812.

[354] SAE International. *Wiring Aerospace Vehicle, AS50881G*. 2019.

[355] ASTM International. *ASTM F3230-17: Standard Practice for Safety Assessment of Systems and Equipment in Small Aircraft*. 2017.

[356] Federal Aviation Administration. *FAA Airports (ARP) Safety Management System. Appendix C. Safety Assessment Tables*. 2021.

Acknowledgements

The author wishes to express his sincere gratitude to all those who have contributed to the completion of this journey. Above all, the author is deeply grateful to the dearest people in his life for their unwavering encouragement and for being a source of comfort and strength during the most challenging times. Special thanks are extended to his brother Claudio, his father Giovanni Battista, and his significant other Maria Vittoria for their endless support, love, and inspiration.

Deep thanks are conveyed to Prof. Fabrizio Nicolosi, whose mentorship, patience, and expertise were critical in navigating the complexities of this research. Special appreciation is extended to all fellow researchers, for their collaborative spirit and their invaluable constructive feedback.

Last but not least, the author's participation in international research projects was also crucial for the development of this thesis work. Special acknowledgments are intended for the ELICA and GENESIS research projects. Both projects have received funding from the Clean Sky 2 Joint Undertaking. The Joint Undertaking receives support from the European Union's Horizon 2020 research and innovation program and the Clean Sky Joint Undertaking members other than the Union. However, the author desires to specify that this thesis only reflects his own view, and the Clean Sky 2 Joint Undertaking is not responsible for any use that may be made of the information it contains.

The ELICA project has received funding under Grant Agreement No. 864551. The author is grateful to all members of the ELICA consortium for their precious feedback on this research topic.

The GENESIS project has received funding under Grant Agreement No. 101007968. The author is grateful to all partners, and particularly to the Department of Environmental and Resource Engineering of the Technical University of Denmark, for their contributions to the realization of this work.

About the Author

Valerio Marciello was born in Naples, Italy, on 29/06/1995. He earned a Bachelor's Degree in Aerospace Engineering from the University of Naples "Federico II" in November 2017. In July 2020, he earned his master's degree in aerospace engineering from the same institution, before enrolling as a Ph.D. candidate in industrial engineering. His research has focused on aircraft design and alternative propulsion solutions for aviation, with a commitment to exploring sustainability and mitigating the environmental impact of future aircraft. Actively engaged in EU-funded projects under the Clean Sky 2 and Clean Aviation programs, he has made significant contributions to initiatives such as projects IRON, ELICA, GENESIS, and HERA.